DEVELOPMENT AND OPERATION OF AN OPEN-CORE DOWNDRAFT GASIFIER SYSTEM

GERAINT DEVENPORT EVANS
Doctor of Philosophy

THE UNIVERSITY OF ASTON IN BIRMINGHAM
October 1992

1

The University of Aston in Birmingham

DEVELOPMENT AND OPERATION OF AN OPEN-CORE DOWNDRAFT GASIFIER SYSTEM

GERAINT DEVENPORT EVANS
Doctor of Philosophy
1992

SUMMARY

The objectives of this research were to gain a greater understanding of the gasification process in an open-core downdraft gasifier and to investigate parameters which affect the performance of open-core downdraft gasifiers.

A gasification system utilising a novel 75 mm diameter transparent quartz glass gasifier was extensively modified to enable more reliable and safer operation. The main modification consisted of replacing the previous gas cooler, gas scrubber and gas pump with a venturi ejector system. The gasifier system can now be operated reliably for periods in excess of three hours if required.

The gasification process in the open-core downdraft gasifier occurs in two stages: flaming pyrolysis followed by char gasification. The time for flaming pyrolysis of a 15 mm diameter bead was 85.4 seconds. The time for a char particle produced from a 15 mm diameter bead to undergo char gasification was 200 seconds. The lengths of the flaming pyrolysis and char gasification zones in the uninsulated gasifier were found to be equivalent to 1.20 and 9.5 mean representative feed particle diameters. The measurements of the flaming pyrolysis zone were compared with a published model of flaming pyrolysis and found to compare well. A new model was developed to predict the length of the char gasification zone. In addition to the measurements made using the uninsulated gasifier, the effect of gasifier insulation on the gasification process was investigated. Gasifier insulation reduced the length of the flaming pyrolysis zone and increased the length of the char gasification zone reducing the equivalence ratio required to maintain stable gasifier operation. Reducing the gasifier air requirement for stable operation by 12% led to an increase in the product gas higher heating value from 3.38 to 4.49 $MJNm^{-3}$ during insulated gasifier operation.

It has been confirmed that stable operation in an open-core downdraft gasifier occurs due to the rate of char production by pyrolysis equalling the rate of char consumption by gasification. Increasing the air flow rate into the gasifier will result in increased oxidation of the gaseous products of pyrolysis. The resultant higher temperatures in the char gasification zone lead to an increase in the rate of char consumption by gasification relative to the rate of char production by pyrolysis and the reaction zone will move downwards towards the grate; a state which is termed gasification dominant operation. Operation in the char gasification dominant mode occurred at an higher equivalence ratio compared with stable operation which is in agreement with theory.

Key words: Open-core, downdraft, gasification, stratified, biomass

ACKNOWLEDGEMENTS

TABLE OF CONTENTS

9

Figures

Chapter 3

16

Tables

Plates

1.0   INTRODUCTION

One method of converting solar energy into more usable forms is by the use of biomass which uses solar radiation to convert atmospheric carbon dioxide into a fixed carbon resource as a fuel. It is estimated that throughout the whole of the EC, an area of approximately 20 million hectares of currently agricultural land and 10 to 20 million hectares of currently marginal land will become available by the year 2000 for the production of biomass in the form of forestry products (short rotation forestry, conventional forestry or scrub woodland) or annual crops such as sweet sorghum (Figure 1.1) [1]. This potential energy resource could provide up to two million barrels of oil equivalent per day [1].

Now   Future

million Ha

■ Fallow agricultural land
▨ Permanent agricultural land
▥ Arable agricultural land
■ Other
□ New crops
▨ Woodland
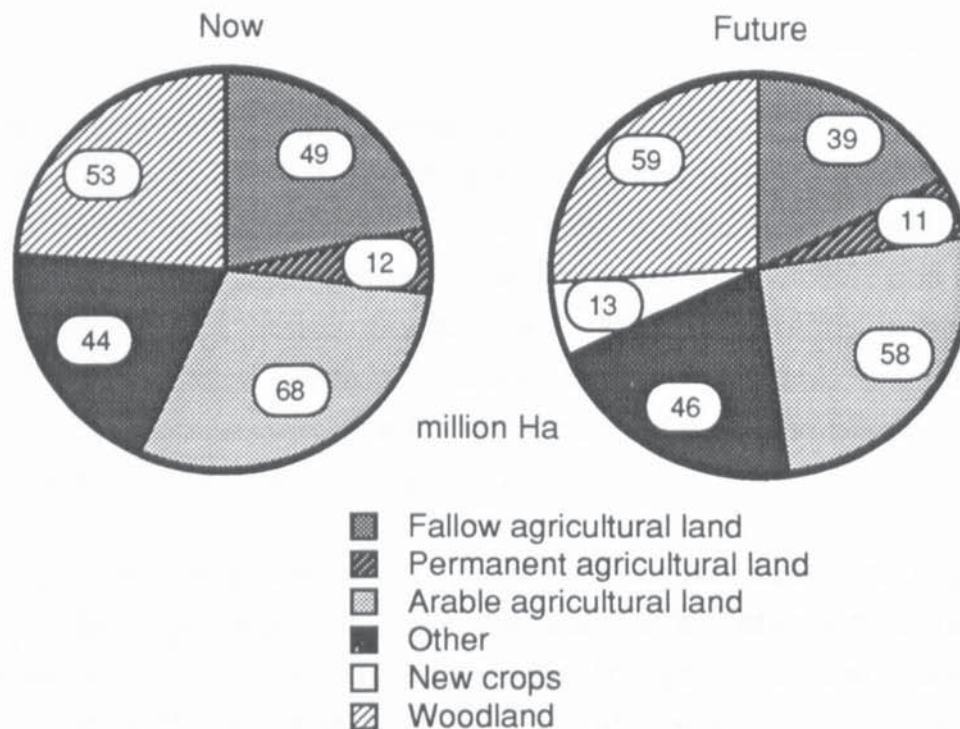
Figure 1.1
European Land Use [1].

Biomass has the advantage over conventional fossil fuels of being renewable, having a higher reactivity, lower sulphur content and a lower ash content. In addition, it is a CO_2 neutral energy source provided that consumption does not exceed annual production [2].

The term biomass can describe a variety of materials which includes crops, wood, agricultural waste, industrial and municipal wastes. Woody biomass was the world's first source of fuels and chemicals but its use declined in

industrial countries when fossil fuels became available. However, interest has been revived during the past two decades due to the uncertainty of fossil fuel prices and supplies. 1988 and 1990 estimates of proven reserves to current production rates for coal oil and gas are presented in Table 1.1.

Table 1.1 Proven Reserves/Current Production Rates Ratios Assuming Production Levels Continue at 1989 Rates [3],[4]			
	Coal	Gas	Oil
1988 reserves/production ratio, years*	218	58	41
1990 reserves/production ratio, years*	238	58	43

* Reserves remaining at the end of the year divided by the production in that year

Biomass utilization is difficult, however, due to its low heating value, high moisture content, low bulk density and non uniform size and shape which makes handling awkward [5]. It is also a diffuse resource making transportation to the point of use difficult and expensive. Conversion to other forms, solid, liquid and/or gaseous will, therefore, greatly enhance its usefulness. Of these, gaseous fuels are particularly valuable since they are clean burning, convenient to use and control and may also be converted to liquid fuels or chemicals (see Figure 1.2) [5].

Gasification is the conversion of a carbonaceous feedstock into a gaseous energy carrier by means of partial oxidation at elevated temperature [6]. Gasification is not a new technology - the first gasifiers having been built approximately 150 years ago [7],[8]. Their use reached a peak during the Second World War when about one million air gasifiers fuelled by wood blocks, peat, charcoal or anthracite were built to fuel road vehicles, boats, trains and electric generators [5],[6].

From the variety of technologies available for the gasification of biomass, fixed bed gasifiers have shown themselves to be simple in design and operation [9],[10]. Of these the downdraft gasifier has received considerable attention because of its ability to produce low tar content gases. Despite being similar in configuration to the conventional throated gasifier, the open-core downdraft gasifier has a number of advantages over the throated type, including not needing a gas tight seal at the fuel feeder, less stringent

reactor size limitations and the ability to accept a wider range of fuels [11],[12].
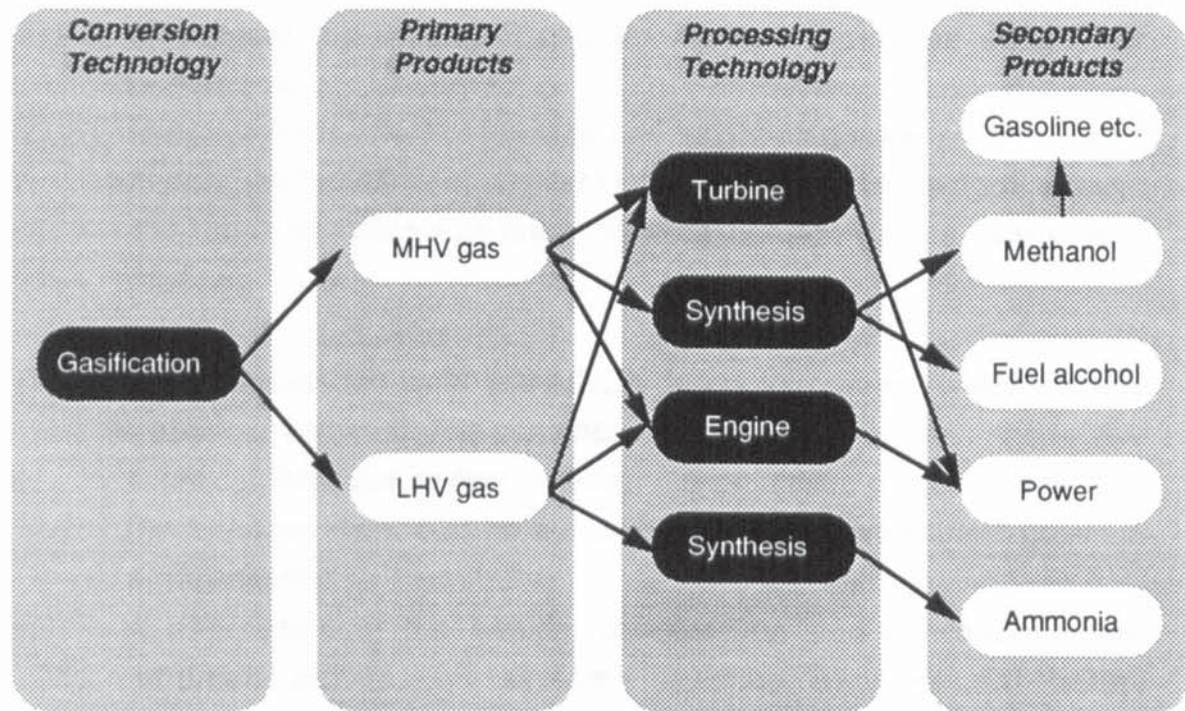
Figure 1.2
Gasification Conversion Technologies [1]

The Aston gasifier is a novel, transparent quartz glass open-core downdraft gasifier which permits direct observation of the gasification process. This can provide unique information which can lead to a greater understanding of the processes occurring within the reaction zone such as size, shape and extent of the reaction front and the degradation process of individual particles. In addition, the influences of the various parameters which affect gasifier performance (such as feed type, size, shape, moisture content) can be directly studied in considerable detail which is impossible with any conventionally built gasifier.

The objectives of this project were to:

i)   Modify an existing 75 mm transparent open-core downdraft gasification system to make gasifier operation easier, safer, more reliable, to allow longer run times and shorter turn around times between runs [12];

ii)   Qualitatively and quantitatively observe the gasification process and study the effect of insulation and feedstock particle size on the gasification process;

iii) Investigate the effects of gasifier mode of operation on gasifier performance;

iv   Investigate the effect of the char bed height on gasifier performance;

v)   Investigate the effect of gasifier insulation on gasifier performance;

vi)   Evaluate the effects of feed moisture content on the gasification process.

This thesis describes the work carried out during this project which aims to meet the above objectives. The contents include:

i)   A critical literature review in which the principles of gasification and the previous work carried out using open-core downdraft gasifiers are discussed,

ii)   A description of the design, construction and operation of the modified gasification system including experimental safety procedures,

iii) A description of the types of fuels and feeding methods employed,

iv)   The results and discussion of this work followed by the conclusions and recommendations for future work.

2.0   THEORY OF OPEN-CORE DOWNDRAFT GASIFICATION AND LITERATURE REVIEW

Gasification is one of several methods for the thermochemical conversion of biomass into more useful and valuable fuels. Of the variety of technologies available for the fixed bed gasification of biomass (Figure 2.1 and Table 2.1), the downdraft gasifier has received considerable attention due to its simplicity and ability to produce low tar content gases. The open-core downdraft gasifier, in its simplest form consisting of an open topped tube, is similar in configuration to the conventional throated gasifier. However, it has a number of advantages over the throated type, including ease of scale up, the ability to accept a wider range of fuels because of the absence of any constrictions within the gasifier, and it does not need a seal at the fuel feeding point as this is the entry point for the air.
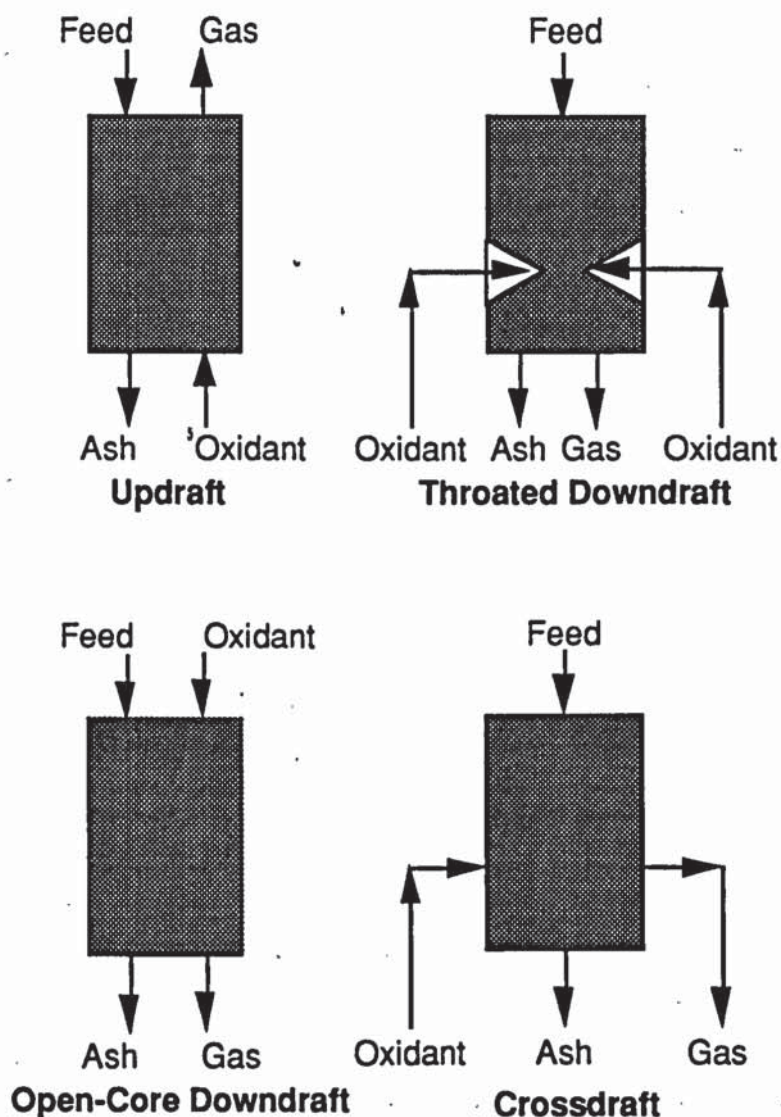
Figure 2.1
Fixed Bed Gasifier Types [9],[13],[14],[15]

Table 2.1
Advantages and Disadvantages of Fixed Bed Gasifier Types [9],[15],[16]

Advantages	Disadvantages
I Updraft (Counter-current)	
Low gas exit temperature; High carbon conversion; Low ash carry over; Simple construction.	High tar yield; Lump or block feed only; Ash fusion or clinkering on grate; Feed channelling or bridging possible.
I Throated Downdraft (Co-current)	
Low tar yield; High carbon conversion; Low ash carry over; Simple construction.	High gas exit temperature; Ash fusion or clinkering on grate; Poor turn down; Lump or block feed only; Feed channelling or bridging possible; Difficult to scale up; Limited feed moisture content.
III Open-Core Downdraft	
Simple construction; Sealed feed inlet not needed; Easier to scale-up than throated gasifier. Less susceptible to feed size variations - [- than throated downdraft gasifier.	High gas exit temperature; Limited feed ash content; Higher tar content gas compared to [- throated downdraft gasifier; Lump of block feed only; Poor turn down ratio; Limited feed moisture content.
IV Crossdraft	
Low reactor weight; Low ash carry over; Low sensitivity to plugging.	High tar yield except with wood char; Difficult to scale up; Ash fusion or clinkering on grate.

This chapter discusses the theory of gasification, the operation of open-core downdraft gasifiers and provides a critical appraisal of previous research work carried out using open-core gasifiers. Data from throated downdraft gasifiers is included where relevant and for comparison, but the main focus is to consider the open-core downdraft gasifier.

2.1   Theory of Gasification in an Open-Core Downdraft Gasifier

2.1.1   Principles of Gasification

Thermochemical gasification is the conversion by partial oxidation at elevated temperature of a carbonaceous feedstock such as biomass or coal into a gaseous energy carrier consisting of carbon monoxide, carbon dioxide, hydrogen, methane, trace amounts of higher hydrocarbons such as ethane and ethene, water, nitrogen (if air is used as the oxidizing agent) and

various contaminants such as small char particles, tars and oils [6],[12]. This conversion can be carried out using air, oxygen, steam or a mixture of these. Air gasification produces a low heating value gas (5-7 MJNm^{-3} higher heating value) [1] suitable for boiler and engine operation but not for pipeline transportation (due to its low energy density), while oxygen gasification produces a medium heating value gas (10-18 MJNm^{-3} higher heating value) suitable for limited pipeline distribution and as synthesis gas for conversion, for example, to methanol and gasoline (See Figure 1.1) [1].

The gasification process consists of several basic steps: drying, pyrolysis, combustion of some of the products of pyrolysis and gasification of the remaining char produced by pyrolysis. A description of the basic principles of gasification in terms of these basic steps is made in Sections 2.1.1.1 to 2.1.1.4.

2.1.1.1 Drying
Heat provided by oxidation (see Section 2.1.1.3) of some of the biomass feedstock heats up and evaporates moisture in the biomass. This process acts as a heat sink as the latent heat for the conversion of biomass moisture to water vapour is no longer available as useful energy to pass into the outlet gas stream.

2.1.1.2 Pyrolysis
Pyrolysis is defined as the thermal decomposition of organic matter at temperatures between 150 and 500°C yielding, in the case of biomass, a gaseous product, a liquid product, char and ash (Equation 2.1) [6]. Pyrolysis can take place in the presence or absence of external reagents.

$$wood + heat \rightarrow Char + CO + CO_2 + H_2O + CH_4 + C_2H_4 + oil/tars........[2.1]$$

Energy for the pyrolysis process is provided by the combustion of some of the products of the pyrolysis process (Section 2.1.3). The relative proportions of the pyrolysis products depend on the chemical composition of the biomass and on the operational conditions under which the pyrolysis takes place such as temperature, pressure, heating rate, residence time and catalysts.

2.1.1.3 Oxidation

Energy for the gasification process is provided by the oxidation of some of the pyrolysis products with a gasifying agent such as air or oxygen yielding carbon dioxide, carbon monoxide, and hydrogen [6]. In the area of oxidation, the temperature within the gasifier will rise sharply to approximately 1000°C (in an open-core downdraft gasifier) [17].

2.1.1.4 Gasification

The products from the previous three stages are converted by endothermic reactions at temperatures in excess of 750°C to produce a gas consisting mainly of hydrogen, carbon monoxide, carbon dioxide, methane, steam, hydrocarbons and, if air is used as the oxidizing agent, nitrogen (see Table 2.2) [12].

Table 2.2

Gasification and Oxidation Process Reactions [12],[18]

a) Heterogenous Gas-Solid Reactions

$$C + O_2 = CO_2 + heat \dotfill [2.2]$$
$$C + \tfrac{1}{2}O_2 = CO + heat \dotfill [2.3]$$

Boudouard Reaction

$$C + CO_2 + heat = 2CO \dotfill [2.4]$$

Water Gas Reaction

$$C + H_2O + heat = H_2 + CO \dotfill [2.5]$$

Methane Formation

$$C + 2H_2 = CH_4 + heat \dotfill [2.6]$$

b) Homogenous Gas-Gas Reactions

$$CO + \tfrac{1}{2}O_2 = CO_2 + heat \dotfill [2.7]$$
$$H_2 + \tfrac{1}{2}O_2 = H_2O + heat \dotfill [2.8]$$

Water Gas Shift Reaction

$$CO + H_2O = CO_2 + H_2 + heat \dotfill [2.9]$$

Reforming

$$CH_4 + H_2O + heat = CO + 3H_2 \dotfill [2.10]$$

Methanation

$$2CO + 2H_2 = CH_4 + CO_2 + heat \dotfill [2.11]$$

Methanation

$$CO_2 + 4H_2 = CH_4 + 2H_2O + heat \dotfill [2.12]$$

Variations in biomass properties, process conditions and the gasifying agent can all affect the gas composition produced by these gasification reactions shown by the wide variation of gas heating values ranging from 3 for atmospheric, air blown gasifiers to 18 $MJNm^{-3}$ for oxygen blown gasifiers [1].

The gasification reactions of the liquid products of pyrolysis are complex and not widely discussed in the literature. They may be gasified via thermal cracking or reactions with the gasifying agent and other pyrolysis products.

2.1.1.5   Air Required for Gasification

The amount of air required for gasification is usually defined either by the equivalence ratio or air factor. Equivalence ratio is defined as the percentage ratio of the actual oxidant to feed ratio to the stoichiometric oxidant to feed ratio. Air factor is defined as the ratio of the oxidant to feed ratio to the stoichiometric oxidant to feed ratio. At low equivalence ratios, below approximately 25%, biomass is converted to gas, a liquid and char in a pyrolysis mode of operation. As the equivalence ratio increases more char is converted by partial oxidation to a fuel gas reducing the yields of liquid and solid products. At an equivalence ratio of approximately 25%, the mole fraction of carbon monoxide is a maximum indicating that efficient gasification occurs at equivalence ratios of approximately 25% (see Figure 2.2) [5]. As the equivalence ratio is further increased, the product gas is increasingly oxidised to carbon dioxide and water and the process approaches combustion. Stoichiometric combustion is indicated by an equivalence ratio of 100% or an air factor of 1.0. The effect of equivalence ratio on the gasification process is described in further detail in Section 2.1.4.1.

2.1.2   Description of the Gasification Process in an Open-Core Downdraft Gasifier

To describe how the open-core downdraft gasifier operates, a single particle is followed through the system. Two physical models have been described by Reed [19] and Earp [12] (Figure 2.3). These models assume the reactor to be one dimensional and split into several distinct zones or strata separated by horizontal boundaries. Earp's model is based on observations made using the transparent quartz glass mark I Aston gasifier (Section 2.3.1) [12].

Mole fraction
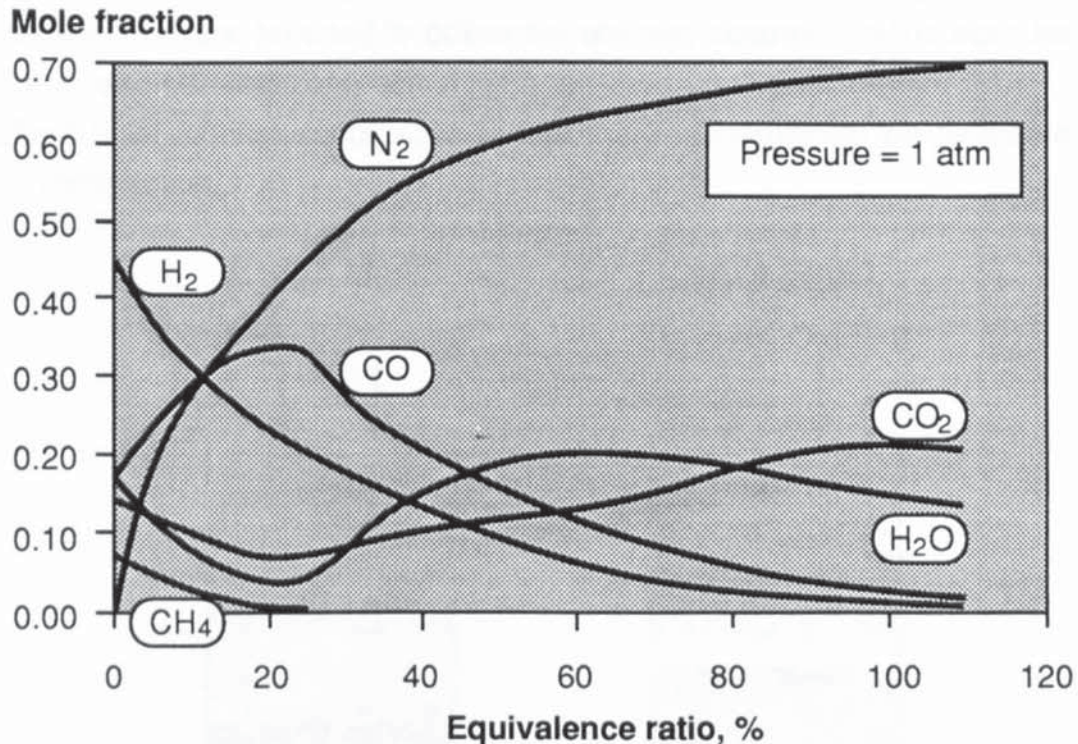
Figure 2.2
Equilibrium Composition for Adiabatic Air/Biomass (dry)
Reaction [5]

2.1.2.1   Unreacted Feed Zone

Oxidant and feed enter through the top of the reactor together and form a non reactive fuel/oxidant reservoir which is claimed to homogenize the flows of fuel and oxidant to the reacting zones below [20]. Due to the consumption of biomass in the gasification process below, the particle moves towards the reaction zone and more biomass is added to the reactor to maintain a suitable preset level of biomass.

As the particle sinks further into the reactor its temperature rises sharply when it sees back radiation from the pyrolysis zone below and moisture begins to evaporate. As the particle dries, it enters the pyrolysis zone where 80 to 95% of the biomass will be converted to gas and tars and 5 to 20% will be converted to a highly reactive charcoal [20],[21].

2.1.2.2   Flaming Pyrolysis Zone

Flaming combustion is a term which has been used to describe the initial phases of wood combustion when the volatiles released by the heat of combustion burn in an excess of air thus producing more heat to sustain the

32

reaction [20]. Reed suggested that a term analogous to flaming combustion, flaming pyrolysis, be used to define the process occurring in the zone below the unreacted feed zone within an open-core downdraft reactor [20]. This differs from flaming combustion in that there is insufficient air available for full combustion.

Reed's Model

Biomass Oxidant

Earp's Model

Biomass Oxidant

Grate

Product gas including some char and ash to downstream processing

Product gas including some char and ash to downstream processing

Unreacted feed

Drying and flaming pyrolysis

Void

Char gasification

Hot char

Inert char
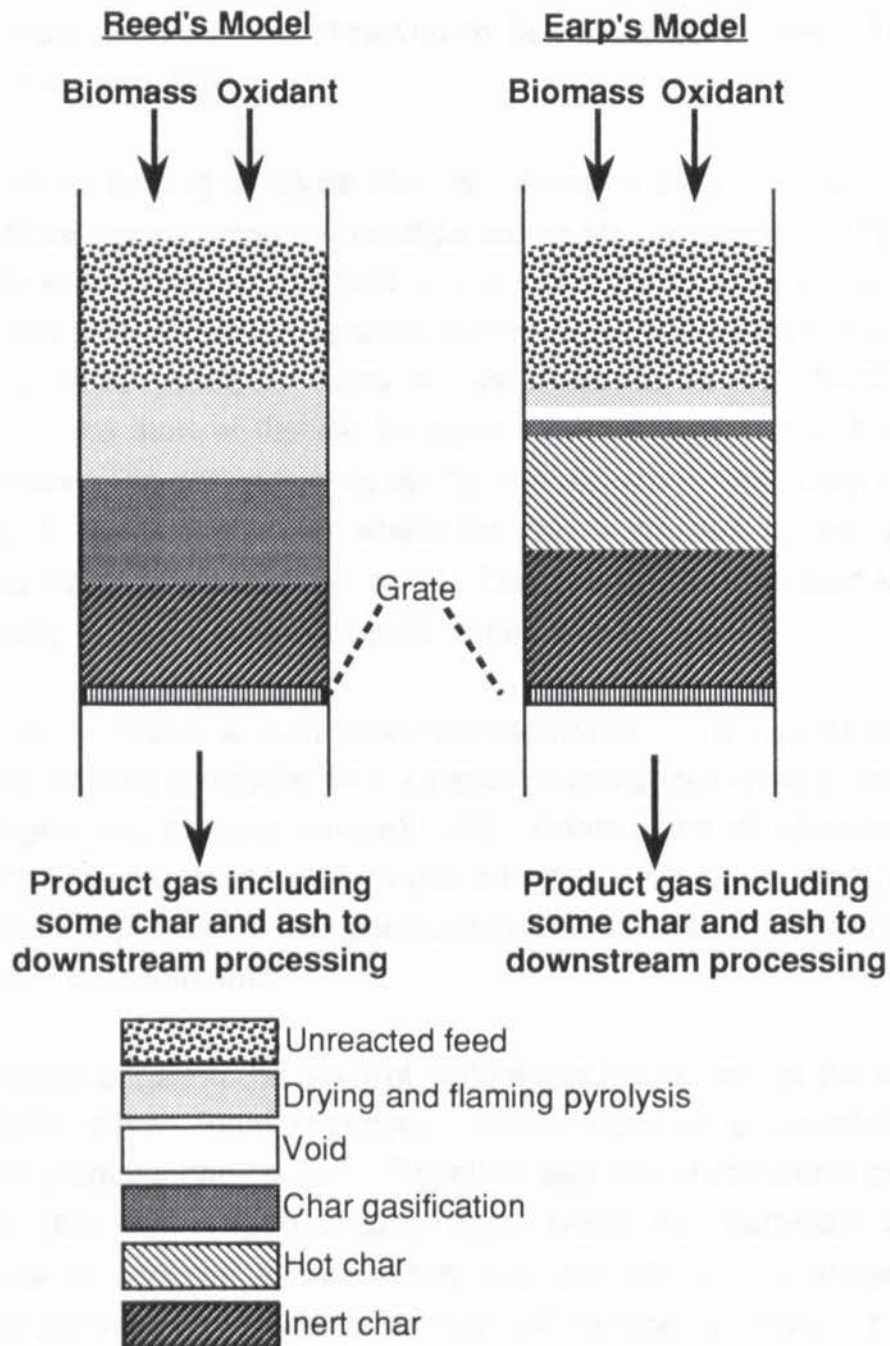
Figure 2.3

Open-Core Downdraft Gasifier Models [12],[20]

On entry to the flaming pyrolysis zone the particle's temperature rises rapidly at its surface by heat transfer by primarily radiation and conduction from the

surrounding hot particles [20]. Reed suggests that the most important heat transfer mechanism is convective heat transfer from upwardly propagating flames [11]. This upward propagation of flames would appear to contradict the expected situation since there is a rapid forced convection of air and gases drawn down through the reactor by the action of the gas pump downstream of the gasifier. In addition, Earp reports that flames from the flaming pyrolysis zone were observed to flow downwards away from the unreacted feed zone [12].

The start of the flaming pyrolysis zone is defined by Earp to be the point at which particles approaching the reaction zones start to blacken [12]. Reed defines the start of flaming pyrolysis as the top of the glowing reaction zone in the gasifier [11]. However, particles commencing flaming pyrolysis will not be glowing since pyrolysis starts at temperatures above 250°C. The definition for the start of flaming pyrolysis reported by Earp is, therefore, more accurate. The end of flaming pyrolysis is defined by both Earp [12] and Reed [22] to be the point at which the flame emitted by the particle undergoing flaming pyrolysis dies away. The definitions of the start and end of the flaming pyrolysis zone will be confirmed in this thesis.

Equation 2.13 shows a simplified representation of a typical biomass undergoing flaming pyrolysis with a typical flaming pyrolysis product gas (with nitrogen and tars/oils omitted) [20]. Combustion of some of these gases with oxygen from the air provides energy for the gasification process. The gasification process in an open-core gasifier is, therefore, energetically self sufficient or autothermal.

Large volumes of gas in the order of 1000 times the volume of the biomass are released, which Reed suggests, provide a buffering boundary layer around the biomass particle [20]. Together with the endothermic pyrolysis reactions, this buffering boundary layer limits the particle's surface temperature to between approximately 800 and 900°C and prevents the reaction of pyrolysis gases with solid char until flaming pyrolysis is complete [20].

$$CH_{1.4}O_{0.6} + 0.4\ O_2 \rightarrow 0.2\ C + 0.45\ CO + 0.35\ CO_2 + 0.45\ H_2 + 0.25\ H_2O$$

$$\dots\dots\dots\dots\dots\dots\dots\dots\dots\dots\dots\dots\dots [2.13]$$
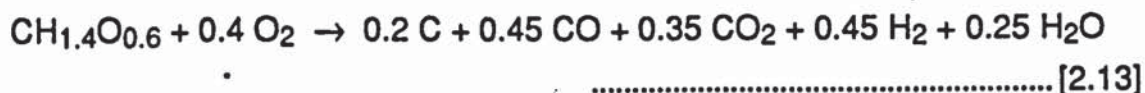
Although the temperature within this zone is high, the temperature within the particle rises slowly due to the poor thermal conductivity of wood. This will result in a thermal wave which passes upwards through the particle with pyrolysis occurring wherever the temperature rises above about 250°C [21]. Pyrolysis will, therefore, not be uniform throughout the particle and there will be a pyrolysis zone within the particle moving in a wave like manner through the particle, leaving char behind where pyrolysis has been completed [21].

Both Reed and Earp report that on completion of flaming pyrolysis, the charred particle and the gaseous products of flaming pyrolysis (mainly hydrogen, carbon monoxide, carbon dioxide and water) move down into the next zone (see Figure 2.3). Alternative views concerning the exact nature of this zone are put forward by both Earp [12] and Reed [11],[19],[20]. Earp suggests (Figure 2.3) that the particle falls through a void zone reported to be one to two particle diameters deep, containing flaming pyrolysis gases and on to the char bed below. The void forms due to the shrinkage of biomass particles during flaming pyrolysis and is supported by particles bridging across the flaming pyrolysis zone [12]. Collapses of bridged particles will produce a non-uniform void zone, however. The uniformity of the void zone is not reported by Earp [12]. Observations of the nature of voids formed due to the shrinkage of biomass particles in the flaming pyrolysis zone will be made in this project. Both Chern [21] and Reed [11],[19],[20] suggest that the particle under consideration passes directly from the flaming pyrolysis zone into the char gasification zone and report no void zones. This apparent contradiction will be investigated in this thesis.

The length of the flaming pyrolysis zone is reported by Reed to be of the order of 11 feed particle diameters [20] while Earp reports that flaming pyrolysis occurs within a height of no more than two feed particle diameters [12]. Although both definitions of the start and end of flaming pyrolysis reported by Earp [12] and Reed [20] are similar, there are wide variations between the reported flaming pyrolysis zone lengths which will be investigated in this project.

A model to predict the length of the flaming pyrolysis zone in an open-core downdraft gasifier is reported by Reed [22]. It is suggested that in combination with a model to predict the char gasification zone length

(Section 2.1.2.3), this model can be used to calculate the dimensions of a gasifier as a function of feed properties and gasifier operating conditions.

The length of the flaming pyrolysis zone is calculated from the flaming pyrolysis time. The flaming pyrolysis time is calculated using an empirically based model of flaming pyrolysis devised by Huff [23] and modified by Reed (Equation 2.14) [22]. Huff measured the time required for flaming combustion of a wood particle in a furnace of controlled temperature as a function of particle size, shape, density, wood moisture content and furnace temperature [23]. The start and end of flaming combustion were determined visually [23]. From his data, Huff derived an empirical formula to describe flaming combustion. Huff reports that the flaming combustion times predicted by his model were within 3% of the measured values [23]. Reed modified the Huff model by including the effect of oxygen concentration [22].

$$t_{fp} = \frac{0.207.\rho.F_s.(1 + 1.76F_m).D.(1 + 0.61D) \exp(\frac{4369}{RT})}{(1 + 3.46F_{O_2})} \quad \ldots\ldots [2.14]$$

where:

t_{fp} Time for flaming pyrolysis, seconds

ρ particle absolute density, gcm^{-3}

F_s Sphericity

F_m Particle moisture content (fraction)

D   Particle characteristic dimension, (Volume$^{0.333}$), cm

R   Gas constant, 1.987 $calK^{-1}mol^{-1}$

T   Flaming pyrolysis temperature, K

F_{O_2} Initial fraction of oxygen in the ambient gas (0.21)

Reed compared experimentally determined flaming pyrolysis times with the predicted flaming pyrolysis times calculated using Equation 2.14 for wood dowels. This data is presented in Table 2.3. It can be seen that the predicted time calculated using Equation 2.14 compares well with the experimentally determined flaming pyrolysis time. The predictions are within 20% of the measured values.

The length of the pyrolysis zone is calculated from the flaming pyrolysis time, feed rate and bulk density of the feed using Equation 2.15.

$$L_{fp} = \frac{4 \cdot t_{fp} \cdot F}{3600 \cdot \rho_{bulk} \cdot r^2 \cdot \pi} \quad \text{.................................} \quad [2.15]$$

where:

L_{fp} Flaming pyrolysis zone length, m

F   Feedstock feedrate to gasifier, kgh^{-1}

ρ_{bulk} Feedstock bulk density, kgm^{-3}

r   Gasifier radius, m

Table 2.3
Comparison of Predicted and Measured Flaming Pyrolysis Times [20]

Dowel size d x l (mm)	Experimental time (seconds)	Predicted time (seconds)
6.35 x 25.4	30	24
11.1 x 25.4	54	54
19.1 x 12.7	132	108
25.4 x 38.1	156	168

Reed does not, however, compare the predicted flaming pyrolysis zone lengths calculated using Equation 2.15 with measured values of the flaming pyrolysis zone length. Reed does present a calculation based on the gasification of 6.35 mm (0.25 inch) wood chips [20]. The predicted gasification time is 1.44 minutes. This corresponds to a calculated flaming pyrolysis zone length of 10.72 cm equivalent to 13.4 feed particle diameters. This compares well with the measured flaming pyrolysis zone length reported by Reed for 1x1x0.3 cm pine wood chips (9 cm equivalent to 11 feed particle diameters) [20]. However, as noted earlier, there is a discrepancy between the measured flaming pyrolysis zone lengths reported by Earp [12] and Reed [19],[20] which will be investigated in this project.

It is noted that errors will arise using Equation 2.15 since the particle velocity in the flaming pyrolysis zone will change as particle shrinkage due to pyrolysis occurs (it is estimated that the char particle radius will be 50% of the feed particle radius on completion of pyrolysis). If the length of the flaming pyrolysis zone is small as reported by Earp, then the error will be

small and the simplification would be valid. However, the scale of the error will be increased if the flaming pyrolysis zone length is similar to that reported by Reed (9 cm) [20].

Reed developed a new model based on observed heat transfer rates [24]. However, the "new model" is reported to be less accurate than the modified Huff equation (Equation 2.14). The modified Huff equation will, therefore, be used in this project for comparison with the measured flaming pyrolysis times and flaming pyrolysis zone lengths.

2.1.2.3   Char Gasification Zone

It is in the adiabatic char gasification zone that the gases produced in the flaming pyrolysis zone, primarily CO_2, CO, H_2, H_2O and CH_4 react with the char produced by pyrolysis according to the reactions shown in Table 2.2 [19],[21]. The char particle deposited in the char gasification zone was observed by Earp to shrink rapidly and disappear from view as a result of char gasification (see Figure 2.3) [12]. However, there may be some residual oxygen in the char gasification zone not consumed in the flaming pyrolysis zone leading to some char consumption by combustion (see Section 2.1.3).

The temperature of the hot gases entering this zone is approximately 1000°C [12]. This heat provides the energy for the endothermic gasification reactions to take place (see Table 2.2). As gasification proceeds, cooling takes place slowing reaction rates until the temperature falls to approximately 700°C where the rates of the reduction reactions fall to insignificant levels [21]. There is, therefore, the possibility that equilibrium will not be attained in the char gasification zone. Charcoal conversion efficiency may also be reduced by the entrainment of small charcoal particles into the gas stream [19].

The start and end of the char gasification zone in the open-core downdraft gasifier are not clearly defined in the literature. Earp suggests that particles ending flaming pyrolysis fall through a void zone and on to the top of the char gasification zone [12]. This suggests that the void zone is clearly visible. However, from the photographs presented by Earp, the void zone is difficult to observe and is not a clearly defined zone across the whole diameter of the gasifier. This suggests that the start of the char gasification

zone is difficult to observe. The start of the char gasification zone is not defined by Reed. The end of the char gasification zone is defined by Reed as the bottom of the incandescent zone of char in the gasifier [11]. Earp defines the end of char gasification zone during stable gasifier operation as the point at which char particles disappear from view [12]. However, the visual determination of the point of extinction of a small char particle at the bottom of the char gasification zone would be difficult. It is concluded that the start and end of the char gasification zone in the open-core downdraft gasifier are poorly defined in the literature. New definitions will be developed in this project.

Although the start and end of the char gasification zone are not clearly defined, both Earp [12] and Reed [20] report values for the char gasification zone length. The char gasification zone length is reported by Earp to be approximately one feed particle diameter [12]. while Reed reports it to be 6 feed particle diameters [20] This discrepancy will be investigated in this project. Earp suggests that the height of the entire reaction zone consisting of the flaming pyrolysis, void and gasification zones is no more than four to five particle diameters [12].

Measured char gasification times are not reported by either Reed or Earp. The total particle reaction time (flaming pyrolysis and char gasification) is reported by Earp to be approximately 36 seconds for a cubic particle sieved to between 4.75 mm and 6.35 mm [12]. Video and time lapse photography will be used in this project to study the time for char gasification.

A model to calculate the length of the char gasification zone is reported by Reed [22]. It is reported that this model can be used in combination with the flaming pyrolysis zone length model (Equations 2.14 and 2.15) to predict the dimensions of an open-core downdraft gasifier. The model is simple and consists of the length of reactor that the fuel will travel through in 100 seconds (Equation 2.16) [24]. It is suggested by Reed that kinetic studies of the char gasification zone show that the gasification of char particles will be 90% complete in 100 seconds. There is disagreement, however, between various papers written by Reed since some papers suggest that char gasification is 90% complete in 100 seconds [25],[26],[27],[28] while others suggest that char gasification is 90% complete in 140 seconds [19],[20]. In addition, the char particle size is not reported by Reed.

$$L_{CG} = \frac{4 \times t \times G_o}{\rho_{bulk} \times 3.6 \times \pi \times d_o^2} \quad\text{...} [2.16]$$

where:

L_{CG}	Char gasification zone length, cm
G_o	Feed rate through gasifier, kgh^{-1}
ρ_{bulk}	Feed bulk density
d_o	Gasifier diameter, cm
t	Time for gasification (100 seconds)

Reed has not presented data to compare the predicted char gasification zone length calculated by Equation 2.16 with measured char gasification zone lengths. It is reported, however, that the results predicted by the char gasification zone length model are compatible with the zone lengths observed in a quartz gasifier [20].

This model calculates the char gasification zone length from the wood flow rate to the reaction zones and not the char flow rate from the flaming pyrolysis zone into the char gasification zone. Reed does not explain the reason for the use of the wood flow rate and not the char flow rate.

This model will be used in this project for comparison with the measured char gasification zone lengths. However, the simplicity of this model indicates that further work in predicting the length of the char gasification zone is required.

2.1.2.4 Char Zone Below Gasification Zone

Once the charcoal temperature falls to below approximately 700°C, the char particle enters the relatively inert char zone and takes no further part in the gasification reactions although heat losses from this zone to the surroundings will reduce the temperature of the product gas leaving the gasifier. Reed suggests that this charcoal may help reduce the tar content of the product gas by cracking the tars to lower molecular weight material. However, the temperature of this zone is below 900°C below which little tar cracking is reported to occur [29]. Some tar removal may occur as this zone may act as a hot gas filter [30]. During char accumulation operation (see Section 2.1.3) this zone will contain small char particles due to their reduction in size during pyrolysis and gasification. There is, therefore, a

danger that during pyrolysis dominant operation, the reactor pressure drop may rise to unacceptable levels during long periods of operation unless char removal operations are carried out. Channelling may also occur resulting in poor oxidant distribution across the reaction zone thereby reducing gasification efficiency [6].

Earp proposes that the inert char zone below the gasification zone is composed of a hot char zone and an inert char zone (Figure 2.3). It is suggested that the temperature of the hot char zone is high enough to promote tar cracking mechanisms. However, since a temperature of 850°C is reported to be required for tar cracking, tar cracking will only occur in the char gasification zone since char gasification occurs at temperatures greater than 700°C [12],[19]. Heat losses to the surroundings will further reduce the temperature in the char zone below hot char zone (Figure 2.3) leading to the formation of an inert char zone in which the temperature is reported to be too low to sustain tar cracking, although it is suggested that some tar absorption may occur [12]. Earp does not provide a definition for the end of the hot char zone and the start of the inert char zone.

The fate of ash produced during the gasification of biomass in an open-core downdraft gasifier is not reported by Reed [19] or Earp [12]. During stable operation, ash will either accumulate at the interface between the char gasification zone or will be entrained into the product gas.

2.1.2.5 Summary

Two physical, stagewise descriptive models of the gasification process in an open-core downdraft gasifier have been reported. Each model assumes the system to be split into several distinct zones. Reed's model splits the gasifier into four zones each apparently of approximately equal height. Earp derived his own model based on observations made using an earlier version of the gasifier used in this project (mark I Aston gasifier). The disagreement between the zone heights reported by Reed and Earp will be investigated in this project.

The char particles entering the char gasification zone are reported to be gasified by the gaseous products of pyrolysis. It is not reported whether any unreacted residual oxygen is present in the char gasification zone leading to some char consumption by combustion (see Section 2.1.3).

2.1.3 Open-Core Downdraft Gasifier: Mode of Operation

The work of Reed and Markson [11], Earp [12] and Reyes [17] show that an open-core downdraft gasifier can be operated in three regimes (see Figure 2.4):

i)   constant height of char bed (there is no net production or consumption of char in the gasifier). This is termed stable operation by Reed and Markson [11], Earp [12] and Reyes [17] although, in general, small changes in any parameter can cause the reaction zone to drift through either of the mechanisms below;

ii)   increasing height of char bed (there is a net production of char in the gasifier). This is termed pyrolysis dominant operation Earp [12] and Reyes [17];

iii)   decreasing height of char bed (there is a net consumption of char in the gasifier). This is termed gasification dominant operation by Earp [12] and Reyes [17].

The mode of operation in an open-core downdraft gasifier is reported to be primarily altered by varying the equivalence ratio although gasifier heat losses, bed stirring and air injection to the reaction zone will also have an effect [11]. The effect of equivalence ratio on gasifier performance is discussed in Section 2.1.4.1. At a particular equivalence ratio, gasifier operation will be stable and there will be no net production of char in the gasifier. Reducing the gasifier equivalence ratio relative to the equivalence ratio required for stable operation will result in pyrolysis dominant operation. Conversely, increasing the gasifier equivalence ratio relative to the equivalence ratio required for stable gasifier operation will result in char gasification dominant operation.

Relation of biomass pyrolysis rate Vp to char gasification rate Vg	Vg > Vp	Vg = Vp	Vg < Vp	Vg << Vp
Reaction zone motion	Down	None	Up	Fast up
Mode of operation	Char consumption	Stable operation	Char production	Char production
Example condition	Air, no insulation	Air, some insulation	Air, insulation	Oxygen
Typical reaction zone velocity, Vr, cm/min	-0.6	0	+0.6	+50
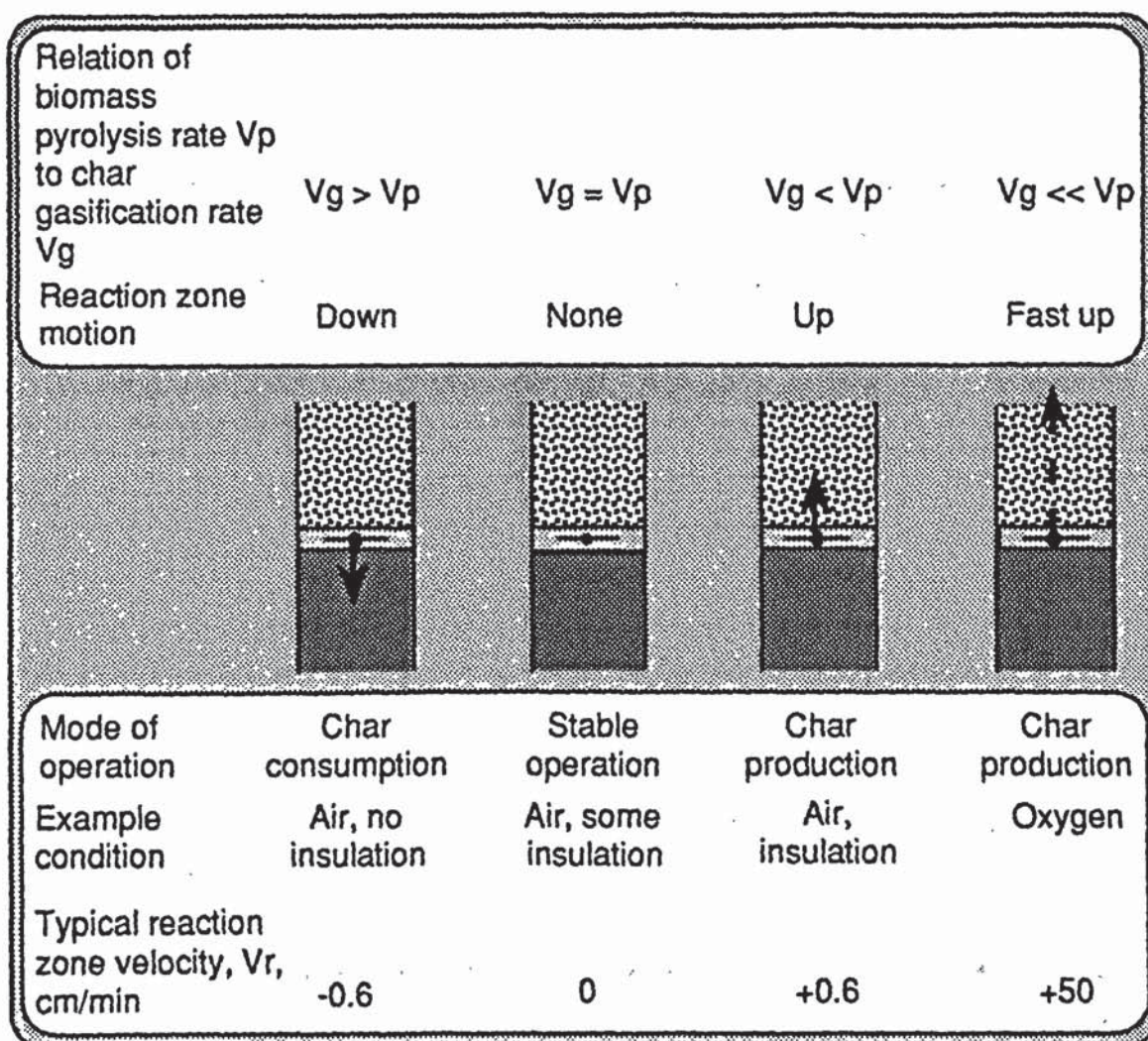
Figure 2.4
Reaction Zone Motion Observed in Open-Core Gasifiers [11]

Reed and Markson report that altering the mode of operation is due to variations in the rates of pyrolysis and gasification [11]. They do not, however, explain whether the equivalence ratio affects the rate of char gasification, the rate of flaming pyrolysis or both [11]. Reed and Markson suggest that if the rate of pyrolysis exceeds the rate of gasification then the reaction zone will rise until it reaches the top of the bed - a state termed top stabilised operation. During top stabilised operation, the reaction zone position will be controlled by the fuel feed rate [11]. Reed notes that if oxygen is used as the oxidant, then the rate of flaming pyrolysis will greatly exceed the rate of gasification and the reaction zone will immediately become top stabilized. If the rate of pyrolysis equals the rate of char gasification then the position of the reaction zone will remain constant relative to the position of the grate. If pyrolysis proceeds more slowly than gasification then the height of the char bed will fall and the reaction zone will

43

approach the grate. Figure 2.4 summarizes the modes of operation of open-core gasifiers described by Reed.

The possibility of stable gasifier operation occuring as a result of the rate of char production by pyrolysis equalling the rate of char consumption by both gasification and combustion is not considered by either Reed or Earp. At high equivalence ratios excess air may pass through the flaming pyrolysis zone (Figure 2.3) unconsumed leading to char consumption by combustion. This theory will be investigated in this project and compared with the theory reported above.

Two open-core downdraft gasifiers fuelled with wood in the literature are reported to have been operated in the three modes listed above. Only data from the stable and pyrolysis dominating modes are reported for the mark I Aston gasifier, however [12]. The gasifier reported by Reed was used to investigate the rate at which the reaction zone moved with or counter to the flow of air or oxygen [20]. Gasifier performance is only reported during stable operation [11],[20].

Stable gasifier operation was only achieved for short periods with the mark I Aston gasifier suggesting that maintaining stable operation in an open-core downdraft gasifier not fitted with a char removal system (see Section 2.1.4.1) is difficult. The longest reported period of stable gasifier operation was 12.4 minutes and the shortest period of stable operation was 3.05 minutes [12]. The ease of maintaining stable operation in the open-core downdraft gasifier is not reported by Reed. The average equivalence ratio at which stable operation in the mark I Aston gasifier was obtained is reported to be 38.9% [12].

It would be expected that during pyrolysis dominant operation when the char bed depth is increasing that the equivalence ratio would decrease. Earp's data, however, shows that during rising bed operation there is a higher air requirement [12]. Earp explains this by considering the heat losses from the uninsulated reactor and the reduction in biomass throughput [12]. During pyrolysis dominant operation, the fractional heat loss from the reactor will be greater than during stable operation since the hot area from which heat is lost is increased compared with that during stable operation [12]. The conversion efficiency of the biomass to gas will be lower due to reduced

44

carbon conversion efficiency during unstable operation (from 91% during stable operation to 84% during unstable operation) [12]. Earp also suggests that the higher reactor heat loss during pyrolysis dominant operation manifests itself in higher product gas CO_2 and H_2O levels reducing the reactor's efficiency to cold clean gas [12]. He concludes that in a period when pyrolysis is dominating the gasification process, the equivalence ratio is reduced relative to that at stable operation but that this change is masked by differences in reactor heat loss [12]. The high equivalence ratio may, however, be due to the failure to obtain a stable reaction operating regime. During the period of pyrolysis dominant operation, the air flow rate into the gasifier may have been progressively increased in an attempt to obtain a stable operating regime resulting in an high average air input rate to the gasifier during the run. A comparison of the air flow rates during stable operation and during rising char bed operation with an insulated reactor will be made in this project to investigate this discrepancy (see Section 2.1.4.3).

Increasing the air flow rate to the reactor should cause the depth of the char bed to decrease. Neither Reed nor Earp report any results or descriptions of the effect of gasifier operation with a net consumption of char (gasification dominant operation). A comparison of the air flow rates during operation with a net consumption of char (gasification dominant operation) and stable operation will be made in this project.

A third open-core downdraft gasifier (the University of California, Davis gasifier fuelled with rice hulls) is shown to have been operated in three modes [29]. Because no ash removal took place, the high ash content of the rice hull feed resulted in an upward moving reaction zone. However, the volume reduction of the rice hulls following reaction and their caking behaviour resulted in a downward movement of the rice hull fuel bed. The significance of the relative velocities of the upward velocity of the reaction zone and the downward velocity of the unreacted fuel bed is not reported by Kaupp [29].

The three modes of operation in which the University of California open-core downdraft gasifier was operated were [29]:

a)   the upward movement of the reaction zone is greater than the downward velocity of the fuel bed;

45

b) the upward movement of the reaction zone equals the downward velocity of the fuel bed, and;

c) the upward movement of the reaction zone is less than the downward velocity of the fuel bed.

One set of data presented by Kaupp shows gasifier operation where the velocity of the reaction zone was greater than the downward velocity of the fuel bed at an equivalence ratio of 32% (mode a). A second set of data shows gasifier operation at an equivalence ratio of 35% where the upward velocity of the reaction zone equals the downward velocity of the fuel bed (mode b). The remaining four data sets show gasifier operation at equivalence ratios between 35% and 52% where the downward velocity of the fuel bed was greater than the upward velocity of the reaction zone (mode c) [29].

The relative rates of char production by pyrolysis and char consumption by gasification in the three modes are not, however, reported by Kaupp. At the point at which the upward velocity of the reaction zone equals the downward velocity of the fuel bed, it is not reported whether the rate of char production by pyrolysis equals the rate of char consumption by gasification. It is concluded that insufficient data is presented to assess the mode of operation according to the definitions i, ii and iii on page 42.

An open-core downdraft gasifier can be operated in three modes (stable operation, pyrolysis dominant operation and char gasification dominant operation). Stable operation is reported to occur due to the rate of char production by pyrolysis equalling the rate of char consumption by gasification. Pyrolysis dominant operation is reported to occur when the rate of char production by pyrolysis exceeds the rate of char consumption by gasification. Char gasification dominant operation is reported to occur when the rate of char consumption by gasification exceeds the rate of char production by pyrolysis. It is not reported whether any unreacted residual oxygen not consumed during flaming pyrolysis is present in the char gasification zone leading to char consumption by combustion.

Two wood fuelled open-core downdraft gasifiers are reported to have been operated in these three modes. However, performance data in the char gasification dominant mode has not been presented.

46

2.1.4   Effects of Process Parameters and Biomass Properties on
               the Gasification Process in an Open-Core Downdraft Gasifier

2.1.4.1   Equivalence Ratio

Gasification with air is reported to occur at equivalence ratios between approximately 25% and 30% [6]. Below equivalence ratios of 25%, pyrolysis becomes increasingly influential while above 25%, combustion becomes increasingly influential [6]. Full combustion normally occurs at equivalence ratios greater than 1 [6]. Figure 2.2 showed the composition of the equilibrium gases produced at equivalence ratios between 0 and 120% [5]. It can be seen that the primary fuel gases in the product gas mixture at equivalence ratios of approximately 25% are carbon monoxide and hydrogen.

Figure 2.5 is a carbon saturation phase diagram which shows the three regions of gasification depending on temperature and relative oxygen addition [5]. Curve XY shows the carbon saturation curve for the gasification of woody biomass in air on to which the adiabatic reaction temperature in air (curve ABC) has been superimposed. The intersection of the adiabatic temperature line (ABC) with the carbon saturation line (curve XY) gives the operating point for an ideal gasifier with no energy losses (the effect of energy losses on product gas quality is discussed in Section 2.1.4.3).

At low equivalence ratios, excess carbon will be in equilibrium with the gas produced. This situation is as would be expected since the equivalence ratio is approaching 0 for pure pyrolysis. At higher equivalence ratios (above 25%) and at temperatures above 800°C, all char produced is converted to a gas. The line XY (Figure 2.5) represents the equivalence ratio at which the gas is said to be carbon saturated and the minimum amount of oxygen required for complete conversion of the char to gas [25].

Reducing the equivalence ratio from approximately 25% towards 0 (pyrolysis) increases the product gas heating value as shown in Figure 2.6. However, since less oxygen is available for flaming pyrolysis, less energy will be produced by the flaming pyrolysis zone resulting in lower reaction zone temperatures. Reducing the equivalence ratio may, therefore, lead to an increase in the product gas tar concentration (Figure 2.5) [25].

Temperature, °C
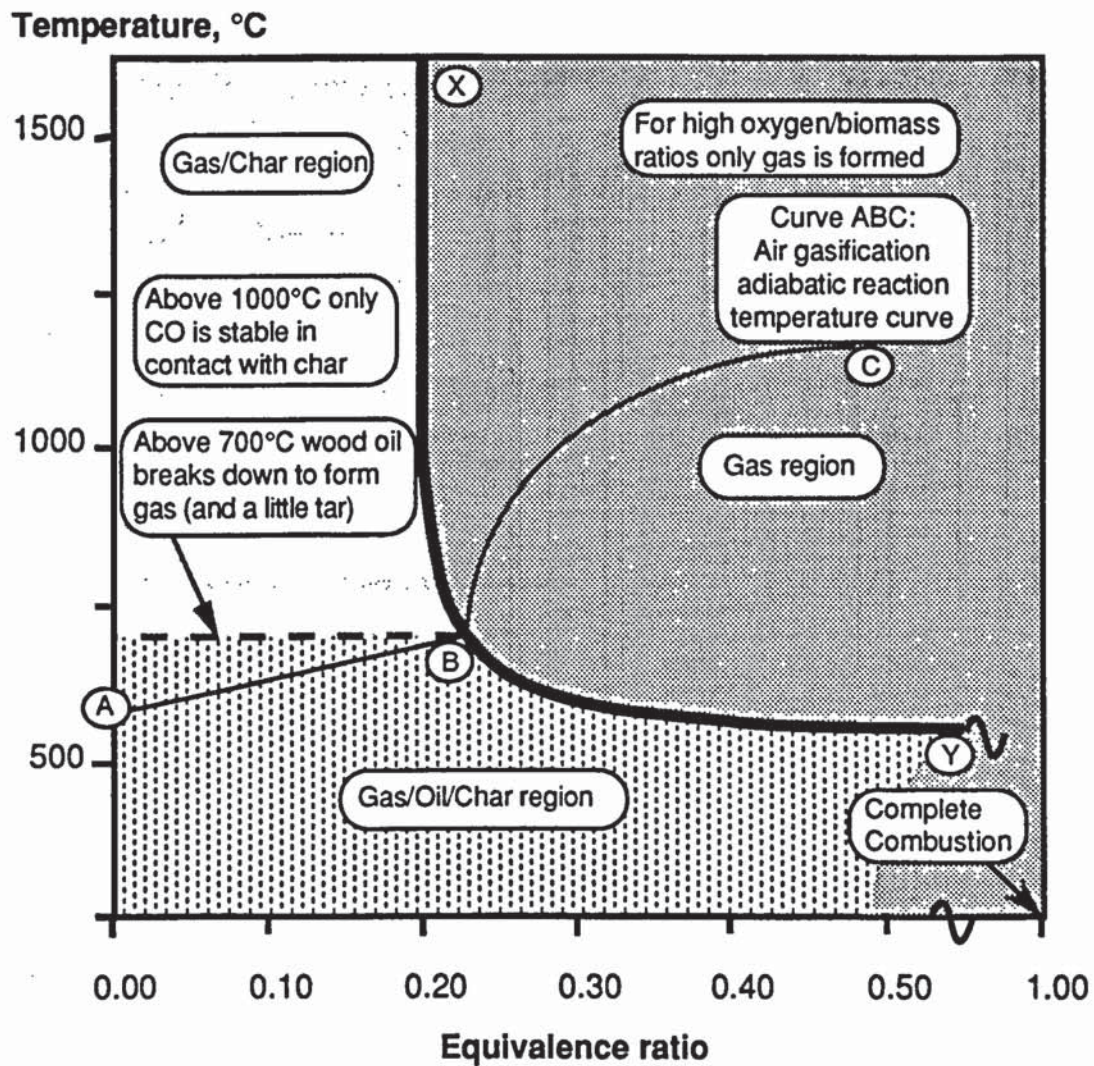
Figure 2.5

Phase Diagram Showing the Three Regions of Gasification [27]
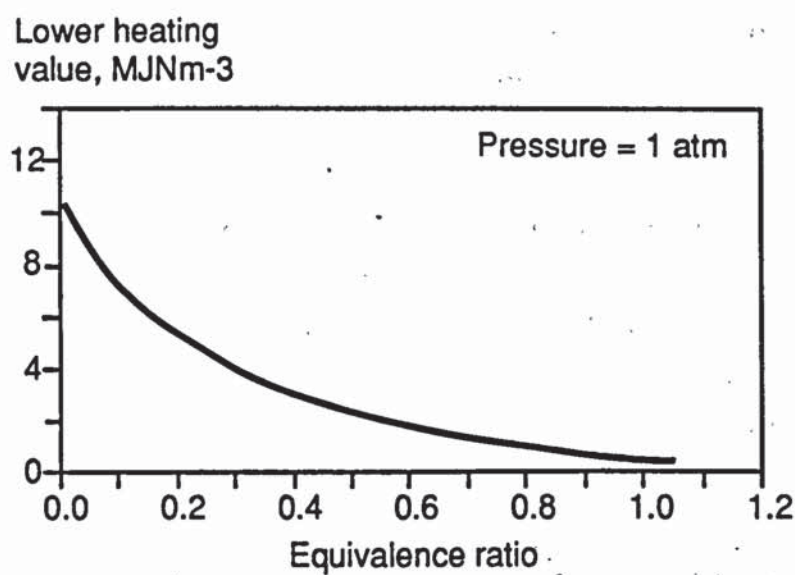
Figure 2.6

Lower Heating Value for Dry Equilibrium Gas for Air-Biomass Reaction [5]

The product gas energy density from an open-core downdraft gasifier can, therefore, be increased by operating at lower equivalence ratios at the expense of the carbon conversion efficiency to gaseous components. Operation to maximize the product gas energy content, however, occurs when there is a net production of char in the gasifier and it would be necessary to utilize a char removal system such as a grate agitation system or screw auger to maintain a constant height of char in the gasifier [25]. Char/ash removal systems are proposed on a 5800 dry kgh^{-1} open-core downdraft gasifier (American Waste and Power Management) gasifying waste wood [30] and a 10-25 kgh^{-1} open-core downdraft gasifier gasifying rice husk (Twente University, Netherlands) [31]. The AWPM gasifier is operated using a char removal system to permit a claimed turn down ratio of 5:1 [30]. At low output rates, the tar production rate in an open-core downdraft gasifier should increase. It is claimed, however, that trace tar levels in the AWPM gasifier product gas will be removed by cracking in the gasification zone and filtration in the char bed below the reaction zones [30]. No product gas tar concentrations are reported by AWPM. Rice husk contains a high ash content of approximately 20% and char and ash is continuously removed from the Twente University gasifier to prevent ash build up in the gasifier [29].

The effect on gasifier performance of reducing the equivalence ratio from approximately 25% towards 0 (pyrolysis) was investigated by Walawender (2.1.4.5) [32]. The Walawender (KSU) gasifier is of open-core configuration but differs from the Aston gasifier as secondary air is injected into the reaction zones to maintain a stable reaction zone (Section 2.3) [32]. Char and ash is broken up by a rotating grate and stirrer system enabling it to percolate through the grate [32]. The air input rate to the gasifier was varied by altering the gas fan rotation speed which is directly proportional to the air input rate and hence the equivalence ratio [32]. The gasifier was operated between equivalence ratios of 10.8 and 22.0% indicating that the KSU gasifier operates under gasification conditions which approach pyrolysis (see Figure 2.5).

Reducing the equivalence ratio and hence air input rate reduced the product gas nitrogen concentration (Figure 2.7) [32]. The concentrations of hydrogen and methane were relatively constant with increase or decrease in

air input rate (Figure 2.8) [32]. A slight decrease in the carbon dioxide concentration is indicated in Figure 2.8 with a corresponding increase in the carbon monoxide concentration [32]. Overall, however, altering the air input rate resulted in minor product gas concentration changes (Figures 2.7 and 2.8) [32]. The decrease in product gas nitrogen and carbon dioxide concentrations with decrease in air input rate result in a gradual linear increase in the product gas higher heating value (Figure 2.9), while the gasifier cold gas efficiency is reported to remain essentially constant since as the air input rate is decreased, there is a reduction in the dry feed throughput (Figure 2.10) [32].

At equivalence ratios up to approximately 25%, char is increasingly converted to fuel gas. Beyond approximately 25%, char is also converted to combustion products and heat thus reducing the product gas heating value (see Figure 2.6). The mark I Aston gasifier is reported to operate at equivalence ratios in excess of 30% due to high heat losses [12],[17]. The product gas from the Aston gasifier [12] (approximate equivalence ratio: 40%) has high product gas carbon dioxide and nitrogen concentrations and a correspondingly low product gas higher heating value compared with the KSU [32] and AWPM [30] gasifiers which operate at equivalence ratios below 25%.
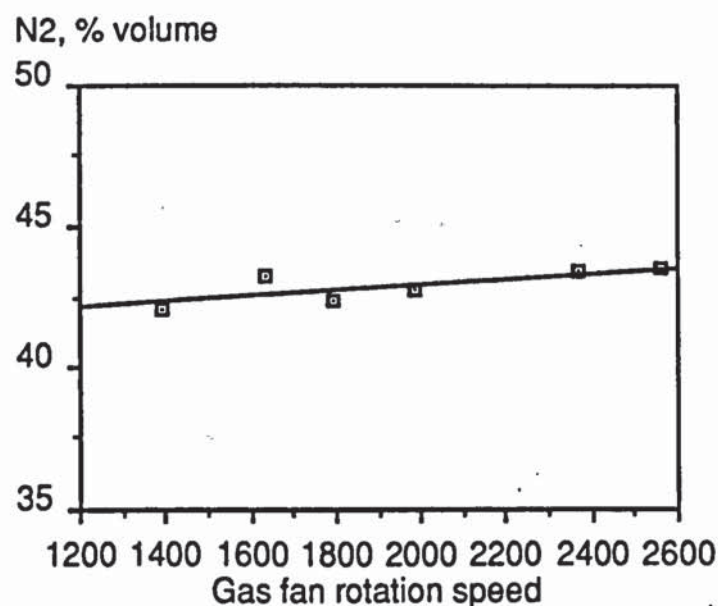
Figure 2.7

Effect of Air Input Rate on Product Gas Nitrogen Concentration
[32]

% volume
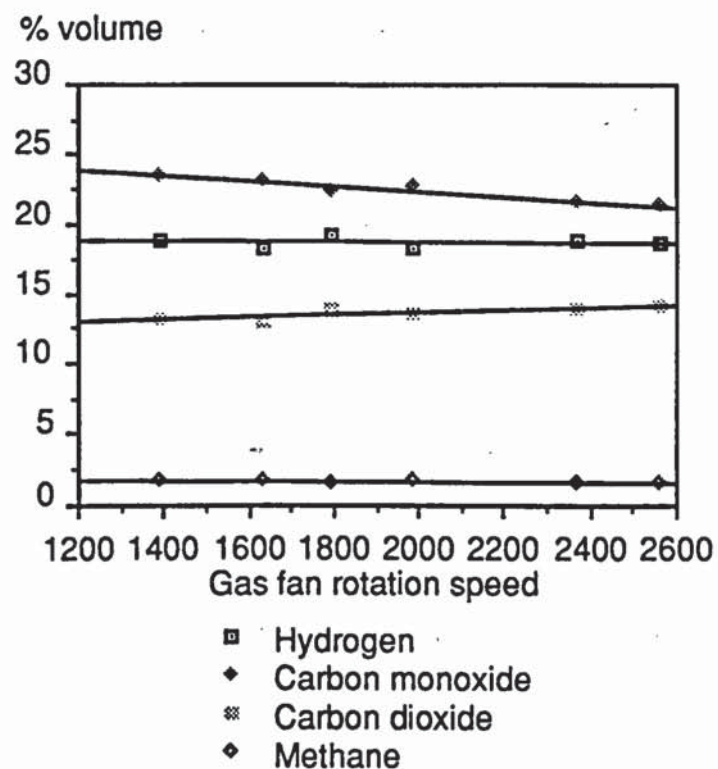
Figure 2.8

Effect of Air Input Rate on Product Gas Composition [32]

HHV, MJNm-3
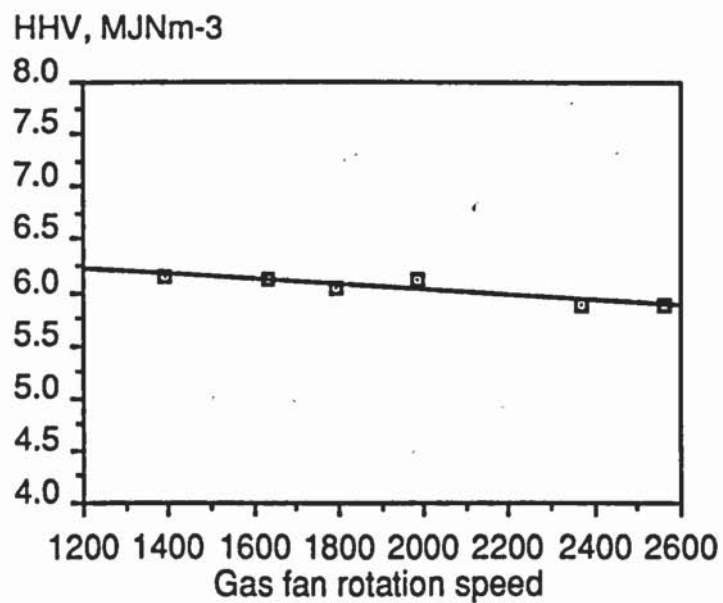
Figure 2.9

Effect of Air Input Rate on Product Gas Higher Heating Value [32]
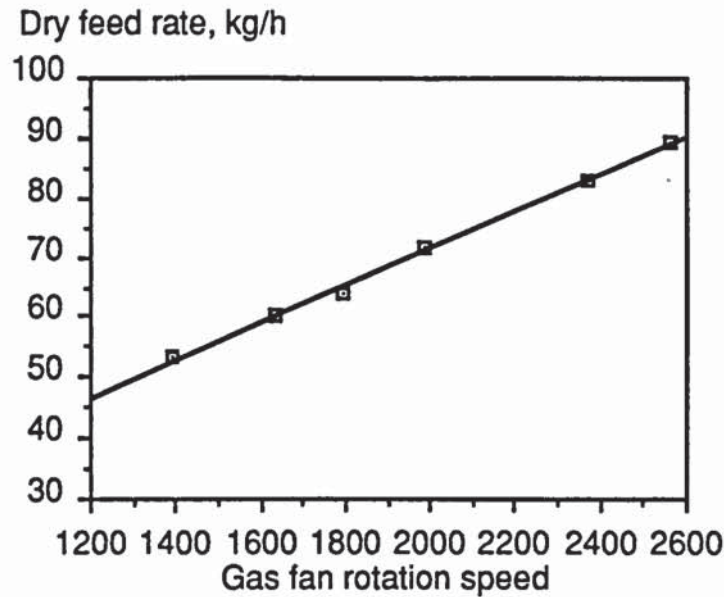
Figure 2.10
Effect of Air Input Rate on Dry Feed Throughput [32]

Operation at low equivalence ratios will maximise the product gas heating value. Kaupp reports that the maximum gas heating value was obtained at the lowest equivalence ratio tested in the open-core downdraft gasifier (University of California, Davis) [29]. However, reducing the equivalence ratio will lead to increased production of char and tar as indicated by Figure 2.5 and the reaction zone in an open-core gasifier will rise up through the gasifier. Operation at high equivalence ratios will lead to a net consumption of char in the gasifier and the reaction zone will descend through the reactor. A comparison of the product gas quality from the gasifier operating in the gasification dominant operation and stable operation has not been reported and will be investigated in this project.

2.1.4.2   Effect of Char Bed Height on Gasifier Performance
As discussed in Section 2.1.3, the height of the char bed in the gasifier can be varied. The effect of the char bed height on gasifier performance was studied by Earp [12] and Reed [20].

Both Reed [20] and Earp [12] report that the gas heating value is improved as the char bed height increases although the results indicate the improvement to be small. Reed reports that the optimum char bed depth is about 24 cm where the optimum gas composition occurs. No explanation for this optimum is given, however [20]. The improved gas quality is attributed

52

by Earp to increased char oxidation due to increased char gas contact time and/or tar cracking in the hot char zone. However, the depth of the char gasification zone will not be affected by the depth of cooler char below the char gasification zone while tar cracking is reported to occur only at temperatures above 900°C [29],[33]. Any tar cracking will, therefore, only occur in the char gasification zone since the rates of gasification reactions will only fall to insignificant levels at temperatures of approximately 700°C [21].

The data used by Earp was collected during pyrolysis dominant operation and with char bed heights greater than 5 cm. Some short experiments running the Aston open-core gasifier with the reaction zone on the grate (grate operation) were carried out but no data are reported [12]. Earp suggests that operating without a char bed should have a disproportional effect on the gas heating value and gas quality particularly in terms of tar loadings (since during grate operation, there is no hot char to perform tar cracking [12]). However, since the gasifier would be operating at a high equivalence ratio to maintain the reaction zone at the grate, the gasification process would be operating beyond the carbon saturation line (Figure 2.5). Tar production levels should, therefore, be low during grate operation [25]. Modelling work based on an open-core downdraft reactor by Reed does not indicate a sharp decrease in gas heating value as the depth of the char bed approaches zero [19]. Extrapolation of Earp's experimental results to calculate gasifier performance with no char bed showed the gas heating value of the gas produced when operating with no char bed to be approximately 85% of the heating value of the gas produced when operating with a 10 cm deep char bed [12]. Partial combustion of the product gas below the grate with excess oxidant used to maintain the reaction zone on the grate is not considered. Product gas combustion below the gasifier grate will be easily observed and will be indicated by high carbon dioxide levels in the product gas compared to gasifier operation with a char bed.

The effect of char bed height on gasifier performance shows that there is a small improvement in gas quality with increased char bed height. There may also be an optimum char bed height at which gasifier performance is maximised. It is necessary to investigate the effect of char bed height on the Aston gasifier performance under stable operating conditions and including gasifier performance data with a char bed height of less than 5 cm to more

fully describe the effect of char bed height on the performance of the Aston gasifier.

2.1.4.3   Effects of Gasifier Heat Losses and Insulation

Heat losses from the reaction zones should be minimised because energy losses from the gasifier will be reflected in a lower product gas heating value and a lower rate of tar cracking. At high feed throughput, heat losses will be a small fraction of the feed energy input. At low feed throughputs, however, heat losses can become increasingly significant [22].

The curve ABC superimposed on Figure 2.5 (adiabatic reaction temperature) shows the temperature reached at equilibrium when biomass reacts with air with no external heat losses or gains [25]. Heat losses will move the operating point (the intersection of the curves ABC and XY shown in Figure 2.5) down the curve resulting in an increase in air consumption and therefore decreasing the gas quality [25]. Insulation should therefore move the operating point nearer to the adiabatic gasifier operating point reducing air consumption and improving gas quality [25].

High temperatures produced during flaming pyrolysis will be better maintained within an insulated reactor and should, therefore, result in an increase in the height of the char gasification zone (see Figure 2.3) leading to increased char conversion. The increased height of the char gasification zone will lead to a lower gasification air requirement for stable gasifier operation since, compared with stable operation in the uninsulated gasifier, a smaller proportion of the gaseous flaming pyrolysis products will be combusted to provide sufficient energy to gasify the char produced by flaming pyrolysis. Stable operation in an insulated reactor will, therefore, occur at a lower equivalence ratio and the `product gas will contain a lower nitrogen content thereby increasing the product gas heating value.

The overall heat losses for the mark I Aston gasifier were estimated by Reyes [17]. She calculated that the overall heat losses from the uninsulated mark I Aston gasifier (primarily by radiation) to be between 23.8 and 38.1% of the dry wood input energy [17]. The wide variation in the gasifier heat loss as a percentage of the dry wood input energy is due to the use of the same estimated gasifier temperatures and hence overall gasifier heat loss for all the runs performed. The gasifier temperature was measured using an array

of type K thermocouples inserted into the gasifier fixed close to the wall and positioned at vertical intervals of 4 cm (see Section 3). The maximum recorded gasifier temperature reported by Reyes was not, however, in agreement with the maximum recorded temperature reported for open-core downdraft gasifiers in the literature [17],[20]. In order to estimate heat losses from the mark I Aston gasifier for all runs, a vertical temperature distribution was assumed by considering a 1 cm deep reaction zone at 1000°C located at 12 to 13 cm above the grate and three cylindrical zones below the reaction zone each of 4 cm height [17]. A step temperature change was assumed just above the reaction zone from 25°C to 1000°C [17]. The estimated average temperatures of each of the three 4 cm zones below the reaction zone were calculated using temperature data recorded in run 8R [17]. The estimated temperatures are shown in Table 2.4. A search thermocouple will be used in this project to measure the temperature at smaller intervals (see Section 3). This will be able to respond better to variations in reaction zone height than the method described by Reyes [17].

Table 2.4
Gasifier Zones Selected for Mark I Aston Gasifier Heat Loss Calculations [17]

Gasifier zone	Height limits from the grate cm	Zone height cm	Mean temperature °C
I	0-4	4	525
II	4-8	4	600
III	8-12	4	825
IV	12-13	1	1000

The lack of gasifier insulation and hence gasifier heat losses were concluded by Earp to mask the actual effects of varying gasifier operating parameters such as equivalence ratio [12] (see Section 2.1.3). An insulated gasifier will be used in this project, therefore, to investigate Earp's conclusion.

Reed carried out experiments using a 5 cm diameter quartz open-core downdraft reactor gasifying 1 cm charcoal chips. His experiments compared the rate of reaction zone ascent and descent using an insulated (using

reactors insulated using gold plate and a 1.4 cm thick fibrous insulation) reactor and an uninsulated reactor [11],[22]. It was found that in an insulated reactor, the reaction zone descended more slowly than in an uninsulated reactor at the same high, air input flow rate while at the lowest air input flow rate, the reaction zone in an insulated reactor ascended faster than that in an uninsulated reactor [11].

Other open-core downdraft reactors found in the literature are insulated as as matter of course where mentioned. No mention is made of insulation fitted to the open-core rice husk gasifier produced by Manurung and Beenackers and from the diagrams it does not appear to be insulated [31].

Gasifier insulation has the effect of minimising heat losses from the gasifier and increasing the product gas heating value and gasifier thermal efficiency. The gasifier air requirement will be reduced reducing the product gas nitrogen content since less biomass is combusted for energy production. Reduced gasifier heat losses will also lead to increased char conversion to carbon monoxide and hydrogen and increased tar cracking to lighter molecular weight compounds.

The effect of gasifier insulation on the performance of the Aston open-core downdraft gasifier and the gasification process will be investigated in this project. This will include a comparison of the air requirement and product gas composition from the insulated and uninsulated gasifier. The method of gasifier insulation is described in Section 3.

2.1.4.4   Feed Particle Size and Shape
Particle size and shape affect the flow of particles through a reactor, the rate of reaction and the pressure drop through the gasifier [34]. Variations in the feed particle size can also lead to channelling in the gasifier. Problems with channelling are reported to become more significant with feedstocks containing a wide range of particle sizes although the limiting dimension is not reported [6].

The open-core gasifier should not be affected by fuel flow problems to the same extent as the throated gasifier since the open-core gasifier contains no internal constrictions restricting material flow. However, feedstocks containing a high proportion of fine particles can bridge in an open-core

reactor causing voids resulting in a non-uniform reaction zone. This may lead to an increase in the product gas tar content, since tars formed in the flaming pyrolysis zone may pass through the gasification zone uncracked [12]. Bridging is also reported to lead to slag formation in small, stationary gas producers due to an increase in the local air/fuel ratio which causes an increase in the local temperature [34]. Small particles may also give rise to unacceptable pressure drops across the gasifier while the use of large particles may cause mal-distribution of the particles near the wall [12].

Size and shape will also affect the particle reaction time [34]. The burning times of various particles was studied by Huff [23]. He found that "stick" (long, thin particles) shapes burn more quickly in terms of minutes/cm (ratio of burning time in minutes to the particle volume/surface area ratio) than chips (approximating to cuboids), although the difference was only slight [23]. Size increases resulted in increased burning times and it was found that burning time was a function of the first and second powers of the particle size defined as the cube root of the particle volume (see Equation 2.17) [23].

$$\text{Burning Time, minutes/cm} = aZ + bZ^2 \quad \text{.................[2.17]}$$
$$\text{where } Z = \sqrt[3]{\text{Particle volume}}$$

The size of the particle during the gasification process will also affect the char yield from pyrolysis [35]. Large particles will yield a greater amount of char than smaller particles [36]. The volatile products formed during pyrolysis will contain reactive and non-reactive components [37]. As the feed particle size increases, the residence time of the volatiles in the particle will increase and allow sufficient time for some of the reactive components to deposit carbon [37]. Hence, char production will increase with particle size [37]. It is reported that the char yield from the pyrolysis of a 5 mm particle was 19% and from a 15 mm particle was 24% [36].

Winship reports that particle size and feed moisture content (see Section 2.1.4.5) are the major factors determining throated downdraft gasifier performance [38]. The highest quality gas (7.23 MJm^{-3}) was obtained with the combination of largest chip size, dry fuel, slowest grate rotation speed and lowest air flow rate. Reducing the chip size reduced the gas heating value to 5.66 MJm^{-3} [38]. Hoi reports that the gasifier cold gas efficiency (throated downdraft gasifier) decreases as the feed particle size increases

(from 1x3x3 cm to 6x3x3 cm chips) while the gas heating value increases to a maximum at a particle size of approximately 3x3x3 cm (see Figure 2.11) [39]. Hoi also reports that the gasification of regularly sized particles results in a better gas heating value compared with the gasification of irregularly shaped particles [39].

The effect of feed size on open-core downdraft gasifiers was investigated by Earp although no quantitative data was presented. Work will therefore be carried out to compare the effect of feed size and shape on open-core downdraft gasifier performance with the results presented by Hoi for a throated downdraft gasifier.
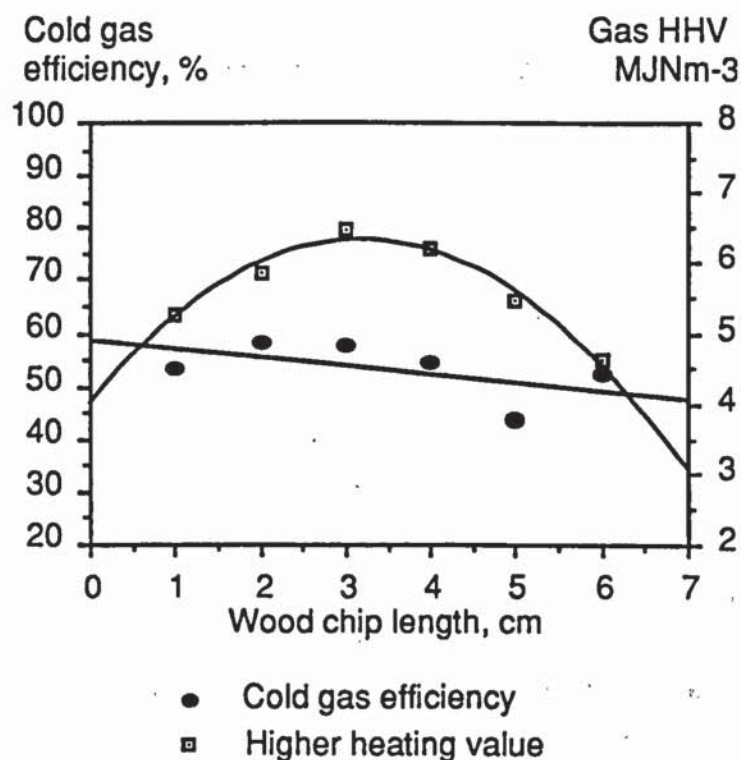
Figure 2.11

Influence of Feed Particle Size on Gasifier Cold Gas Efficiency and Product Gas Heating Value [39]

2.1.4.5   Biomass Moisture Content

The biomass moisture content significantly affects the product gas quality from downdraft gasifiers [40]. Graboski suggests that the air blown Syngas gasifier can tolerate wood moisture contents as high as 30% wet basis [41]. Figure 2.12 (throated downdraft gasifier) shows that as the feed moisture content rises, the reaction zone temperature and gas heating value fall because of the heat removal effects of moisture by both physical evaporation

and the endothermic reactions between carbon dioxide and char (Equation 2.4) and steam and char (Equation 2.5). The presence of moisture within the biomass fuel will also reduce the fraction of biomass available for conversion, therefore, reducing the gasifier feed throughput (dry kgh⁻¹). The cooling of the reaction zone could also produce an increase in the levels of tars and oils contaminating the product gas (see Section 2.1.4.1).

When cut, biomass can typically contain over 50% moisture. For gasification purposes, it is generally desirable to dry biomass containing over 25% moisture [2].
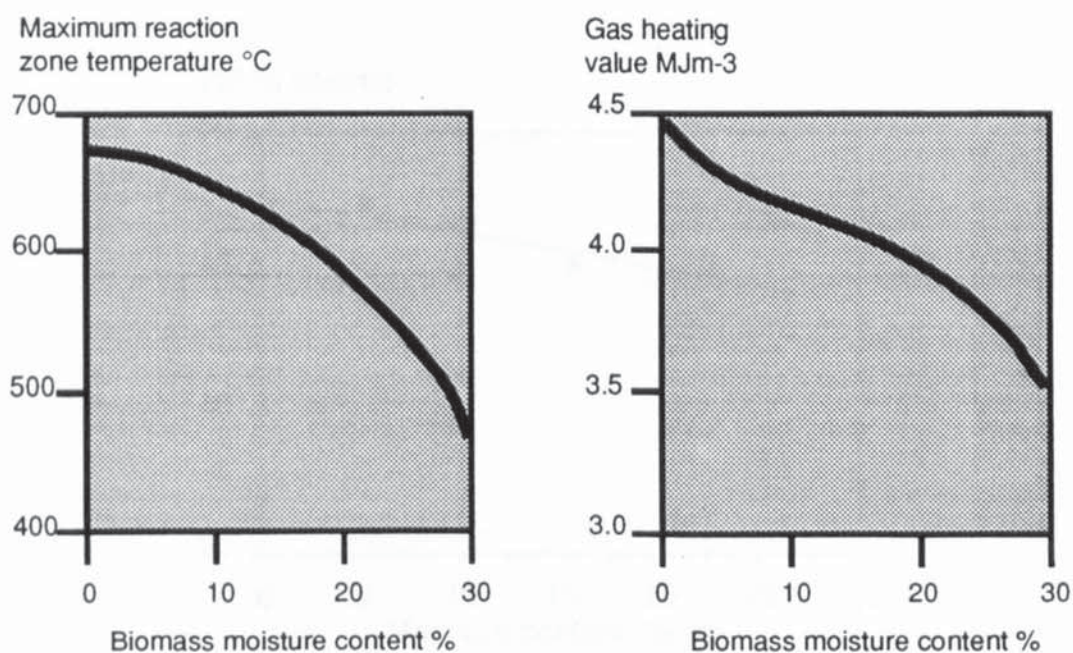
Figure 2.12

Effect of Biomass Moisture Content on Throated Gasifier Reduction Zone Temperature and Gas Heating Value [13]

Walawender investigated the effect on feed moisture content on an hybrid open-core downdraft gasifier (Section 2.3) [32]. The Walawender (KSU) gasifier contained no throat and had an open top (see Section 2.3). Secondary air, however, was introduced into the reaction zone through tuyeres [32]. The effects of feed moisture content on dry product gas composition, air to feed ratio, gas higher heating value and cold gas efficiency reported by Walawender are shown in Figures 2.13 to 2.17. Increasing the feed moisture content is reported to cause a decline in the dry product gas nitrogen content as a result of the decline in the air to feed ratio with increasing chip moisture content (see Figures 2.13 and 2.14) [32]. The

concentrations of carbon dioxide and hydrogen increase with increasing feed moisture content while that of carbon monoxide decreases due to the action of the water gas shift reaction (see Figure 2.15) [32]. The effects of the increased product gas concentrations of nitrogen and carbon dioxide result in a decrease in the product gas higher heating value and gasifier cold gas efficiency (Figure 2.16). The concentration of methane is reported to be small and to remain essentially constant with variation in feed moisture content (Figure 2.15) [32]. The gasifier energy output rate and dry feed rate are reported to show linear decreases with increased feed moisture content, while the wet feed rate is reported to be approximately constant [32].
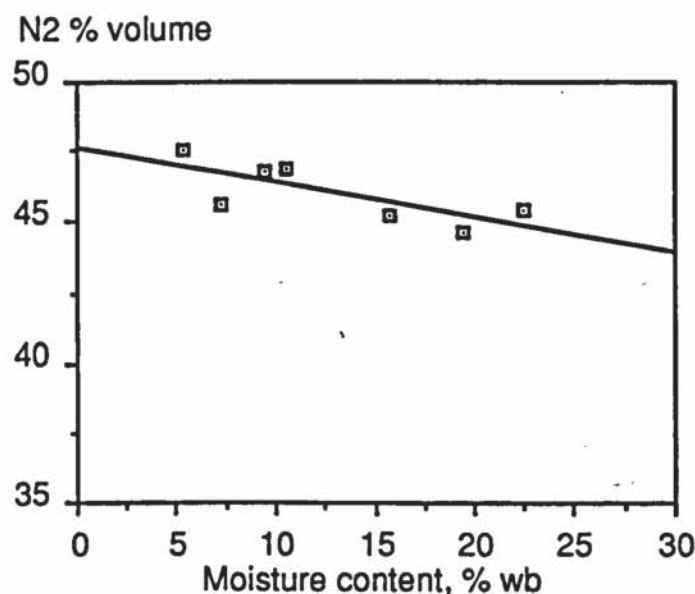
Figure 2.13

Effect of Feed Moisture Content on Dry Product Gas Nitrogen Content [32]
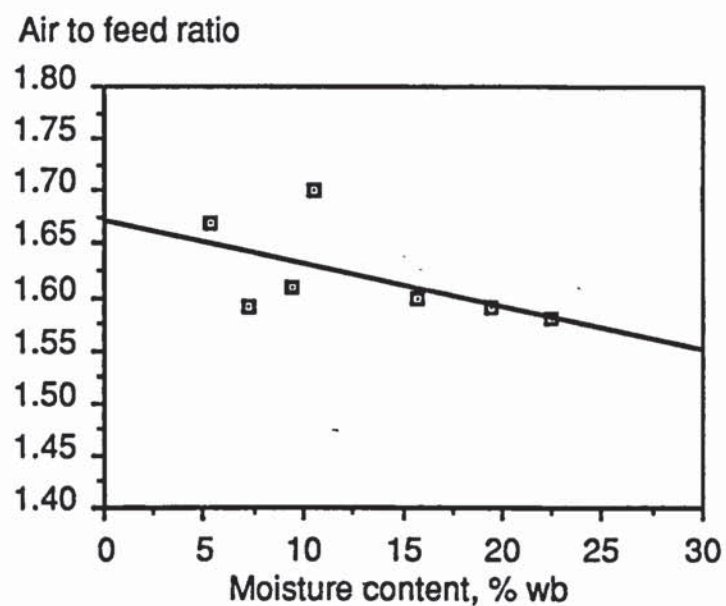
Figure 2.14

Effect of Feed Moisture Content on Air to Feed Ratio [32]

      □ Hydrogen
      ◆ Carbon monoxide
      ※ Carbon dioxide
      ◇ Methane
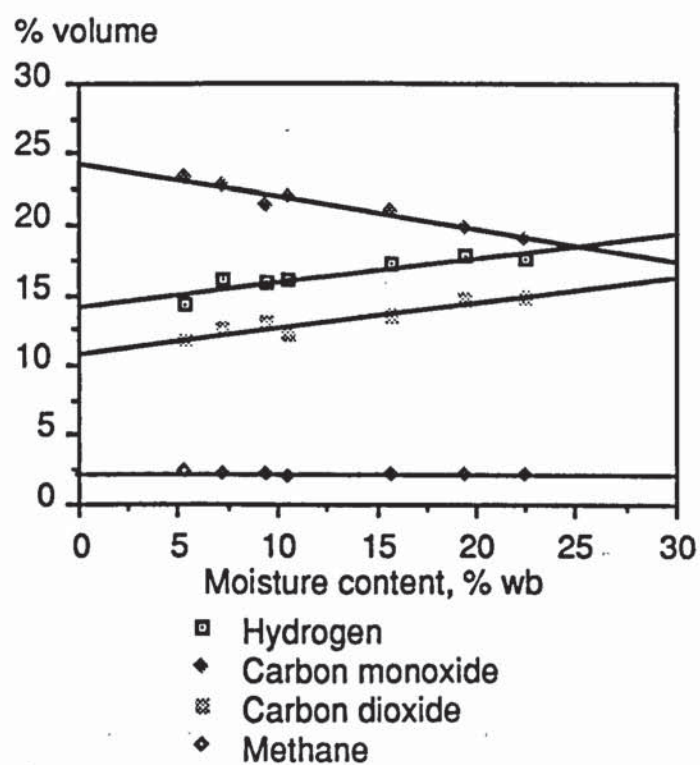
Figure 2.15

Effect of Feed Moisture Content on Dry Product Gas Composition
[32]
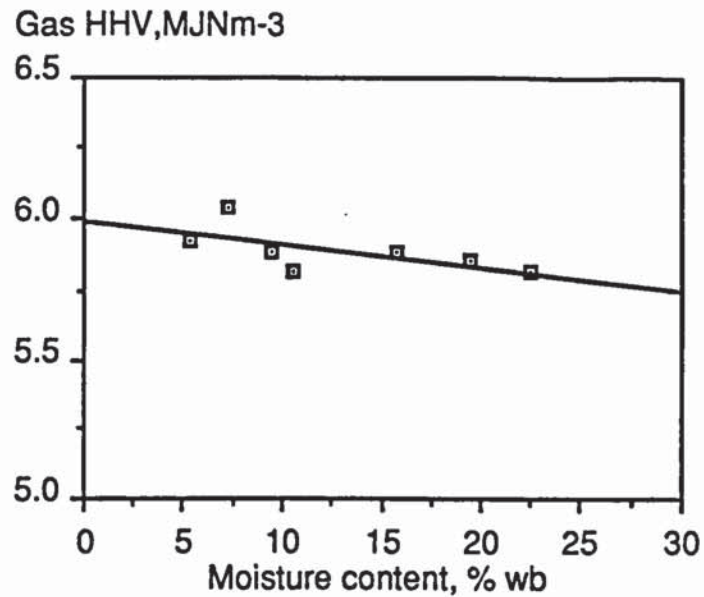
Figure 2.16

**Effect of Feed Moisture Content on Product Gas Heating Value
[32]**
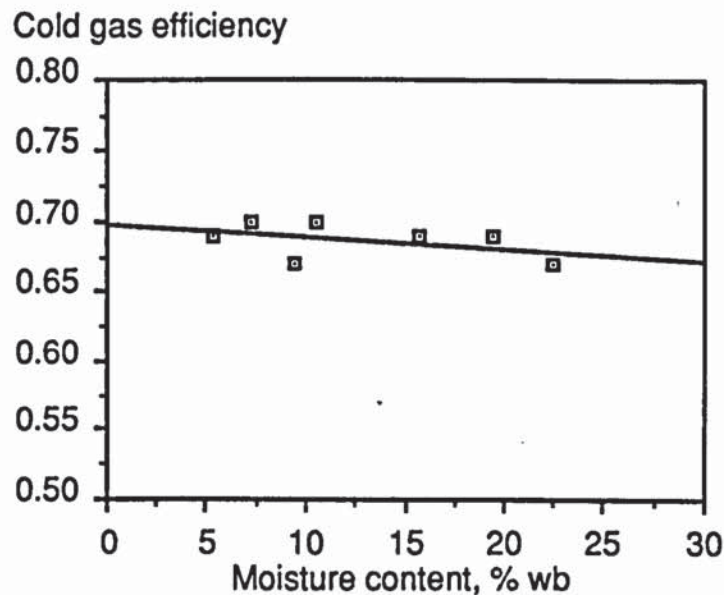
Figure 2.17

**Effect of Feed Moisture Content on Gasifier Cold Gas Efficiency
[32]**

The trends reported by Walawender are in general agreement with those of Hoi (see Table 2.5) [42]. However, the results of Hoi show that as the feed moisture content increases, the methane concentration of the product gas decreases (Table 2.5). Hoi's results also indicate an increased gasifier oxidant requirement with increased feed moisture content.

Table 2.5

**Effect of Feed Moisture Content on Gas Composition from
Rubberwood Open-Core Downdraft Gasifier [42]**

Gas composition, % volume	Moisture content of rubberwood, %		
	10	20	30
H_2	10.0	10.0	5.0
CO	15.5	12.0	8.0
CO_2	11.0	14.0	17.0
CH_4	9.0	3.0	4.0
N_2	53.5	60.2	65.5

The effect of feed moisture on the performance of an oxygen-blown open-core downdraft gasifier at the same feed rates has also been shown by Reed et al to increase the oxygen requirement [22]. On a wet feed basis, gasification of a feed containing 22.8% moisture needed 10% more oxygen than the gasification of a feed containing 12.8% moisture [22]. The H_2/CO_2 ratio also increases with increasing feedstock moisture content [22]. For a 12.8% moisture content feed, the measured H_2/CO_2 ratio is 0.48 and for the 22.8% feed, the ratio is 0.65 [22].

As noted in Section 2.1.4.4, the effects of feed moisture content on the performance of a commercial throated downdraft gasifier were studied by Winship [38]. The highest product gas heating value was obtained from the gasification of dry wood (7.23 MJm^{-3}). Increasing the feed moisture content resulted in a deterioration in the product gas heating value. The highest feed moisture content tested by Winship was 26% yielding a product gas with a heating value of 3.24 MJm^{-3} [19].

Reed and Markson used a computer model to study the effect of feed moisture content on the time required for flaming pyrolysis [19]. Their computer model shows that for a bone dry biomass particle (1 cm pine cubes) the time for flaming pyrolysis is 0.42 minutes while for a biomass particle containing 50% moisture, the flaming pyrolysis time has increased to 0.79 minutes. This increase in time is due to the requirement for the physical

evaporation of water from the particle before pyrolysis can commence. It is also shown that the height of the flaming pyrolysis zone is increased as the biomass moisture content increases [19]. This will increase the heat losses from the reactor leading to decreases in the conversion efficiency of biomass to cold clean gas and in reactor throughput (daf kgh^{-1}). When utilising high moisture content feeds, the sensible heat of the product gas from downdraft gasifiers should be used to dry the feed stock and improve the gasifier efficiency and product gas quality.

Increasing the feed moisture content will reduce the thermal efficiency of a gasifier. Energy is required to remove any moisture in the biomass feed prior to the start of any gasification reactions. The latent heat provided to convert feed moisture to water vapour is lost and can not be recovered for use in the gasification process.

Earp and Reyes did not investigate the effect of feed moisture content on the performance of the Aston open-core gasifier. The effect of feed moisture content on the performance of the Aston open-core downdraft gasifier will be made in this project. The results will be compared with those described above.

2.2 Advantages and Limitations of Open-Core Downdraft Gasifiers

2.2.1 Advantages of Open-Core Gasifiers

The open-core gasifier as previously described has proven to be a conceptually and mechanically simple method of gasifying biomass [19]. Compared with the throated downdraft gasifier, the open core gasifier has a number of advantages including ease of feeding, safety and scale-up.

2.2.1.1 Feeding

The open top of atmospheric open-core downdraft gasifiers permits easy and, if required, continuous fuel feeding using, for example, screw feeders. This provides the open-core gasifier with a major advantage both economically and operationally. This advantage disappears, however, if pressurized or oxygen operation is used since reactor sealing would be required.

2.2.1.2 Safety Advantages of Open-Core Gasifiers

There is little literature available concerning the safety aspects of open-core gasifiers. Earp [12] carried out a short hazard and safety analysis of the mark I Aston open-core downdraft gasifier. Assessment of both the toxic and explosive hazards associated with the whole gasification system was undertaken. However no comparison of the safety aspects of open-core downdraft gasifiers with other gasifier types was made.

Conventional throated downdraft gasifiers typically produce between 0.1 and 0.2% (dry feed input) tars [20]. The low quantity of tars produced by downdraft gasifiers represent not only a saving in economic terms as a result of the need for less gas cleanup and an high cold clean gas efficiency but also provide a safety advantage to the downdraft gasifier as tars from gasifiers are taken by analogy with mineral oils to be carcinogenic (see Section 5.3.2).

Gasification plants produce a toxic gas (carbon monoxide) which when mixed with air is explosive - the explosion limit is approximately 4% volume oxygen in the gas mixture [43]. Due to the bulk forced convection currents of air and gas down through an open-core gasifier, gas will not leak from the gasifier itself reducing the possibility of carbon monoxide poisoning and explosion.

The open top of the air blown open-core downdraft gasifiers ensures that any explosions will be directed upwards allowing the explosive force to escape. The sealed top of the conventional downdraft gasifier would prevent the escape of gases and could result in a more serious explosion. This advantage does not apply in the case of an oxygen fed open-core downdraft gasifier which requires a sealed method of feeding.

2.2.1.3 Scaling

Conventional throated downdraft gasifiers are widely believed to be limited to a maximum size of approximately 700 kgh^{-1} since, as the reactor size increases, oxygen penetration at the throat region diminishes producing uneven oxidant distribution in the reaction zone [12]. This will result in tars passing through the reaction zones uncracked hence increasing the tar loading of the product gas and reducing the main advantage of throated downdraft gasifiers - the production of a relatively tar free gas. In addition,

increases in gasifier diameter may cause the reaction zone at the throat to collapse [12].

It is claimed that oxidant distribution is kept relatively uniform in open-core downdraft reactors by the non reacting fuel reservoir which is thought to distribute the flow of oxidant to the reaction zone below [20]. This is believed to reduce the incidences of cold spots within the reaction zone and maintain a uniform temperature distribution across the bed. Feed containing regularly shaped and sized particles will perform an effective oxidant distribution to the reaction zone. Feeds containing varied shapes and sizes may not, however, distribute oxidant flows evenly due to poor material flow within the non reacting feed zone.

As the reaction zone of open-core downdraft gasifiers is completely supported by a grate, increases in reactor diameter will have no affect on reaction zone support. By comparison with updraft gasifiers, which also operate as plug flow reactors, Earp estimated that the maximum practicable size of an open-core gasifier would be of the same order as an updraft gasifier - ie. approximately 10 tonnes/hour although no explanation of this statement is given [12]. To date, the largest open core downdraft reactor built is of 0.762 m diameter with a feedstock throughput of 900 kgh^{-1} with oxygen or 670 kgh^{-1} with air [41].

2.2.2   Limitations of Open-Core Downdraft Gasifiers
This section describes the limitations which affect the performance of open-core downdraft gasifiers.

2.2.2.1   Feedstock
The open-core downdraft gasifier has less stringent feedstock limitations than the conventional throated downdraft gasifier since it consists basically of a smooth tube with no internal constrictions or air injection systems to restrict solids flow within the gasifier.

Acceptable particle sizes for moving bed gasifiers are generally between 1 and 100 mm [6]. The minimum size will be set by the maximum allowable reactor pressure drop. The grate design will also affect the feed particle size since a grate designed for use with small particles may not successfully permit the efficient gasification of large particles [12]. A large volume of fines

may also lead to high reactor pressure drops frequently followed by channelling [6]. The upper particle size limit will be set by the reactor size and the particle reaction time. Complete pyrolysis must occur before the particle enters the gasification zone for efficient gasification [17]. The effect of particle size and shape was more fully discussed in Section 2.1.4.4.

The recommended feed moisture content upper limit for use in an open-core downdraft gasifier is 40% [44]. Moisture acts as a heat sink, it reduces the fraction of useful components available for conversion to gas, reduces the gas mass and volumetric yields and increases the gas tar content [18]. In addition, wet biomass is difficult to handle and has poor flow characteristics [6]. The effect of biomass moisture content on the gasification process in an open-core downdraft gasifier was discussed in further detail in Section 2.1.4.5.

Woody biomass generally has a very low ash content. Feedstocks with high ash contents are not suitable for open-core downdraft gasifiers unless an ash removal system is installed. Ash sintering is unlikely to occur unless the pure ash is exposed to temperatures in excess of 1000°C [6]. In the Aston open-core downdraft gasifier, the highest temperature recorded was 902°C. Ash sintering is not, therefore, expected in this project [17]. If ash sintering does occur in an open-core gasifier, then there will be an increase in reactor pressure drop, poor oxidant distribution across the reaction zone and poor solids flow [31]. The open-core gasifier is less susceptible to ash sintering problems from high ash/low fusion temperature feedstocks than the conventional throated gasifier due to the more even temperature distribution across the reaction zone of open-core reactors and the lack of local hot spots encountered in the vicinity of the oxidant injectors of throated gasifiers [12]. The use of feeds with low ash fusion temperatures should be avoided, however, to simplify open-core gasifier operation.

The ability of the open-core downdraft gasifier to gasify a difficult feedstock is demonstrated by the Twente University 0.45 m diameter rice husk gasifier which gasifies rice husk, producing a gas considered suitable for engine applications [31]. Rice husk is considered to be a difficult fuel to gasify since it has a high ash content (approximately 20%), is small in size (average particle characteristic size, 50 μm [29]) and has a low bulk density

(approximately 0.1 kgl^{-1}) [31]. In addition, during pyrolysis, the rice husks swell causing flow difficulties [31].

2.2.2.2   Turn-Down

Maximum turn-down ratio is defined as the ratio of maximum gas output to the minimum gas output at which gasifier operation becomes unstable. In commercial applications, gasifier systems often need to be able to respond to load changes imposed upon them.

Earp states that for any particular reactor configuration there is only one air/fuel ratio at which operation (see Section 2.1.3) can be achieved indicating that this reactor configuration has no turn-down capacity [12]. Increasing the air flow rate has the effect of reducing the height of the char bed while reducing the air flow rate leads to pyrolysis dominant operation and the height of the char bed increases (see Section 2.1.3) [11],[12].

The utilization of a char and ash removal system such as that used by Manurung and Beenackers for the gasification of rice husk could permit a degree of gasifier turn-down by removing any build up of char and ash during low output periods when the gasifier would be operating at low equivalence ratios and, therefore, in the pyrolysis dominating mode [11]. The removal of char would maintain a stable reaction zone but would lead to a reduced carbon conversion efficiency and conversion efficiency to cold clean gas. The American Waste and Power Management open-core gasifier (see Section 2.3) also utilizes a char removal system resulting in a claimed turn down ratio of 5:1. The char removed from the gasifier is claimed to approximate to activated charcoal [30].

2.2.2.3   Gas Quality

Open-core downdraft gasifiers operate at higher equivalence ratios than other gasifier types such as the throated downdraft gasifier (see Section 2.1.3). The higher air flow rate will increase the product gas nitrogen content (if air is used as the oxidant) and carbon dioxide content due to increased char conversion, thereby reducing the product gas heating value.

The tar content of the product gas from an open-core downdraft gasifier may be higher than the tar content from a similarly sized throated downdraft gasifier. As a result of localized hot spots and reduced cross sectional area

68

at the throat of conventional throated downdraft gasifiers, a high proportion of the tars produced by pyrolysis are cracked to lower molecular weight components. The open-core downdraft gasifier does not contain a high intensity temperature zone through which tars must pass. The reaction zone in an open-core gasifier may contain low temperature areas due to poor material flows permitting tars to leave the reactor uncracked.

The effect of equivalence ratio on open-core gasifier product gas quality is discussed in Section 2.1.4.1.

2.2.3 Summary

The open-core downdraft gasifier has a number or advantages and limitations imposed by its configuration. The open-core gasifier is simple and requires no seal at the feed inlet permitting easy insertion of instruments into the gasifier. The absence of a throat reduces the frequency of material bridging compared with the throated downdraft gasifier design. The feed particle size distribution is, therefore, not as critical as that required for a throated downdraft gasifier.

However, the reaction zone in an open-core downdraft gasifier is cooler than the reaction zone in a conventional throated downdraft gasifier [45]. As the temperature in the reaction zone is lower, there may be less cracking of tars produced in the flaming pyrolysis zone of an open-core gasifier than in the reaction zone of the conventional throated downdraft gasifier. In addition, the reaction zone position and shape in an open-core gasifier are poorly defined and some tars may bypass the hot zone uncracked [12],[45]. The product gas from an open-core downdraft gasifier may, therefore, contain a higher tar loading compared with the product gas from a throated downdraft gasifier.

2.3 Open-Core Downdraft Gasifiers in the Literature

2.3.1 Aston Mark I Gasifier

The mark I Aston gasifier, constructed in 1986, consists of a 75 mm diameter, 500 mm high transparent quartz glass tube. The gasifier has been used to study individual particle reaction, to investigate the effect of operation in various modes of operation and the effect of char bed height on gasifier performance [12]. A limited number of mass and energy balances were performed [17]. Heat losses from this gasifier are high due to the absence of

gasifier insulation leading to a low overall gasifier thermal efficiency compared with the NREL gasifier which is of similar design and incorporates gasifier insulation.

Table 2.6					
Open-Core Downdraft Gasifier Performance in the Literature					
	Aston mark I	NREL	KSU	Open Unlv.	AWPM *
References	[12]	[11]	[32]	[46]	[29][47]
Grate diameter, mm	75	54	600	120	nr
Operating pressure, atm	1.0	1.0	1.0	1.0	1.0
Feed	wood chips	wood chips	wood chips	carrot fibre	wood pellets
Feed size, mm	4.75-6.35	10x10x3	0-12.7	10x30x30	nr
Feed moisture content, % wb	10	nr	9.99	0	11
Specific capacity, $kgm^{-2}h^{-1}$	296	540	200	208	636¶
Mass yield, $kgkg^{-1}$	3.30	nr	nr	nr	1.93
Volumetric yield, Nm^3kg^{-1}	2.81	2.68	1.87	1.53	nr
Gas HHV, MJm^{-3}	3.78	4.32	6.08	3.10	8.08
Cold gas efficiency, %	54.60	71.5	72.0	28.2	60.0
Gas composition. % volume					
H_2	11.08	nr	15.1	9.1	19.8
CO	14.95	nr	19.6	12.7	16.3
CO_2	9.98	nr	14.6	24.6	15.2
CH_4	1.22	nr	3.09	1.8	4.2
N_2	62.78	nr	46.4	49.1	42.4
	Twente	Syngas	UCD✛	FRIM♦	DTU
References	[31][48]	[41]	[29]	[39][42]	[49][50]
Grate diameter, mm	450	762	162.1	450	nr
Operating pressure, atm	1.0	1.0	1.0	1.0	1.0
Feed	Rice Husk	Wood chips	Rice hulls	Rubberwood chips	Straw
Feed size, mm	nr	nr	nr	10x10x10	nr
Feed moisture content, % wb	12.0	11.1	12.4	15	nr
Specific capacity, $kgm^{-2}h^{-1}$	110	1450	160	nr	nr
Mass yield, $kgkg^{-1}$	nr	nr	nr	nr	nr
Volumetric yield, Nm^3kg^{-1}	1.37	2.62	2.11	nr	2.35
Gas HHV, MJm^{-3}	4.6	5.44	5.0	nr	7.0
Cold gas efficiency, %	43.9	79.5	61.1	nr	nr
Gas composition. % volume					
H_2	17.5	17.8	8.8	10.0	33
CO	19.7	21.2	34.9	15.5	18
CO_2	12.7	10.9	13.5	11.0	12
CH_4	3.5	2.9	4.1	9.0	3
N_2	42.7	45.8	55.8	53.5	34

nr   not reported
¶   Wet briquette feed rate (diameter not reported)
*   American Power and Waste Management
✛   University of California, Davis (Batch fed)
♦   Forest Research Institute of Malaysia. Throated gasifier operating with throat removed
DTU   Technical University of Denmark

2.3.2 National Renewable Energy Laboratory

This adaptation of the conventional throated downdraft reactor by removing the throat and replacing it with a grate was first reported in 1980 by the National Renewable Energy Laboratory (formerly Solar Energy Research Institute) in Colorado [2],[11],[19]. Other versions have also been produced as shown in Table 2.6.

The Aston gasifier is similar to the NREL quartz open-core gasifier. The NREL reactor was used to investigate reaction zone stability and has a higher specific capacity than the uninsulated Aston gasifier [11]. It is reported that this reactor has been operated with and without insulation [11]. The effect of insulation on reaction zone stability was investigated and was found to increase the rate of char conversion [11].

2.3.3 Kansas State University

Although described as an open-core downdraft gasifier, the Kansas State University gasifier is slightly different from the Aston gasifier. Secondary air is injected into the bed to maintain a stable reaction zone and in-bed stirring is used to prevent bridging and to break up char and ash in a ceramic ball bed to enable the char and ash to percolate through the grate. The cold gas efficiency of the KSU gasifier is higher than the Aston gasifier cold gas efficiency due possibly to a lack of insulation applied to the Aston gasifier. The use of in-bed air injection permits a degree of turn-down while maintaining a stable reaction zone. Energy output rates of between 320 and 1400 MJh^{-1} have been reported [51].

2.3.4 Open University

The Open University gasifier was used to investigate the gasification of carrot fibre in open-core downdraft gasifiers [46]. The Open University gasifier differs from the mark I Aston gasifier in that it has a diameter of 120 mm, is insulated and incorporates a manually operated in-bed stirrer [46]. The gasifier thermal efficiency to cold clean gas is very low compared with other open-core downdraft gasifiers (see Table 2.6) [46]. This is attributed to shrinkage of the carrot fibre during pyrolysis leaving voids [46]. Inefficient stirring in the gasifier led to the formation of vertical channels which permitted air to pass into the gasification zone increasing the product gas carbon dioxide content (see Table 2.6) [46]. In addition, approximately 14% of the feed input by mass is produced as char, ash and unreacted feed [46].

2.3.5 American Power and Waste Management

The American Power and Waste Management gasifier is an open-core downdraft gasifier which operates with a net production of char in the gasifier (pyrolysis dominant operation - Section 2.1.3). Operating the gasifier with a net production of char results in a higher product gas heating value than if the gasifier is operated with a stable reaction zone since the product gas contains high carbon monoxide and hydrogen concentrations and a low nitrogen concentration (see Figure 2.2 and Section 2.1.3). To maintain a stable reaction zone, char is periodically removed on a batch basis [30]. This results in a reported turn down ratio of 5:1. It is also reported to give a tar free gas due to breakdown of tar in the char bed below the char reduction zone (see Section 2.1.4.1) [30].

2.3.6 Twente University

The Twente University rice husk gasifier incorporates an ash removal system to enable operation with the high ash fuel (rice husk ash content is 19.5% [31]). This system operates at a lower specific capacity than the mark I Aston gasifier. This may be due to the poor flow characteristics of rice husk and the small particle size. The volumetric gas yield is also low compared with the Aston gasifier as a result of poor flow of the rice husk feed in the gasifier and poor oxygen distribution within the gasifier because of the small feed particle size.

2.3.7 Syngas

The Syngas Inc. gasifier was a cylindrical refractory lined gasifier. The Syngas gasifier was operated with a minimal depth of unreacted feed and char removal was performed to maintain a stable reaction zone [41]. This was reported to permit rapid startup and shutdown [41]. Grate agitation was used to eliminate fuel flow problems in the gasifier. The pilot Syngas gasifier operated with a propane burner to maintain the reaction zone on top of the bed within the gasifier although it was intended to replace the use of propane with product gas. Coupled with the blasting of air to the reaction zone, this results in the very high specific capacity reported for this gasifier. The use of the propane burner will also favour tar cracking mechanisms which may account for the higher gas heating value compared with the Aston gasifier.

72

2.3.8 University of California, Davis

The UCD rice husk gasifier was used to obtain relevant operational data on rice husk gasification in an open-core downdraft gasifier [29]. Due to the absence of an ash removal system, the gasifier operated using an upward moving reaction zone [29]. Tests were terminated when the reaction zone reached the very top of the gasifier [29]. This gasifier has a similar cold gas efficiency to the mark 1 Aston gasifier.

2.3.9 Forest Research Institute of Malaysia

The FRIM gasifier is a throated gasifier in which the throat was removed [42]. Air was fed into the reactor through 3 of 6 nozzles radially distributed around the periphery of the gasifier and positioned 5 cm inside the chamber to ensure sufficient air reached the centre of the gasifier [42]. The air input to the gasifier is heated by the exiting hot product gas using an annular layer around the gasifier as an heat exchanger [42]. Ash collects in the base of the gasifier and is removed using a screw. A continuous supply of good quality gas was obtained only when operating with a feed moisture content of less than 20% while the product gas carbon monoxide concentration reduced to unacceptably low levels at feed moisture contents above 30% (see Section 2.1.4.5) [42].

2.3.10 Technical University of Denmark

The pyrolysis and gasification stages in this gasifier are separate [50]. Feed is firstly pyrolysed in a screw feeder which feeds the products of pyrolysis (char, liquid and gas) to an open-core downdraft gasification reactor where the char is gasified [50]. Energy for pyrolysis and char gasification is provided by waste heat from the utilization of the product gas in an internal combustion engine [50]. Ash is removed from the reactor batchwise [52]. The rate of production of char is made equal to the rate of char consumption by adjusting the screw feeder speed [52]. Increasing the temperature in the char gasification reactor increases the gasifier output [52]. The maximum temperature is limited by the ash softening point of the straw feed (800-900°C) [50].

The product gas from this gasifier contains a high percentage of hydrogen compared with the Aston gasifier as a result of steam injection with air into the gasifier. Current plans (1992) include scale-up by a factor of ten [52].

2.4   Summary

The open-core downdraft gasifier consists of an open-topped tube through which biomass and oxidant move down towards a narrow reaction zone supported on a bed of char. Biomass gasification in the open-core downdraft gasifier occurs in three stages: drying, pyrolysis and gasification of the char produced by pyrolysis.

The open-core downdraft gasifier can be operated in three modes:

i)   Pyrolysis dominant operation (there is a net production of char in the gasifier);

ii)   Char gasification dominant operation (there is a net consumption of char in the gasifier), and;

iii)   Stable operation (there is no net production or consumption of char in the gasifier).

A number of open-core gasifiers have been reported in the literature. A short description of each and a comparison of the performance of each has been presented.

74

3. EXPERIMENTAL APPARATUS

3.1 Introduction

At the start of this project, the mark I Aston gasification system had not been operated on a regular basis for a period in excess of 6 months. The gas pump was not operating correctly and required either overhaul or replacement. Damage to the pump appeared to have made gasifier control difficult [12]. Due to the damage caused to the pump by tars in the product gas, it was concluded that the existing scrubber was not effective and required replacement or modification. It was not known whether the seals in the gasification system had deteriorated. The mark I gasification system was also understood to have caused unpleasant smells in the laboratory during the previous project. The opportunity was taken, therefore, to extensively modify the gasification system. The design process which was undertaken can be summarised as follows:

i)   Identification of the inadequately functioning items of equipment,

ii)   The selection of suitable equipment to replace those identified in (i),

iii)   The design and subsequent construction or purchase of the equipment required,

iv)   The evaluation of the installed equipment followed by any necessary modification.

This chapter describes the redesign process through which the mark I Aston gasification system has been subjected resulting in the mark II Aston gasification system. Each section of the system is considered separately.

A flow diagram of the original mark I Aston gasification system is shown in Figure 3.1. A flow diagram and photograph of the completed mark II Aston gasification system are shown in Figure 3.2 and Plate 3.1.
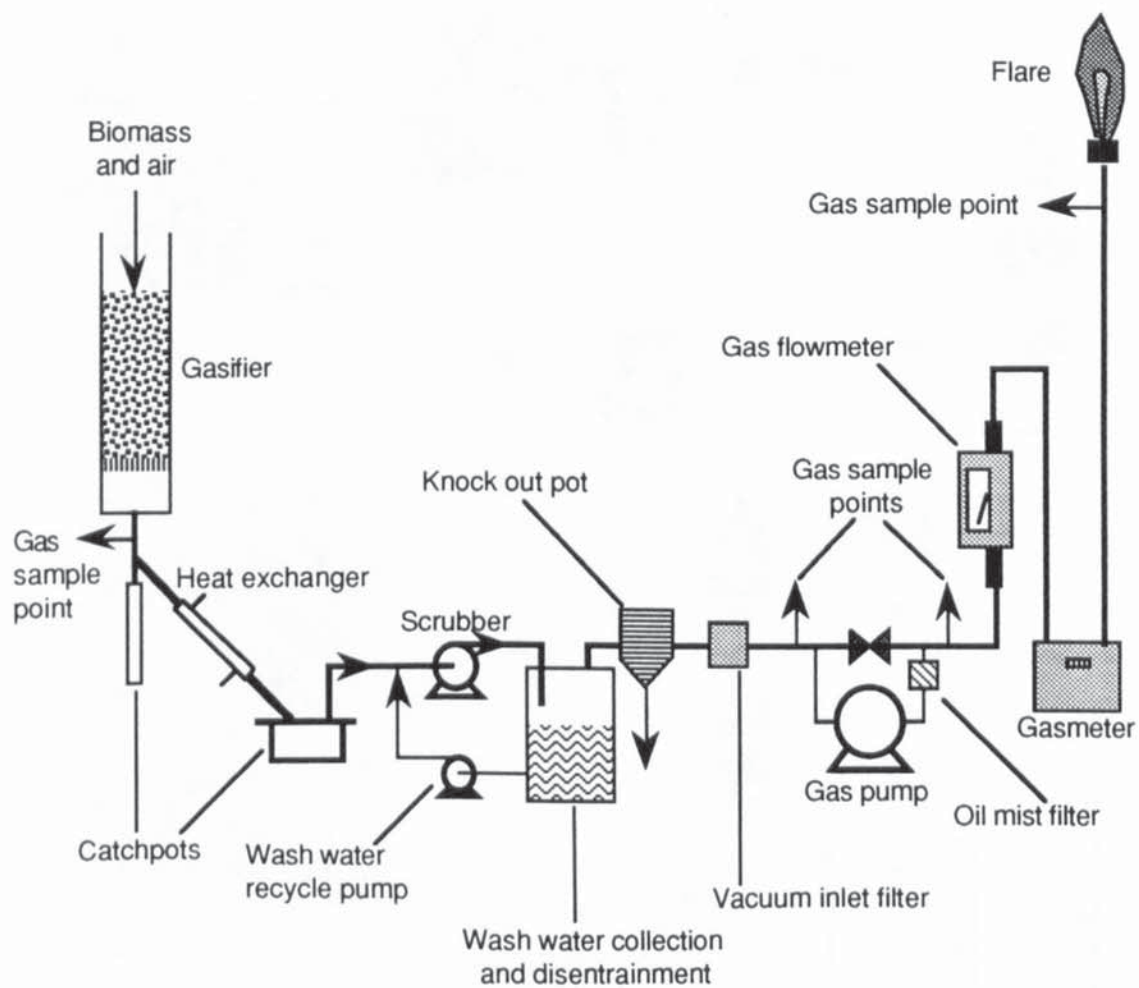
Figure 3.1
Mark I Aston Gasification System Flow Diagram [12]
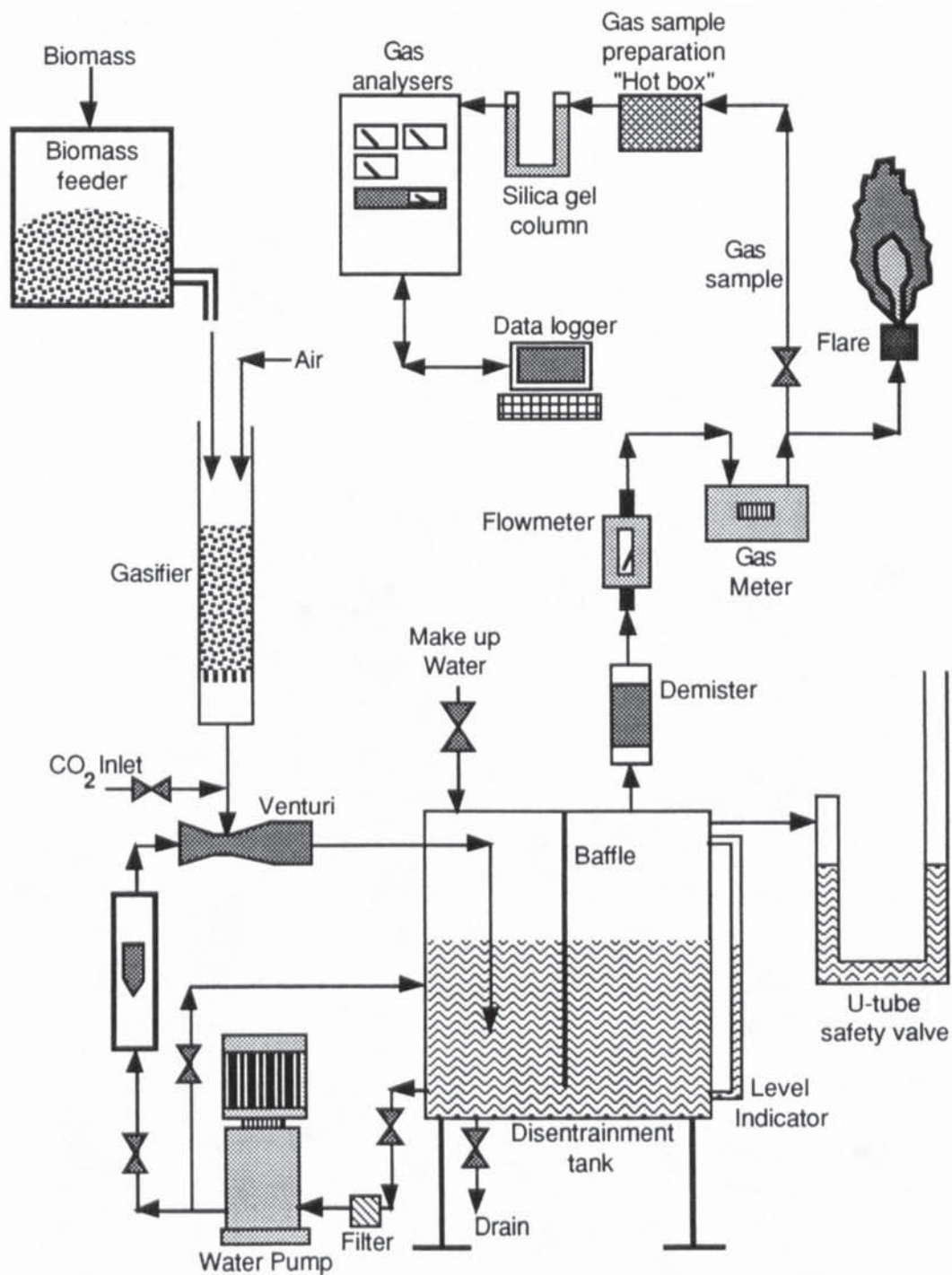
Figure 3.2
Mark II Aston Gasification System Flow Diagram
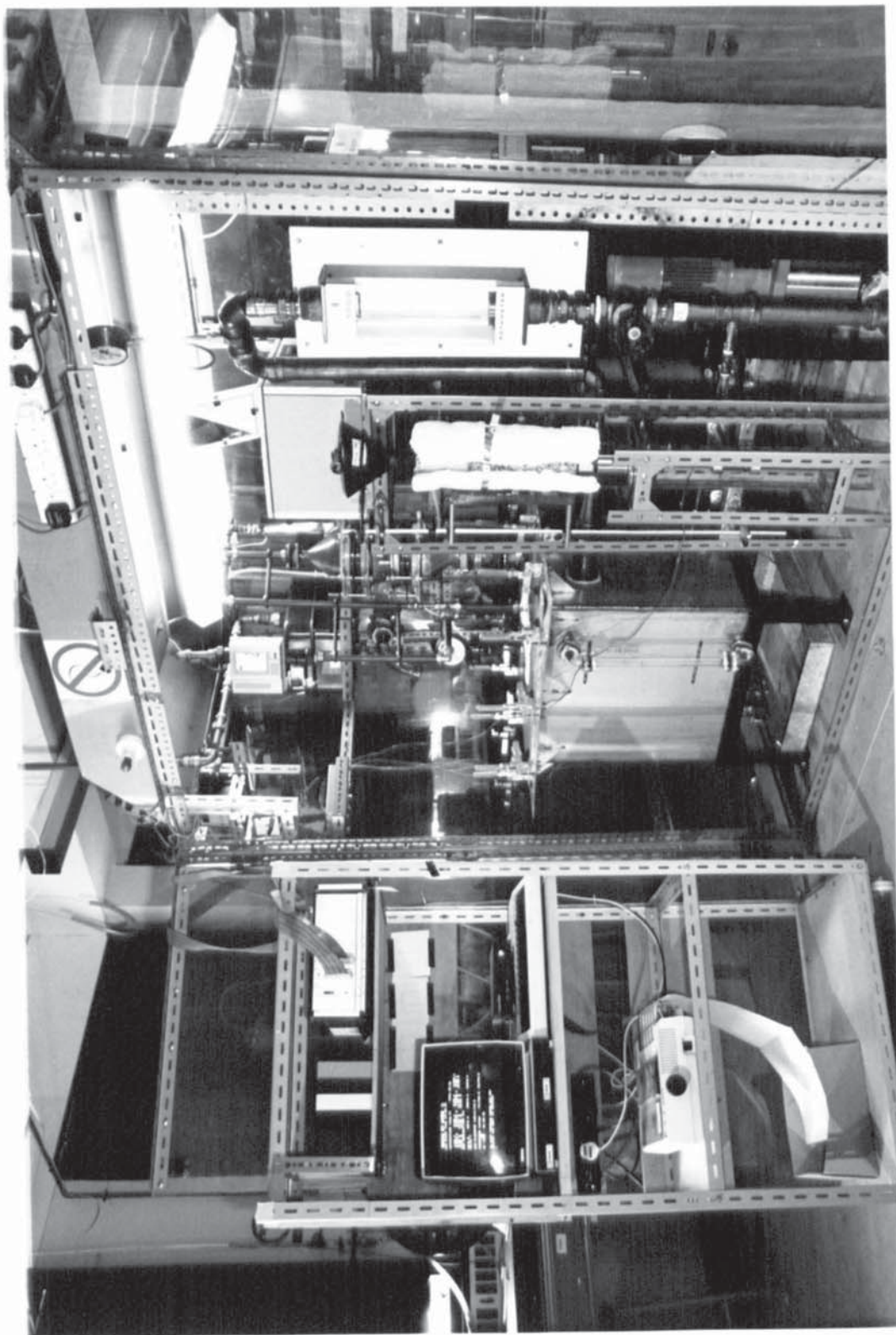
Plate 3.1
Mark II Gasifier System

78

3.2   Fuel Feeding

Previous work used a manual batch feeding system through the open top of the gasifier using a funnel [12],[17]. It was decided to use an automatic screw feeder to simplify operation and enable attention to be focussed on operation, data collection and observation. A suitable feeder (Model 302 Accurate dry material feeder fitted with a 3/4" diameter centreless screw) with approximate feed rates in the range 0.3-7.2 kgh^{-1} and a claimed accuracy of about ±5% was available. The "Accurate" dry material feeder will only accept material in bulk densities in the range 150 - 250 kgm^{-3}. Only feedstocks consisting of particles which had passed through the 6.35 mm sieve were suitable for the feeder, therefore. Batch feeding was used for feeds consisting of particles which had not passed through the 6.35 mm sieve.

A calibration curve for this feeder using wet wood chips (moisture content: 10% wet basis) in the size range 4.75 - 6.35 mm is shown in Figure 3.3. The graph (Figure 3.3) was drawn using the data shown in Table 3.1. Each test run shown in Table 3.1 was of five minutes duration.
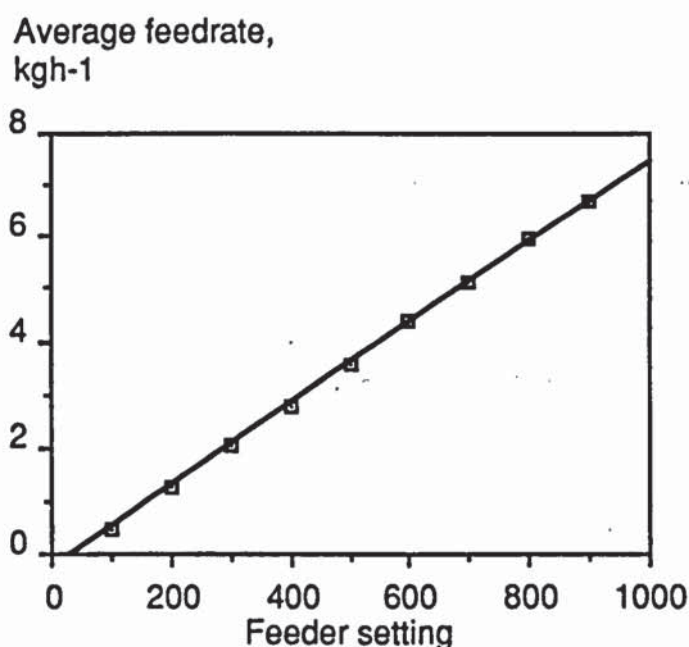
Figure 3.3

Calibration Curve for "Accurate" Screw Feeder

Table 3.1

Screw Feeder Calibration Data

Feeder	Feedrate, kgh^{-1}		Average
setting	Test 1	Test 2	feedrate, kgh^{-1}
100	0.4771	0.4986	0.4878
200	1.1736	1.3344	1.2540
300	1.9238	2.1137	2.0188
400	2.6744	2.8656	2.7700
500	3.4597	3.6757	3.5677
600	4.2799	4.5023	4.3911
700	5.0136	5.2837	5.1487
800	5.8915	6.0324	5.9620
900	6.6546	6.7651	6.7099

It was found during runs 1 to 3 of this project that it was extremely difficult to find the correct feeder setting at which there was neither insufficient or excessive fuel feed to the gasifier. During runs 1 to 3, the feeder setting required continuous adjustment to maintain a stable fuel level in the gasfier. Manual batch feeding was found to be easier to control and record. In addition, the wood chip feed used for standard case operation was unsuitable for the Accurate feeder as the standard case feed consisted of particles which were too large for the Accurate feeder's screw auger.

3.3 Reactor

3.3.1 Reactor Vessel

The previous (mark I gasifier) reactor consisted of a 500 mm long, 75 mm diameter quartz glass tube. The reactor was supported by a stainless steel collar (see Figure 3.4) which was used to connect the reactor to the downstream processing units [12]. The design procedure for this reactor is described in full by Earp [12].

A larger diameter reactor of the same design was considered for use in this project. Above 7.5 cm internal diameter, quartz glass tube of the kind already used in this application was available with internal diameters of 10 cm, 12.5 cm and 15 cm. A larger reactor would use a larger amount of wood (estimated to be 2.7 kgh^{-1} for a 10 cm diameter reactor) increasing the wood

preparation time and making gasifier operation more difficult if manual batch feeding were in use.

It was decided to use the same size gasifier as used in the mark I gasification system. This would enable the use of the existing spare reactors and the re-use of the reactor support collar and grate reducing the overall system design and construction time. It would also enable a close comparison to be made between the results from this project and the work of Earp [12] and Reyes [17].
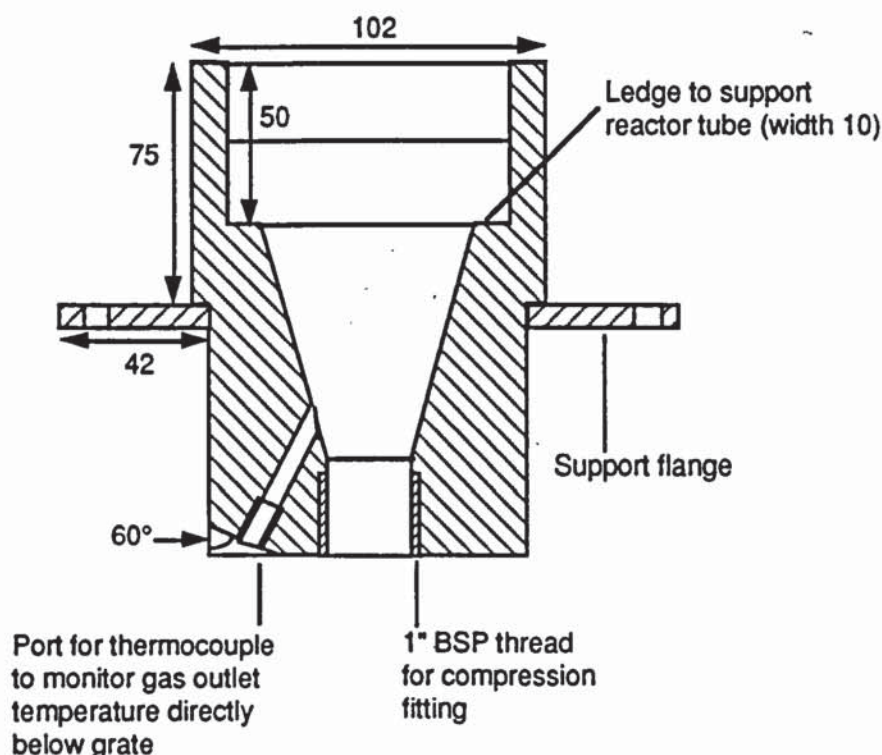
Not to scale - (All dimensions in mm unless otherwise stated)

Figure 3.4
Stainless Steel Reactor Support Collar [12]

3.3.2   Grate Design

The grate used on the mark I Aston gasification system consists of a type 304 stainless steel plate, 73 mm in diameter (to permit thermal expansion) perforated with 62 5 mm diameter holes [12]. The grate is supported by four legs which are themselves supported on the ledge machined into the reactor connecting collar (see Figure 3.4). No problems were recorded by Earp or Reyes concerning this component and it was decided to re-use it with no modification.

It was decided to investigate the effect of char bed height on gasifier performance. During operation with char bed heights of less than 2 cm, it was predicted that heat transferred from the reaction zones could damage the reactor·support collar (Figure 3.4). A grate extension was, therefore, constructed to prevent possible damage to the reactor support collar. This consisted of two stainless steel rings 73 mm outer diameter and 55 mm inner diameter joined together using four legs 90 mm in length (Figure 3.5). The outer diameter selected permits an adequate average tolerance of 1 mm on the reactor internal diameter to allow for thermal expansion up to 1500°C. This diameter was found to be suitable during both Earp's project [12] and the intial stages of this project. The inner diameter is the same as the inner diameter of the existing grate's base. The height of the grate extension was chosen to provide an effective reactor height of 250 mm from the reactor top to the grate.
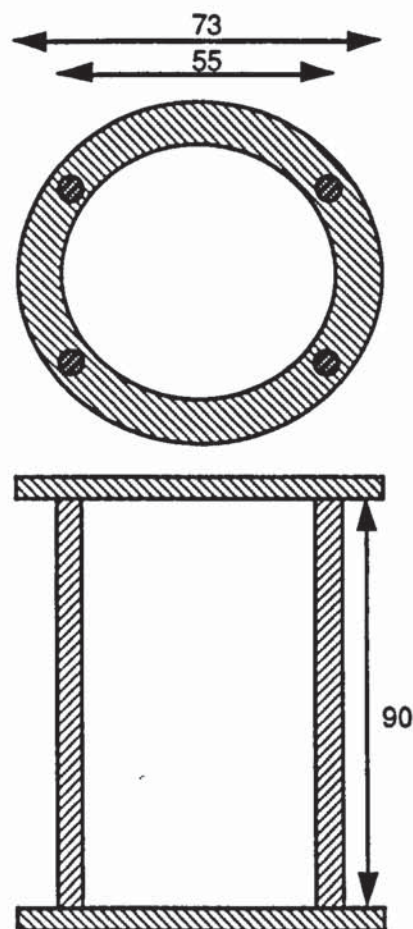
To scale - All measurements in mm

Figure 3.5
Grate Extension

3.3.3   Reactor Insulation

The quartz glass reactor had previously been used without insulation leading to high heat losses estimated to be between 20 and 34% of the total energy input [17].

Insulation of the gasifier would enable an assessment of the effects of heat loss on gasifier performance to be made (see Section 2.8.3). The novel gold insulation system developed by Reed was considered difficult to obtain (see Section 2.8.3). Reed and Markson reported that a quartz glass gasifier could be well insulated using a riser sleeve constructed from 14 mm fibrous, high temperature ceramic insulation with a 5 mm vertical slot cut into the insulation to permit observation of the gasification process [11],[22]. Reed used this system (ceramic insulated reactor) to study the rate at which the reaction zone moved with or counter to the flow of air or oxygen [22].

High temperature ceramic fibrous fibre insulation is easy to obtain, cheap and can be quickly cut to size and moulded into simple shapes. It had also been used on the (mark I) gasification system as the sealing material to seal the reactor tube into the gasifier support collar. It is available in yarn, rope lagging, twisted rope, cabled rope, paper, bulk fibre blanket, stiff board and moist felt [53]. Of these, the paper and blanket types were considered. Paper was considered too thin for this application being available only in thicknesses of up to 3 mm. Ceramic blanket is available as standard in thicknesses of 6, 13, 25, 38 and 50mm [53]. In addition, it can also be hardened to various degrees to form solid shapes [53].

To enable selection of a suitable insulation thickness, the reduction in gasifier heat losses for various (available) thicknesses of insulation was predicted using heat loss data presented for the uninsulated mark I Aston gasifier by Reyes (Table 3.2) [17]. The heat loss from the uninsulated mark I Aston gasifier was estimated by Reyes by measuring the gasifier temperature in four zones and calculating the convective and radiative heat losses using Equations 3.1 and 3.2 [17]. Using her data (as this was the only data available), the outside temperature and heat loss of an insulated gasifier using the available thicknesses of ceramic insulation was predicted using Equations 3.3 and 3.4 [54],[55].

Table 3.2

Reported Uninsulated Gasifier Temperature and Heat Loss Data [17]

Zone	Height above grate, cm	Zone temperature °C	Zone height cm	Thermal conductivity $wm^{-1}k^{-1}$ 24	Uninsulated reactor heat loss, w
1	0-4	525	4	0.110	253.1
2	4-8	600	4	0.125	351.0
3	8-12	825	4	0.170	820.1
4	12-13	1000	1	0.220	357.1

Ambient temperature, $T_a = 25°C$

$$Q_{conv} = 1.18.\pi.d^{0.75}.L_i.(T - T_a)^{1.25} \quad \ldots\ldots\ldots\ldots\ldots[3.1]$$

where:

Q_{conv}	Reactor heat loss due to convection, watts
d	Reactor diameter (including insulation), m
L_i	Zone length, m
T	Outside temperature of glass reactor tube, K
Ta	Temperature of surrounding air, K

$$Q_{rad} = \sigma.\varepsilon.\pi.d.L_i.(T^4 - T_a^4) \quad \ldots\ldots\ldots\ldots\ldots[3.2]$$

where:

Q_{rad}	Reactor heat loss due to radiation, watts
σ	Emissivity of insulation, 0.94 [56]
ε	Stefan-Boltzman constant, 5.67×10^{-8} $wm^{-2}k^{-4}$

$$\frac{q}{L} = \frac{2.\pi.(T - T_a)}{\frac{1}{h.r} + \frac{\ln\left(\frac{r}{r_i}\right)}{K}} \quad \ldots\ldots\ldots\ldots\ldots[3.3]$$

where:

L	Length of pipe, m
h	Outer surface convection coefficient. For free convection in air, this is 5 $wm^{-2}k^{-1}$ [57]
r	Radius (outer) of gasifier and insulation, m
r_i	Gasifier outer diameter, 0.081 m

K   Thermal conductivity of insulation, $wm^{-1}k^{-1}$

$$\frac{q}{L} = \frac{2.\pi.K.(T - T_s)}{\ln\left(\frac{r}{r_i}\right)} \quad \text{......................................[3.4]}$$

where:

T_s External surface temperature of insulated reactor, K

L   Length of pipe, m

Using a spreadsheet, the heat loss for each of the four zones shown in Table 3.2 was calculated for each available thickness of insulation and the percentage of the total heat loss from the uninsulated reactor calculated using Equation 3.5 (see Figure 3.6).

$$\frac{\text{Heat loss from insulated gasifier}}{\text{Heat loss from uninsulated gasifier}} \times 100\% \quad \text{.................[3.5]}$$

% of total heat loss from
uninsulated gasifier
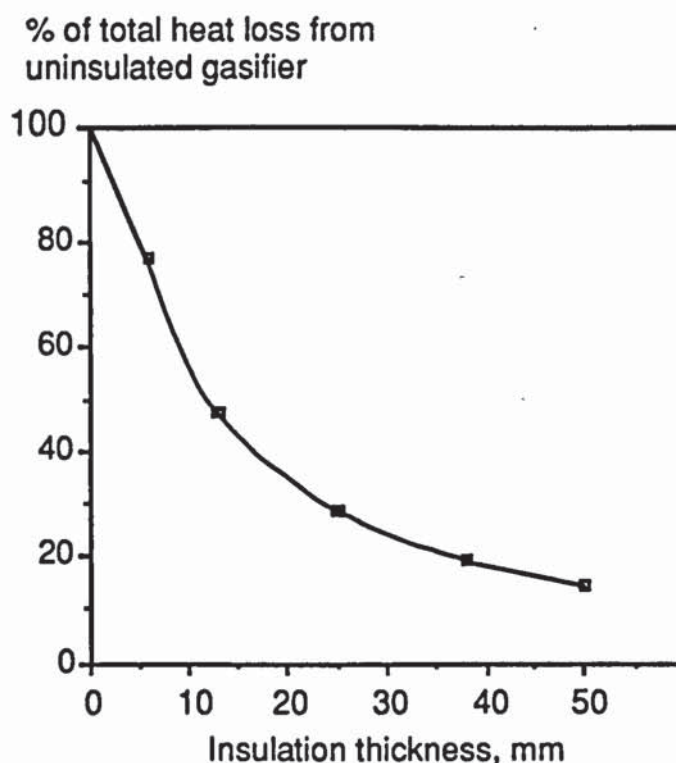
Figure 3.6

Percentage of Heat Loss (Calculated) from Uninsulated Reactor Lost by Insulated Reactor Fitted with Various Insulation Thicknesses

Figure 3.6 shows that the rate of heat loss from the gasifier becomes less significant at insulation thicknesses of 38 mm and above. The choice of 50mm thick insulation would provide minimal additional insulation compared with 38 mm thick insulation. In addition, 50mm thick insulation would be difficult to cut to size and would increase the chances of leaving vertical channels between the external surface of the gasifier and the internal surface of the insulation due to folding. The outer temperature and heat loss data for a reactor insulated with 38 mm thickness Kaowool is presented in Table 3.3.

Table 3.3

Predicted Outer Temperatures and Heat Losses from Gasifier Insulated Using 38 mm Kaowool Insulation

Zone (Table 3.1)	Outer temperature °C	Heat loss convective W	Heat loss radiative W	Total heat loss W
1	173.7	6.11	33.59	39.70
2	211.8	8.13	49.80	57.93
3	341.5	5.71	141.60	147.31
4	472.1	6.05	78.95	85.00

A reactor tube was used as a former to produce an insulating sleeve from 38 mm Kaowool blanket leaving a 20 mm sight strip. The sleeve was "case" hardened to produce a degree of robustness while maintaining a soft inner surface which could be squeezed tightly around the gasifier eliminating gaps between the reactor and the insulation. The insulation sleeve was attached to the reactor using metal straps (see Plate 3.2).
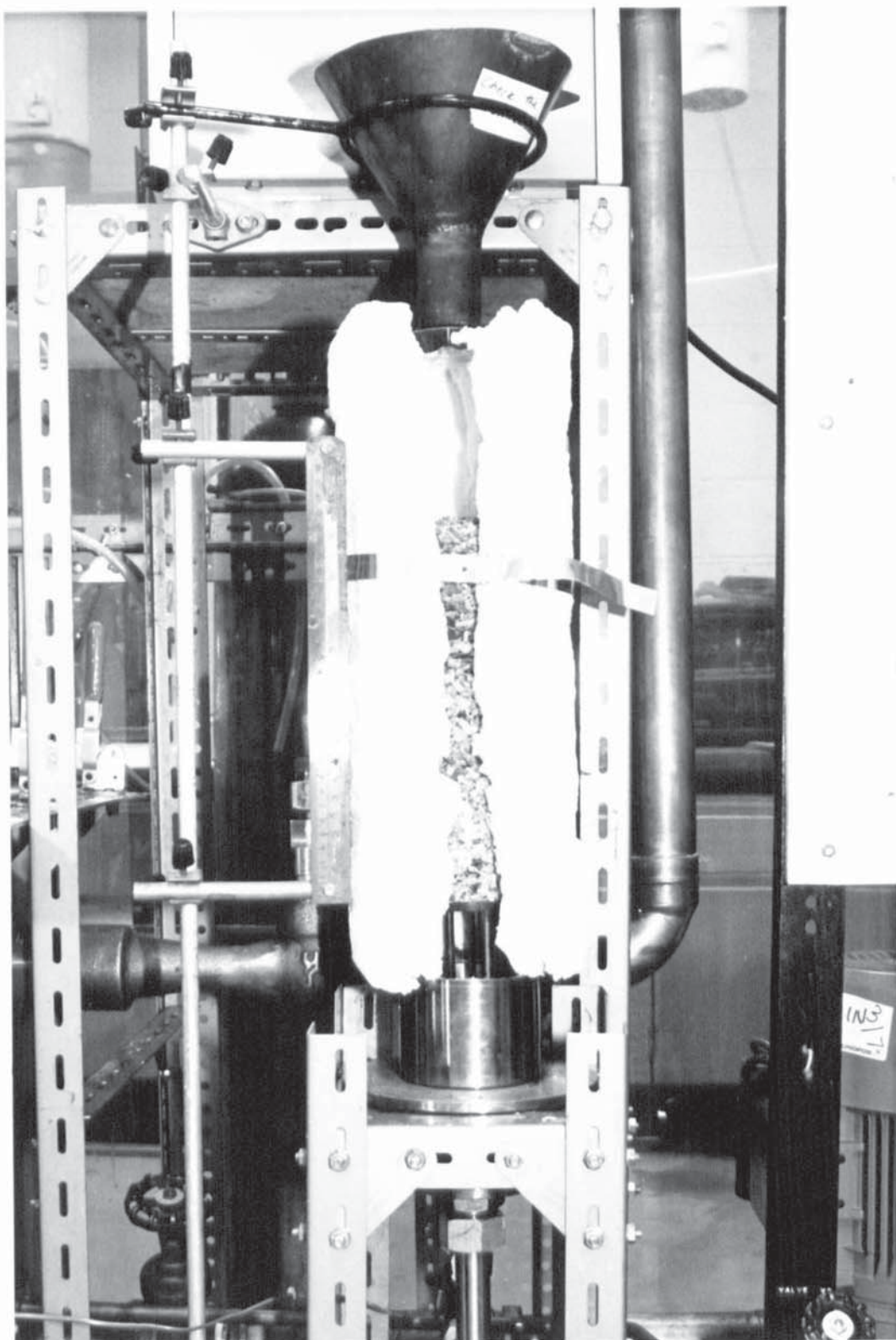
Plate 3.2
Gasifier Fitted with Insulation

During the first run in which an insulated gasifier was used, it was found that the high temperatures occurring in the reactor (approximately 1000°C-1100°C) maintained at the surface by the insulation caused the quartz glass reactor tube to become opaque making observation of the gasification process difficult (the softening temperature of quartz glass is 1250°C [56]). Sufficient transparency was maintained through the sight strip, however. Higher temperature resistant glass was available but was extremely expensive. Further experiments using an insulated reactor were, therefore, carried out using the existing quartz glass tubes. Further damage was encountered but it was noted that damage did not occur each time an insulated run was carried out indicating that the temperatures to which the quartz glass tube is subjected when operating with the insulation sleeve is fitted are close to the maximum acceptable operating temperature of the quartz glass tube.

3.4   Product Gas Processing

One of the principal objectives of this project was to rebuild the gasification system built by Earp [12]. to provide a more robust and efficient gasification system. This section describes the design process through which the product gas processing system was taken.

3.4.1   Product Gas Processing - Mark I Gasification System

The previous gas processing and moving system designed by Earp consisted of three separate stages [12]. These were: gas cooling using a heat exchanger, gas cleaning using a water scrubber and gas pumping using a gas pump (see Figure 3.1).

3.4.1.1   Gas Cooling

The temperature of the gas below the grate in previous experiments ranged from 425 to 530°C [12]. Gas cooling was carried out to protect the pressure transducers and gas flowmeter downstream of the gasifier from temperatures greater than the maximum pressure transducer operating temperature (70°C) [58]. A counter current water cooled concentric tube heat exchanger of length 0.75 m and internal diameter 2.54 cm was used which cooled the gases from approximately 700 to 150°C [12].

3.4.1.2 Gas Cleaning

Depending on the use to which the product gas from a gasifier will be put, gas clean-up to varying degrees may or may not be required. Product gases for use in boilers or furnaces require minimal cleaning. Product gases to be used in engines are required to be almost free of particulates and tars. The raw product gas from the Aston gasfier would contain particulates approximately 1 micron in size, liquid droplets (greater than 10 microns) and mists (less than 10 microns) of tars and oils (condensibles) [59]. The objective of gas cleaning processes is to efficiently remove as much as possible of the particulates and condensibles in the product gas.

Several methods of gas cleaning were employed by Earp [12] and Reyes [17]. The final assembly consisted of two catchpots to remove any particulates (solid char particles entrained in the gas) and a high energy centrifugal contacting wet scrubber (see Figure 3.7). The gas and water mixing was carried out using a Stuart Turner No. 12 centrifugal pump while the scrubber water was recycled using a Stuart Turner No. 10 centrifugal pump (Figure 3.7). It is not reported whether any wash water was forced back through the dirty gas inlet (Figure 3.7) and into the heat exchanger (Figure 3.1).
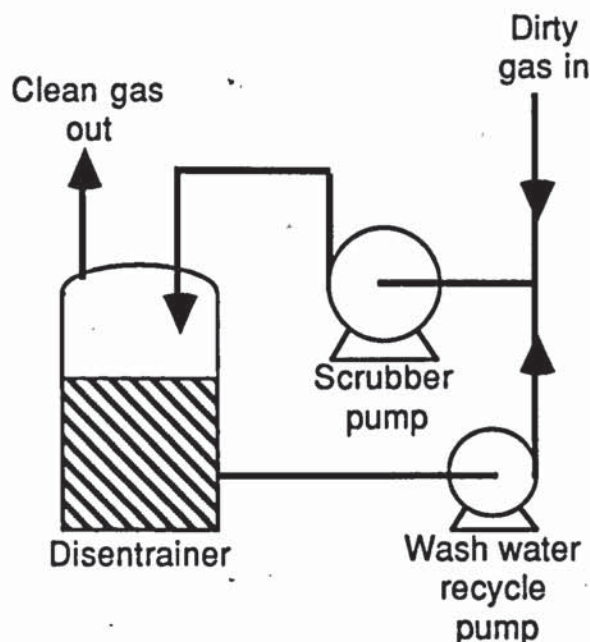
Figure 3.7
Flow Diagram of Final Scrubbing System Used by Earp [12]

89

Earp [12] and Reyes [17] had particular problems with fine droplets of tars affecting the performance of the gas pump. Extra gas clean-up stages (a knock out pot and two filters fitted downstream of the scrubber) had to be added to to protect the gas analysers, flowmeter and gasmeter from tars (see Section 3.11.1.2 and Figure 3.6). The performance of the second scrubber was not described or quantified by Earp [12].

3.4.1.3 Gas Pumping

A Werner Rietschle VL10 positive displacement pump rated at 10 m^3h^{-1} was used to move the product gases through the mark I gasification system [12]. The Werner Rietschle pump employed a once through lubrication system selected due to the manufacturers concern over the possibility of contamination of the lubrication oil with tars, moisture and other contaminants in the product gas [12]. This pump was damaged by tars in the product gas and required overhaul during Earp's project. At the completion of Earp's project, the gas pump was operating unevenly and noisily indicating that further damage had occurred. A second overhaul or replacement was, therefore, necessary.

This Werner Rietschle pump required relatively long start-up and shut-down procedures which, when added to the other tasks required during the start-up and shut-down procedures for the gasification system as a whole, reduced the amount of time available for carrying out an experiment. The pump also caused some discomfort due to noise (during normal operation).

3.4.2 Gas Moving and Cleaning Modifications
3.4.2.1 Gas Pumping

A method of drawing air into the gasifier and moving the product gas from the gasifier, through a cleaning system and to a burner was required. The open-top of the open-core downdraft gasifier necessitates the use of a negative pressure system to draw air into the gasifier to ensure that ease of feeding and ease of instrument insertion into the gasifier is maintained. A forced draught system was not considered as this would increase the complexity of the gasification system to an unacceptable degree. Hence, it was necessary to position the pump downstream of the reactor.

90

Three options were considered:

i   Overhaul the existing pump and replace or improve the gas cleaning equipment;

ii   Purchase a new gas pump and replace or improve the gas cleaning equipment;

iii   Purchase a venturi ejector to move and clean the product gas.

The positive displacement pump previously used had been shown to be unsuitable unless an improved method of gas cleaning was utlilised upstream of the pump (see Section 3.4.1.3). A number of scrubbers were tested during the previous project [12]. However, it was found that tars were not completely captured [12]. It was predicted that both the overhauled gas pump or a new gas pump containing moving internal parts would become damaged by any tars and particulates escaping the gas cleaning operations and were, therefore, considered unsuitable for this application.

It was decided that a venturi ejector would be suitable for this application as venturi ejectors have the advantage of having no moving parts and can handle a wide range of gases or vapours including those containing sticky or solid particles as in this application. In addition, they can be constructed from a wide range of materials including plastics [60]. Suction pressures of down to 50 mmHg (abs) should be possible using single stage ejectors whilst multistage ejectors using two or more ejectors fitted in parallel can produce vacuums down to approximately 1 mmHg (abs) [54],[60]. The design simplicity also results in a low maintenance requirement and a long life at a sustained efficiency although energy is required to operate the venturi. Due to the difficult handling characteristics of the raw product gas from a gasifier, it was decided that the simple construction and operation of the venturi ejector would provide an efficient and reliable means of gasifier operation and control.

Ejector venturis work by expanding a fluid (in this case, water) at high pressure through a nozzle which results in the formation of an area of low pressure in the chamber into which the nozzle discharges the fluid. Fluid from the system to be evacuated is sucked in at the throat of the ejector and mixed with the motive fluid (see Figure 3.8) [56],[61]. Following gas and water mixing, the gas must be separated from the water using a disentrainment device (see Section 3.7 and Figure 3.8). The suction

produced by a venturi ejector can be controlled using a valve controlling either the gas or the water flowrate into the venturi ejector.

The use of a venturi ejector also offered the advantage of being able to cool and clean the gas in addition to moving the gas. This would simplify the design process, construction and gasifier operation.
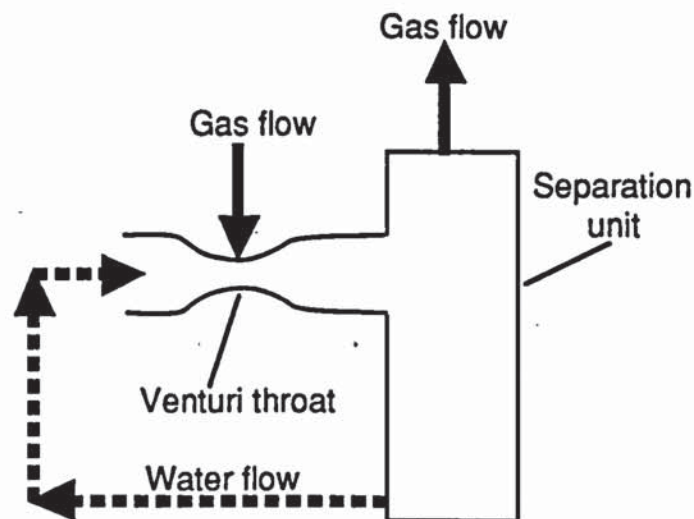
Figure 3.8
Method of Operation of a Venturi Scrubber [59]

The sizing of the venturi ejector for this project is presented in Section 3.5.1.

3.4.2.2   Venturi Ejectors for Gas Cleaning

The venturi ejector designed for gas moving will also scrub a gas. Venturi scrubbers are a highly efficient form of gas cleaning and can collect condensible liquids in addition to solid particulates [59]. Venturi scrubbers are a type of preformed gas atomised spray scrubber utilising spray nozzles to atomise liquid droplets which, travelling at high velocity with respect to the gas flow, collect the larger particles in a gas stream by impaction and the smaller particles by diffusion due to the high surface area of the atomized water droplets [62].

Venturi ejector scrubbers are simple in design, do not plug easily and should be capable of removing more than 99% of sub 5μm particles and 97% of one micron particles (see Table 3.4) [59],[63]. A water jet scrubber has been shown to be superior in tar removal relative to a spray tower

92

Table 3.4
Summary of Gas Cleaning Equipment Performance and Efficiency [64]

Gas Cleaning Equipment Performance:

Type of Equipment	Field of Application	Pressure loss Nm^{-2}
Settling chambers	Removal of coarse particles , larger than about 100-150 μm	< 50
Low pressure drop cyclones	Removal of fairly coarse dusts down to about 50-60 μm	< 250
High effiency cyclones	Removal of average dusts in the range 10-100 μm	250-1000
Wet washers (including spray towers, venturi scrubbers etc.)	Removal of fine dusts down to about 5 μm (or down to sub-micron sizes for the high pressure drop type).	250-600 or more
Bag filters	Removal of fine dusts and fumes down to about 1 μm or less	100-1000
Electrostatic precipitators	Removal of fine dusts and fumes down to 1 μm or less	50-250

Gas Cleaning Equipment Efficiency:

Type of Equipment	Efficiency, %		
	at 5 μm	at 2 μm	at 1 μm
Medium efficiency cyclone	27	14	8
High efficiency cyclone	73	46	27
Electrostatic precipitator	99	95	86
Fabric filter	99.8	97	92
Spray tower	94	87	55
Wet impingement scrubber	97	95	80
Venturi scrubber	99.8	99	97

scrubber [48]. The tar content of the product gas from a rice hull fuelled open-core downdraft gasifier cleaned using a spray tower was 1 gNm^{-3} while the tar content of the product gas from the same gasifier cleaned using a venturi scrubber was 0.37 gNm^{-3} [48]. Droplet and particulate removal efficiency is proportional to the degree of mixing between the gas and scrubbing liquid and is normally constant for a given droplet removal efficiency [59]. Increasing the pressure drop across the scrubber will increase the degree of gas and liquid mixing and hence increase the droplet and particulate removal efficiency. However, increasing the pressure drop increases the energy input requirement to a system [59].

The use of a venturi ejector for gas cleaning was predicted to provide an efficient and simple gas scrubbing system. Earp suggested that the construction of a venturi ejector system would be difficult since he only considered the in-house manufacture of a venturi ejector [12].

A computerized database search using the "ENERGY" database was carried out as part of this project during 1989. No reference was found, however, concerning the use of a venturi ejector as both a prime gas mover and gas cleaning system for a downdraft gasifier.

3.5   Venturi Choice
3.5.1   Venturi Size
Earp [12] estimated gas flow rates of $10m^3h^{-1}$ would be required for this gasifier but the gas flowrate in his experiments never exceeded 4 Nm^3h^{-1} as shown in Table 3.5 (approximately 11 m^3h^{-1} at a gas temperature of 500°C). Sizing calculation procedures (see Appendix II) showed that a 54 mm (2 inch) single nozzle water jet ejector would be suitable for this duty [65]. The maximum gas moving capacity of this size and type of ejector was calculated as 18.6 m^3h^{-1} using a water pressure of 4.22 barg (60 psig) and 21.8 m^3h^{-1} using a water pressure of 5.51 barg (80 psig) at a suction pressure of 635 mmHg abs. and a water temperature of 21°C (see Figure 3.9). The approximate water consumption for a 54 mm venturi is presented in Figure 3.10.

Table 3.5
Previous Gas Throughputs of Aston Gasifier [12]

Run Number	C6	R7	R7	R8	R9	R9
Gas flowrate Nm^{3}h^{-1}	2.97	2.91	3.89	2.56	2.25	2.84

Air handling capacity m3h-1

Water pressure, barg
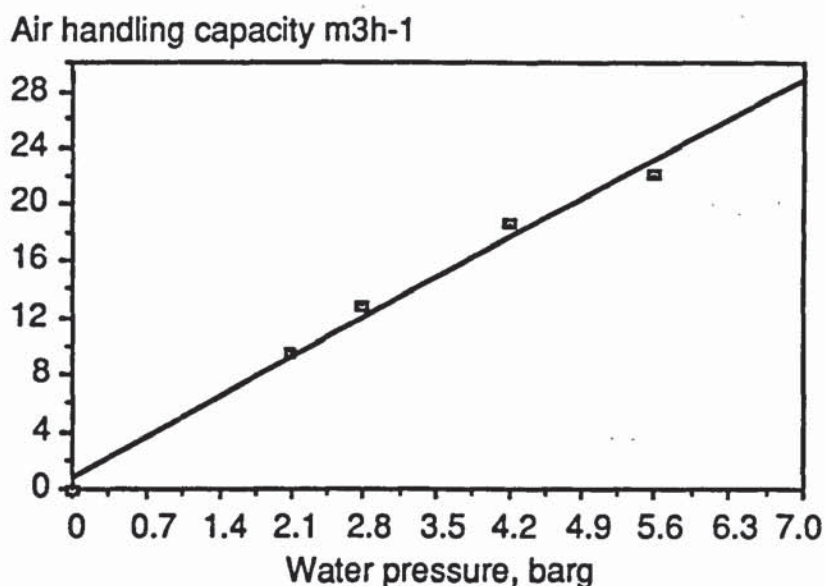
Figure 3.9

Air Moving Capacity of 54 mm (2 inch) Type 484 Standard AVE Water Jet Ejector at Various Water Pressures

Water consumption litres/minute

Water pressure, barg
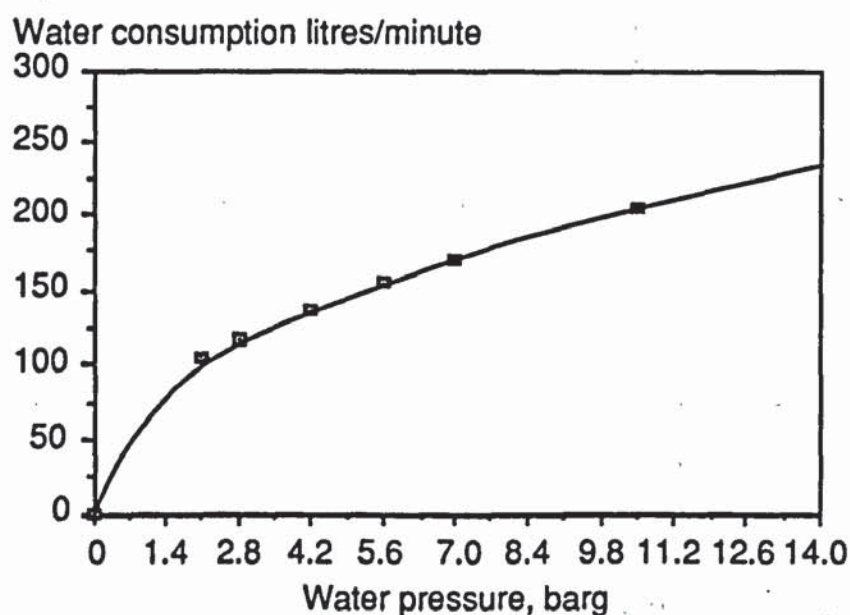
Figure 3.10

Approximate Water Consumption for a 54 mm (2 inch) Type 484 Standard AVE Water Jet Ejector

Venturi back pressure is minimized by discharging the venturi directly into the disentrainment tank (Section 3.7). The estimated back pressure in the disentrainment tank was calculated at 0.227 barg, 3.3 psig (see Appendix II for calculations). The greatest back pressure observed during any runs was found to be 0.207 barg (3 psig). Information from the venturi suppliers indicated that the venturi would operate efficiently at this back pressure and that a similar venturi had been successfully operated against back pressures up to 0.620 barg (9 psig) [66].

Once installed, a correlation between the water flowrate and the air flowrate through the cumulative gasmeter was obtained. The results of this test are shown in Figure 3.11.

Gasmeter flowrate m3h-1

Water flowrate l/min
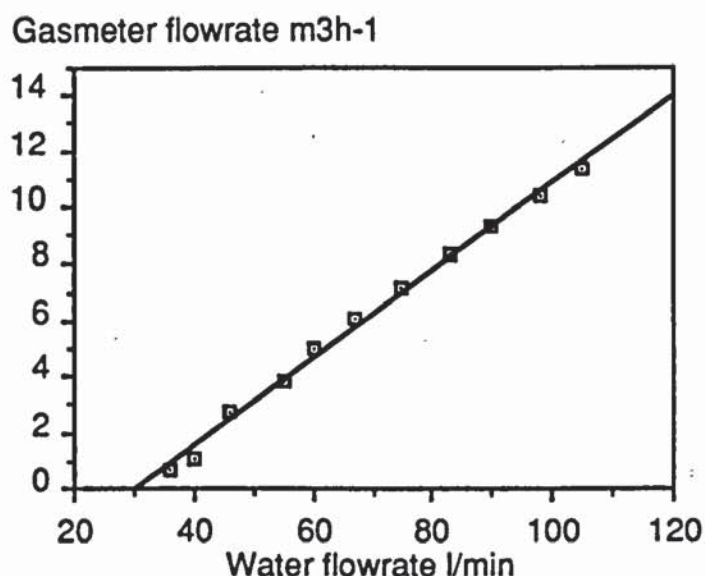
Figure 3.11

Cold Gas Flowrate Through Gasmeter versus Water Flowrate Through Venturi

3.5.2   Scrubbing Medium

Wet scrubbers usually use water as the scrubbing media since water is easy to obtain and cheap. However, hydrocarbon oil (or a combination of oil and water) and solvents can also be used [59]. Gas scrubbing equipment can be constructed from cheaper materials if oil is used as the scrubbing media as oil will not become acidic during operation. The system would, however, be more complex and large volumes of oil would have to be purchased and stored (approximately 140 litres of liquid is required to operate the

gasification system). The gas may also entrain some of the oil and become saturated with the more volatile components of the oil [59]. The use of a solvent as the scrubbing media was discounted due to volatility of the solvents and disposal of large volumes of used solvent following each run.

Due to its ease of use and availability it was decided to use water as a scrubbing medium and driving force for the venturi. During gasifier operation the water will become corrosive due to the presence of absorbed carbon dioxide and organic and inorganic water-soluble acids in the gas (condensate pH is approximately 3.6 [67]) [62]. From data available in the literature, it was calculated that a downdraft gasifier of 1.5 kgh^{-1} feed throughput would produce approximately 305 $ml.h^{-1}$ of condensate (see Appendix II) [67]. From the data shown in Table 3.6, the concentration of acetic acid in water would be approximately 4.01 $x10^{-3}$ % and that of phenols in water would be 3.4 $x10^{-4}$ % in 140 litres of water after five hours operation if 500 $ml.h^{-1}$ of condensate were produced during a run (see Appendix II). The pH of the water was estimated to be 6.2 due to the absorption of carbon dioxide from the product gas (see Appendix II).

Table 3.6 Summary of Condensate Analysis - Downdraft Gasifier [67]	
pH	3.9
Phenols mg/l as phenol	4990.0
Organic acids mg/l as acetic	37430.0
Methanol mg/l	15310.0
Acetone mg/l	3550.0
Tannin and Lignin mg/l as tannic acid*	7040.0
* Determined on residue after distillation of phenols	

3.5.3   Material of Construction

Due to the acidity of the water in use, the venturi ejector was specified in 316 stainless steel. Corrosion properties of type 316 stainless steel are presented in Table 3.7.

97

Table 3.7			
Corrosion Properties of type 316 Stainless Steel [56]			
Acid	Maximum Temperature °C	Maximum Concentration %	Corrosion inch/yr
Acetic	100	75	<0.02
Formic	52	100	<0.02
Phenol	427	100	<0.02

3.5.3 Water Pump

As the water used in the venturi is recycled, the concentrations of solid particulates and liquid contaminants will rise and could damage the pump drive and motor. A quotation for a seal less pump with a magnetic drive system was requested. This would have cost over £2000 and was rejected as an alternative.

A Grundfos CRN 8-50 multistage centrifugal pump was selected due to its competitive price, efficiency, ease of maintenance (if required) and the in-line design of inlet and outlet pipe connections making installation easy. Due to the acidity of the water in use, the pump was specified in 316 stainless steel.

As centrifugal pumps are designed for pushing fluids rather than pulling, the pump was placed as close as possible to the source of water (the disentrainment tank) with the minimum number of bends in the pipework between the tank and pump.

3.5.4 Reactor to Venturi Connection

This component transfers raw product gas from the gasifier to the downstream processing equipment. It should be as short as possible and contain the minimum number of bends to minimize the pressure drop and maximize the venturi efficiency

The simplest method would be to attach the gasifier collar directly on top of the venturi suction chamber. However, this would not have left sufficient clearance below the fumehood ceiling to install the screw feeder or to permit

hand feeding. In addition, it was proposed to fit an iso-kinetic gas sampling probe into this pipework suitable for taking representative raw gas samples just downstream of the gasifier which would require a specified length of straight pipe to comply with the requirements of the British Standard.

During cold commissioning runs with a short (80 mm height) venturi to collar connection, it was occasionally found that when the water pump supplying high pressure water to the venturi was switched off, water rose up into the gasifier which, during hot operation, could cause the gasifier to break and possibly explode. The escape of water upwards into the gasifier was caused by a small amount of "dead water" in the venturi throat being pushed into the low pressure region in the venturi to gasifier connection by high pressure just downstream of the venturi. This resulted in water being forced up through the venturi connector and towards the gasifier. A simple shut-down procedure was conceived to eliminate this problem. However, during emergency shut-down, the problem could re-occur causing cold water to enter the hot reactor.

A system of 25.4 mm (1 inch) diameter 316 stainless steel pipes connected using Ermeto stainless steel compression fittings and incorporating a catchpot was constructed (see Figure 3.12). The catchpot will act as a course particulate (>5 mm) removal system. Any water ejected out of the venturi would, therefore, be collected before reaching the gasifier. It was decided to use 25.4 mm (1 inch) diameter pipe since the gasifier collar connection diameter was a 1 inch male Ermeto straight compression joint. This was connected to the female 54 mm (2 inch) BSPT thread at the throat of the venturi using an in-house manufactured adaptor also made from 316 stainless steel (see Figure 3.13). The adaptor was fitted with a tapping to permit connection to a bottled carbon dioxide supply.

An iso-kinetic sample probe constructed according to BS 893: 1978 was incorporated into the design of the venturi to gasifier connection system [68]. The design procedure is outlined in Appendix II. As the raw gas emerging from the gasifier could be up to 1000°C and contain corrosive constituents, 316 stainless steel was used for the construction of this probe. To permit removal for inspection and maintenance, the iso-kinetic sample probe was installed through the solids catchpot.

99
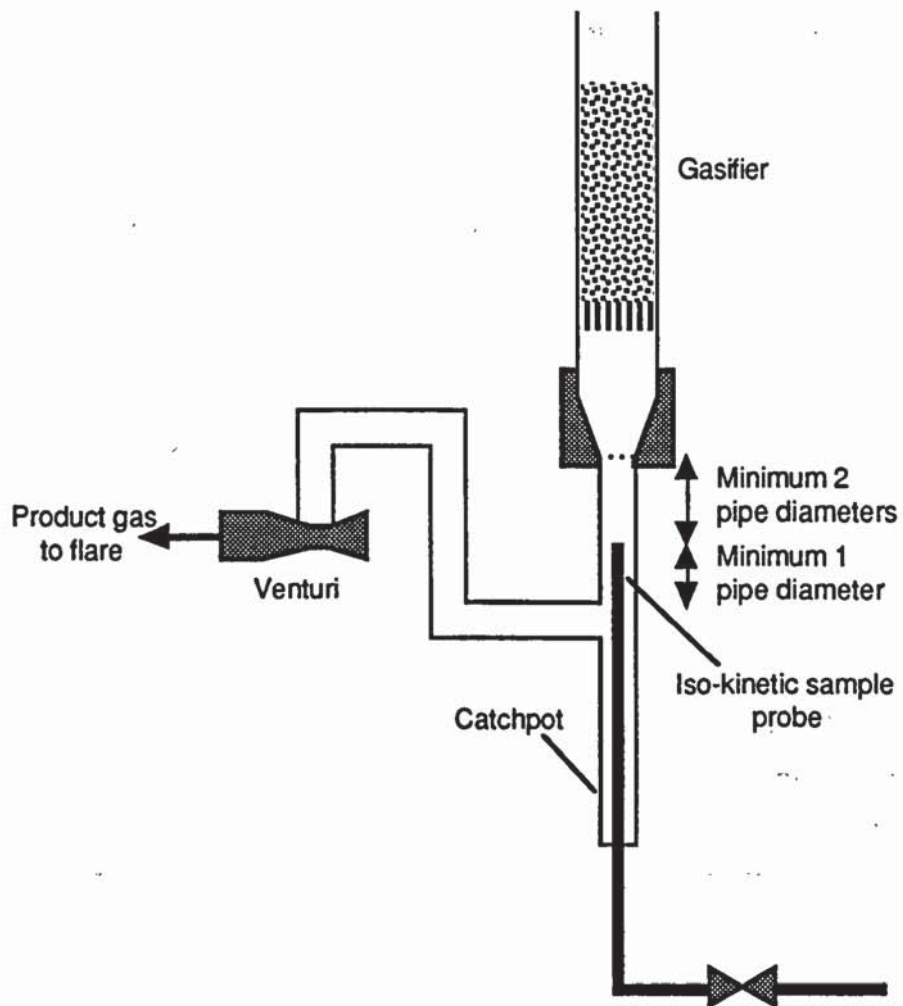
Figure 3.12
Venturi to Gasifier Connection System Configuration
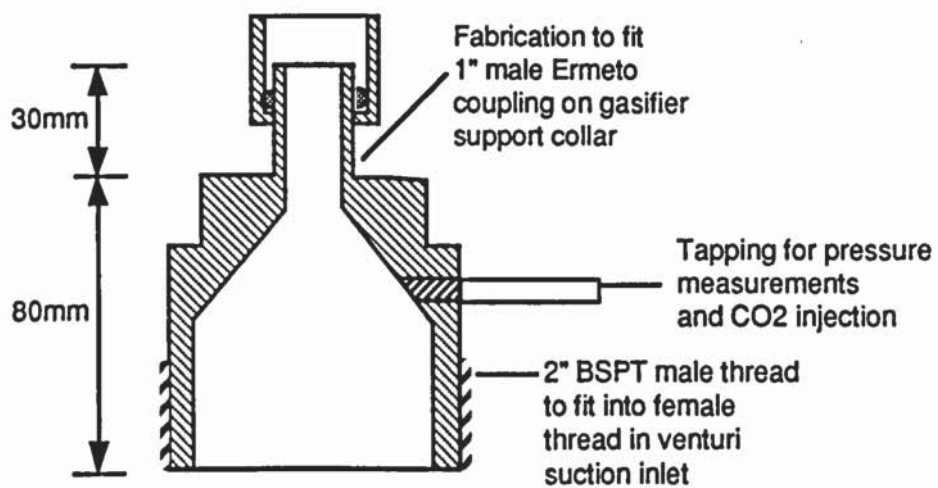
Figure 3.13
Adaptor to Connect Venturi Ejector to 25.4 mm (1 Inch) Pipework

100

Time constraints meant that a tar and condensate sampling system could not be built as part of this project. However, the iso-kinetic sample probe was left in position for use in the next project [69].

3.6   Water Circuit Pipework and Valves

3.6.1   Venturi Circuit Pipe Diameter

The venturi circuit pipe diameter was dictated by the size of the input and output connections to the venturi ejector and Grundfos water pump (54 mm, 2 inch BSP) [70].

3.6.2   Pipework Construction Material

Two materials were considered - unplasticised PVC and copper with brass fittings.

UPVC pipe is simple to handle, cheap to buy and easily available. Construction could be made quickly and easily. UPVC pipe is suitable for use between 5 and 60°C and can withstand 8.269 barg (120 psig) at 20°C and 2.067 barg (30 psig) at 60°C [56],[71]. Higher grades of uPVC give greater] pressure resistance. Table 3.6 shows the main corrosive components in the condensate from the gasification of wood to be phenols recorded as phenol and organic acids recorded as acetic acid [67]. Table 3.8 shows the resistance of uPVC to acetic acid and phenol at various temperatures.

Copper has good resistance to acidic solutions and is suitable if superior materials are uneconomic or unavailable [56]. The use of copper pipework with brass fittings would give greater flexibility if redesign became necessary and would give greater resistance to temperature and pressure fluctuations than uPVC pipework. It was, therefore, decided to construct the venturi water circuit from 54 mm diameter copper pipework with brass fittings. Small copper and brass fittings up to 25 mm in size are stored in the departmental stores making their acquisition easy.

101

Table 3.8
Resistance of uPVC to Attack From Acetic Acid and Phenol [56]

Acid	Temperature °C			
	24	40	52	70
Acetic	Complete resistance from a 75% solution	Complete resistance from a 25% solution		Resists some attack from a 25% solution
Phenol		Complete resistance from a 20% solution	Satisfactory resistance from a 100% solution	

3.6.3   Venturi Water Circuit Configuration

A schematic flow diagram and photograph of the mark II gasification system showing the water circuit configuration were shown earlier in Figure 3.2 and Plate 3.1. The main limitations on the design of the water circuit configuration were the pump installation guide-lines, the position of the gasifier and the available space under the fumehood.

The suction pipework between the outlet of the disentrainment tank and the inlet connection of the pump was made as short and straight as possible to minimize friction losses. A gate valve was fitted in this pipework to enable isolation of the pump if required. Between the gate valve and the pump, a brass Y shaped line filter fitted with a 100 micron mesh screen (the finest mesh size available) from Reliance Water Controls was installed to prevent any particulate material in the water damaging the pump. The mesh filter is easily removed for cleaning by unscrewing the cap from the filter housing and removing the mesh. The disentrainment tank was placed at a level such that there is always a positive head of water acting on the pump (when the system contains water).

Between the water outlet of the pump and the water inlet of the venturi ejector, a 54 mm (2 inch) needle valve (labelled valve V3 on Figure 3.19) was fitted to control the water flowrate to the venturi and hence the air

flowrate into the gasifier. The suction produced by the venturi can be reduced by closing the gate valve (V3). The water flowrate and pressure to the venturi is monitored using a 65 G Rotameter (stainless steel float) calibrated between 20 and 195 lmin^{-1} of water at 20°C and a Bourdon pressure gauge calibrated between 0 and 10.54 barg (0 and 150 psig).

A pump safety bypass pipe (12 mm diameter copper pipe) was fitted to short circuit the venturi in case the valve on the discharge side of the pump (Valve 3) was left closed with the pump running (see Figure 3.2). This would ensure that sufficient water (at least 7.5% of the full water throughput is recommended by the pump manufacturers) passed through the pump for lubrication and cooling purposes. A gate valve was fitted into this pipe to permit the maximum flowrate of water to pass through the venturi if required. The bypass pipe enters the disentrainment tank at a point below the operational tank water level to prevent re-entrainment of gas into the scrubber water by the jet of water.

To minimize back pressure, the discharge pipe from the venturi was made as short as possible. The discharge pipe from the venturi passes through a right angle before discharging water and gas into the disentrainment tank under the tank water level. This ensures that there is a water seal at this point forming a flame trap.

Soldered joints were used for all bends in the venturi water circuit to provide reliable, water and gas tight seals. Soldered joints are able to withstand pressures of 12.059 barg (175 psig) at a temperature of 38°C to 5.168 barg, 75 psig, at 121°C. Soldered joints were, therefore, considered suitable for the pressures and temperatures expected in this application (not higher than 4.824 barg (70 psig) in the high pressure section of the circuit and approximately 35°C). Other fittings which may require removal for inspection and maintenance were fitted using compression fittings.

3.7   Disentrainment Tank

A disentrainment tank is required to serve as a gas-water separator tank and a water reservoir for the venturi circuit. Three options were considered:

i)   Reuse the existing 25 litre capacity glass QVF vessel used in the mark I Aston gasifier. The inlet and outlet aperture diameters (25 mm) in this

vessel were too small to match the venturi circuit pipework diameter. In addition, the capacity of this vessel (25 litres) was considered to be too small for use with the new gas cleaning system since a water flowrate of 136 l.min^{-1} would result in a water hold up time in the tank of only 11 seconds (a water circulation rate of eight times per minute). Product gas disentrainment efficiency from the water will increase with water residence time in the tank and, therefore, as the tank size increases. The existing disentrainment vessel was, therefore, considered unsuitable.

ii)   Purchase a prefabricated tank. The use of domestic hot water tanks and plastic cold water tanks was considered. Copper hot water cylinders were discounted because there were no suitable apertures to permit cleaning and inspection. Domestic cold water tanks were discounted as the manufacturers stated that they were only suitable for water storage and would not accept any additonal pressure to that exerted by the water. In addition, the tank lids could not be made to provide a gas tight seal.

iii) Fabricate a tank. The construction of specially designed tank would have the advantage of permitting efficient space utilisation within the confines of the fumehood in which the gasification system was to be sited and would permit the tank to be constructed from a suitable material (Section 3.7.4). In additon, suitable features such as a large aperture to permit easy and efficient cleaning could be incorporated into the design. It was decided, therefore, that the construction of a specially designed tank would provide the most suitable solution.

This section describes the design and construction of the disentrainment tank shown in Figure 3.2.

3.7.1   Disentrainment Tank Size

The disentrainment tank was located within the confines of the fumehood as the disentrainment provides a potential source of poisonous gas leakage from the gasification system. The area of the fumehood under which the gasification system was to be sited limited the size of the base of the tank to approximately 60 cm x 60 cm.

The pressure expected within the tank was predicted to be 0.227 barg (3.3 psig) calculated from pressure drop measurements presented by Reyes for the mark I Aston gasification system (see Appendix II) [17]. The tank was, therefore, designed to resist 0.586 barg (8.5 psig) allowing a margin in excess of 100% for safety. Since a cubic tank could be constructed to resist this pressure (Appendix II) permitting a greater water capacity for a given cross sectional area, a cubic design was selected.

The height of the tank was limited by the available height under the fumehood, the height required to fit a drain under the tank (25 cm), the height of the demister (80 cm) to be fitted on top of the tank (Section 3.8) and the remaining headroom under the fumehood (95 cm). Allowing a working height to permit space for connections and maintenance of 40 cm resulted in the tank height of 60 cm.

To ensure that the water level in the tank was higher than the top of the pump, a minimum depth of water in the disentrainment tank of 15 cm is required. The maximum water level in the tank is limited by the position of the connection to the U-tube safety manometer. The maximum water level in the tank is, therefore, 45 cm. This results in a maximum water capacity of 162 litres. At 2.81 barg (40 psig) water pressure (the maximum water pressure predicted for use with the mark II Aston gasifier), the water flowrate through the venturi is 117.4 litres/minute. The disentrainment tank size, therefore, permits a water hold up time of only 1.4 minutes at the maximum expected water flowrate. The water hold up time will increase as the water flowrate decreases, however. As it was not possible to provide a disengagement space above the liquid level equivalent to the representative diameter of the disentrainment tank [72], a knitmesh demister was fitted to the disentrainment tank gas outlet to improve the gas liquid separation (Section 3.8). In addition, a baffle was fitted in the tank (Figures 3.14 and 3.15) to simulate a long tank and hence improve gas liquid separation.

Drawings of the disentrainment tank are shown in Figures 3.14 and 3.15.
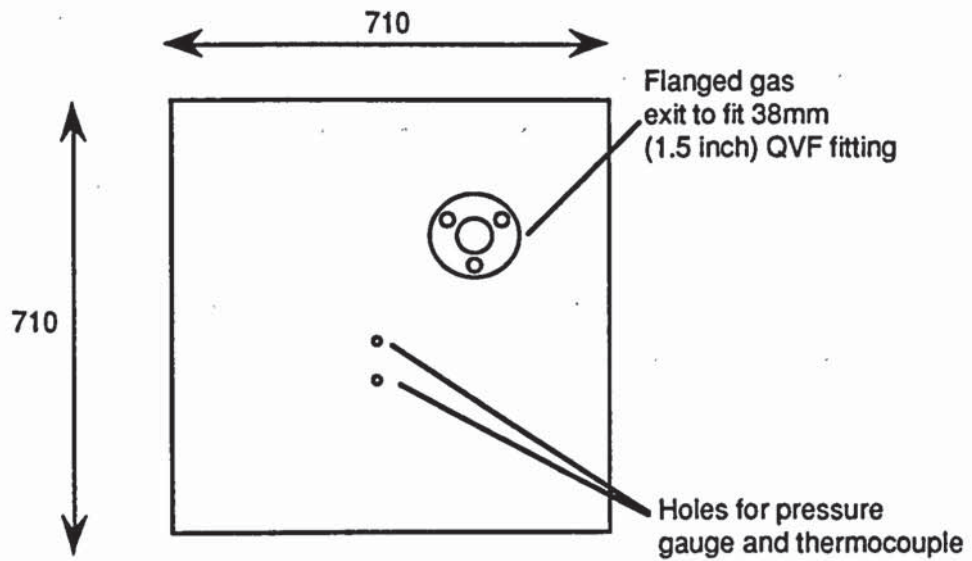
Disentrainment Tank Lid - Top View
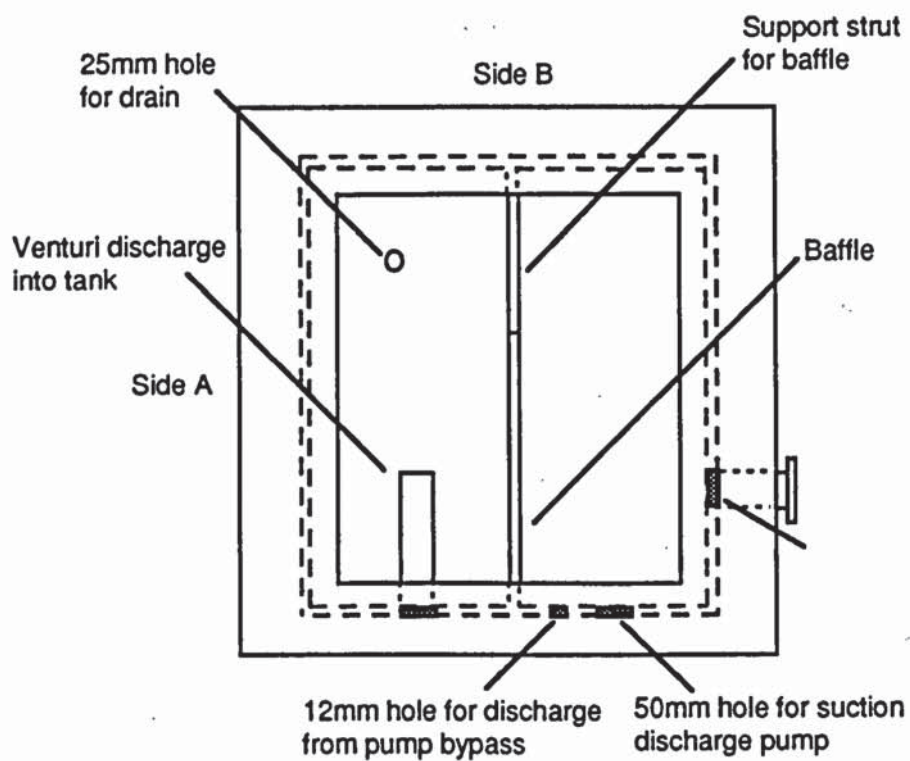
Disentrainment Tank - Top View (Lid Not Fitted)

all measurements in mm

Figure 3.14

Top Views of Disentrainment Tank and Lid
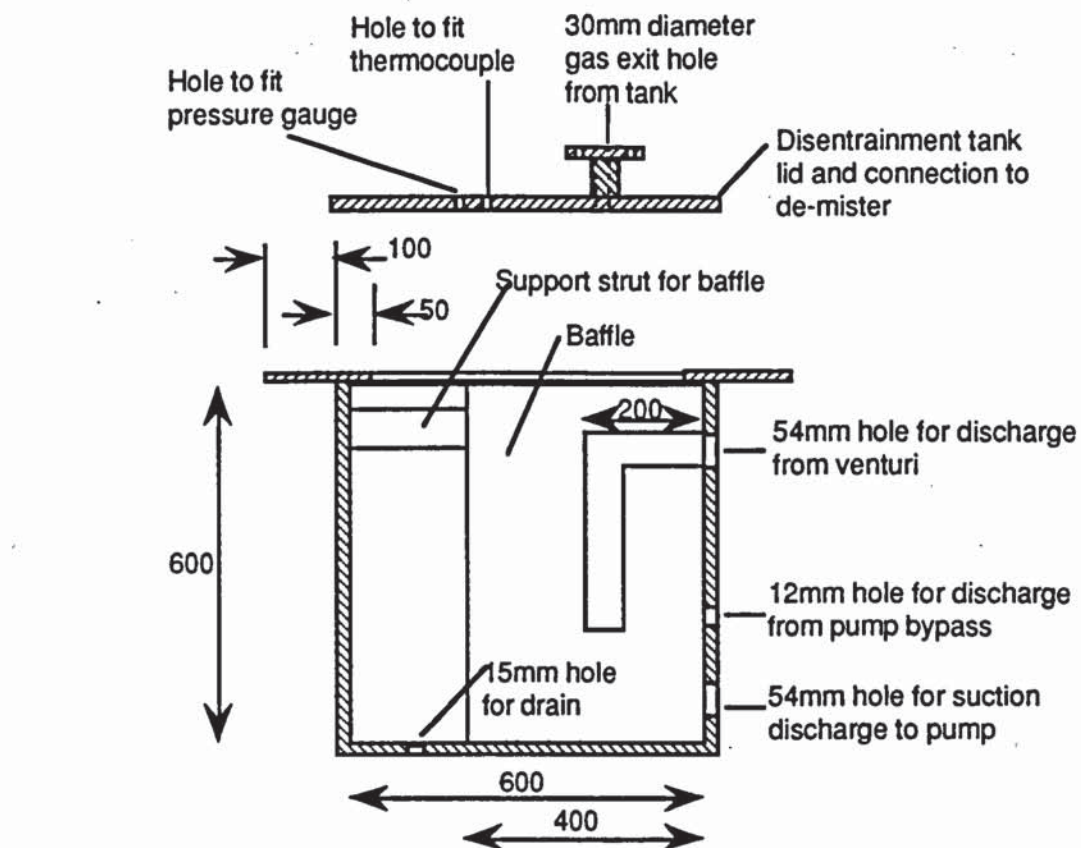
Disentrainment Tank Lid and Disentrainment Tank
Viewed from Side A
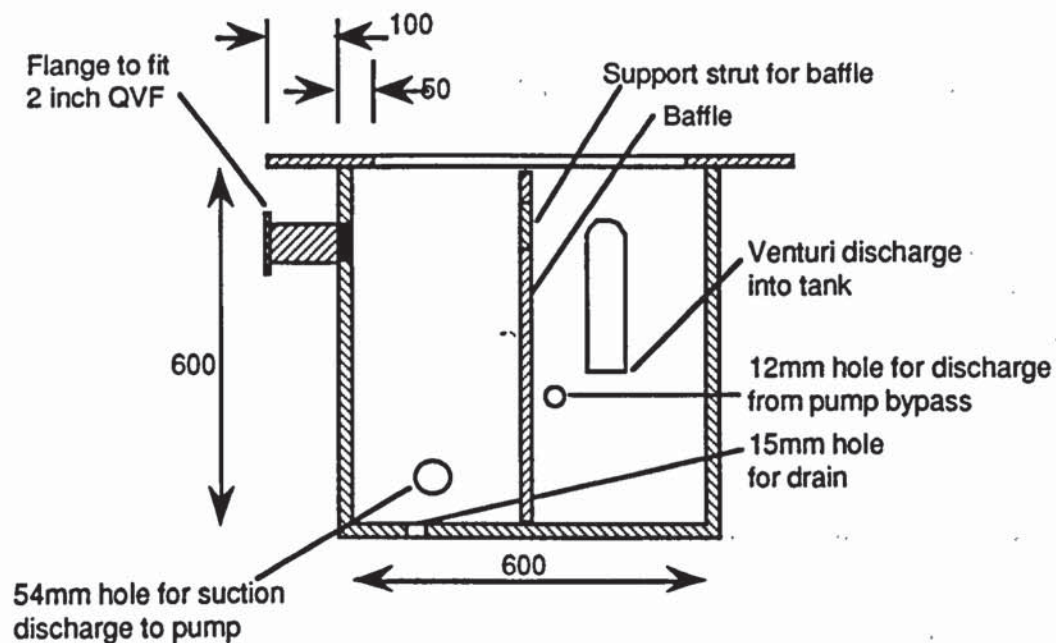
Disentrainment Tank - Viewed from Side B

all measurements in mm

Figure 3.15
Side Views of Disentrainment Tank and Lid

3.7.2   Disentrainment Tank Fittings

Connections between the tank and the 54 mm diameter venturi circuit pipework were made using brass tank connectors permitting the tank and pipework to be separated for maintenance as required. The copper pump safety bypass discharge to the tank was connected in position (again using a brass tank connector) below the expected tank liquid level to prevent re-entrainment of the disentrained product gas by the water entering the tank through the pump safety bypass pipe (Figure 3.2).

A 25 mm (1 inch) diameter drain hole was cut into the bottom of the tank connected to the drains using 25 mm stainless steel pipe. The QVF glass water manometer safety system was connected to the tank using a flanged 54 mm diameter pipe (see Section 3.7.5).

3.7.3   Disentrainment Tank Lid and Gasket

It was decided to fit a full width lid to enable easy access for tank cleaning and maintenance.

The disentrainment tank lid was designed to fit on to the flange on the top of the disentrainment tank. The gasket material originally chosen to effect a gas tight seal between the disentrainment tank and the lid was a PTFE joint sealant (Walflon joint sealant number 256) since it would be resistant to the tars and condensates found in the tank during gasifier operation [73]. The tank seal was tested up to 0.232 barg (3.3 psig) by pressurising trapped air in the top of the tank using a rising water level inside the tank. The tank pressure was monitored for a test period of 60 minutes. During tank pressure testing it was found that the PTFE material did not provide an effective seal since the tank pressure slowly decreased during the pressure test. The second method tried was a rubber seal used with silicone sealant. This system provided an effective seal but was difficult to apply and once sealed, was difficult to remove. The most successful gasket material used was Plumbers Mait - a non setting putty. This was easy to apply, easy to remove and provided an effective seal between the disentrainment tank and its lid.

A 30 mm hole was cut into the top of the lid to permit the disentrained product gas to leave the tank. This size hole would ensure that the gas was travelling at the correct velocity (see Appendix II for calculation) on entrance

to the demister to ensure efficient removal of any water droplets from the gas while minimizing the re-entrainment of water droplets back into the gas (see Section 3.8).

A Bourdon pressure gauge calibrated between 0 and 0.7 barg (0 and 10 psig) and a thermocouple were fitted to the tank lid to give a visual indication of the disentrainment tank gas pressure and water temperature (see Sections 3.11.4 and 3.11.5).

Two methods of clamping the disentrainment tank lid on to the disentrainment tank were considered. These were bolts and quick release clamps. It was decided to use clamps as they would make lid removal easier and faster. 12 Braur V150/2B toggle clamps each capable of remaining shut against 150 kgf were calculated to be necessary for this application (see Appendix II) [74].

3.7.4 Disentrainment Tank Construction Material

Stainless steel (316) was considered to be most suitable for this application due to the expected acidity of the scrubbing water during gasifier operation (see Section 3.5.2). 3.2 mm (1/8 inch) and 6.4 mm (1/4 inch) thicknesses were considered. 3.2 mm thick 316 stainless steel was purchased as calculations predicted that a cubic tank constructed from this thickness of steel would be suitable for pressures up to 0.6 barg (see Appendix II for calculation).

3.7.5 Disentrainment Tank Pressure Relief System

For safety reasons, a pressure relief system was fitted to the disentrainment tank. Pressure relief valves were discounted because tars in the product gas could cause a valve to jam, regular testing is required to ensure correct operation and once used, a valve would require replacement as the seal could have been damaged. Bursting discs are unreliable at low pressures and are susceptible to pressure fluctuations.

A water manometer was selected as it could be built from available materials, could be easily tested, could be easily reset for re-use, could be made quickly and cheaply and was versatile in respect of pressure changes.

As a section of the manometer would be exposed to the same pressure as the tank, it was necessary to ensure that the materials used in the construction of the manometer are able to withstand the maximum pressure expected.

QVF glass tubing is available in a number of diameters. The pressure resistance of various diameters of QVF glass tube is shown in Table 3.9. In this application, pressures up to 0.227 bara (3.3 psig) were predicted. Allowing a 100% margin for safety, any diameter of QVF below 80 mm was considered suitable.

The minimum acceptable manometer diameter was chosen by calculating the size of bursting disk required to give a suitable gas escape velocity [76]. Basing the calculation on air at 25°C and assuming a perfect gas, Equation 3.6 is used to calculate the volumetric discharge rate (m^3h^{-1}) through a bursting disc for low pressure gases (0.07 to 0.3 bara) [76].

$$D_{e_{(air, 25°C)}} = 0.3 \times d^2 \dots\dots\dots\dots\dots\dots\dots\dots\dots[3.6]$$

where:

D_e = Volumetric gas discharge rate, m^3h^{-1}

d = Bursting disc diameter, mm

Table 3.9
Pressure Resistance of QVF Glass Tube [75]

Diameter, mm	Pressure Resistance, bar	
	bara	mmHg (abs)
25	4.0	3001.0
40	4.0	3001.0
50	4.0	3001.0
80	3.0	2250.7
100	2.0	1500.5
150	2.0	1500.5

Table 3.10 gives the approximate times calculated using Equation 3.6 for the expected volume of gas in the disentrainment tank during normal gasifier operation ($0.072m^3$) to escape. The data are illustrated by Figure 3.16.

Table 3.10
Gas Escape Times Through Various Diameter Pipes

Tube diameter, mm	Escape time, seconds
15	3.84
25	1.38
40	0.54
50	0.35
80	0.14

It can be seen that the gas escape time decreases to an asymtotic minimum value above diameters of approximately 50mm. It was, therefore, decided to use 50mm QVF pipe for the water manometer. 50mm QVF pipe would also provide a higher pressure resistance than 80 mm QVF pipe.

Gas Escape Time, seconds

Manometer Diameter, mm
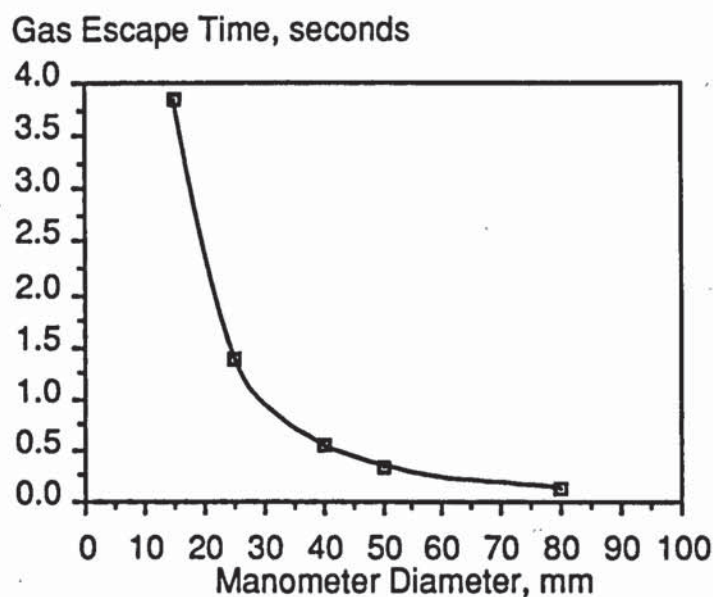
Figure 3.16
Gas Escape Times Through Various Sized Bursting Discs

The laboratory in which the gasifier is sited has a headroom of 3.71 m. The largest length of 50mm QVF tube available in the department was 1 m. In order to minimize the number of joints required, a manometer height of 2.325 m was constructed (giving a total pressure protection to the disentrainment tank of 0.232 barg, 3.31 psig).

The manometer was built on to the back wall of the gasifier outside the fumehood enclosure due to the headroom requirement (see Plate 3.3). The discharge end of the manometer was inserted inside the fumehood enclosure while the gas side of the manometer was connected via a standard QVF connection technique to a flange on the side of the disentrainment tank (see Figures 3.14 and 3.15). The fume extraction system would extract any discharges of gas. Water discharges are directed towards the floor of the fume hood behind the disentrainment tank since this would provide immediate indication of safety valve operation.

Testing the manometer against the maximum operating pressure of the water pump proved this length of manometer to be suitable. During gasifier operation, a larger manometer was not required. However, the facility exists to increase its height, if necessary.

3.8   Demisting Device

Following disentrainment from the scrubbing water, the cleaned product gas saturated with water and carrying water droplets leaves the tank through a hole in the disentrainment tank lid. To protect the instruments fitted downstream of the disentrainment tank, a demisting device was installed.

The original gasification system used a small knitted wire pad fitted into a section of QVF glass incorporated into the disentrainment vessel [12]. The performance of the pad is not reported. However, a knock-out pot was fitted into the copper pipework between the demister pad and the gas pump to remove water from the gas.

Two types of demister were considered in this project. These were a knitted mesh (Knitmesh) pad and a plate demister. The former was chosen as it could be easily and quickly constructed and should provide a more efficient means of water removal (above 99% is reported [72]) with a low pressure drop (usually less than 25 mm H_2O [56],[77]).

112
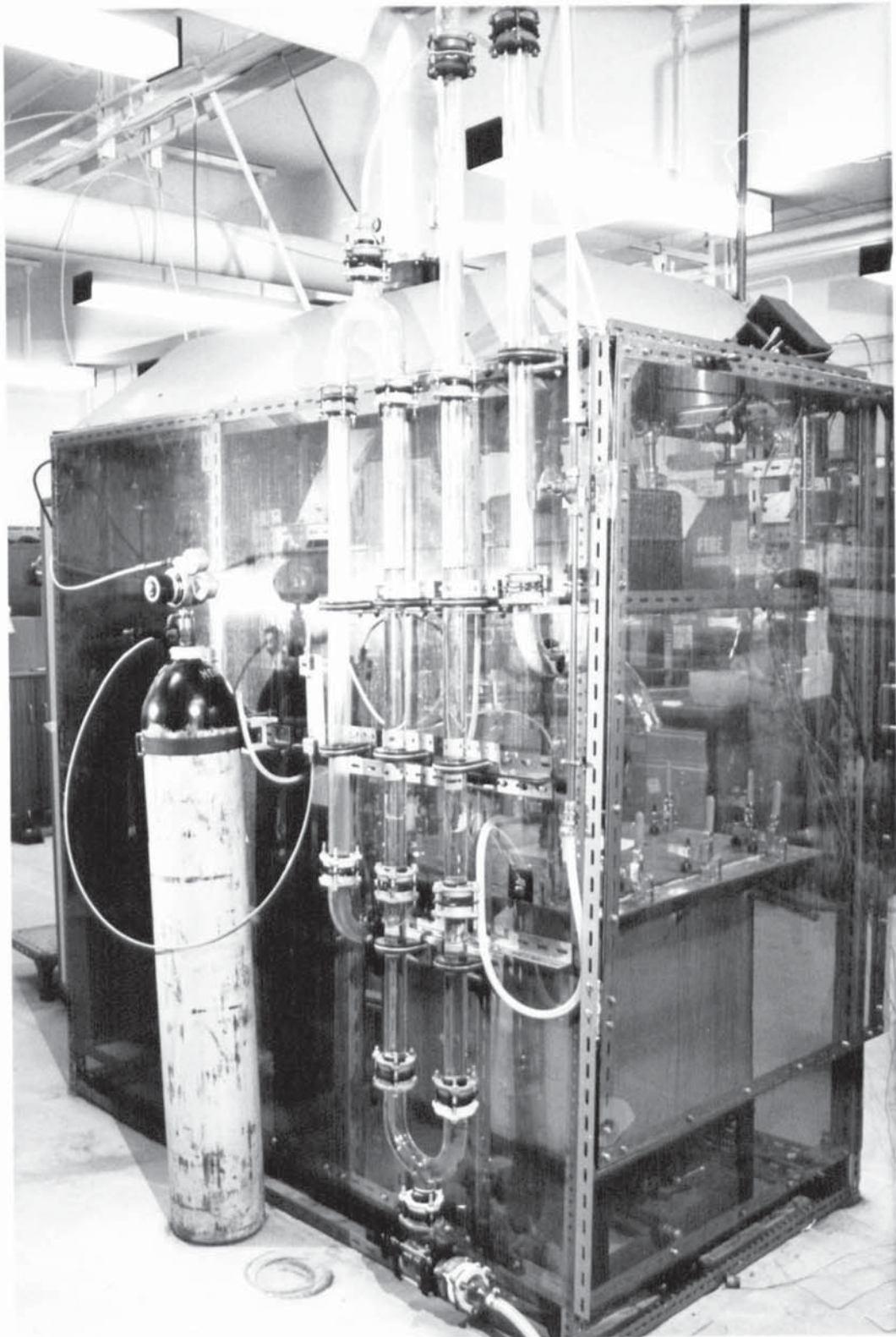
Plate 3.3
Disentrainment Tank Pressure Relief System

Knitmesh consists of knitted fabric of interlocking asymmetrical loops of metal (or plastic) [56]. A high collection efficiency is obtained by inertial and direct impaction (for large particles over 2-3 µm) and by brownian diffusion (small particles less than 2 µm) [56]. Once collected, the water droplets flow down the wires of the knitted pad. At the base of the wires, the liquid droplets are held by surface tension until they become large enough for gravity to exceed the combined effect of gas velocity and surface tension and fall away. There will, therefore, be a minimum and maximum gas velocity between which a demister will operate correctly. Below the minimum velocity, entrained droplets will follow streamlines around the wires in the knitmesh pad and collection efficiency will be low. Above the maximum gas velocity, re-entrainment of the removed water droplets will occur [77].

The three basic principles involved in separation (impingement, coalescence and drainage) are all affected by the velocity of the gas stream through the demister. The basic design is assessed to meet gas velocity requirements. The sizing calculations to calculate the size of the demister are shown in Appendix II. A drawing of the demister constructed from QVF glass is shown in Figure 3.17.

The diameter of the gas entry pipe to ensure the correct gas velocity through the demister was calculated and found to be 30 mm (Appendix II) [77]. A 30 mm hole was cut into the disentrainment tank lid and a fitting constructed to connect the QVF demister to the disentrainment tank lid. Finally, the expected pressure drop through the Knitmesh pad was calculated and found to be 1.02 mmH$_2$O (g) [77].

3.9   Gas Pipework Sizing
This pipework is used to transport the cleaned product gas from the demister exit to the lean gas burner (see Section 3.10) while minimising the pressure drop between the demister and burner.

3.9.1   Pipe Construction Material
Of the piping materials readily available (copper, mild steel, stainless steel, PVC), copper was selected for ease of construction and corrosion resistance from condensation products.

114

Gas to burner

25mm (1") QVF fitting
to fit 22mm copper pipe

Knitted mesh pad

150mm

200mm (8") diameter
QVF cylinder

Gas in from 30mm
hole in disentrainment
tank lid
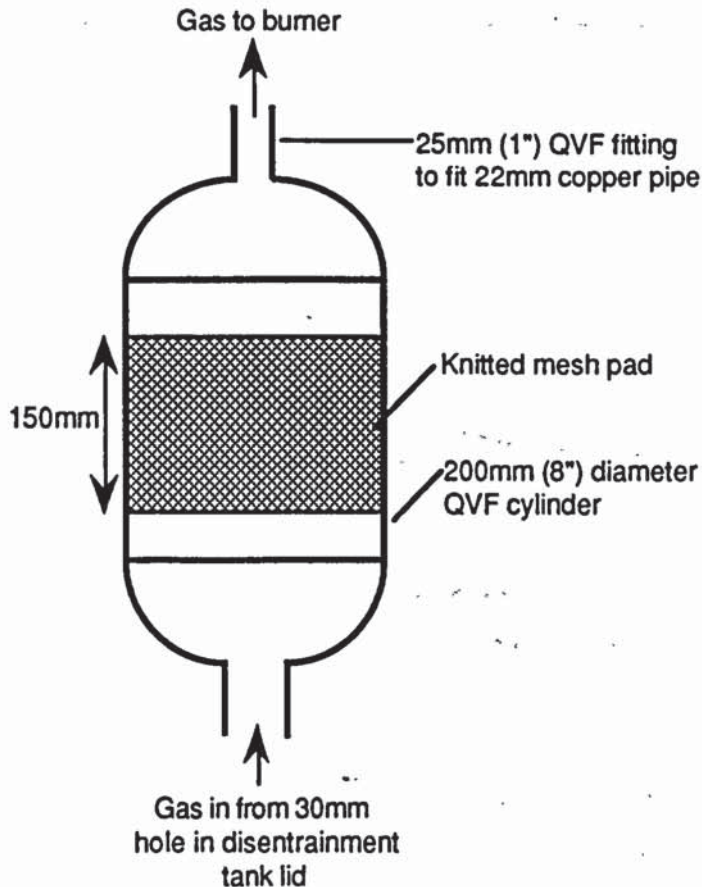
Figure 3.17
Diagram of Demister

3.9.2   Pipe Size and Fittings

The pipework between the demister and lean gas burner was built as
smooth and as straight as possible with the minimum number of bends and
changes in pipe diameter to minimize the back pressure acting on the
venturi ejector. As existing equipment was fitted with 22 mm fittings, 22 mm
pipework was used where possible minimizing changes in pipe diameter. It
can be seen from Figure 3.18 that there is little difference in the power
required to pump gas through pipes above 22 mm in this application.

A tapping downstream of the gasmeter is used for gas sampling (see Figure
3.2). Iso-kinetic sampling is not required in this case since only gas is being
sampled [56].
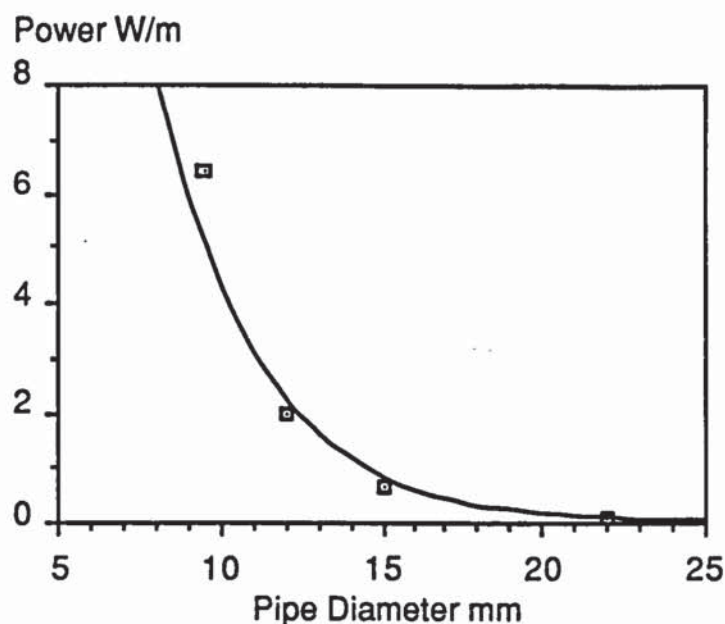
Figure 3.18
Power Required to Pump Air Through Copper Pipe

3.10 Lean Gas Burner

Due to the poisonous and explosive nature of the product gas, it is necessary to flare it. The existing lean gas burner was apparently effective and trouble free and was retained [12]. It contains a pilot light, a pilot light failure alarm and flame trap.

3.11 Instrumentation

An efficient and comprehensive system of monitoring the process parameters of the gasification system is required to enable a reliable evaluation of the the system performance to be made. This section describes the instrumentation used in the gasification system. A piping and instrumentation diagram is shown in Figure 3.19 (the key to the diagram is shown in Appendix IV). The symbols used are those listed by Austin [78].

3.11.1 Gas Analysis

The primary objective of a gasification system is to produce a fuel gas. The gas composition should be known to evaluate the gas heating value and mass and energy balances. The original Aston gasification system utilized a dedicated on-line analysis system detecting hydrogen, carbon monoxide, carbon dioxide and methane.
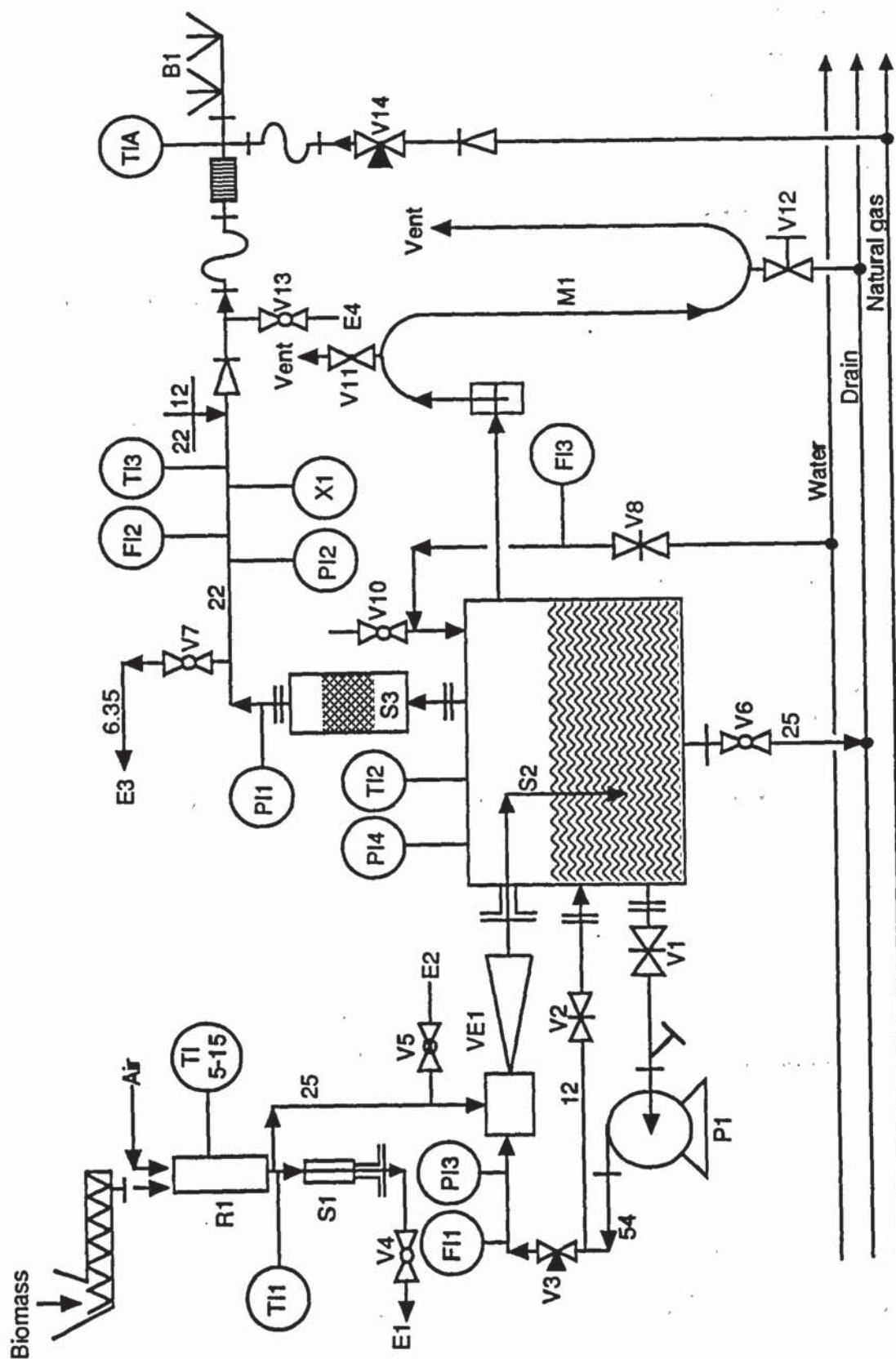
Figure 3.19

Piping and Instrumentation Diagram of Gasification System
For key to diagram, see **Appendix** IV

3.11.1.1 Gas Analysis System Description

The gas analysis system consists of a stand alone analyser cubicle unit housing four separate gas analysers. Hydrogen is detected using a Leybold-Hereaus Hydros thermal conductivity meter calibrated between 0 and 25%. Carbon monoxide, carbon dioxide and methane are detected using MSA Lira 3000 infra red meters calibrated between 0 and 25% (carbon monoxide), 0 and 30% (carbon dioxide) and 0 and 10% (methane). Figures 3.20 and 3.21 are flow diagrams of the analyser cubicle. These analysers were recalibrated prior to each experimental run. The nitrogen concentration of the product gas is calculated by difference.

In addition to an analogue display, each meter produces an electrical output of between 0 and 100 mV which is proportional to the gas composition. This signal is recorded using the BBC datalogging system (see Section 3.11.8).

Prior to the start of experimental work, the MSA analysers were overhauled by the manufacturers.

FSC: Final sampling conditioning unit
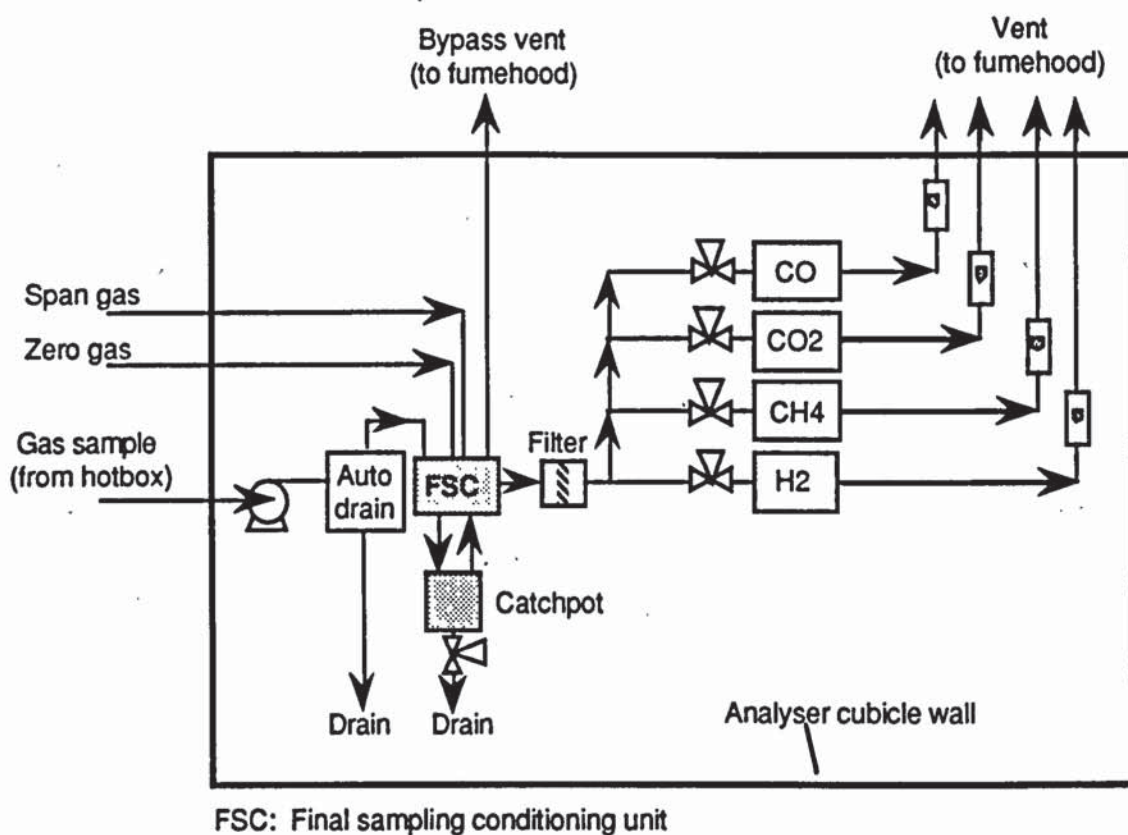
Figure 3.20

. Analyser Cubicle Flow Diagram [12]

118
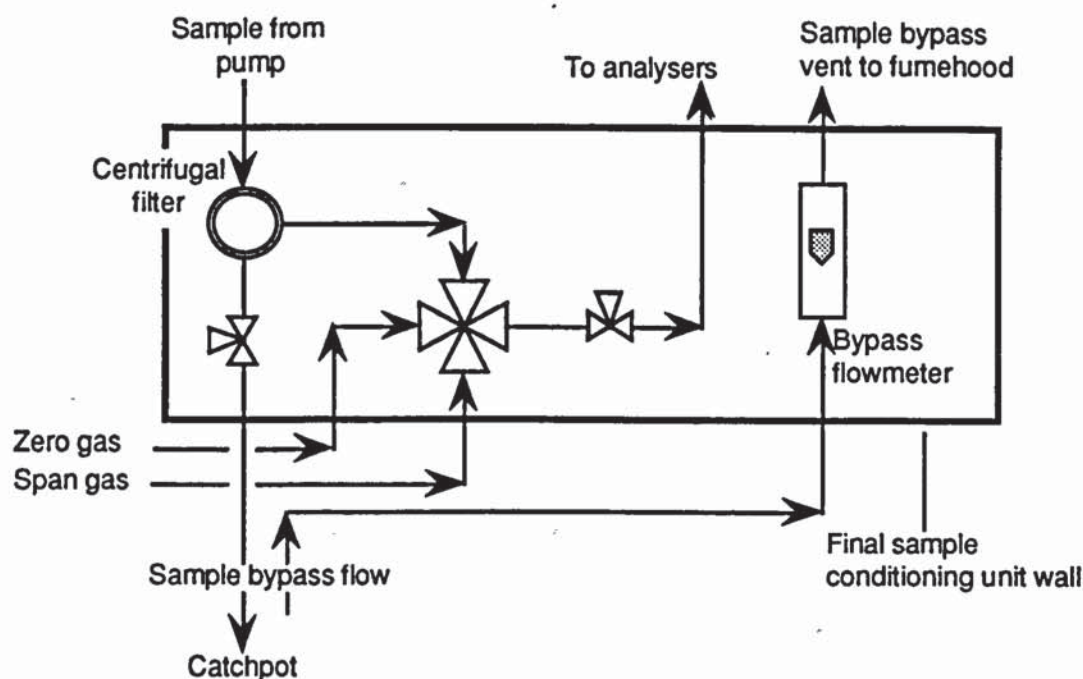
Figure 3.21
Final Sampling Conditioning Unit Flowsheet [12]

3.11.1.2   Gas Sample Port and Clean-Up Unit

Static tap sampling ports act as convenient 10 micron inertial pre-filters [2]. Earp initially sampled gas from a position just downstream of the heat exchanger (as shown in Figure 3.1). This reduced the time lag between sampling and analysis. However, gas sampling could only take place for 45 to 60 minutes since the U-tube filled with silica gel through which the gas sample stream was passed before entering the gas analyser cabinet became overloaded with tars [12]. To make operation easier and to permit gas analysis to operate for longer periods, Earp moved the gas sample point to a position between the scrubber and gas pump (see Figure 3.1) [12]. In this arrangement, the gas analysis system worked satisfactorily [12]. It was, therefore, decided to sample gas from a position just downstream of the cumulative gasmeter to permit the gas analysis system to operate for long periods of time (see Figure 3.2).

Figure 3.22 shows a diagram of the primary gas clean-up unit (hotbox) used to prepare the sampled gas for analysis (Perma Pure model 4112). The gas sample entering the hotbox firstly passes through a heated (120°C), sintered stainless steel, bypass filter which is claimed to remove condensible liquids and particulates down to one micron [79]. The sample bypass is then vented to the fumehood with the eductor air.

119
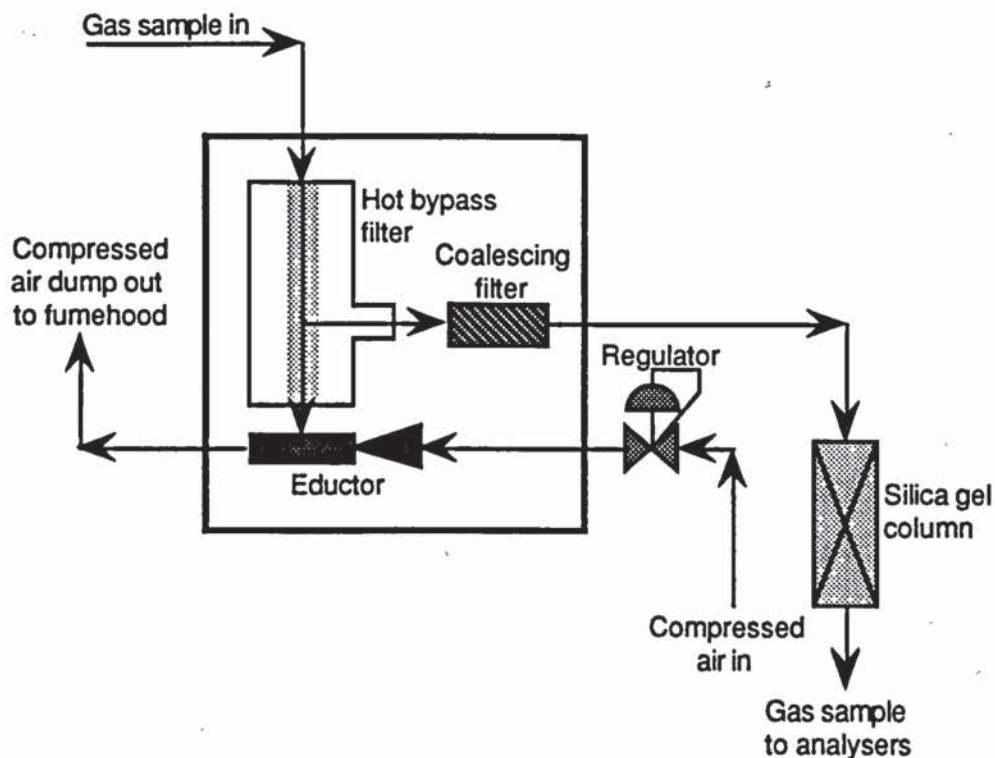
Figure 3.22
Gas Sample Clean-Up System Flow Diagram [12]

The filtered gas (approximately 4 lmin^{-1} out of a total of 10 lmin^{-1} sampled) then passes through a wound string filter. An additional silica gel column was fitted between the hotbox and the analyser cubicle to prevent tars entering the analyser cubicle and was found to be effective (tested by noting the colour of a filter cartridge in the sample line inside the analyser cubicle at regular intervals). The silica gel column would also absorb any moisture present in the test gas stream.

During the course of this project, replacement wound string filters of the correct design for the coalescing filter could not be obtained. A new coalescing filter housing was, therefore, fabricated from stainless steel to house the new filters supplied by Perma-Pure. This new filter housing was found to be more effectively sealed against air ingress than the previous Perma-Pure item. This system operated well and no filter clogging was experienced.

3.11.1.3 Batch Gas Analysis

To check the accuracy of the gas analysers and to detect the levels of gases other than hydrogen, carbon monoxide, carbon dioxide and methane, a

batch gas sampling system was used. Gas was sampled using gas sample bags from a gas sampling port upstream of the lean gas burner at valve 13 (see Figure 3.19). Due to the accumulation of water in the sample pipe leg, it was necessary to open valve 13 prior to sampling to prevent water entering the sample bag. The sampled gas was then analysed by gas chromatography.

3.11.2   Gas Flowrate

Two types of instruments were used to measure the flowrate in the original Aston gasification system. These were a Platon Flowbits CMIE Rotameter with an analogue display and analogue electrical signal directly proportional to the gas flowrate; and a standard gasmeter.

The Platon flowmeter records gas flowrates over the range 0.8 to 8.0 m^3h^{-1} for air at atmospheric pressure (760 mmHg) and at a temperature of 20°C [12]. It was positioned downstream of the demister (see Figure 3.2) in a vertical position with straight pipe 5 diameters in length upstream of the flowmeter and straight pipe 2 diameters in length downstream of the flowmeter [80].

The gasmeter was used to measure the cumulative volume of gas produced. For more accurate determinations of gas flow through the gasmeter, it is fitted with a test dial. Each revolution of the test dial corresponds to one cubic foot of gas at 50 mbar and room temperature [81].

3.11.3   Water Flowrate and Pressure Through Venturi

The air flow rate into the gasifier is controlled by altering the water flowrate into the venturi ejector (Section 3.4.2.1). To aid control of the gasifier, a 65S Rotameter (stainless steel float) and a Bourdon pressure gauge were installed downstream of the water pump.

3.11.4   Gas and Reactor Temperatures

Temperatures throughout the gasification system were collected to provide data for gasifier control, gasification process analysis and for the preparation of mass and energy balances. The datalogging equipment permits the use of up to 15 thermocouples. Type K thermocouples were used for all temperature measurements. Table 3.11 and Figure 3.19 give the positions of the thermocouples fitted to the gasification system.

Table 3.11

Gasifier Thermocouple Positions

Thermocouple number	Position
1	Gas temperature below grate
2	Water temperature within disentrainment tank
3	Gas temperature at gasmeter
4	Air inlet temperature to gasifier
5	Search thermocouple used to measure in-bed temperatures
6	Used to measure gasifier outside temperature
7	Used to measure gasifier outside temperature
8	Used to measure gasifier outside temperature
9	Used to measure gasifier outside temperature
10	Used to measure gasifier outside temperature
11	Used to measure gasifier outside temperature
12	Used to measure gasifier outside temperature
13	Used to measure gasifier outside temperature
14	Used to measure gasifier outside temperature
15	Used to measure gasifier outside temperature

It is important to monitor the vertical temperature profile through the gasifier as it helps to locate the positions of the various zones through the reactor and indicate the effects of feed properties on the gasification process. Earp had difficulties measuring the vertical temperature profile through the reactor. He initially used an array of three 1 mm diameter stainless steel thermocouples sheathed in a stainless steel tube [12]. It was found that it was difficult to move the array of thermocouples up and down the tube when the array was in position within the reactor and to accurately locate the position of the three thermocouples [12]. It was replaced with an array of 7 stationary 1 mm diameter stainless steel sheathed thermocouples placed at 30 mm intervals from 0 to 180 mm above the grate. However, this system caused problems with biomass flow through the reactor and damage to thermocouples occurred [12]. In this project, a search thermocouple was used to measure the internal vertical temperature profile of the gasifier. A single 1 mm stainless steel thermocouple was fitted into a stainless steel sheath. This search thermocouple was positioned along the vertical central

axis of the reactor. No problems were encountered with the flow of biomass through the reactor with the search thermocouple in position and thermocouple location was relatively simple. However, measuring the temperature profile through the reactor using this method was time consuming and only one temperature at one position at a time could be obtained. When measuring the gasifier vertical temperature profile using the search thermocouple, it was important to ensure that the reaction zone was stationary. In addition to the search thermocouple, a disappearing filament pyrometer was used to monitor the maximum gasifier temperatures.

It was initially decided to measure the external uninsulated gasifier temperatures using thermocouples strapped to the external surface of the gasifier using metal straps. To prevent errors due to convection effects, small pads of mineral insulation were used. However, due to the high temperatures around the gasifier, the metal straps rapidly burnt out. To estimate the uninsulated gasifier heat loss, therefore, the gasifier vertical temperature profile measured using the search thermocouple was used.

During the runs where the insulated gasifier was used, the external temperature of the insulation applied to the gasifier was measured using thermocouples inserted a small distance (approximately 1 mm) into the insulation and held in place using silicone sealant. This method proved to be satisfactory.

Due to the small diameter of the Aston gasifier and the difficulties encountered by Earp when inserting a number of thermocouples into the gasifier during operation, no attempt was made to measure the radial temperature distribution through the reactor.

3.11.5   Gas Pressure
The gas pressure is monitored at three positions. A Bourdon pressure gauge is used to monitor the disentrainment tank pressure (psig) while the gas pressure at the demister and at the gasmeter (see Figure 3.19) are measured using two pressure transducers (Data Instruments - Model AB) giving an analogue signal of 0 to 100 mV inversely proportional to the measured pressure [12].

3.11.6 Feed Rate

Two methods were used to measure the feedrate to the gasifier. Initially, the Accurate dry material feeder was used. This was calibrated prior to each run to enable the average feedrate to the gasifier to be measured (Section 3.2). However, fuel feed control using the Accurate feeder was difficult. In additon, the feeder was unsuitable for use with the standard case feed (Section 4). Batch feeding was used, therefore, for the majority of runs performed.

3.11.7 Char Bed Height

Earp suggested that the height of the char bed in an open-core gasifier is an important parameter (see Section 2.8.2) [12]. It was thought necessary to investigate its effect on gasifier performance since gasifier performance data collected by Earp were not collected during stable gasifier operation. The height of char bed was measured using a 30 cm steel ruler mounted by the side of the reactor.

3.11.8 Data Recording

Earp purchased an automatic datalogging system for the Aston gasification system [12]. It was proposed to re-use this system in this project as no previous difficulties had been noted. The datalogging system records all the output data produced by the four gas analysers, two pressure transducers, the Platon flowmeter and up to 15 thermocouples.

3.11.8.1 Data Logging Hardware

The datalogging hardware system consists of three main components. The Biodata Microlink interface conditions and digitizes the analogue signals from the thermocouples, flowmeter, pressure transducers and gas analysers before passing it on to a BBC microcomputer via the IEEE 488 databus (a physical link between two or more devices). The BBC microcomputer controls the Microlink interface, the flow of data over the IEEE 488 databus, converts the digital signals to the appropriate instrument reading, displays the readings on its screen and writes the data to floppy disc [12] (see Figure 3.23). The datalogging hardware appeared to work well during the previous project and the system was reused in this project without modification.

124

Gas flowrate   Temperatures   Pressures   Gas compositions

Flowmeter   Thermocouples   Pressure
                              Transducers   Gas Analysers

Analogue Inputs
(Voltage Signals)

Microlink

IEEE 488 Databus

BBC Microcomputer

VDU   Magnetic
       disc storage   Printer

Key to digital signals

Control signals   Data transfer
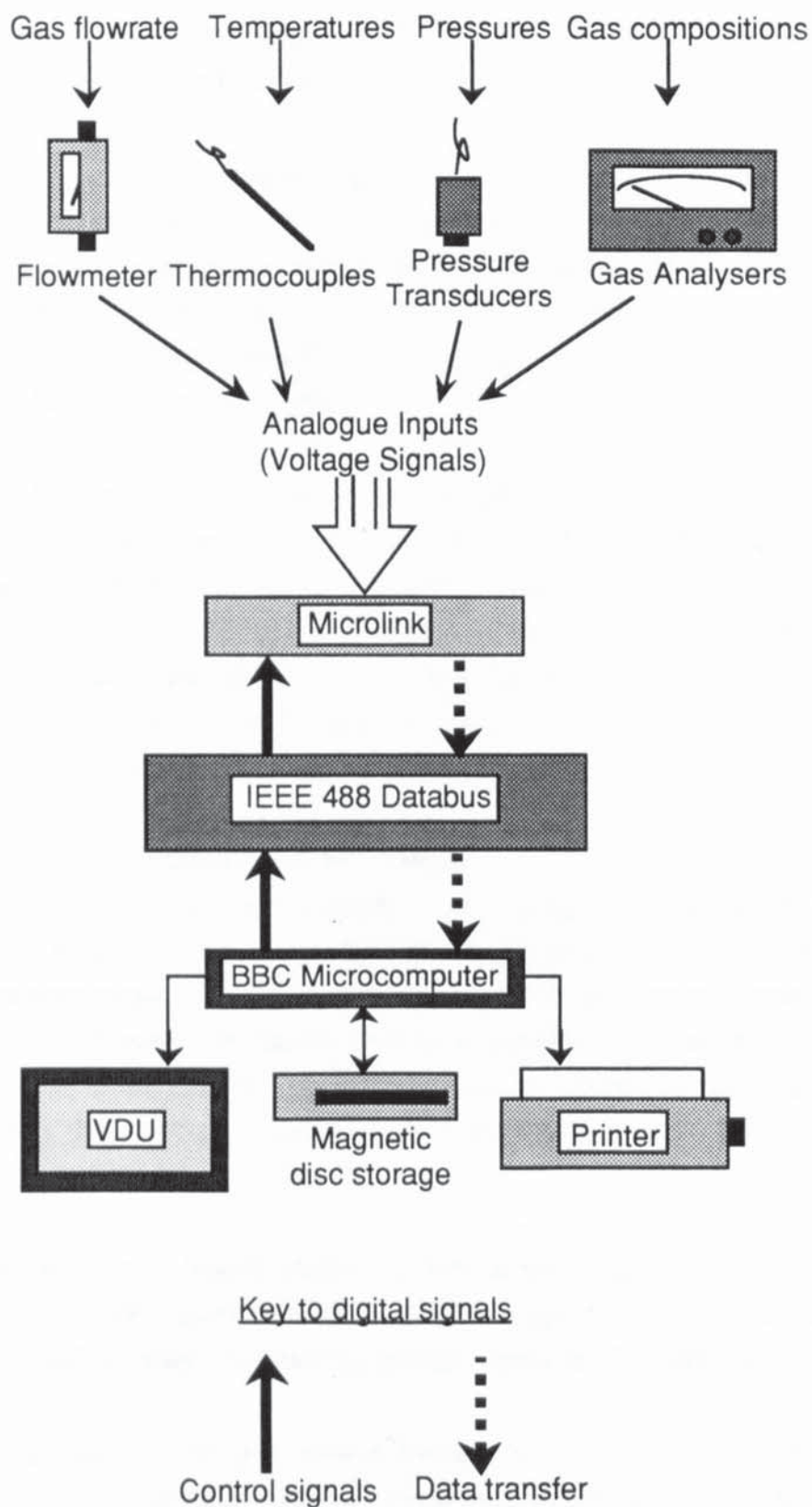
Figure 3.23

Data Logging System (Hardware) Flow Diagram [12]

The design and construction of the data logging hardware is not covered under this project and is discussed in greater detail by Earp [12].

3.11.8.3   Data Processing

Analysis and plotting of the data collected by the data-logging equipment was previously carried out using the GINO routines on the University's VAX 8650 Cluster system using the Kermit file transfer system to transfer the ASCII data files from the BBC microcomputer to the VAX via the University's Accent local area network [82].

Due to the author's experience with spreadsheets and personal computers, it was decided to analyse and plot the data collected using commercially available Macintosh software. Kermit was used to download the data from the VAX mainframe computer to an Apple Macintosh. Using a text processor the ASCII data files were converted to a tab delimited form. They were then loaded into Excel 2.2 and saved in Excel format. Graphs were produced using Cricket Graph 1.6.

3.12   Experimental Safety

The primary intention of this section is to highlight the necessary precautions required to ensure that the downdraft gasification system used in this project is operated safely and that experiments are carried out in a safe and reliable manner to prevent accidents and to safeguard the operators. A process should be designed to prevent dangerous situations developing and to minimize the consequences of any incidents that arise from the failure of safeguards built into the system.

In addition to this safety section, a Hazop analysis has been carried out to highlight the operability of the gasification system and to indicate potential hazards which may arise during gasifier operation (Appendix VI).

The operation of this gasification system is potentially hazardous since the products of gasification are both toxic and flammable. The hazard analysis was carried out by considering the following headings [72]:

i   Identification and assessment of the hazard

ii   Control of the hazards. For example, by containment of flammable and toxic materials

iii   Control of the process. Prevention of hazardous deviations in process variables by provision of alarms and trips etc. together with good operating practices and management

iv   Limitation of the loss. The damage and injury caused if an incident occurs: Pressure relief, provision of fire fighting equipment etc.

3.12.1   Feedstock Considerations

During wood preparation is was necessary to be aware of the danger from wood splinters, wood dust, noise and fast moving machinery (from the granulating machine and bandsaw). Following chipping the wood was sieved to extract the undersize and oversize fractions. During wood preparation, dust masks, goggles and laboratory coats were worn for protection from airborne dust. In addition, ear-plugs and leather gloves were worn when using the granulating machine and bandsaw.

The storage of wood and wood chips in the laboratory presented both fire and dust explosion hazards. No figure is given for the minimum explosion concentration of wood in any form in a report on Explosivity Tests for Industrial Dusts by the Joint Fire Research Organization [83]. Only small quantities of wood (up to 10 kg) were stored and sieved in the laboratory at any one time and the cutting and chipping operations were carried out in other laboratories. The risk from this hazard was, therefore, minimal.

3.12.2   Gasification Considerations

Biomass gasifiers produce a number of products which are toxic and flammable.

3.12.2.1   Gaseous Gasification Products

This mixture of gases produced by a gasifier are toxic and flammable (Table 3.12). Carbon monoxide is a colourless, odourless, tasteless and highly toxic gas. The long term occupational exposure limit for this gas is 50 ppm for an eight hour day, five day week and in the short term, 400 ppm (10 minutes) [84].

Table 3.12
Typical Gasifier Gas Composition with Associated Toxic Effects

	Typical Product Gas Composition % vol, dry	Toxic Effects
Hydrogen	11.0	Asphyxiant
Carbon Monoxide	15.5	Poisonous
Carbon Dioxide	17.0	Asphyxiant
Methane	1.3	Narcotic at high concentration in the absence of oxygen
Nitrogen	55.2	Asphyxiant

The other constituents of the product gas are not toxic. However they do form a potential hazard mainly as asphyxiants (see Table 3.12). The product gas also presents an explosion (with or without fire) and/or fire hazard in the event of a gas leak out of or an air leak into the gasification system. The flammability limits (ie the lowest and highest concentrations at normal temperature and pressure at which a flame will propagate through a mixture) of the flammable constituent gases in air in the mixture are given by Table 3.13.

Table 3.13
Flammability Limits of Gases in Air [85]

Component	Flammability Limits, %		Ignition Temperature
	Lower	Upper	°C
Hydrogen	4.0	74.2	585
Carbon monoxide	12.5	74.2	609
Methane	5.0	15.0	537

Four safety precautions have been incorporated to minimize the risk of a gas leak, to warn of a gas leak, to minimize the effects of a gas leak and to allow emergency action to be carried out in the event of gas leak. Some of these precautions will also apply to those for fire and explosion protection.

i   The system has been sited within the confines of a fumehood (which was tested prior to use).

ii   The system has been designed to be gas tight. During cold commissioning, the pressure of the system was raised to 0.227 barg, 3.3 psig (50% above the expected operating pressure) using air and the pressure monitored for 30 minutes using a pressure transducer. Soapy water was used to detect any leaks.

iii A Crowcon Toxiguard carbon monoxide alarm previously purchased [12] was used to warn of excess levels of carbon monoxide in the laboratory. During normal operation with levels of carbon monoxide below 50 ppm the alarm gives a slow clicking sound. If the carbon monoxide level rises above 50 ppm, then the tempo of the alarm starts to rise. Levels of carbon monoxide of 200 ppm and above causes the alarm note to change to a 'siren' and a warning light flashes. During gasifier operation, this alarm was placed on the computer stand next to the operators' position. Prior to the the start of the experimental work, this alarm was re-calibrated and overhauled by the manufacturers. The alarm was tested prior to each run or weekly - whichever was the more frequent.

iv   The laboratory is equipped with a compressed air breathing apparatus to allow emergency procedures to be effected should the atmosphere within the laboratory become unsafe. This was serviced prior to the start of this project.

The same precautions used to prevent toxic gas leaks will also reduce the risk of fire or explosion due to escaping gas. However, other precautions were necessary to reduce the danger of explosion as a result of high pressure.

The system is protected from high pressure explosions by a water manometer fitted to the disentrainment tank constructed from 50mm diameter QVF glass tube (itself capable of withstanding up to 4.0 barg [86]). This permits the tank to reach a pressure of 0.227 barg (3.3 psig) before the water is blown out of the U-tube and into the fumehood enclosure relieving the pressure in the disentrainment tank (see Section 3.7.5). Calculations show that the pressure relief should take approximately 0.35 seconds [76]. Following such a release of pressure, all persons should leave the

laboratory leaving one person wearing breathing apparatus to shut down the gasification system and make the laboratory safe.

An explosion port was built into the plastic shielding around the gasifier to direct the force of any explosion away from the operators. Any major release of water due to the tank failing would be contained within the area of the gasifier by a 30 mm high bund surrounding the gasifier.

The system is fitted with two flame traps to prevent the propagation of flames through the system should the flame from the burner flash back. The first forms an integral part of the lean gas burner and consists of a chamber partly filled with glass beads and water while the second results from the fact that the venturi ejector discharges water and product gas below the water level in the disentrainment tank.

The system is also fitted with a burner pilot light alarm consisting of a thermocouple placed in the pilot flame. Using a set point controller (set at 100°C), a red warning light indicates whether the pilot light is lit.

3.12.2.2 Liquid Gasification Products

The pyrolysis liquids or tars produced, although low in volume, require attention as they are made up of a number of toxic and, by analogy with coal pyrolysis and mineral oils, carcinogenic compounds [87],[88],[89]. The water miscible liquid products will contaminate the scrubber water causing it to become toxic. Hence, care will be needed when handling the scrubber water and when cleaning the gasification system after a run - especially the interior of the disentrainment tank.

Little is known about the effects of breathing in gasification oil vapours or oils over extended periods or in high concentrations [88]. However, it must be assumed that breathing in pyrolysis oils and skin and eye contact with pyrolysis oils should be avoided.

3.12.2.3 Solid Gasification Products

During operation, there will be three types of solid product requiring handling, ash, char and unreacted feed. The amount of ash produced is extremely small while the small amount of unreacted wood remaining was

returned to the feed storage bin. Partially reacted wood was disposed of safely.

Small quantities of char mixed with ash (approximately 100 g) remain in the reactor after each run. This was sieved (following the removal of any unreacted feed) to produce start-up fuel for the next run during which time dust was produced (for approximately ten minutes). No figures for the minimum explosive concentration of wood charcoal are available although the minimum ignition temperature is reported to be 470°C [83]. Although the explosive hazard was considered small, sieving operations were found to be uncomfortable and inhalation of the dust from wood charcoal was avoided by the use of dust masks. Excess char/ash mixtures were disposed of regularly and not permitted to build up in the lab.

3.12.3 General Laboratory Safety Considerations

In addition to the precautions already discussed, clear access was maintained around the gasifier at all times to permit fast and efficient laboratory evacuation if required.

A weekly record of the testing and condition of the laboratory safety equipment was kept . This recorded the last service date and results of the regular tests carried out on the Crowcon carbon monoxide alarm, the condition and last service date of the laboratory fire fighting equipment, the condition and last service date of the laboratory breathing apparatus and the presence of the laboratory eye-wash bottle.

Start-up and shut-down procedures were drawn up to ensure safe and efficient gasifier operation (see Appendix V). During gasifier operation, the Crowcon carbon monoxide alarm and disentrainment tank pressure should be continuously monitored. Any deviations from normal operation should be immediately investigated.

A clear set of emergency shut down instructions were drawn up and copies were placed on the gasification rig, next to the fire extinguishers and next to the laboratory entrance.

3.13 Summary

A gasification system incorporating an open-core downdraft gasifier constructed from transparent quartz glass has been extensively modified to permit easier, safer and more reliable operation. The primary modification involved the replacement of the previous gas pump, gas scrubber and gas cooler with a venturi ejector which carries out the gas moving, cooling and scrubbing functions in one process stage.

An on-line dedicated gas analysis system is used to continuously monitor the levels of hydrogen, carbon monoxide, carbon dioxide and methane in the product gas. The output from the gas analysers together with data from other instruments is recorded using a microcomputer based data-logging system.

In addition to a description of the modifications made to the gasification system, the design process involved a HAZOP analysis and a system safety evaluation.

4. FEEDSTOCK SELECTION, PREPARATION AND CHARACTERIZATION

This chapter describes the selection, preparation and properties of the feedstocks used in this project. Variations in feedstock characteristics such as moisture content, ash content, particle size and shape will effect the gasification process [6]. When selecting a feedstock for a particular gasifier, therefore, consideration must be given to these characteristics to ensure satisfactory performance.

4.1 Feedstocks Selection and Preparation

Due to the difficulties encountered in the previous project due to poor feedstock flow through the gasifier and the resultant voiding and bridging in the bed causing the reaction zone to slope, it was decided to obtain a spherical feedstock for use as the standard case feedstock. A spherical feed would exhibit superior flow characteristics through the gasifier and would enable a more exact comparison to be made with computational models of gasification which assume particles to be spherical.

4.1.1   Feed A - Beads

A suitable specification was firstly established. A spherical wooden feed was required with a diameter of less than 10 mm at a reasonable cost. It should have no varnish or paint coating or be impregnated with any oils. The presence of a hole through each bead was acceptable although it was preferred that there be no holes. The type of wood was of secondary importance. Assuming a gasifier feedrate of 1.83 kgh^{-1} (the maximum feedrate used by Earp and Reyes [12],[17]) it was calculated that approximately 1250 15 mm diameter beads would be required per hour (a 15 mm diameter bead was available for calculation purposes).

Various sources were selected to find beads. These were local craft shops and craft shop suppliers, builders merchants, manufacturers of wood products and educational timber suppliers.

Craft shops and craft shop suppliers were able to supply beads in a number of suitable sizes (<10 mm diameter) but they were supplied with holes and varnished. It was not possible to obtain from any craft shops the names of their suppliers. An educational timber supplier was also unable to provide beads or balls.

Builders merchants were not able to supply spherically shaped wood. However, the addresses of two manufacturers of wood products were obtained from one builders merchant. Both local companies contacted, however, were unable to produce the quantities of beads required. Other companies contacted, however, produce beads which are impregnated with oils. Of these, a supplier was found who could supply birch beads in sizes 15, 19, 22 and 25 mm diameters. Due to the difficulty of obtaining any beads, it was, therefore, decided to purchase 1000 15 mm (5/8 inch) diameter beads for test.

As it was not possible to obtain sufficient quantities of beads for the duration of this project, a secondary feed was required.

4.1.2   Feed B - Dowells (Cylinders)

A cylindrical shaped feed would exhibit good flow properties through the gasifier. Several lengths of 6.35 mm diameter dowel were purchased and cut into 5 mm lengths using a bandsaw. This production method, however, was slow and laborious and it was decided that this was not an effective means of producing feed for the gasifier.

4.1.3   Feed C - Chips

Due to the difficulties experienced obtaining feed materials, it was decided to produce wood chips from 25x25 mm softwood. Several lengths of 25x25 mm softwood were purchased from a local timber merchant and cut into 5 mm thick slabs using a bandsaw. These slabs were then chipped using the Atlas hand grinding mill and hand sieved using three 457 mm (18 inch) diameter sieves of 4.75 mm, 6.35 mm and 12.7 mm aperture size.

Initially, the fraction sieved between 4.75 mm and 6.35 mm was produced. However, the time required to produce this size fraction led to the use of chipped wood in the size range 6.35 to 12.7 mm. This proved to be much easier to produce and exhibited better flow characteristics through the gasifier than the smaller sized wood.

Feed C was produced in several size fractions to enable an investigation of the effect of feed size on gasifier performance to be made (Table 4.1).

Table 4.1
Feed C - Size Fractions

| | Sieve Size, mm | |
Feed Designation	Lower	Upper
C1 Wood chips	3.35	4.75
C2 Wood chips	4.75	6.35
C3 Wood chips	6.35	9.50
C4 Wood chips	6.35	12.70
C5 Wood chips	9.50	12.70

4.1.4 Feed D - Commercial Wood Chips

A large quantity of the feed designated "Feed A" by Earp was available in the laboratory in an unsieved form. It was decided to use this feed sieved between 4.75 and 6.35 mm to check Earp's results.

4.1.5 Feed E - Dry Sewage Sludge

2 kg of this material was supplied by Ventec Ltd. for gasification tests. The analysis of this material shown in Section 4.2 was provided by Ventec. This would enable an investigation of the effect of feedstock properties on gasifier performance to be made. It was predicted that due to the high ash content of this feedstock, its gasification in the Aston gasifier would be difficult.

4.2 Feed Materials Characterization

The ultimate and proximate analyses of feeds A to D were carried out by British Gas (for this project). The proximate and ultimate analyses of the sewage sludge were provided by Ventec. Table 4.2 lists the proximate and ultimate analyses of the feedstock types used in this project.

4.2.1 Higher Heating Value

The biomass higher heating value can either be measured or calculated.

The higher heating value for feed C (72 mesh) was measured experimentally using a Bomb calorimeter. The results of the measurements are shown in Table 4.3. The average heating value for feed C was found to be 18.56 MJkg^{-1}. However, these experiments were not carried out strictly in accordance to British Standard since the titrations were not carried out. In

addition, it was not possible to crush feeds A, B and D to 72 mesh. For calculation purposes, therefore, the use of calculated heating values was considered.

Table 4.2
Feed Materials - Ultimate and Proximate Analyses

Feed	Beads	Dowells	Chips	Chips	Sewage
Feed designation	(A)	(B)	(C)	(D)	(E)
Dry basis					
Volatile matter	84.82	81.55	84.75	80.21	nr
Fixed carbon	15.11	17.66	15.19	19.41	nr
Ash	0.07	0.79	0.07	0.38	31.80
Carbon	49.47	50.13	53.01	50.74	45.19
Hydrogen	6.47	6.34	6.12	5.62	5.29
Oxygen	43.49	42.32	39.86	43.05	nr
Nitrogen	0.48	0.41	0.93	<0.20	4.51
Sulphur	0.01	0.01	0.01	<0.01	nr
Higher heating value					
(calculated)	21.23	20.18	20.36	19.50	21.38
Dry, ash-free basis					
Volatile matter	84.88	82.20	84.81	80.51	nr
Fixed carbon	15.12	17.80	15.19	19.48	nr
Carbon	49.51	50.53	53.04	50.93	66.26
Hydrogen	6.48	6.39	6.12	5.64	7.76
Oxygen	43.52	42.66	39.90	43.21	nr
Nitrogen	0.48	0.41	0.93	<0.20	6.61
Sulphur	0.01	0.01	0.01	<0.01	nr
H/C atomic ratio	1.57	1.52	1.39	1.33	1.40

nr not reported

Table 4.3
Measured Wood Chip Heating Value - Bomb Calorimeter

Feed Moisture content: 10%

Determination number	Heating value (dry) MJ/kg
1	15.57
2	16.25
3	17.82
4	17.17
Average	16.70
Average (dry basis)	18.56

A number of equations are available for the calculation of a solid's fuel heating value. A comparison of three equations (Dulong-Bertholot, Tillman and IGT) has been made by Graboski and Bain [90]. The Dulong-Bertholot equation is reported to consistently under predict the heating value of fresh biomass feeds - the average error being -6.8%. The Tillman method uses only the carbon content of the fuel and is more accurate than the Dulong-Bertholot method - the average error for fresh biomass feeds being 2.5%. The IGT method is reported to be the most accurate of the three methods for the calculation of biomass heating value - the average error for fresh biomass being 1.7%.

The higher heating values of the biomass feedstocks used in this project were calculated from the biomass ultimate analyses using the IGT equation (Equation 4.1) [90]. The calculated heating values for each of the feeds tested are shown in Table 4.2.

$$HHV = 0.341C + 1.323H + 0.068S - 0.0153A - 0.12 (O + N)....[4.1]$$

where:

HHV = Higher heating value, $MJkg^{-1}$

C = Carbon, % weight

H = Hydrogen,% weight

S = Sulphur, % weight

A = Ash, % weight

O = Oxygen, % weight

N = Nitrogen, % weight

By comparison of the average measured and calculated higher heating values for feed C (Tables 4.2 and 4.3), it can be seen that the calculated value is within 10% of the measured value. Due to the difficulty in producing 72 mesh wood from feeds A, B and D, it was decided to use the IGT equation to calculate the heating value of the feedstocks used in this project (Table 4.2).

4.2.2   Feed Moisture Content

The effects of the feed moisture content on the gasification process in an open-core downdraft gasifier were discussed in Section 2.1.4.5. It is reported that increasing the feed moisture content has a detrimental effect on gasifier performance because moisture acts as a "heat sink" [91]. For successful open-core downdraft gasifier operation, it is reported that the biomass moisture content should be less than 30% wet basis [41]. For 'standard case' experiments (Section 8.1), it was decided that the feed moisture content should be as low as possible.

The feed moisture content was determined using the oven dry method described by TRADA [92]. The oven method is simple to carry out and the moisture content of the wood prior to each run could be measured easily since the necessary equipment was available in the laboratory. No other methods for the determination of feed moisture content could be used to measure the feed moisture content on the same day as a gasification experiment as operators had to remain in the laboratory to attend to the gasification system.

The oven dry method involves drying small, representative samples of wood in a fan assisted oven at a temperature of 103 ±2 °C until the mass of the wood is constant. Three samples were dried prior to each run and the mean moisture content calculated. This method may drive off small amounts of volatiles which could be wrongly counted as water, however [92]. Care was taken, therefore, to ensure that the oven temperature did not exceed 105°C.

The feedstocks used in this project were stored in open bins in the laboratory. The feedstocks used for gasification were, therefore, near their equilibrium moisture contents. The feed moisture content was measured

prior to each run since the feed moisture content will vary with humidity and room temperature.

As noted above, for "standard case" runs, air dried wood was used. However, following purchase, the wood was often wet and required drying. Some runs were performed using wet wood to observe the effect of feed moisture content on gasifier performance.

4.2.3   Feed ash Content

The Aston gasifier is not fitted with an ash removal system such as that fitted to the rice husk gasifier operated by Manurung and Beenackers [31]. During stable operation, ash particles not entrained into the product gas flow will accumulate at the interface between the char gasification and inert char zones. The use of high ash fuels may prevent gasifier stable operation because of ash build up, lead to high reactor pressure drops and the formation of slag which could prevent successful gasifier operation [6].

Feed ash content was evaluated as part of the ultimate and proximate analyses performed by British Gas Plc. at the Midland Research Station, Solihul. Ultimate and proximate analyses of each feed type used are presented in Table 4.2.

4.2.4   Feed Size and Shape

The particle size is limited by the automatic screw feeder (if in use), the size of the gasifier and the pumping system capacity. The size of the screw feeder helix is such that any particle with a dimension greater than 8 mm is not acceptable. The use of a feed larger than 8 mm would, therefore, require manual batch feeding. Small particles could bridge over the feeder helix stopping feed flow to the gasifier although the minimum acceptable particle size is not reported.

By comparing the gasifier to a packed column, Earp suggested that the upper particle size is limited to approximately one eighth of the reactor diameter to limit wall effects (in this case, 9.4 mm) [12],[72]. Earp carried out no tests, however, using feeds consisting of particles greater than 9.4 mm.

139

No proof was provided of poor gasifier performance using particles greater than 6.35 mm in diameter. It was, therefore, decided that tests should be conducted using particles above this size.

The minimum particle size is limited by the permissible pressure drop across the gasifier (set by the capacity of the pumping system) [12]. Poor flow characteristics through the gasifier exhibited by particles sieved between 2.8 and 4.75 mm (sieve sizes) resulted in only one run being carried out using this feedstock by Earp and Reyes [12].

Particle shape will effect the flow of solids through the reactor. A knowledge of the particle size and shape will give an indication of the behaviour of the fuel in the gasifier and whether gasifier stirring or shaking is required. Stick or pin shaped particles are reported to be prone to bridging and will restrict the flow of particles to the reaction zones [12]. Bridging may also lead to a poorly defined reaction zone shape (ie sloping zone). During the previous project, large voids and sloping reaction zones (up to 45°) were observed when using feedstocks containing small, mixed shape particles [12]. Earp concluded that tars could escape cracking due to the presence of voids in the reaction zone within the gasifier hence increasing tar levels in the product gas [12].

Particle shape in the previous project was defined by observation (ie, whether the particle appeared to be of a specific shape) [12]. In addition to this method (ie, beads, cylinders or chips), particle shape was characterised in this project by the particle sphericity. Particle sphericity is defined by Equation 4.2 [19].

$$\text{Sphericity} = \frac{\left(\begin{array}{c}\text{Surface area of a sphere having}\\ \text{the same volume as the particle}\end{array}\right)}{\text{Surface area of the particle}} \quad \text{...........[4.2]}$$

Feed particle size was defined in this project as the characteristic size (cubic) and characteristic diameter. Characteristic size is defined as the length of side of a cube having the same volume as the particle under consideration (Equation 4.3). Characteristic diameter is defined as the diameter of a sphere having the same volume as the particle under consideration (Equation 4.4). The characteristic size, characteristic diameter and sphericity of the feeds used in this project are presented in Table 4.4.

$$\text{Characteristic dimension} = \sqrt[3]{\left(\text{Particle volume}\right)} \quad\text{............ [4.3]}$$

$$\text{Characteristic diameter} = \sqrt[3]{\left(\frac{6 \times \text{Particle volume}}{\pi}\right)} \quad\text{........ [4.4]}$$

Table 4.4
Feed Particle Physical Properties

Feed	Bulk density gcm^{-3}	Absolute density gcm^{-3}	Voidage %	Average Dimensions, mm		
				a	b	c
Beads (A)	0.51	0.83	38.77	15.00 (diameter, ø)		
Dowells (B)	0.42	0.61	30.92	6.35 ø	5.00	-
Chips (C1)	0.23	0.51	48.99	2.18	4.10	5.94
Chips (C2)	0.26	0.51	45.78	3.24	5.31	7.24
Chips (C3)	0.28	0.51	45.11	5.17	7.66	10.72
Chips (C4)	0.28	0.51	45.06	4.81	8.42	11.14
Chips (C5)	0.27	0.51	46.49	4.97	11.05	17.02
Chips (D) [12]	0.15	0.48	68.00	1.55	4.20	10.60

Feed	Surface area mm^2	Volume mm^3	Particle mass, g	Characteristic size (cubic) mm	Characteristic diameter mm	Sphericity
Beads (A)	706.86	1767.14	1.460	12.09	15.00	1.00
Dowells (B)	163.08	158.34	0.122	5.41	6.71	0.87
Chips (C1)	91.68	52.39	0.020	3.65	4.52	0.71
Chips (C2)	158.30	124.13	0.050	4.89	6.07	0.74
Chips (C3)	158.30	430.59	0.178	7.48	9.28	0.77
Chips (C4)	384.62	477.19	0.204	7.62	9.46	0.76
Chips (C5)	655.32	898.46	0.328	9.49	11.77	0.68
Chips (D)	133.40	65.25	0.023	4.03	4.99	0.59

The average dimensions of the beads and dowels were relatively easy to determine due to their uniform size and shape. The size determination of the irregularly shaped feedstock particles was more difficult. The dimensions of the irregularly shaped particles were carried out by assuming each particle to be cubic, measuring the three dimensions, a, b and c and averaging the results (see Figure 4.1). This procedure was carried out ten times for each feed type shown in Table 4.4 using different particles in each test. From these measurements, the particle surface area (for irregularly shaped particles, the surface area of a cuboid having the same dimensions was calculated), the particle volume (for the irregularly shaped particles the volume of a cuboid having the same dimensions was calculated), the characteristic dimension (Equation 4.3), the characteristic diameter (Equation 4.4) and the sphericity (Equation 4.5) of each type of feed particle were determined.
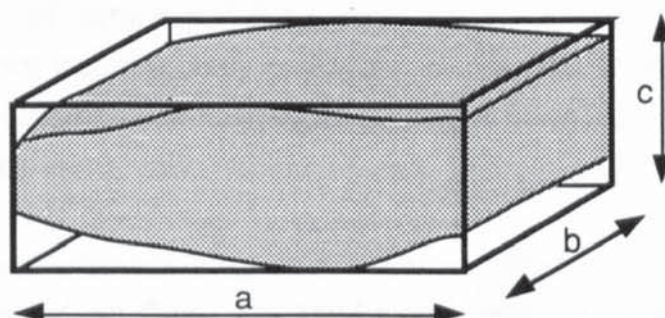
Figure 4.1
Particle Measurement Technique

4.2.5 Bulk Density

The bulk density (loose, uncompacted) was measured by filling a measuring cylinder with approximately one litre of feed. The measuring cylinder was then shaken vigorously and the volume of feed measured. The mass of the feed was then determined and the bulk density calculated. This was repeated twice and the average bulk density was recorded. Bulk density varies with moisture content [90]. The bulk densities of the feed materials presented in Table 4.4 were measured using air dried wood. The average moisture content of the air dried wood in this project was 9.7%. The bulk density of the dry biomass can be calculated using Equation 4.5.

$$\rho_{dry} = (1 - M) \cdot \rho_{wet} \quad \text{...[4.5]}$$

where:

ρ_{dry} :   Density of dry wood

142

ρ_{wet} :   Density of wet wood

M :   Moisture content of wood

The absolute density of feeds A, B and C was found by weighing and calculating the volume of unchipped timber. This procedure was carried out ten times for each feed.

The fractional voidage for each feed was calculated using Equation 4.6.

$$\text{Fractional voidage} = \frac{\text{Absolute density - Bulk density}}{\text{Absolute density}} \quad \text{........[4.6]}$$

4.3   Summary

It was initially decided that a feedstock consisting of spherical particles should be used for this project. A lack of commercial availability led to the investigation of other wood sources including dowells. Wood chips produced from commercially available 25x25 mm lengths of wood were found to be obtainable efficiently in sufficient quantities and were used for most of the experimentation in this project.

Proximate and ultimate analyses of the wood used in this project were carried out by British Gas. The feed higher heating values were calculated using the IGT equation. Particle size was defined as the characteristic size and characteristic diameter. Particle shape was defined as the particle sphericity. Feeds consisting of particles ranging in characteristic diameter from 4.03 to 15.00 mm and sphericity from 0.59 to 1.00 were gasified in this project.

5. VARIABLE SELECTION AND EXPERIMENTAL PROGRAMME

This section describes the selection of the variables for investigation, the operating procedures devised for gasifier operation and summarises the experiments completed.

5.1 Variable Selection

The gasification process in an open-core downdraft gasifier is affected by a number of variables. The parameters for investigation in this project together with their limitations are presented in Table 5.1. Variations in gasifier performance are compared with a standard (base) case performance defined in Section 8.1.

Table 5.1
Experimental Variables for Investigation

Experimental variables	Limitations
Reactor mode of operation	Stable, pyrolysis dominant, char consumption (gasification) dominant
Carbon dioxide enrichment of input air	Zero to a maximum where gasification will be extinguished
Reactor char bed height	0 - 40 cm
38 mm Kaowool insulation	With or without.
Feed moisture content	0 - 40%
Particle size	8 mm maximum for screw feeder.
Particle shape	Commercial availability (chips, spheres, cylinders)
Feed type	Wood, dry sewage sludge

5.2 Gasifier Operation

The same method of gasifier operation was used for all the gasification experiments. Methodical operating procedures are important to ensure safe and correct operation of the gasifier and the collection of reliable results. Gasifier operation is divided into four parts: startup, data collection, shut down and gasifier cleanup and preparation for the next run (a run is defined as the period of operation between gasifier start up and shutdown).

Operator duties and startup, shutdown and emergency shutdown procedures are shown in Appendix VII.

During gasifier operation, the following parameters were recorded every 30 seconds using the BBC microcomputer:
- Dry gas composition (H_2, CO, CO_2 and CH_4);
- Temperatures measured by thermocouples fitted to the gasification system (Table 3.11);
- Gas flowrate measured using the Platon flowmeter;
- Gas pressures at the demister and at the gasmeter measured by the two pressure transducers, PT1 and PT2;
- Time since the start of the run.

Following each run, data recorded by the BBC microcomputer was converted to a spreadsheet format to simplify analysis (Section 3).

The following parameters were manually recorded at an approximate frequency of every two minutes:
- The gas flow rate measured using the gasmeter;
- The char bed height and the position of the start of pyrolysis above the grate;
- The maximum temperature in the gasifier measured using a disappearing filament pyrometer;
- The gas pressure in the disentrainment tank using a Bourdon pressure gauge;
- The Rotameter setting indicating the water flowrate through the venturi;
- The water pressure downstream of the water pump;
- The screw feeder setting (if in use).

During gasifier operation when manual batch feeding of wood was used, batches of wood of known mass measured to an accuracy of ±0.01 g were added regularly to ensure that the upper wood level in the reactor was at no time more than 3 cm below the top rim of the gasifier. The wood addition rate was recorded manually against time.

The following measurements were calculated indirectly:
- Product gas nitrogen content (by difference as described in Section 3);
- Wet and dry air input flowrate (by nitrogen balance);

145

- Dry product gas flowrate (by assuming the gas to be saturated following disentrainment from the scrubber water and knowing the gas temperature and pressure) [56].

Gasifier performance data were calculated from the dry gas analyses, measured and calculated stream rates and the feed properties (Section 6). The gas mass yield; gas volumetric yield; air to fuel ratio; cold, hot and raw gas efficiencies serve as gasifier efficiency indicators as defined in Appendix VII. Feed properties were determined by British Gas (see Section 4). System throughput is indicated by the specific capacity - the ratio of the dry ash free feed rate to the grate area.

5.3 Summary of Experiments

During this project, a total of 26 experiments have been performed. Raw data are available on request from the Department of Chemical Engineering and Applied Chemistry, Aston University. The operating conditions and objectives for the experiments performed are summarized below and in Table 5.2.

Experiment 1	Duration 72 minutes
Objectives	Shakedown experiment using insulated reactor to yield initial results on insulated gasifier performance.
Feed used	Woodchips (4.75-6.35 mm)
Feed moisture content	7.9% wet basis
Data collected	Gas composition, gasifier temperatures from 8 thermocouples fitted in between insulation and reactor, system temperatures, gas volume using Platon flowmeter and manually using gasmeter, gas pressure at gasmeter, char bed height
Average feedrate	1.48 kgh^{-1}
Average gas flowrate	6.81 Nm^{3}h^{-1} (Platon)
Average gas HHV	3.45 MJNm^{-3}
Reason terminated	Reaction zone reached the top of the reactor. Gasifier was damaged by excess heat.

Experiment 2	Duration 36 minutes
Objectives	Base case experiment

Feed used	Woodchips (6.35-12.7 mm)
Feed moisture content	12.0% wet basis
Data collected	Gas composition, system temperatures, gas volume using Platon flowmeter and manually using gasmeter, gas pressure at gasmeter, char bed height, average tar production rate over whole run
Average feedrate	1.81 kgh^{-1}
Average gas flowrate	5.16 Nm^{3}h^{-1} (gasmeter)
Average gas HHV	4.19 MJNm^{-3}
Reason terminated	Experiment completed

Experiment 3	Duration 32 minutes
Objectives	Experiment using small chips
Feed used	Woodchips (3.35-4.75 mm)
Feed moisture content	11.1% wet basis
Data collected	Gas composition, system temperatures, gas volume using Platon flowmeter and manually using gasmeter, gas pressure at gasmeter, char bed height
Average feedrate	1.52 kgh^{-1}
Average gas flowrate	3.66 Nm^{3}h^{-1} (gasmeter)
Average gas HHV	3.91 MJNm^{-3}
Reason terminated	Experiment completed

Experiment 4	Duration 40 minutes
Objectives	Gasifier performance using sewage sludge feed
Feed used	Sewage sludge (4.75-6.35 mm)
Feed moisture content	10.3% wet basis
Data collected	Gas composition, system temperatures, gas volume using Platon flowmeter and manually using gasmeter, gas pressure at gasmeter, char bed height
Average feedrate	0.35 kgh^{-1}
Average gas flowrate	2.13 Nm^{3}h^{-1} (gasmeter)
Average gas HHV	1.58 MJNm^{-3}
Reason terminated	Reaction zone reached top of gasifier

Experiment 5	Duration 22 minutes
Objectives	Experiment using small wood chips
Feed used	Woodchips (3.35-4.75 mm)
Feed moisture content	11.1% wet basis
Data collected	Gas composition, system temperatures, gas volume using Platon flowmeter and manually using gasmeter, gas pressure at gasmeter, char bed height
Average feedrate	1.40 kgh^{-1}
Average gas flowrate	3.90 Nm^{3}h^{-1} (gasmeter)
Average gas HHV	4.10 MJNm^{-3}
Reason terminated	Experiment completed

Experiment 6	Duration 45 minutes
Objectives	Experiment using of dowels
Feed used	Dowels (6.35ϕ x 5 mm)
Feed moisture content	10.0% wet basis
Data collected	Gas composition, system temperatures, gas volume using Platon flowmeter and manually using gasmeter, gas pressure at gasmeter, char bed height
Average feedrate	1.39 kgh^{-1}
Average gas flowrate	3.81 Nm^{3}h^{-1} (gasmeter)
Average gas HHV	4.29 MJNm^{-3}
Reason terminated	Experiment completed

Experiment 7	Duration 26 minutes
Objectives	Experiment using small wood chips
Feed used	Woodchips (4.75-6.35 mm)
Feed moisture content	9.5% wet basis
Data collected	Gas composition, system temperatures, gas volume using Platon flowmeter and manually using gasmeter, gas pressure at gasmeter, char bed height
Average feedrate	1.24 kgh^{-1}
Average gas flowrate	3.91 Nm^{3}h^{-1} (gasmeter)
Average gas HHV	3.64 MJNm^{-3}
Reason terminated	Experiment completed

Experiment 8	Duration 33 minutes
Objectives	Experiment using beads (measure length of flaming pyrolysis and gasification zone, investigate interface between flaming pyrolysis and gasification zones)
Feed used	beads (15 mm ϕ)
Feed moisture content	10.0% wet basis
Data collected	Gas composition (recorded manually), Gas recorded manually using gasmeter, char bed height (Computer recorded data lost due to disk error)
Average feedrate	1.56 kgh^{-1}
Average gas flowrate	4.62 Nm^3h^{-1} (gasmeter)
Average gas HHV	3.34 $MJNm^{-3}$
Reason terminated	Experiment completed

A video recording of this experiment is available on request from the Department of Chemical Engineering and Applied Chemistry, Aston University.

Experiment 9	Duration 14 minutes
Objectives	Operation with no char bed
Feed used	Woodchips (4.75-6.35 mm)
Feed moisture content	9.5% wet basis
Data collected	Gas composition, system temperatures, gas volume using Platon flowmeter and manually using gasmeter, gas pressure at gasmeter, char bed height
Average feedrate	1.24 kgh^{-1}
Average gas flowrate	2.48 Nm^3h^{-1} (gasmeter)
Average gas HHV	3.09 $MJNm^{-3}$
Reason terminated	Problem with gas analysers not measuring gas composition. Blockage found in hot box and rectified.

Experiment 10	Duration 15 minutes
Objectives	Investigate effect of injecting CO_2 into gasifier (10 $lmin^{-1}$)

Feed used	Woodchips (6.35-12.7 mm)
Feed moisture content	9.5% wet basis
Data collected	Gas composition, system temperatures, gas volume using Platon flowmeter and manually using gasmeter, gas pressure at gasmeter, char bed height, CO_2 flowrate
Average feedrate	1.54 kgh^{-1}
Average gas flowrate	2.89 Nm^{3}h^{-1} (gasmeter)
Average gas HHV	3.42 MJNm^{-3}
Reason terminated	Experiment completed

Experiment 11	Duration 15 minutes
Objectives	Investigate effect of injecting CO_2 into gasifier (2 lmin^{-1})
Feed used	Woodchips (6.35-12.7 mm)
Feed moisture content	9.5% wet basis
Data collected	Gas composition, system temperatures, gas volume using Platon flowmeter and manually using gasmeter, gas pressure at gasmeter, char bed height, CO_2 flowrate
Average feedrate	0.80 kgh^{-1}
Average gas flowrate	3.01 Nm^{3}h^{-1} (gasmeter)
Average gas HHV	3.34 MJNm^{-3}
Reason terminated	Experiment completed

Experiment 12	Duration 14 minutes
Objectives	Investigate effect of injecting CO_2 into gasifier (5 lmin^{-1})
Feed used	Woodchips (6.35-12.7 mm)
Feed moisture content	9.5% wet basis
Data collected	Gas composition, system temperatures, gas volume using Platon flowmeter and manually using gasmeter, gas pressure at gasmeter, char bed height, CO_2 flowrate
Average feedrate	0.85 kgh^{-1}
Average gas flowrate	4.77 Nm^{3}h^{-1} (gasmeter)
Average gas HHV	3.32 MJNm^{-3}
Reason terminated	Experiment completed

Experiment 13	Duration 34 minutes
Objectives	Operation using commercially produced woodchips
Feed used	Commercially produced woodchips (4.75-6.35 mm)
Feed moisture content	9.5% wet basis
Data collected	Gas composition, system temperatures, gas volume using Platon flowmeter and manually using gasmeter, gas pressure at gasmeter, char bed height
Average feedrate	0.69 kgh^{-1}
Average gas flowrate	3.06 Nm^{3}h^{-1} (gasmeter)
Average gas HHV	3.51 MJNm^{-3}
Reason terminated	Excessive bridging in gasifier

Experiment 14	Duration 22 minutes
Objectives	Experiment using large wood chips
Feed used	Woodchips (9.5-12.7 mm)
Feed moisture content	9.7% wet basis
Data collected	Gas composition, system temperatures, gas volume using Platon flowmeter and manually using gasmeter, gas pressure at gasmeter, char bed height
Average feedrate	1.44 kgh^{-1}
Average gas flowrate	4.58 Nm^{3}h^{-1} (gasmeter)
Average gas HHV	3.12 MJNm^{-3}
Reason terminated	Experiment completed

Experiment 15	Duration 44 minutes
Objectives	Experiment using woodchips sized between 6.35 and 9.5 mm
Feed used	Woodchips (6.35-9.50 mm)
Feed moisture content	9.7% wet basis
Data collected	Gas composition, system temperatures, gas volume using Platon flowmeter and manually using gasmeter, gas pressure at gasmeter, char bed height

Average feedrate	1.81 kgh^{-1}
Average gas flowrate	4.99 Nm^{3}h^{-1} (gasmeter)
Average gas HHV	3.89 MJNm^{-3}
Reason terminated	Experiment completed

Experiment 16	Duration 25 minutes
Objectives	Investigate effect of feed moisture content
Feed used	Woodchips (6.35-12.7 mm)
Feed moisture content	32.1% wet basis
Data collected	Gas composition, system temperatures, gas volume using Platon flowmeter and manually using gasmeter, gas pressure at gasmeter, char bed height
Average feedrate	0.68 kgh^{-1}
Average gas flowrate	1.36 Nm^{3}h^{-1} (gasmeter)
Average gas HHV	3.31 MJNm^{-3}
Reason terminated	Experiment completed

Experiment 17	Duration 40 minutes
Objectives	Investigate effect of feed moisture content
Feed used	Woodchips (6.35-12.7 mm)
Feed moisture content	32.1% wet basis
Data collected	Gas composition, system temperatures, gas volume using Platon flowmeter and manually using gasmeter, gas pressure at gasmeter, char bed height
Average feedrate	0.97 kgh^{-1}
Average gas flowrate	2.14 Nm^{3}h^{-1} (gasmeter)
Average gas HHV	3.30 MJNm^{-3}
Reason terminated	Experiment completed

Experiment 18	Duration 46 minutes
Objectives	Investigate effect of feed moisture content, check gas composition measured by gas analysers against gas chromatography results
Feed used	Woodchips (6.35-12.7 mm)
Feed moisture content	32.1% wet basis

Data collected	Gas composition, system temperatures, gas volume using Platon flowmeter and manually using gasmeter, gas pressure at gasmeter, char bed height, gas sample taken for gas chromatography analysis
Average feedrate	0.69 kgh^{-1}
Average gas flowrate	2.14 Nm^{3}h^{-1} (Platon)
Average gas HHV	2.78 MJNm^{-3}
Reason terminated	Experiment completed

Experiment 19	Duration 81 minutes
Objectives	Investigate effect of feed moisture content
Feed used	Woodchips (6.35-12.7 mm)
Feed moisture content	18.6% wet basis
Data collected	Gas composition, gasifier maximum temperature using disappearing filament pyrometer and system temperatures, gas volume using Platon flowmeter and manually using gasmeter, gas pressure at gasmeter, char bed height
Average feedrate	1.10 kgh^{-1}
Average gas flowrate	3.15 Nm^{3}h^{-1} (gasmeter)
Average gas HHV	3.10 MJNm^{-3}
Reason terminated	Experiment completed

Experiment 20	Duration 17 minutes
Objectives	Investigate effect of feed moisture content
Feed used	Woodchips (6.35-12.7 mm)
Feed moisture content	18.6% wet basis
Data collected	Gas composition, gasifier maximum temperature using disappearing filament pyrometer and system temperatures, gas volume using Platon flowmeter and manually using gasmeter, gas pressure at gasmeter, char bed height
Average feedrate	2.05 kgh^{-1}
Average gas flowrate	4.43 Nm^{3}h^{-1} (gasmeter)
Average gas HHV	3.65 MJNm^{-3}
Reason terminated	Experiment completed

Experiment 21   Duration 15 minutes
Objectives   Investigate effect of feed moisture content
Feed used   Woodchips (4.75-6.35 mm)
Feed moisture content 18.7% wet basis
Data collected   Gas composition, gasifier maximum temperature using disappearing filament pyrometer and system temperatures, gas volume using Platon flowmeter and manually using gasmeter, gas pressure at gasmeter, char bed height
Average feedrate   0.89 kgh^{-1}
Average gas flowrate   3.40 Nm^{3}h^{-1} (gasmeter)
Average gas HHV   2.41 MJNm^{-3}
Reason terminated   Experiment completed

Experiment 22   Duration 74 minutes
Objectives   Extended base case experiment
Feed used   Woodchips (6.35-12.7 mm)
Feed moisture content 8.9% wet basis
Data collected   Gas composition, gasifier maximum temperature using disappearing filament pyrometer and system temperatures, gas volume using Platon flowmeter and manually using gasmeter, gas pressure at gasmeter, char bed height
Average feedrate   1.33 kgh^{-1}
Average gas flowrate   3.92 Nm^{3}h^{-1} (gasmeter)
Average gas HHV   3.31 MJNm^{-3}
Reason terminated   Experiment completed

Experiment 23   Duration 52 minutes
Objectives   Investigate effect of gasifier insulation
Feed used   Woodchips (6.35-12.7 mm)
Feed moisture content 8.8% wet basis
Data collected   Gas composition, gasifier maximum temperature using disappearing filament pyrometer and system temperatures, gas volume using Platon flowmeter and manually using gasmeter, gas pressure at gasmeter, char bed height
Average feedrate   1.59 kgh^{-1}

Average gas flowrate   3.90 Nm^3h^{-1} (gasmeter)
Average gas HHV   4.18 $MJNm^{-3}$
Reason terminated   Experiment completed

Experiment 24   Duration 21 minutes
Objectives   Investigate operation in pyrolysis dominant regime
                        using insulated reactor
Feed used   Woodchips (6.35-12.7 mm)
Feed moisture content   8.8% wet basis
Data collected   Gas composition, gasifier maximum temperature
                        using disappearing filament pyrometer and
                        system temperatures, gas volume using Platon
                        flowmeter and manually using gasmeter, gas
                        pressure at gasmeter, char bed height
Average feedrate   1.37 kgh^{-1}
Average gas flowrate   4.01 Nm^3h^{-1} (gasmeter)
Average gas HHV   3.73 $MJNm^{-3}$
Reason terminated   Reaction zone reached top of reactor

Experiment 25   Duration 41 minutes
Objectives   Investigate effect of gasifier insulation
Feed used   Woodchips (6.35-12.7 mm)
Feed moisture content   10.1% wet basis
Data collected   Gas composition, gasifier maximum temperature
                        using disappearing filament pyrometer and
                        system temperatures, gas volume using Platon
                        flowmeter and manually using gasmeter, gas
                        pressure at gasmeter, char bed height
Average feedrate   2.02 kgh^{-1}
Average gas flowrate   5.93 Nm^3h^{-1} (gasmeter)
Average gas HHV   4.79 $MJNm^{-3}$
Reason terminated   Experiment completed

Experiment 26   Duration 44 minutes
Objectives   Base case experiment
Feed used   Woodchips (6.35-12.7 mm)
Feed moisture content   10.1% wet basis

Data collected	Gas composition, gasifier maximum temperature using disappearing filament pyrometer and system temperatures, gas volume using Platon flowmeter and manually using gasmeter, gas pressure at gasmeter, char bed height
Average feedrate	1.32 kgh^{-1}
Average gas flowrate	5.48 Nm^{3}h^{-1} (gasmeter)
Average gas HHV	3.45 MJNm^{-3}
Reason terminated	Experiment complete

5.4   Summary

A total of 26 experiments have been performed to investigate the gasification process in an open-core downdraft gasifier and the parameters which influence the gasification process. The average experiment length was 35.4 minutes and the average as received wood feed rate was 1.27 kgh^{-1}.

Table 5.2
Summary of Experiments Performed

Experiment number	Duration minutes	Feed type*	Feed moisture content %	Feed rate kgh^{-1}	Gas flowrate Nm^{3}h^{-1}	Gas HHV MJNm^{-3}
1	72	C2	7.9	1.48	6.81	3.45
2	36	C4	12.0	1.81	5.16	4.19
3	32	C1	11.1	1.52	3.66	3.91
4	40	E	10.3	0.35	2.13	1.58
5	22	C1	11.1	1.40	3.90	4.10
6	45	B	10.0	1.39	3.81	4.29
7	26	C2	9.5	1.24	3.91	3.64
8	33	A	10.0	1.56	4.62	3.34
9	14	C2	9.5	1.24	2.48	3.09
10	15	C4	9.5	1.54	2.89	3.42
11	15	C4	9.5	0.80	3.01	3.34
12	14	C4	9.5	0.85	4.77	3.32
13	34	D	9.5	0.69	3.06	3.51
14	22	C5	9.7	1.44	4.58	3.12
15	44	C3	9.7	1.81	4.99	3.89
16	25	C4	32.1	0.68	1.36	3.31
17	40	C4	32.1	0.97	2.14	3.30
18	46	C4	32.1	0.69	2.14	2.78
19	81	C4	18.6	1.10	3.15	3.10
20	17	C4	18.6	2.05	4.43	3.65
21	15	C4	18.7	0.89	3.40	2.41
22	74	C4	8.9	1.33	3.92	3.31
23	52	C4	8.8	1.59	3.9	4.18
24	21	C4	8.8	1.37	4.01	3.73
25	41	C4	10.1	2.02	5.93	4.79
26	44	C4	10.1	1.32	5.48	3.45

* see Tables 4.1 and 4.2

6. MASS AND ENERGY BALANCES

The aim of this section is to present and discuss the mass and energy balances performed for each experiment. The methods used to evaluate the mass and energy balances and the detailed mass and energy balances for each experiment performed are presented in Appendix VII.

6.1 Mass Balance

In any process, mass is neither created nor destroyed (Equation 6.1). This applies to the total mass of the system and to the components within that system.

$$\{Mass\ in\} = \{Mass\ out\} + \{accumulation\ (or\ depletion)\ within\ system\} \quad ....[6.1]$$

During stable gasifier operation (ie there is no net production or consumption of char in the gasifier), the accumulation of material within the gasifier is zero and the amount of material within the system does not enter into the calculation. The mass balance closure is, therefore defined as:

$$Mass\ balance\ closure = \frac{Total\ mass\ out}{Total\ mass\ in} \times 100\% \quad ....[6.2]$$

The mass balance closure should equal 100%. The size of any deviation from 100% will indicate the quality of the balance.

Over the gasifier used in this project, the material inputs and outputs are:

Inputs	Outputs
as received feed	product gas
air	tars and condensate
	ash

In addition to the overall mass balance, elemental balances (carbon, hydrogen and oxygen) and performance indicators have been determined. The gasifier performance indicators (discussed in Section 8) are evaluated using a variety of measures determined from the dry gas composition, mass balance data and supporting measurements. These performance indicators are defined by Equations 6.3-6.7.

158

Mass Yield

This is defined as the ratio of the mass of dry product gas and the mass of dry feed input to the gasifier (Equation 6.1).

$$\text{Mass yield, kgkg}^{-1} = \frac{\text{Dry gas mass flowrate + Tar mass flowrate}}{\text{Dry feed input rate to gasifier}} \quad ...[6.31]$$

Volumetric Yield

The volumetric yield is defined as the ratio of the dry gas normal volumetric flowrate and the dry feed input rate to the gasifier.

$$\text{Volumetric yield, Nm}^3\text{kg}^{-1} = \frac{\text{Normal dry gas volumetric flowrate}}{\text{Dry feed input rate to gasifier}} \quad ....[6.4]$$

Air / Fuel Ratio

This is defined as the ratio of dry air mass flow into the gasifier and the dry feed input rate to the gasifier.

$$\text{Air/fuel ratio, kgkg}^{-1} = \frac{\text{Dry air mass flowrate into gasifier}}{\text{Dry feed input rate to gasifier}} \quad ....[6.5]$$

Mass Conversion to Dry Product Gas

This is the ratio, expressed as a percentage, of the dry gas mass flowrate to the sum of the dry feed flow and the dry air input rate to the gasifier.

$$\text{Mass conversion; \%} = \frac{\text{dry gas mass flowrate}}{\text{dry gas mass flowrate+dry air input rate}} \times 100 ....[6.6]$$

Specific Capacity

This is the dry fuel flow rate divided by the grate cross sectional area $(\text{kg.h}^{-1}.\text{m}^{-2})$.

$$\text{Specific capacity, kg.h}^{-1}.\text{m}^{-2} = \frac{\text{dry fuel feed rate}}{\text{grate cross sectional area}} ....[6.7]$$

6.1.1   Mass Balance Measurements

The feed flow rate into the gasifier and gas flow rate out of the gasifier were measured directly. The methods used to measure these quantities were described in Section 3. The air flow rate into the gasifier was measured by

159

nitrogen balance assuming that the nitrogen in the product gas equalled the nitrogen in the air entering the gasifier.

There was insufficient time to design and construct a raw gas particulate, tar and condensate sampling system for this project. As the raw gas water content was not measured, the mass balances are evaluated on a dry basis. It is recommended that future workers install a tar sampling system to quantify the tar, condensibles and particulate content of the raw product gas (see Section 10). An iso-kinetic sampling probe is fitted into the venturi to gasifier connection system (Appendix II.10). From a review of product gas tar contents reported in the literature and from a simple evaluation of the tars produced in experiment 2, the raw gas tar content was taken to be equal to 1% of the wet gas mass flowrate (see Table 6.1). The simple evaluation of the overall tar production rate from a run was carried out by thoroughly cleaning the whole gasification system following the run with acetone and weighing the residue collected following evaporation of the acetone. This process gives only a rough indication of the product gas tar content over the whole operational period of a run including the startup and shut down periods. In addition, it is a difficult and time consuming task. It was not, therefore, repeated following experiment 2.

Table 6.1
Reported Raw Gas Tar Contents in the Literature

Reference	Gasifier type	Raw product gas tar content % weight
Brown [93]	Throated downdraft	0.005-0.05
Reed [11]	Open-core downdraft	0.02-0.2
Graham [94]	Throated downdraft	1-6
Esplin [95]	Throated downdraft	1.6
Chee [96]	Open-core downdraft	0.1
Walawender [51]	Open-core downdraft	0.13
Experiment 2 (simple evaluation)	Open-core downdraft	1.05
Mean:		0.90

For the purposes of calculating the mass balance, it is assumed that no char exits the gasifier with the product gas during stable operation. Walawender reports that only about 3% by mass of the char remains following the gasification process - some of which will be entrained into the product gas flow leaving the gasifier [51]. The error arising from this simplification should, therefore, be small.

The mass balance closure will be affected by inaccuracies in the product gas flow measurement. The Platon flowmeter was shown to be inaccurate and erratic in performance during this project. The accuracy of the gasmeter during cold operation was compared with an 18A Rotameter and found to be accurate to within ±5%. Table 6.2 shows a comparison between the air flow through the gasification system at room temperature measured by the cumulative gasmeter and an 18A Rotameter calibrated between 0 and 6.6 m^3h^{-1}. These tests were carried out using the test dial fitted to the gasmeter (each revolution of the test dial equals 1 ft^3). These two instruments were fitted in series into the gasification system; the 18A Rotameter was fitted into the position normally occupied by the Platon flowmeter (see Figure 3.1). This data is graphically presented in Figure 6.1. It can be seen that the air flow rate measured using the gasmeter compares well with the air flowrate measured using the 18A Rotameter. It was concluded that the gasmeter provides an accurate measurement of the gas flowrate through the gasification system.

Table 6.2						
Flowrate Measurement - Cumulative Gasmeter, 18A Rotameter						
Water flow through venturi (Rotameter setting)	Gas flow measured by 18A Rotameter, m^3h^{-1}			Gas flow measured by gasmeter, m^3h^{-1} *		
	Test 1	Test 2	Mean	Test 1	Test 2	mean
2	1.41	1.38	1.39	1.33	1.27	1.30
3	2.73	2.64	2.68	2.55	2.52	2.53
4	3.84	3.81	3.82	3.58	3.67	3.62
5	4.98	4.77	4.87	4.80	4.60	4.70
6	-	5.79	5.79	-	5.55	5.55
* Test duration = 5 minutes						
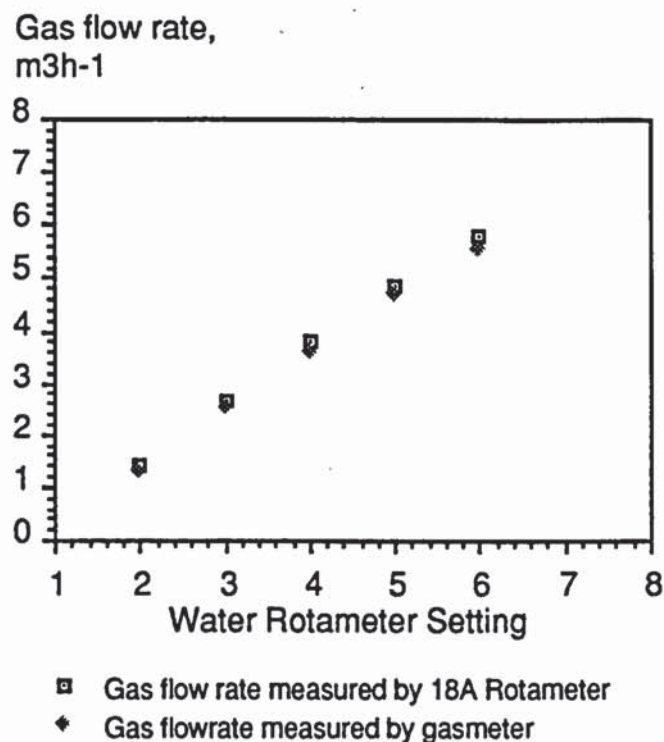
Figure 6.1

Accuracy of Gasmeter Compared with an 18A Rotameter

Table 6.3 shows a comparison between the air flow rate through the gasification system (at room temperature) measured by the cumulative gasmeter and the Platon flowmeter. In a second test (Table 6.4), the air flowrate through the gasification system was progressively increased to an indicated 6 m^3h^{-1} and then progressively reduced to 3 m^3h^{-1}. It can be seen from Tables 6.3 and 6.4 that the Platon flowmeter gave inaccurate and inconsistent readings especially at low flowrates. The float within the Platon flowmeter also often became stuck as shown in Table 6.4.

Table 6.3			
Flowrate Measurement - Cumulative Gasmeter, Platon Flowmeter			
Platon flowmeter	Gasmeter flow, m^3h^{-1} *		
reading, m^3h^{-1} *	Test 1	Test 2	Mean
2	3.45	3.60	3.52
3	4.54	4.54	4.54
4	5.30	5.36	5.83
5	6.19	6.38	6.28
* Test duration = 5 minutes			

162

Table 6.4

Gas Flowrate Measurement - Comparison Between Cumulative Gasmeter and Platon Flowmeter

Water flow through venturi (Rotameter setting)	Platon flowmeter reading, m^3h^{-1}	Gas flow rate measured by gasmeter, m^3h^{-1}
3	0	1.30
4	0	1.86
5	1.8	3.26
6	4.1	4.86
6	4.1	4.86
5	3.4	3.83
4	2.4	2.84
3	2.4	2.04

A standard 18A Rotameter (manually read) was used to measure the product gas flowrate in place of the Platon flowmeter during three experiments (3, 4 and 5) but it was found that the inside surface of the Rotameter became coated with tars preventing measurement. In addition, the Rotameter float filled with water during the run. Standard Rotameters could not, therefore, be used to measure the product gas flowrate.

The gas flow used for mass balance calculations was, therefore, taken from the gasmeter. However, during operation, the gasmeter can only be read to an accuracy of ±10 ft^3 (±283 litres). This error was minimized by reading the gasmeter as soon as possible following a change in the gasmeter display.

6.1.2   Mass Balance Results and Discussion

Mass balances were performed for each experiment carried out. A summary of the mass balances is shown in Table 6.5. Figure 6.2 illustrates the mass balance closures. The mass balance for experiment 18 is not included as the gas flowrate was not correctly measured. The average mass balance closure is 96.09%. The poorest mass balance closure is 83.80%. 84% of the mass balances in Table 6.5 are within 10% of closure while 56% are within 5% of 100% closure. The mass balance closures were fairly

<table>
<thead>
<tr><th rowspan="3">Expt</th><th colspan="3">Inputs, kgh^{-1}</th><th colspan="3">Outputs, kgh^{-1}</th><th colspan="4">Closures, %</th></tr>
<tr><th>Dry</th><th>Dry</th><th>Total</th><th>Dry</th><th>Tar</th><th>Total</th><th>Overall</th><th>C</th><th>H</th><th>O</th></tr>
<tr><th>feed</th><th>air</th><th></th><th>gas</th><th></th><th></th><th></th><th></th><th></th><th></th></tr>
</thead>
<tbody>
<tr><td colspan="11">**Table 6.5**
Mass and Elemental Balance Summary</td></tr>
<tr><td>1</td><td>1.09</td><td>2.43</td><td>3.53</td><td>3.29</td><td>0.03</td><td>3.32</td><td>94.18</td><td>85.59</td><td>69.86</td><td>90.45</td></tr>
<tr><td>2</td><td>1.59</td><td>4.14</td><td>5.73</td><td>5.47</td><td>0.05</td><td>5.53</td><td>96.54</td><td>95.52</td><td>70.70</td><td>92.27</td></tr>
<tr><td>3</td><td>1.50</td><td>3.30</td><td>4.80</td><td>4.21</td><td>0.04</td><td>4.25</td><td>88.51</td><td>73.06</td><td>54.70</td><td>78.29</td></tr>
<tr><td>4</td><td>0.45</td><td>2.35</td><td>2.80</td><td>2.52</td><td>0.00</td><td>2.52</td><td>90.11</td><td>102.13</td><td>40.04</td><td>64.71</td></tr>
<tr><td>5</td><td>1.26</td><td>3.03</td><td>4.29</td><td>4.22</td><td>0.04</td><td>4.26</td><td>99.37</td><td>96.44</td><td>67.67</td><td>102.96</td></tr>
<tr><td>6</td><td>1.24</td><td>2.84</td><td>4.08</td><td>4.02</td><td>0.04</td><td>4.06</td><td>99.41</td><td>101.10</td><td>66.31</td><td>100.94</td></tr>
<tr><td>7</td><td>1.12</td><td>3.32</td><td>4.45</td><td>4.41</td><td>0.04</td><td>4.45</td><td>100.16</td><td>105.95</td><td>64.54</td><td>100.54</td></tr>
<tr><td>8</td><td>1.41</td><td>4.16</td><td>5.57</td><td>5.50</td><td>0.05</td><td>5.55</td><td>99.78</td><td>110.88</td><td>53.15</td><td>97.52</td></tr>
<tr><td>9</td><td>1.13</td><td>3.09</td><td>4.22</td><td>3.88</td><td>0.04</td><td>3.92</td><td>93.00</td><td>84.66</td><td>45.88</td><td>85.92</td></tr>
<tr><td>10*</td><td>1.32</td><td>5.05</td><td>6.37</td><td>5.29</td><td>0.05</td><td>5.34</td><td>83.83</td><td>78.10</td><td>49.61</td><td>78.72</td></tr>
<tr><td>11*</td><td>1.13</td><td>2.63</td><td>3.76</td><td>3.57</td><td>0.04</td><td>3.61</td><td>90.50</td><td>79.04</td><td>43.46</td><td>92.42</td></tr>
<tr><td>12*</td><td>0.77</td><td>2.53</td><td>3.30</td><td>2.79</td><td>0.03</td><td>2.82</td><td>85.45</td><td>76.51</td><td>40.77</td><td>83.40</td></tr>
<tr><td>13</td><td>1.02</td><td>1.85</td><td>2.87</td><td>2.53</td><td>0.02</td><td>2.55</td><td>88.85</td><td>71.82</td><td>40.55</td><td>84.22</td></tr>
<tr><td>14</td><td>1.30</td><td>4.05</td><td>5.35</td><td>5.26</td><td>0.05</td><td>5.31</td><td>99.36</td><td>103.10</td><td>56.81</td><td>99.36</td></tr>
<tr><td>15</td><td>1.63</td><td>4.10</td><td>5.74</td><td>5.82</td><td>0.06</td><td>5.88</td><td>102.58</td><td>104.16</td><td>62.96</td><td>110.83</td></tr>
<tr><td>16</td><td>0.46</td><td>1.17</td><td>1.63</td><td>1.64</td><td>0.02</td><td>1.66</td><td>101.78</td><td>99.17</td><td>55.00</td><td>111.07</td></tr>
<tr><td>17</td><td>0.66</td><td>1.91</td><td>2.57</td><td>2.74</td><td>0.03</td><td>2.77</td><td>108.03</td><td>118.51</td><td>63.53</td><td>124.46</td></tr>
<tr><td>19</td><td>0.89</td><td>2.76</td><td>3.65</td><td>3.67</td><td>0.04</td><td>3.71</td><td>101.51</td><td>106.18</td><td>62.06</td><td>105.81</td></tr>
<tr><td>20</td><td>1.73</td><td>3.63</td><td>5.37</td><td>5.02</td><td>0.05</td><td>5.07</td><td>94.52</td><td>80.48</td><td>51.90</td><td>96.68</td></tr>
<tr><td>21</td><td>0.72</td><td>2.21</td><td>2.29</td><td>2.67</td><td>0.03</td><td>2.69</td><td>91.75</td><td>80.80</td><td>42.69</td><td>81.95</td></tr>
<tr><td>22</td><td>1.21</td><td>3.50</td><td>4.71</td><td>4.51</td><td>0.04</td><td>4.56</td><td>96.63</td><td>94.46</td><td>58.45</td><td>93.42</td></tr>
<tr><td>23</td><td>1.45</td><td>3.82</td><td>5.27</td><td>5.09</td><td>0.05</td><td>5.15</td><td>97.61</td><td>98.74</td><td>76.74</td><td>94.32</td></tr>
<tr><td>24</td><td>1.25</td><td>3.62</td><td>4.87</td><td>4.72</td><td>0.05</td><td>4.77</td><td>97.82</td><td>99.07</td><td>71.66</td><td>94.81</td></tr>
<tr><td>25</td><td>1.82</td><td>4.30</td><td>6.12</td><td>5.97</td><td>0.06</td><td>6.03</td><td>98.50</td><td>99.68</td><td>76.09</td><td>97.22</td></tr>
<tr><td>26</td><td>1.23</td><td>3.37</td><td>4.60</td><td>4.19</td><td>0.04</td><td>4.23</td><td>91.94</td><td>85.25</td><td>48.64</td><td>81.51</td></tr>
<tr><td colspan="7">Mean closures:</td><td>96.09</td><td>94.76</td><td>59.97</td><td>93.91</td></tr>
</tbody>
</table>

* CO_2 was injected into gasifier - dry air input includes CO_2 mass flowrate

Mass balance closure, %
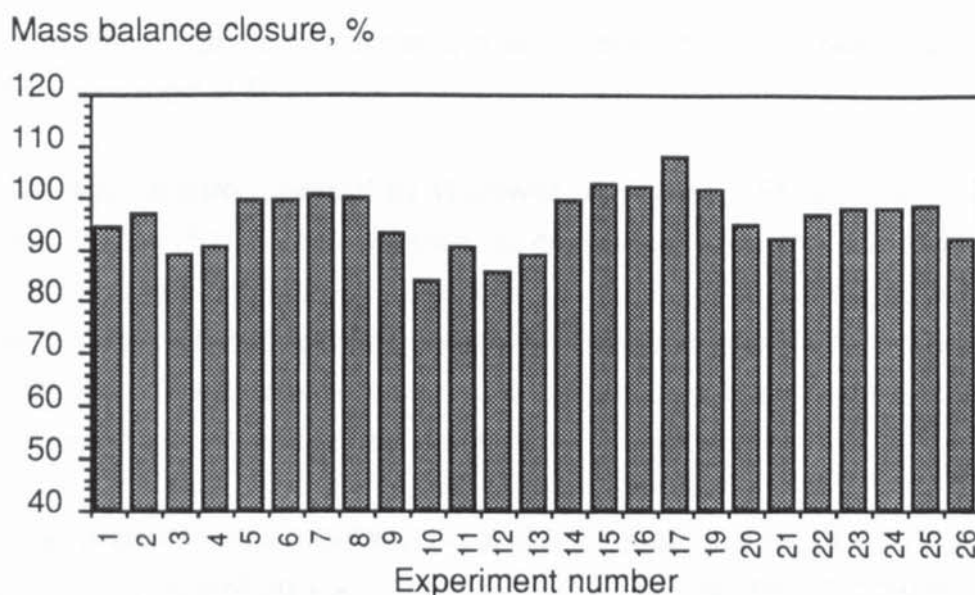
Figure 6.2

Mass Balance Closures

consistent over the range of operating conditions investigated. The poor hydrogen and oxygen balances are attributed to the fact that the moisture content of the gasifier output stream was not measured (see Sections 3 and 7). The mass balances for the experiments in which carbon dioxide was inputted to the gasifier are poor as it was not possible to ensure that all the carbon dioxide exiting the carbon dioxide injection pipe entered the gasifier. Excluding experiments 10, 11 and 12, 91% of the mass balances are within 10% of 100% closure and 59% of the mass balance closures are within 5% of 100% closure.

Mass balances over open-core downdraft gasifiers have been presented by Reyes [17], Graboski [41] and Walawender [51].

Reyes presented two mass and energy balances over the mark I Aston gasifier [17]. The first mass and energy balance was performed for a commissioning experiment (run 6C) during a three minute period of stable operation. The second mass and energy balance (run 8R) was performed over a 36 minute period of stable operation. The first mass balance closure was 92.6% and the second mass balance closure was 91.6%. These compare well with the closures obtained in this project. The carbon balances reported by Reyes are consistent with the carbon balances presented in this project. The hydrogen and oxygen balances presented by

Reyes are less satisfactory since the water content of the raw product gas was not measured [17].

The average closure reported by Walawender for the KSU gasifier is 93.3% (Section 2.3.3) [51]. This balance is consistent with the average mass balance closure presented in Table 6.5 for the mark II Aston gasifier. The average carbon, hydrogen and oxygen closures are 95.12%, 91.62% and 103.87% [8]. The reported carbon and oxygen closures are consistent with the carbon and oxygen closures presented in Table 6.5 [8].

Graboski presents mass balances for the Syngas gasifier for both air and oxygen blown operation (Section 2.3.7) [41]. For air blown operation, the closure is within 10% of 100% closure which is considered by Graboski to be satisfactory for quantifying gasifier performance [41]. The average carbon, hydrogen and oxygen elemental balances for air blown operation are 108.5%, 117.8% and 106.6% respectively [41]. No explanation for these high balances are provided. However, an error of ±10% in the measurement of propane and ±3% in the measurement of air entering the gasifier are reported [41].

Discussion of gasifier performance indicators is made in Section 8.

6.2 Energy Balance

In any plant or unit, energy is conserved. Equation 6.8 illustrates the principle of energy balances. In this case, the unit is the gasifier.

$$\begin{pmatrix} \text{Heat added or removed} \\ \text{from a process} \end{pmatrix} = \begin{pmatrix} \text{enthalpy of} \\ \text{products} \end{pmatrix} - \begin{pmatrix} \text{enthalpy of feed} \\ \text{streams} \end{pmatrix} \quad \text{......[6.8]}$$

Energy inputs to the gasifier are:

- Feed (chemical energy and sensible energy)
- Air (sensible energy and latent energy of any moisture)

Energy outputs from the gasifier are:

- Hot, wet, raw gas (chemical energy, latent energy, chemical energy of tars, sensible energy of tars, latent heat of tars, sensible heat of moisture and latent heat of moisture,

- Heat losses from the gasifier.

The procedures used to calculate the energy balances for each experiment are shown in Appendix VII.

The process performance in terms of energy is defined by the cold gas efficiency, the hot gas efficiency and the raw gas efficiency as defined by Equations 6.9-6.11. For applications in which a cold, clean gas is required such as an internal combustion engine, the cold gas efficiency is considered. For applications in which a hot, clean gas is required (eg. a gas turbine) the hot gas efficiency is considered. For applications (eg. kilns) where a hot gas containing tars can be tolerated, the raw gas efficiency is considered.

$$\text{Cold gas efficiency} = \left(\frac{E^g_{cold}}{E^f_{chem}} \right) \times 100\% \dots \dots [6.9]$$

$$\text{Hot gas efficiency} = \left(\frac{E^g_{chem} + E^g_{sens}}{E^f_{chem}} \right) \times 100\% \dots \dots [6.10]$$

$$\text{Raw gas efficiency} = \left(\frac{E^g_{chem} + E^g_{sens} + E^t_{chem} + E^t_{sens}}{E^f_{chem}} \right) \times 100\% \dots [6.11]$$

where:

E^g_{cold} is the chemical energy of the product gas

E^f_{chem} is the chemical energy of the feedstock

E^g_{sens} is the sensible energy of the raw product gas

E^t_{chem} is the chemical energy of the tars in the raw product gas

E^t_{sens} is the sensible energy of the tars in the raw product gas

6.1.2 . Energy Balance Measurements

Energy balances have been calculated using the mass flow rates of the streams entering and leaving the gasifier; the compositions of the streams

167

and the available and estimated data for each stream. The energy input to the gasifier is the chemical energy of the wood. The datum temperature for each run was taken to be room temperature. The energy outputs from the gasifier during stable operation are the chemical energy of the gas; the sensible energy of the gas; the chemical energy of the tars and condensates; the sensible energy of the tars and condensates; and the heat losses from the gasifier. The quality of the energy balance will depend on the quality of the mass balance upon which it is based and the estimation of gasifier heat losses. The quality of the mass balance is described above in Section 6.1.

The method used to measure the heat loss from the uninsulated gasifier was similar to that reported by Reyes [17]. This method involved measuring the vertical temperature profile through the gasifier and assuming the radial temperature distribution in the gasifier to be constant. Reyes measured the temperature at four heights in the gasifier [17]. In this project, the temperature was measured every centimetre using a 3.5 mm type k thermocouple fitted inside a closely fitting, stainless steel sheath placed near the central vertical axis of the gasifier such that the tip of the thermocouple could be positioned at any height above the grate. This method was described in more detail in Section 3. The maximum temperature recorded by the search thermocouple was checked against the maximum gasifier temperature measured using a disappearing filament pyrometer. The method used in this project to measure the gasifier vertical temperature profile has resulted in a more detailed vertical temperature profile through the gasifier compared with that reported by Reyes since she assumed the reaction zone and char bed height to always be 13 cm (see Section 8.6) [17]. The outside temperature of the insulated gasifier was measured by fitting the tips of thermocouples a short distance into the outer wall of the insulation. Heat losses from the insulated and uninsulated Aston gasifier are discussed in Section 6.2.2.

6.2.2 Energy Balance Results and Discussion

Energy balances were performed for each experiment carried out except for experiment 18 as the gas flowrate was not correctly measured. The calculation procedures (performed using a spreadsheet) used to determine the energy balances are shown in Appendix VII. A summary of the energy balances is shown in Table 6.6 and Figure 6.3.

Table 6.6
Energy Balance Summary

Expt	Total inputs MJh^{-1}	Outputs, MJh^{-1}					Efficiencies, %		
		Dry gas	Tars	Losses	Total	Closure	Cold gas	Hot gas	Raw gas
1¢	23.32	15.65	1.23	5.40	22.29	95.59	55.87	67.23	72.53
2	33.94	24.19	2.04	11.76	37.99	111.91	59.66	71.39	77.40
3	32.02	16.63	1.55	11.78	29.97	93.60	44.61	52.04	56.90
4	7.21	4.22	0.00	1.89	6.12	84.88	42.82	58.91	58.91
5	26.91	16.61	1.53	9.15	27.29	101.43	54.34	61.83	67.54
6	25.41	16.64	1.46	9.13	27.23	107.17	57.91	65.66	71.44
7	23.92	15.60	1.59	11.79	28.98	121.16	54.89	65.37	72.03
8	28.43	17.78	1.97	11.79	31.54	110.92	51.87	62.68	69.61
9	24.01	12.00	1.39	7.70	21.09	87.81	39.80	50.05	55.84
10*	28.21	16.78	1.90	11.01	29.69	105.22	51.03	59.61	66.34
11*	24.17	10.81	1.29	8.04	20.14	89.43	39.13	44.82	56.27
12*	16.40	8.58	1.01	11.02	20.61	136.40	44.41	52.45	69.32
13	19.87	9.93	0.90	11.77	22.60	113.74	44.64	50.08	54.61
14	27.65	16.19	1.88	11.74	29.82	107.84	47.77	58.71	65.53
15	34.83	21.56	2.10	11.76	35.41	101.67	53.51	62.02	68.06
16	9.78	4.93	0.58	7.96	13.47	137.78	43.58	50.56	56.50
17	20.60	7.85	0.96	7.96	16.78	81.44	33.82	38.17	42.84
19	19.00	10.84	1.31	14.05	26.19	137.88	47.80	57.22	64.10
20	36.84	17.90	1.81	14.04	33.75	91.63	41.27	48.67	53.60
21	15.37	6.19	0.94	14.03	21.16	137.63	32.78	40.39	46.52
22	25.83	14.89	1.63	11.73	28.24	109.32	47.49	57.77	64.08
23¢	30.92	22.96	1.89	3.33	28.18	91.12	60.32	74.40	80.54
24¢	26.65	18.99	1.74	4.24	24.96	93.69	56.45	71.42	77.96
25¢	38.77	31.14	2.24	1.02	34.40	88.71	66.71	80.47	86.28
26	26.28	13.90	1.51	11.72	27.13	103.26	45.89	53.04	58.81
Mean:						107.29	49.62	59.22	66.11

* CO_2 was injected into gasifier

¢ Insulated gasifier

Energy balance closure/
cold gas efficiency, %
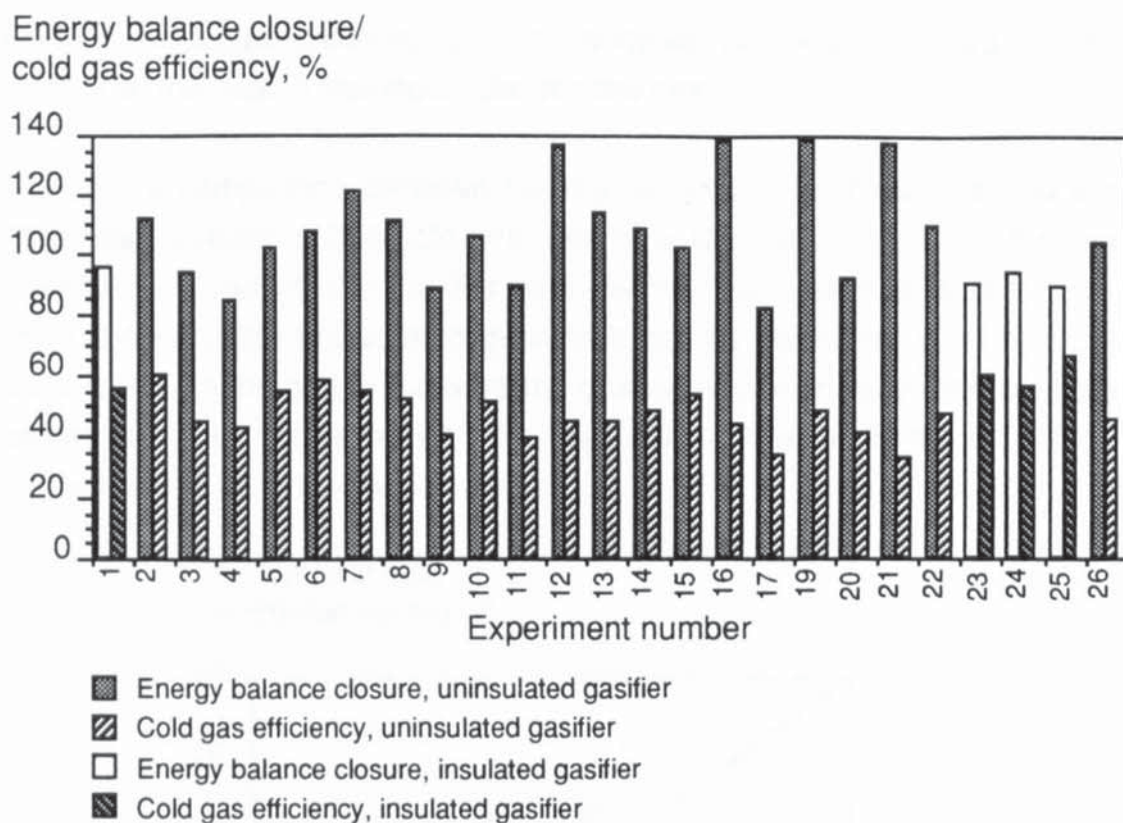
Figure 6.3

**Energy Balance Closures and Cold Gas Efficiencies**

The overall average energy balance closure was 107.29% (Table 6.6). 48% of the closures are within 10% of 100% closure. Excluding those experiments in which carbon dioxide was inputted into the gasifier, the average energy balance closure was 105.01% (Table 6.6). 50% of those closures were within 10% of 100% closure.

The average closures for the uninsulated gasifier experiments are high (the average closure for the uninsulated experiments from Table 6.6 is 107.84%). This is attributed to high estimations of the gasifier outside temperature leading to high gasifier heat losses since the mass balance closures are satisfactory (see Section 6.2.1).

Comparing visual observations firstly, temperatures in excess of 700°C were measured in the black zone of char below the glowing reaction zone during experiment 26 suggesting that there is variation in the radial temperature distribution in the gasifier since black coloured bodies indicate temperatures of less than 600°C (see Section 7.2.2) [110]. It was not possible to measure the radial temperature distribution in the gasifier since insertion of an array of thermocouples would excessively disturb the flow of material through the

gasifier. Acceptable disturbances to material flow were caused by the insertion of the search thermocouple into the gasifier.

Secondly, a comparison between the measured gasifier heat loss and the difference between 100% closure and the raw gas efficiency for the experiments in which the gasifier was operated uninsulated is shown by Figure 6.4. For the uninsulated gasifier, it can be seen that in all but four cases, the method used to measure the gasifier heat loss over-estimates the gasifier heat loss compared with the heat loss calculated by the difference between 100% and the raw gas efficiency.

Gasifier heat loss
(by difference) MJh-1
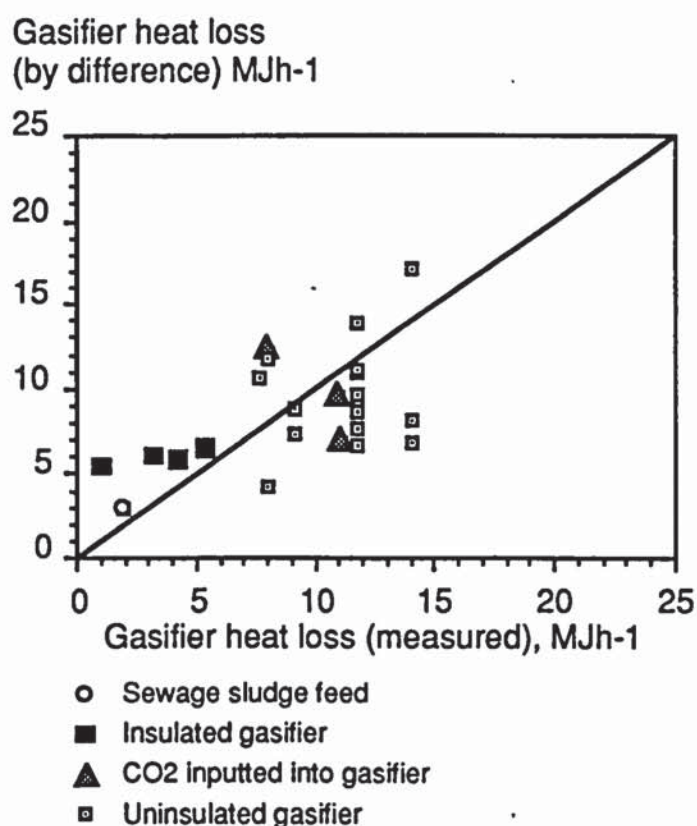
Figure 6.4

Comparison Between Measured Gasifier Heat Loss and Gasifier Heat Loss Calculated by Difference

Thirdly, the heat losses from the uninsulated Aston gasifier can be compared with heat losses for similar, uninsulated open-core downdraft gasifiers in the literature. Heat losses from the Aston gasifier occur by radiation and convection. The primary form of heat loss is by radiation, however. This is illustrated by the heat losses from experiment 26. The radiative heat loss was 10.16 MJh-1 equal to 38.75% of the chemical energy of the feed input to the gasifier. The convective heat loss from the gasifier was 1.56 MJh-1 equal

171

to 5.96% of the chemical energy of the feed. This results in a total heat loss during experiment 26 (uninsulated operation) of 44.71% of the chemical energy of the feed. During standard case operation, the average heat loss from the uninsulated gasifier was 45.0% of the chemical energy of the feed (average of experiments 22 and 26) while the heat loss from the insulated gasifier (see Section 8.6.7) was 13.1% of the chemical energy of the feed. Standard case operation is defined as uninsulated gasifier operation with wood chips sieved to between 6.35 mm and 12.7 mm and with a stable reaction zone (see Section 8.1).

Heat loss measurements for uninsulated open-core downdraft gasifiers are reported only by Reyes for the mark I Aston gasifier [17]. Reyes performed two energy balances over the mark I gasifier [17]. The heat losses from the mark I Aston gasifier are reported to be 24% and 38% of the chemical energy of the feed [17]. The average heat loss from the uninsulated mark II Aston gasifier (45%) compares well with the 38% heat loss reported for the uninsulated mark I Aston gasifier but compares badly with the 24% heat loss. The measured heat loss from the uninsulated Aston gasifier would, therefore, appear to be high (see Section 6.2.2).

The measured heat losses from the uninsulated Aston gasifier are high compared with the difference between 100% and the raw gas efficiency and the heat losses for similar gasifiers in the literature. This has resulted in high energy balance closures for the uninsulated gasifier experiments.

The average closure for the insulated gasifier experiments is low (92.3%) although acceptable. This is attributed to under estimations of the overall gasifier heat loss from the insulated gasifier. Figure 6.4 shows that the heat loss calculated from the difference between 100% and the raw gas efficiency for the insulated gasifier experiments is higher than the measured gasifier heat loss. The measured heat loss is low because there is additional heat loss from the sight strip cut into the insulation to permit observation of the gasification process.

The heat loss from the insulated gasifier can be compared with reported heat losses for open-core downdraft gasifiers in the literature since gasifiers in the literature are insulated. Heat losses from open-core downdraft gasifiers in the literature have only occasionally been evaluated. Energy

balances are reported for the KSU gasifier (Section 2.3.3) [8] and the Syngas gasifier (Section 2.3.7) [41]. The heat loss from the KSU gasifier was evaluated by assuming that heat is dissipated from the gasifier at an uniform temperature of 900 K to the surroundings at 298 K [8]. This resulted in a gasifier heat loss of 10% [8]. The hot gas efficiency of the Syngas gasifier is reported to be 93.8% indicating the overall gasifier heat loss to be 6.2%. The average heat loss from the insulated Aston gasifier (experiments 1, 23, 24 and 25) is equal to 13.1% of the chemical energy of the feed. Due to the small size of the Aston gasifier compared with the KSU (200 mm diameter) and Syngas (762 mm) gasifiers, heat losses will be magnified. The measured heat loss from the insulated Aston gasifier is, therefore, reasonable.

Comparing now the cold gas and hot gas efficiencies. The cold gas efficiency is defined as the ratio of the heating value of the product gas to the heating value of the feed input to the gasifier (Equation 6.9). The hot gas efficiency includes the sensible energy of the hot product gas (Equation 6.10). The cold gas efficiencies during uninsulated and insulated gasifier operation under standard case operation (experiments 22 and 26) were 46.69% and 63.51% respectively. This indicates that when cool, clean gas is required, 53.31% and 36.49% of the input feed energy is lost in the gasification process during uninsulated and insulated gasifier operation respectively. The average hot gas efficiency (this project) during standard case operation (uninsulated gasifier) was 55.40% (experiments 22 and 26). The sensible heat accounts for 8.71% of the input energy of the feed to the gasifier. During insulated gasifier operation, the average hot gas efficiency was 73.38%. During insulated operation, therefore, sensible heat accounts for 9.87% of the chemical energy of the feed.

The reported cold gas and hot gas efficiencies for the mark I Aston gasifier were 57.9% and 67.7% respectively. The high efficiencies are attributed to the very low nitrogen content (52.9%) reported for run 8R leading to a high product gas heating value [17]. This product gas nitrogen content could only be replicated in this project during insulated gasifier operation. However, the difference between the hot gas and cold gas efficiencies (9.8%) is consistent with those reported in Table 6.6.

The cold and hot gas efficiencies for the KSU gasifier (Section 2.3.3) are reported to be 72% and 80% [8]. The average cold and hot gas efficiencies reported for the Syngas gasifier are 70.9% and 93.85% respectively [41]. The hot gas efficiency reported for the Syngas gasifier is high compared with the hot gas efficiencies reported in this project and the literature. The difference between the cold and hot gas efficiencies is 22.95% which is also higher than those reported in the literature. In addition, the data presented does not match the reported efficiencies [41]. The cold and hot gas efficiencies for the insulated Aston gasifier are lower than those reported for the KSU gasifier. This is due to the higher heat loss from the Aston gasifier.

6.3   Summary

Mass and energy balances have been performed for each experiment carried out. The average mass balance closure was 96.09% and the average energy balance closure was 107.29%. The high energy balance closures are attributed to high estimations of the gasifier heat losses. Heat losses have been evaluated for both the insulated and uninsulated mark II Aston gasifier. The average heat loss from the insulated gasifier is equal to 13.1% of the chemical energy of the feed and the average heat loss from the uninsulated gasifier during stable operation is equal to 45.0% of the chemical energy of the feed.

7. DESCRIPTION OF THE OBSERVED GASIFICATION PROCESS

Previous work (Section 2.1.2) has shown that during operation, an open-core downdraft gasifier contains a number of zones with the gasification process occurring in two steps; flaming pyrolysis followed by char gasification. However, there is disagreement in the literature concerning the definitions and order of each zone in the gasifier. In addition, the dimensions of each zone have not been satisfactorily measured. Only qualitative measurements of the flaming pyrolysis and char gasification zone lengths are reported in the literature. Earp reports the length of the flaming pyrolysis zone length to no more than two particle diameters in length [12] and Reed reports the length of the flaming pyrolysis zone to be of the order of 11 feed particle diameters (Section 2.1.2) [19],[20]. The aim of this section is to describe the gasification process in an open-core downdraft gasifier, to confirm the definitions of the zones present in an open-core downdraft gasifier, to quantify the lengths of the flaming pyrolysis and gasification zones and to quantify the times for single particles to undergo flaming pyrolysis and char gasification.

7.1 Methodology and Basic Results

The use of the transparent quartz gasifier and the feed consisting of 15 mm diameter wooden beads (experiment 8) enabled the gasification process to be studied in detail. Observations of the behaviour of four single spherical particles made during steady state operation in experiment 8 are shown in Figures 7.1, 7.2, 7.3 and 7.4 (drawn using a video film of experiment 8). Experiment 8 was ended by "freezing" the gasification process using excess carbon dioxide (over 25 l.min^{-1}) and a number of particles were extracted for analysis. Photographs of these particles (including an unreacted particle) are shown in Plates 7.1 - 7.9. Two partially reacted balls were split and photographs of these sections are shown in Plates 7.10 and 7.11.

A photograph taken during experiment 8 is shown in Plate 7.12 and a schematic of the gasification process drawn from photographs of experiment 8 is shown in Figure 7.5. It can be seen that the spherical feed minimised the formation of bridges and voids in the reactor and led to well defined, horizontal reaction zones (Plate 7.12). From Plate 7.12 and Figure 7.5, the improved diagram showing the zones in an open-core downdraft gasifier has been deduced (Figure 7.6).

0 seconds
Particle diameter=15

70.8 seconds.
Diameter=14.42
Slight glow visible on
underside of particle.

3.5   2.3

10.2 seconds
Particle diameter =15
Initial charring

1.06

80.8 seconds.
Diameter=14.42
Bottom section of
particle now glowing

1.1   2.9
          2.3

20.6 seconds, further
charring. Particle
diameter=15

1.7

4.0   6.3

92.4 seconds.
Length=14.42,
width=12.69.
Bottom half of particle
still glowing.

0.6

30.5 seconds
Diameter=15

2.3

4.0   6.3

101.3 seconds.
Length=13.85,
width=11.54.
Not glowing as much
as before.

40.3 seconds.
Diameter=14.42

2.3

4.0

111.1 seconds.
Length=13.85,
width=8.65

50.0 seconds.
Diameter=14.42

2.3

3.5

121.8 seconds
Length = 12.69,
width = 8.65.
Particle fully charred.

60.1 seconds.
Diameter=14.42.
No glow or flame visible

3.5   2.3

Ball disappeared from view
after122 seconds

Unreacted wood

Charred wood

Glowing wood

To scale
All measurements in mm unless otherwise stated

Figure 7.1

**Observed Flaming Pyrolysis Process Undergone by Spherical
Feed Particle A**

0 seconds, ball is slightly charred in from previous contact with another, hotter ball below it (heat transfer by conduction). Ball diameter is 15mm.

33.02 seconds. Diameter=15mm.

46.1 seconds. Diameter=15mm

53 seconds. Length=15mm, width=13.85 mm.

63 seconds. Length=15mm, width=3.85 mm

69 seconds. Length=15 mm, width=13.27 mm Particle flaming a little

79.2 seconds. Length=14.42 mm, width=13.85, particle flaming from one glowing area

92.7 seconds. Length=14.42 mm, width=13.85 mm

102.5 seconds: Particle completely charred and resting on char bed.

126 seconds. Particle glowing. Length=13.85 mm, width=10.96 mm

134.7 & 144.7 seconds. Length=10.96 mm, width=8.08 mm

240.8 seconds Length=7.35mm width=5.88mm

242 seconds - particle disappeared from view

Unreacted wood

Charred wood

Glowing wood

To scale
All measurements in mm unless otherwise stated

Figure 7.2

Observed Gasification Process Undergone by Spherical Feed Particle B

Fresh particle on entering FP zone. 0 seconds. Particle diameter=15mm

8 seconds, slight charring to particle underside. Particle diameter=14.42mm

16 seconds, further charring. Particle diameter=14.42mm

20.4 seconds, particle diameter = 14.42mm

24 seconds, particle diameter=14.42mm

32 seconds, particle length=14.42mm, particle width=11.54mm

40 seconds. Particle almost completely charred. Particle length=13.27mm, particle width=114 mm

54 seconds, Particle completely charred-end of all flaming pyrolysis Particle length=11.54mm, particle width = 9.81mm

62 seconds, particle length=10.96 mm, particle width = 7.5mm

67.6 seconds, particle length=9.81mm, particle width=5.19mm

79.1 seconds, particle length=6.92mm, particle width=3.46mm

90.5 seconds, particle length=5.19mm, particle width=3.46mm

105.7 seconds, particle length=2.88mm, particle width=2.31mm

125.8 seconds, particle lands on char bed. Too difficult to see to measure size

Unreacted wood

Charred wood

Glowing wood

To scale
All measurements in mm unless otherwise stated

Figure 7.3

Observed Gasification Process Undergone by Spherical Feed Particle C

3.2 seconds, particle diameter=15 mm. Flames leaving particle travelling downwards

87.8 seconds, particle completely charred, FP complete, particle length and width=11.54mm

12.8 seconds, particle diameter = 15mm Particle rotated

119.1 seconds, particle length and width =10.96 mm

32.8 seconds, particle length=15mm, particle width=14.42 mm

129.1 seconds, particle length=10.38 mm, width=9.81 mm

42.8 seconds, particle length =15mm, particle width = 14.42 mm. Bottom of particle is glowing

148.8 seconds, particle length=10 mm, width = 9.23 mm

43.8 seconds, particle rotated. Length=15mm, width =14.42 mm

158.8 seconds, particle length=9.81 mm, width=9.23 mm

168.8 seconds, particle length and width =9.81mm

Area glowing

58.8 seconds, particle length =14.42 mm, particle width=12.69 mm

Glowing area

189.8 seconds, partile length=9.23 width=9.81 mm

262.3 seconds. Particle size=6.07 x 6.07 mm. Very difficult to see and measure.

79.8 seconds, particle length and width=12.11 mm

Unreacted wood

Charred wood

Glowing wood

To scale
All measurements in mm unless otherwise stated

Figure 7.4

Observed Gasification Process Undergone by Spherical Feed Particle D

Plate 7.1
Unreacted Bead (Mass 1.48 g)

Plate 7.2
Bead (1) Entering Flaming Pyrolysis Zone (Mass 1.13 g)

Plate 7.3
Bead (1) Entering Flaming Pyrolysis Zone (Mass 1.13 g)

Plate 7.4
Bead (2) Entering Flaming Pyrolysis Zone (Mass 0.91 g)

Plate 7.5
Bead (3) Entering Flaming Pyrolysis Zone (Mass 0.84 g)

Plate 7.6
Bead (3) Entering Flaming Pyrolysis Zone (Mass 0.84 g)

Plate 7.7
Bead (4) Entering Flaming Pyrolysis Zone (Mass 0.78 g)

Plate 7.8
Charred Bead (1) Removed from Char Gasification Zone (Mass 0.20 g)

Plate 7.9
Split Charred Particle (2) Removed from Char Gasification Zone
(Total Mass 0.54 g)

Plate 7.10
Section of Bead (5) Entering Flaming Pyrolysis Zone

184

Plate 7.11
Section of Bead (6) Entering Flaming Pyrolysis Zone
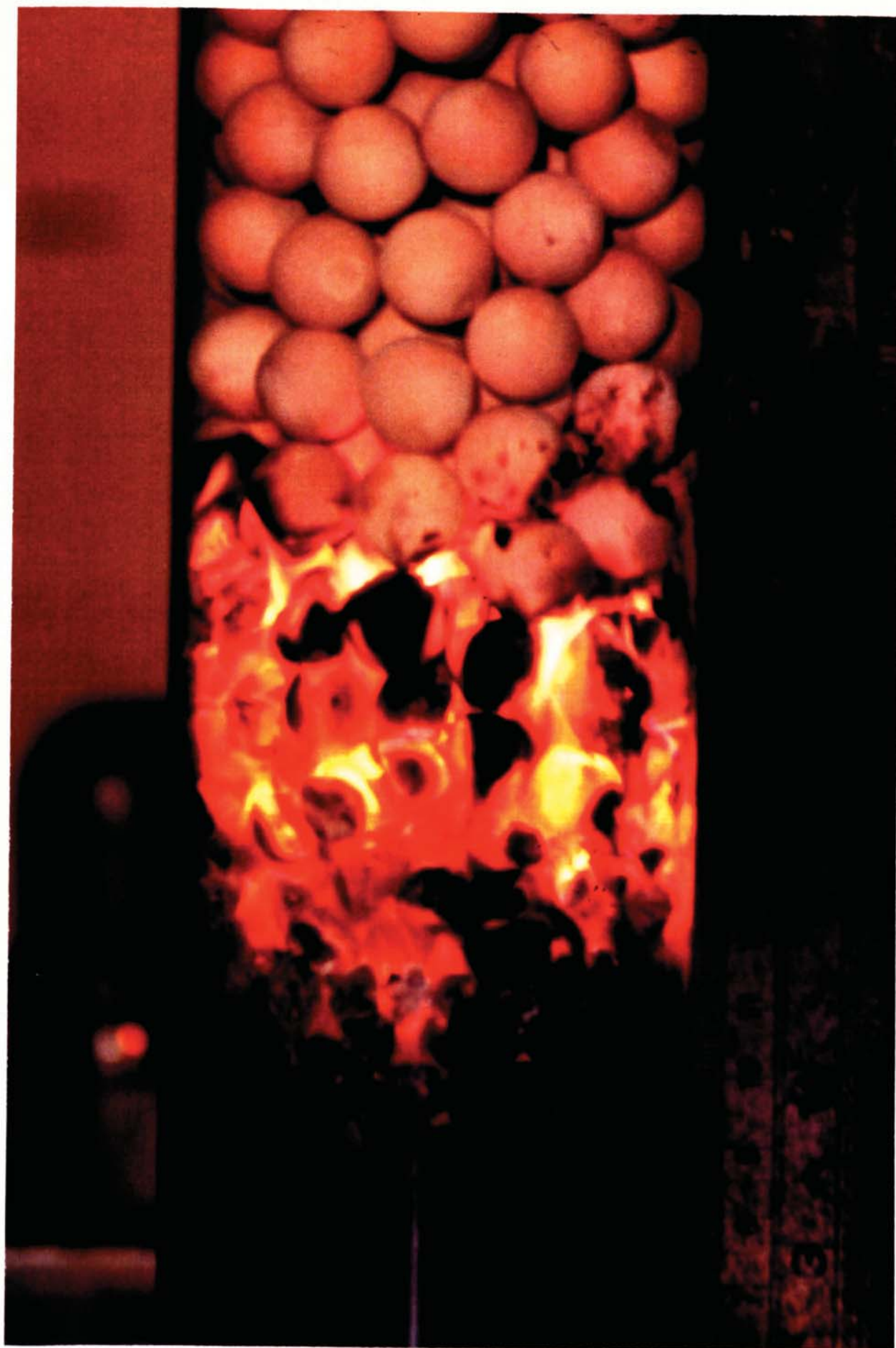
Plate 7.12
Gasification of 15 mm Beads (Experiment 8)

Flow of feed and air towards reaction zone

Particles undergoing drying, flaming pyrolysis and initial stage of gasification

Narrow voids form under flaming particles

Flaming gases flowing downwards due to action of venturi

Particles completing pyrolysis and commencing gasification

Unreacted feed

Emerging pyrolysis gases in boundary layer

1-2 diameters

0.75 diameter

0.5 diameter

Grate

Product gas

KEY

Unreacted wood

Charring due to pyrolysis

Glowing particles undergoing gasification (Orange: 900-1100°C)

Charred particles in hot char zone below gasification zone (Cherry red: 700-900°C)

Charred particles in hot char zone below gasification zone (Black with some red areas)

Black char particles in non reactive char zone

drawn to scale

Figure 7.5

Schematic of Observed Gasification Process Drawn Using Plate 7.12

187

Biomass Oxidant

Grate

**Product gas including
some char and ash to
downstream processing**

Unreacted feed

Drying and flaming pyrolysis

Char gasification

Ash

Inert char
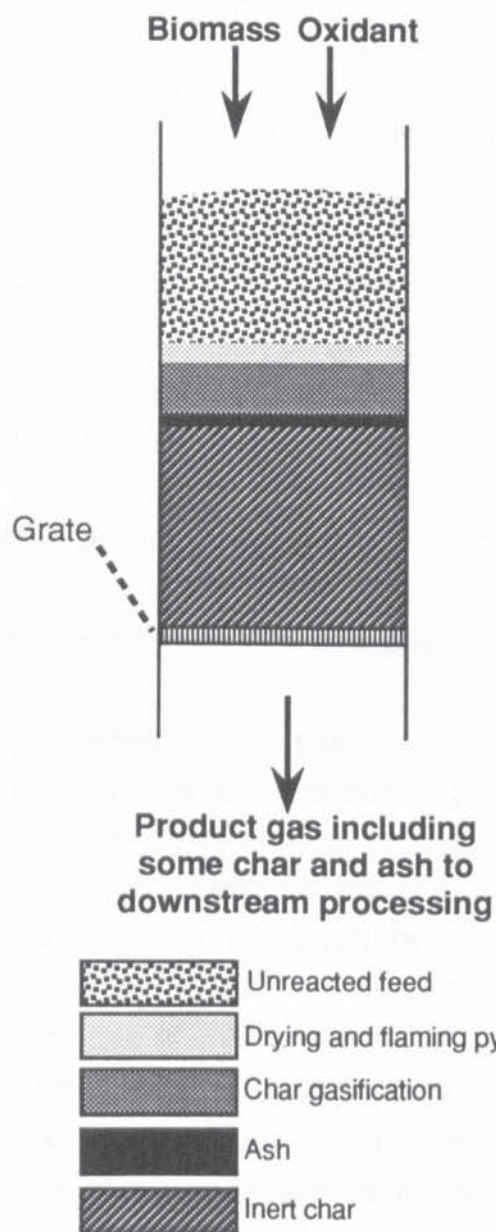
Figure 7.6
Zones in the Open-Core Downdraft Gasifier

7.2   Mechanism for Stable Gasifier Operation

Before considering and discussing the processes occurring in the open-core downdraft gasifier (Sections 7.3-7.4), the mechanism by which an open-core gasifier operates is discussed. An open-core downdraft gasifier can be operated in three modes:

i)   Stable operation: there is no net production of char in the gasifier;

ii)   Char consumption (gasification) dominant operation: there is a net consumption of char in the gasifier;

iii)   Pyrolysis dominant operation: there is a net production of char in the gasifier.

For a given open-core gasifier, the mode of operation is altered by the varying the air to feed ratio in the gasifier.

Open-core gasifier operation in these three modes has been reported by Reed [11] and Earp [12]. However, the mechanisms by which the different modes of operation are not discussed.

Two mechanisms for stable gasifier operation are proposed in this project:

i)   The oxygen entering the gasification zone is fully consumed by oxidation with the volatiles evolved during pyrolysis. No oxygen passes through the flaming pyrolysis zone and enters the char gasification zone. Energy produced by the oxidation of the volatiles provides sufficient energy to fully consume the char produced by flaming pyrolysis in the char gasification stage. Stable operation occurs as the rate of char production by pyrolysis equals the rate of char consumption by gasification. Increasing the air flow rate into the gasifier will increase the quantity of volatiles consumed increasing the energy available in the char gasification zone. There will be more energy in the char gasification zone than is required to consume the char produced by flaming pyrolysis and there will be a net consumption of char in the gasifier. Reducing the air input rate to the gasifier compared with stable operation will result in pyrolysis dominant operation. Pyrolysis dominant operation occurs as there is reduced oxidation of volatiles in the flaming pyrolysis zone. There will be insufficient energy in the char gasification zone to completely consume the char produced in the flaming pyrolysis stage by gasification.

ii)   Oxygen entering the gasifier is not fully consumed in the flaming pyrolysis zone and will enter the char gasification zone. Char consumption will occur, therefore, by oxidation and gasification. Char consumption (gasification) dominant operation will occur as increased amounts of oxygen will pass through the flaming pyrolysis zone unconsumed increasing the rate of char consumption by oxidation and gasification. Pyrolysis dominant operation will occur as less oxygen compared with stable operation will pass through the flaming pyrolysis zone reducing the level of char consumption by oxidation and gasification.

An indication of the mechanism occurring to maintain stable operation can be obtained by performing a theoretical mass balance over the flaming pyrolysis zone. The presence of carbon monoxide and hydrogen in the gases leaving the flaming pyrolysis zone suggests that there is incomplete combustion of the pyrolysis gases and that oxygen entering the gasifier is completely consumed during flaming pyrolysis. Char oxidation will not occur in the flaming pyrolysis zone as the volatiles emerging from the pyrolysing particles provide a buffering layer between the particle and flames preventing char reaction before completion of flaming pyrolysis. The buffering effect will also prevent the reduction of carbon dioxide to carbon monoxide before the completion of flaming pyrolysis.

Theoretical Mass Balance Over Flaming Pyrolysis Zone
(Units: kg. basis: 1 hour):
Assumptions:
- Empirical wood formula = $C_6H_{8.31}O_{3.38}$ ($CH_{1.385}O_{0.563}$) from analysis shown in Table 4.2
- Balance based on experiment 26 (stable operation)
- Experiment 26 equivalence ratio = 38.1%
- Nitrogen supplied by input air passes through the flaming pyrolysis zone unreacted
- Char is 100% carbon (density = 0.36 gcm^{-3}) [56]
- Char yield is 12.2% (Table 7.2 later)
- Methane is omitted to simplify the calculations
- Nitrogen in feed is negligable

<u>Inputs, kgh⁻¹</u>

Wood (daf)		1.23
Air		3.37
Total		4.60

<u>Outputs, kgh⁻¹</u>

Char		0.15
Gas+ vapourised liquids		4.45
Total		4.60

<u>Nitrogen Balance:</u>

All nitrogen in the air passes through the FP zone unreacted.

Nitrogen in air = 0.77 % by mass

Nitrogen in air = 0.77 x 3.37 = 2.59 kgh⁻¹ = nitrogen in product gas leaving of zone

<u>CHO Balances:</u>

% char remaining = 12% (see Table 7.2 later)

$$CH_{1.385}O_{0.563} + 0.381O_2 = 0.12C + xCO_2 + yCO + aH_2 + bH_2O \quad \text{...............[7.1]}$$

Carbon:	$x + y = 0.88$	....[7.2]
Oxygen:	$2x + y + b = 1.32$	....[7.3]
Hydrogen:	$2a + 2b = 1.38$	....[7.4]

from [7.2], $y = 0.88 - x$

from [7.4], $b = 0.69 - a$

substitute into [7.3]

$$2x + 0.88 - x + 0.69 - a = 1.32 \quad \text{..[7.5]}$$

$$a - x = 0.25 \quad \text{..[7.6]}$$

Either the % CO_2 or H_2 or CO or H_2O is needed.

from Reed [20], the CO_2 concentration at the end of the FP zone is 0.35 moles.

Giving x= 0.35, a = 0.60, b = 0.09 and y = 0.53

Substitute into [1],

$$CH_{1.38}O_{0.56} + 0.381O_2 = 0.12C + 0.35CO_2 + 0.53CO + 0.60H_2 + 0.09H_2O$$

$$\text{..[7.7]}$$

Mass flow rate (basis: per kmol feed) CO_2: $\dfrac{0.35 \times 44 \times 1.23}{22.39}$ = 0.85 kgh^{-1}

CO: $\dfrac{0.53 \times 28 \times 1.23}{22.39}$ = 0.81 kgh^{-1}

H_2: $\dfrac{0.60 \times 2 \times 1.23}{22.39}$ = 0.07 kgh^{-1}

H_2O: $\dfrac{0.09 \times 18 \times 1.23}{22.39}$ = 0.09 kgh^{-1}

Total   1.82 kgh^{-1}

% of total by mass (excluding nitrogen):
CO_2 46.70 %
CO 44.50 %
H_2 3.85 %
H_2O 4.94 %

From the overall mass balance over the flaming pyrolysis zone, the mass of gas at the end of the FP zone = 4.45 kgh^{-1}. The percentage of each component by mass including nitrogen is:

CO_2 19.10 %
CO 18.20%
H_2 1.57 %
H_2O 2.02 %
N_2 58.20 %

The theoretical mass balance over the flaming pyrolysis zone shows that there is incomplete combustion in the flaming pyrolysis zone. This supports the theory that oxygen entering open-core downdraft gasifiers is completely consumed by flaming pyrolysis and that oxygen is not available in the char gasification zone to enable char consumption by gasification and oxidation. Energy for the gasification process is provided by combustion of a proportion of some of the biomass.

The composition of the gaseous output from the flaming pyrolysis zone calculated by the theoretical mass balance over the flaming pyrolysis zone can be compared with the composition of the product gas (by mass) leaving the gasifier. The measured product gas composition from the gasifier during experiment 26 (the theoretical mass balance over the flaming pyrolysis zone was calculated using data from experiment 26) is shown below:

% of total by mass (including nitrogen): CO_2 19.26 %

CO   15.81%

H_2 0.64 %

CH_4 0.54 %

N_2 62.73 %

tars   1.00 %

The carbon dioxide concentration of the product gas leaving the gasifier is similar to the carbon dioxide concentration of the gases leaving the flaming pyrolysis zone. The concentrations of hydrogen and carbon monoxide are reduced in the product gas leaving the gasifier compared with the gases leaving the flaming pyrolysis zone. The reduction in carbon monoxide and hydrogen may be due to the action of the water gas shift reaction forming carbon dioxide and hydrogen (Equation 2.9) and the methanation reaction forming methane and carbon dioxide from carbon monoxide and hydrogen (Equation 2.11).

Stable operation in the open-core gasifier will occur since sufficient energy will be produced by flaming pyrolysis to enable complete consumption by gasification of the char produced by flaming pyrolysis.

7.3   Description of the Observed Gasification Process

It has been reported [12],[20] and observed in this project (Figure 7.5) that gasification in an open-core downdraft gasifier occurs in two steps; flaming pyrolysis followed by gasification of the char produced by flaming pyrolysis. In this section, a qualitative description of the flaming pyrolysis zone is firstly made followed by a description of the char gasification step.

7.3.1   Flaming Pyrolysis Step

A biomass particle in the unreacted feed zone (Figure 7.6) will approach the flaming pyrolysis zone due to the consumption of biomass in the reaction zones below. It is noted that unreacted feed moves downwards through the reactor towards the reaction zone as a plug. The start of the flaming pyrolysis zone is defined as a visible, broadly horizontal, black line within the particles undergoing flaming pyrolysis. Within one particle diameter of the flaming pyrolysis zone, the temperature at the bottom of the particle starts to rise rapidly due to back radiation from the hot zones below (Figure 7.7).

193
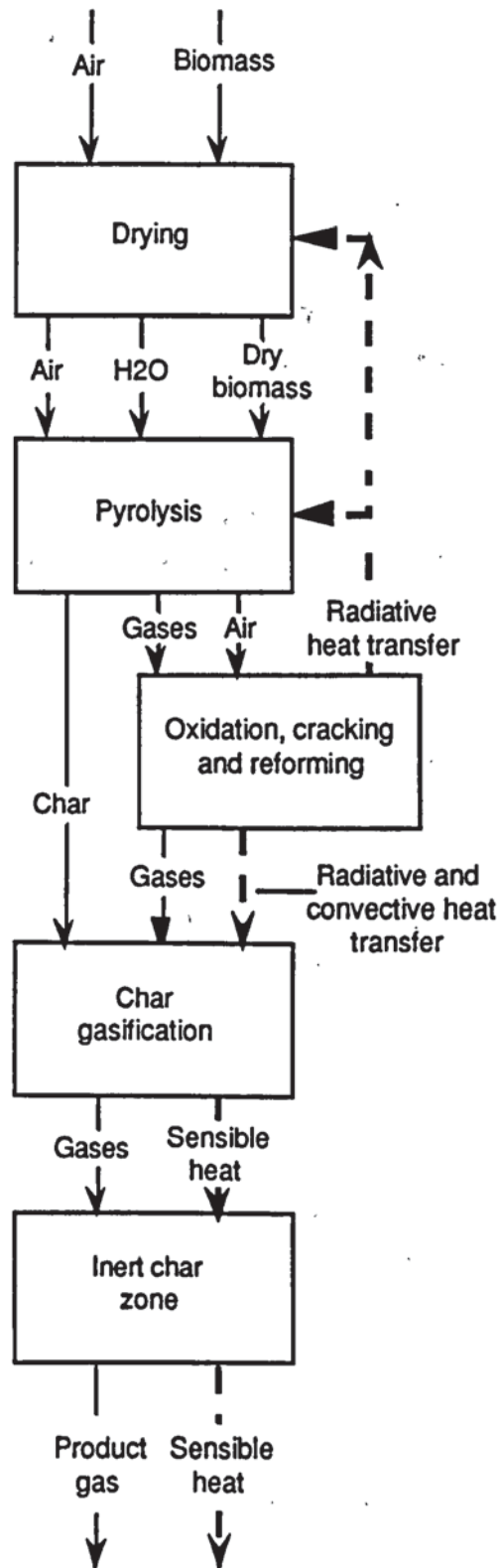
Figure 7.7
Flow Diagram of Gasification Process During Stable Operation
. in an Open-Core Downdraft Gasifier

194
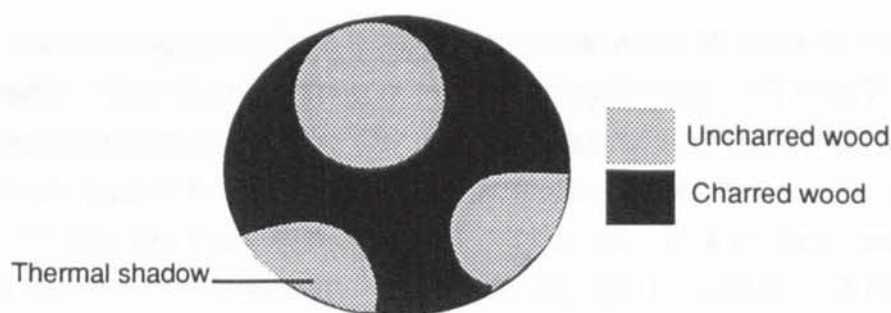
Figure 7.8

Sketch of Thermal Shadows Formed on Wood Particle Removed from Above Flaming Pyrolysis Zone

"Thermal shadows" formed on beads removed from just above the flaming pyrolysis zone (Figure 7.8) indicate radiation to be the main form of heat transfer to the unreacted feed at this point. There will be little heat transfer by convection and conduction to the unreacted feed. The bulk flow of gases through the gasifier is downwards and hot gases are drawn away from the incoming unreacted feed by the action of the venturi. Wood is a poor heat conductor - the thermal conductivity of white pine across the grain is 0.11 $wm^{-1}K^{-1}$ [57]. In addition, the incoming feed is kept cool by air entering the gasifier. Incoming unreacted particles will not start to pyrolyse, therefore, until they "see" radiation from the hot particles below. The rate of back heat transfer from the hot particles below the incoming unreacted particles will control the rate of flaming pyrolysis. During the gasification tests conducted in this project, the gasifier temperature at the bottom of the flaming pyrolysis zone in the uninsulated gasifier measured using a disappearing filament pyrometer was found to be approximately constant (Table 7.1) The rate of pyrolysis in the gasifier during standard operation will, therefore, be approximately constant and there will be just one feed rate at which the gasifier can be operated at stable operation.

Table 7.1

Temperature at Bottom of Flaming Pyrolysis Zone

Experiments	Experiment description	Temperature at bottom of FP Zone, °C		
		Average	Maximum	Minimum
22,26	stable operation	1018	1028	1009
2-22,26	All uninsulated gasifier experiments	1035	1074	1009

·During the flaming pyrolysis process, a thermal wave is seen to rise through the particle. This thermal wave is illustrated by Plates 7.10 and 7.11. Plate 7.10 shows a particle during the initial stages of flaming pyrolysis. Plate 7.11 shows a particle in the later stage of flaming pyrolysis. It can be seen in Plate 7.11 that the base of the particle is charred. This particle can be seen to have been simultaneously undergoing drying, pyrolysis and gasification at the point at which it was removed from the gasifier. During the gasification of spheres, the depth of the flaming pyrolysis zone was often observed to be less than one diameter with particles simultaneously undergoing drying, pyrolysis and gasification (see Figure 7.1).

As the thermal wave rises through the particle, moisture is firstly expelled and the particle subsequently pyrolyses (Figure 7.7). The thermal wave is observed as a progressive blackening moving upwards through the particle as shown in Figures 7.1-7.4. A few seconds after the start of pyrolysis, a flame can be seen around the particle separated from the particle by a boundary layer of emerging pyrolysis gases propagating down into the gasification zone below. From observations made during experiment 8, the depth of the flaming pyrolysis zone was observed to be approximately one particle diameter thick (see Section 7.4).

As the particle pyrolyses, its base can be seen flattening off and the particle shrinks (see Section 7.4 and Plates 7.1-7.6). Due to bridging of the pyrolysing particles and unreacted feed above, a very narrow, poorly defined void filled with burning pyrolysis gases sometimes appears below some pyrolysing particles. Voids were more prominent when using irregularly shaped wood chips. Periodically, the bridge forming the void collapses and the void zone disappears. Pyrolysing particles then fall directly on to the char bed below (Figures 7.6 and 7.7). Due to the high temperatures of approximately 1000°C found at the top of the char gasification zone, such particles more rapidly complete pyrolysis. During the gasification of wood chips, voids were never more than 5 mm in depth. During the gasification of beads in experiment 8, voids were not observed due to the superior flow characteristics of spheres compared with chips (Plate 7.12). Voids had no effect on the wood addition rate to the gasifier as shown by Figure 7.9.
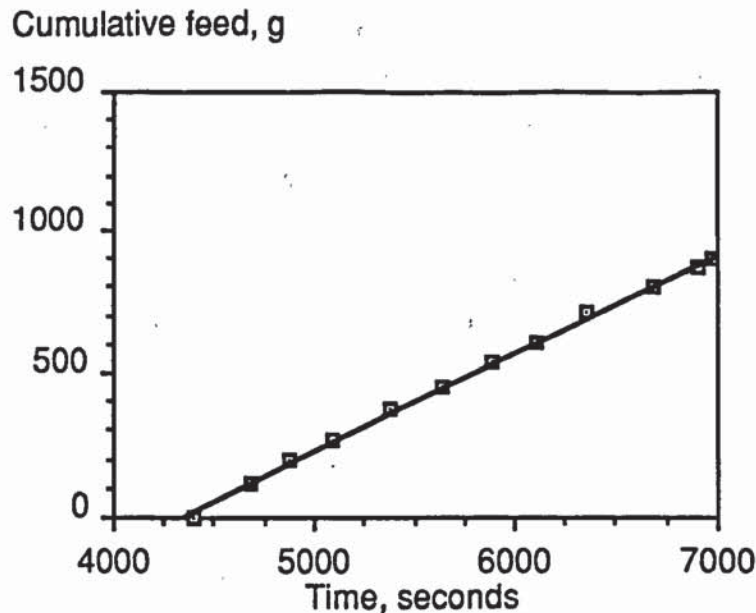
Figure 7.9
Wood Input Rate (Experiment 26-Stable Operation, Uninsulated Reactor)

The temperature in the flaming pyrolysis zone has been measured using a search thermocouple. The temperature in the flaming pyrolysis zone in the uninsulated reactor was found to be 561.7°C (an average of 14 measurements made during experiment 26). The temperature in the flaming pyrolysis zone in the insulated gasifier was found to be 710.6°C (an average of 11 measurements made during experiment 25). Gasifier vertical temperature profiles are shown in Section 8.6. These measurements suggest that the temperature in the gasifier does not immediately rise to approximately 1000°C at the interface between the unreacted feed and flaming pyrolysis zones as indicated by Earp [12], Reyes [17] and Reed [20]. The temperature in the gasifier rises to a pyrolysis zone temperature of approximately 550°C in the narrow pyrolysis zone (in the uninsulated gasifier) before rising further to the maximum gasifier temperature (approximately 1000°C in the uninsulated gasifier) at the top of the char gasification zone (Figures 7.5 and 7.6).

Following flaming pyrolysis, the charred particle commences char gasification (Section 7.3.1 and Figure 7.7).

7.3.1 Char Gasification Step

In the char gasification zone, char produced by flaming pyrolysis is consumed by gasification with the gaseous products of flaming pyrolysis

according to the reactions shown in Table 2.2. Energy for the gasification process is provided by oxidation of some of the gaseous products of pyrolysis with oxygen entering the gasifier. Heat transfer from the hot gases to the gasifying char particles will be by radiation and convection.

As the particle nears the end of flaming pyrolysis, the emission of burning volatiles dies away and the pyrolysed particle of char moves into the char gasification zone (see Figures 7.6 and 7.7). Definitions of the start and end of the char gasification zone are presented in Section 7.4.

The char gasification zone appears as a bright orange zone of char particles as shown in Figure 7.5 and Plate 7.12. Flames from the flaming pyrolysis zone were observed to flow down into the char gasification zone.

The temperature at the start of the char gasification zone in the uninsulated gasifier is 1018°C (Table 7.1) and 1043°C (experiment 26) in the insulated gasifier. These high temperatures provide sufficient energy to drive the gasification reactions (Section 7.2). Mass transfer of gas to the char particle, therefore, will be the rate controlling step. As the char particle gasifies, it cools due to the endothermic gasification reactions (Table 2.2) and reduces in size due to reactions at the particle external and internal surfaces (see Figures 7.3 and 7.4). Plates 7.3, 7.4, 7.5 and 7.6 show the char entering the char gasification zone to be cracked suggesting that char gasification occurs at both the particle external and internal surfaces. Towards the bottom of the glowing orange zone, the temperature reduces and the colour of the char darkens through cherry red, dull red to black. At temperatures below 700°C, there will be insufficient energy for the gasification reactions to proceed (Section 2.1.2.3). Once a particle enters the black area of char, it is likely that gasification reaction rates will be extremely slow.

At the end of the char gasification zone, the particle will be completely consumed (during stable operation) leaving a small amount of ash. The particles located at the interface between the char gasification zone and the inert char zone will be the smallest in the gasifier, therefore. Any ash which is not entrained with the product gas will collect at the bottom of the char gasification zone during stable operation (Figure 7.6). During pyrolysis dominant operation (Section 8.3), particles at the end of the char gasification zone will move into the unreactive, cool char zone and will not disappear

(Figure 7.6). It was not possible to visually determine the end of the gasification zone. A definition of the end of the char gasification zone is presented in Section 7.4.

Below the char gasification zone is a zone of char (Figures 7.6 and 7.7) in which gasification rates are insignificant since the temperature in this zone is below 700°C (below which temperature it is reported that rates of gasification reactions are insignificant [20]). The temperature in the cool char zone will also be too low for thermal cracking since a tar temperature of 900°C is required [29]. During stable gasifier operation, the char in inert char zone takes no part in the gasification reactions although it may act as a hot gas filter. Due to heat losses to the surroundings from the inert char zone, the product gas temperature falls to between approximately 500 and 600°C at the grate depending on the height of the char bed and the extent of gasifier insulation (see Section 8.6).

7.4   Quantitative Evaluation of the Flaming Pyrolysis and Char Gasification Zones

In this section, the measured times for a particle to undergo flaming pyrolysis and char gasification and the flaming pyrolysis and char gasification zone lengths in the uninsulated gasifier are reported and compared with calculated particle flaming pyrolysis and char gasification times and flaming pyrolysis and char gasification zone lengths. Data on the duration of the steps in gasification and the gasification zone lengths are valuable to aid construction of models.

7.4.1   Flaming Pyrolysis Zone

In this section, the particle mass loss during flaming pyrolysis, the time for flaming pyrolysis and the flaming pyrolysis zone length are reported.

7.4.1.1   Particle Mass Loss During Flaming Pyrolysis

The size of particles before and after flaming pyrolysis measured from a video film of experiments 7 and 8 was used to measure the percentage mass loss experienced by particles undergoing flaming pyrolysis (assuming the density of the char particles to be constant and equal to 0.36 gcm^{-3} [56]). These are presented in Table 7.2.

Table 7.2
Particle Weight Loss During Flaming Pyrolysis

Feed type	Initial volume cm³	Char volume cm³	Char density gcm⁻³ [56]	Initial mass g ×10²	Char mass g ×10³	Reduction in volume %	Reduction in mass %
Woodchips*	0.052	0.004	0.36	2.67	1.45	92.3	94.6
Beads	1.767	0.769	0.36	146.00	277.00	56.5	81.0
Average						74.4	87.8

*   Sieved to between 4.75 and 6.35 mm

It is noted that during flaming pyrolysis, there is only a small reduction in particle diameter (from 15 mm to 11.4 mm for the beads gasified in experiment 8) of 24.2%. This reduction in diameter, however, results in a reduction in volume of 56.5%.

There is an average weight loss during flaming pyrolysis of 87.80% (Table 7.2) which is in agreement with the published weight loss on flaming pyrolysis for wood of between 80 and 95% [19],[20]. An average of 12.2% by mass of the original particle remains as char to be gasified in the char gasification zone (Table 7.2). This char yield is equivalent to the char yield from flash pyrolysis [1]. During flaming pyrolysis, volatiles exiting pyrolysing particles are rapidly drawn downwards away from the particle and undergo partial combustion. Secondary pyrolysis reactions which result in higher char yields from wood for conventional pyrolysis technologies (30-35%) will not, therefore, occur [1].

The char yield from the larger beads is greater than the char yield from the smaller wood chips (Table 7.2). The volatiles released during pyrolysis are composed of reactive and non-reactive components. As the particle size is increased, some of the reactive components will have sufficient time to deposit carbon within the particle before leaving the particle increasing the char yield during pyrolysis [37].

7.4.1.2   Flaming Pyrolysis Zone Length and Time for Flaming
               Pyrolysis

The start of flaming pyrolysis is defined as the point at which a particle starts to blacken (Figures 7.1-7.4). The start of flaming pyrolysis in the gasifier was observed as a horizontal black line in the wood feed entering the reaction zone. The end of flaming pyrolysis of a particle was defined as the point at which the particle is completely blackened and no flames are emitted from the particle. Plate 7.11 shows that the centres of particles undergoing flaming pyrolysis will be charred before the top of the particle. This suggests that when a particle is fully blackened, then flaming pyrolysis will be complete and the particle will be fully charred.

The flaming pyrolysis time for individual particles (seconds) and the flaming pyrolysis zone length (mm) in the uninsulated gasifier were measured for three different particle sizes (experiments 7, 8, 22). The time for flaming pyrolysis was measured using a stopwatch directly during experiments and using video film. The flaming pyrolysis zone length was measured from still photographs of the gasifier (Plate 7.12).

Table 7.3 presents the measurements of flaming pyrolysis time and flaming pyrolysis zone length for the uninsulated gasifier. From Figures 7.1-7.4, the time for pyrolysis to reach 50% completion (ie. 50% of the particle is blackened) is approximately half the time required for 100% completion of pyrolysis.

From Table 7.3, it can be seen that the flaming pyrolysis zone has an average length of 1.20 feed particle diameters. As noted in Section 7.2.1, however, particles (especially during experiment 8) were often observed to simultaneously undergo drying, pyrolysis and gasification as shown in Plate 7.10. From Plate 7.10, the depth of the flaming pyrolysis zone for such a particle was 3.6 mm.

The data in Table 7.3 is presented graphically in Figure 7.10. It can be seen that the time for flaming pyrolysis and the flaming pyrolysis zone length increase with particle characteristic diameter (size).

Table 7.3

Flaming Pyrolysis Times and Flaming Pyrolysis Zone Lengths for Different Sized Particles (Uninsulated Reactor)

Particle descrip- -tion	Size range mm	Particle characteristic diameter, mm	FP time seconds	FP zone length mm	FP zone length, characteristic diameters
chips*	3.35-4.75	4.52	28.8	5.8	1.28
chips*	6.35-12.7	9.46	46.7	10.0	1.06
beads§	15ø	15.00	85.4	18.8	1.25
Average					1.20

* Average of six determinations

§ Average of 8 determinations
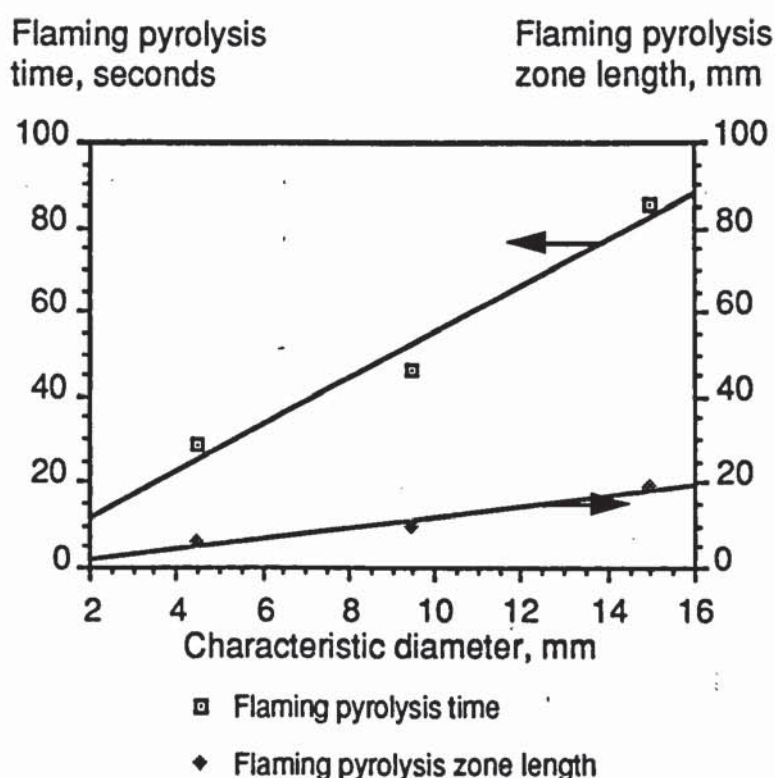
Figure 7.10

Flaming Pyrolysis Time and Flaming Pyrolysis Zone Length v Feedstock Characteristic Diameter (Experimental Results - Uninsulated Reactor)

The average length of the flaming pyrolysis zone (defined as the distance between the point at which a particle started to blacken and the point at which the particle is fully blackened and no flames are emitted) has been

found to be 1.2 feed particle diameters. The length of this zone has been found to increase with feed particle size. The time for flaming pyrolysis has also been found to increase with particle size. The time for flaming pyrolysis for the 15 mm beads was 85.44 seconds.

7.4.1.3 Flaming Pyrolysis Zone Modelling

Modelling of the flaming pyrolysis zone length is important to enable the determination of gasifier dimensions. Equations 2.14 and 2.15 (Section 2.1.2.2) can accurately predict the flaming pyrolysis zone length and the time for flaming pyrolysis in an open-core downdraft gasifier. These equations were used to calculate the time for flaming pyrolysis and the length of the flaming pyrolysis zone for the different sized feedstocks shown in Table 7.3 for comparison with the experimental results (see Table 7.4). These data are graphically presented in Figure 7.11 with the measured results from Table 7.3 superimposed. The flaming pyrolysis zone length was calculated from the average wood flow rates in experiments 7 (4.52 mm representative diameter chips), 26 (9.46 mm representative diameter wood chips) and 8 (15 mm diameter beads). The flaming pyrolysis zone temperature used to calculate the flaming pyrolysis time (Equation 2.14) was 600°C as the measured temperatures in the flaming pyrolysis zone were approximately 600°C (Section 7.3). Feed data used in the calculation are shown in Table 4.4.

Table 7.4 Calculated Flaming Pyrolysis Times and Flaming Pyrolysis Zone Lengths (Uninsulated Reactor)					
Particle characteristic diameter mm	Particle sphericity	Particle description	FP time seconds	FP zone length, mm	FP zone length Characteristic diameters
4.52	0.71	chips	16.71	5.60	1.24
9.46	0.76	chips	45.25	13.22	1.40
15.00	1.00	beads	110.28	19.00	1.27
Average					1.30

203
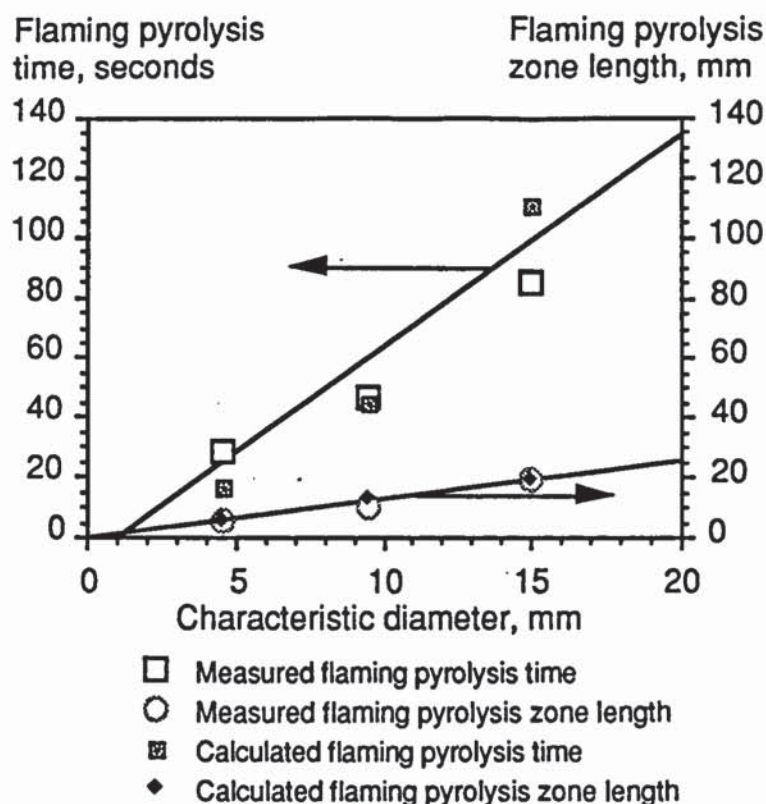
Figure 7.11

Comparison Between Measured and Calculated Flaming Pyrolysis Times and Flaming Pyrolysis Zone Lengths

As noted by Reed, the flaming pyrolysis time equation (Equation 2.14) predicts that the the flaming pyrolysis time and flaming pyrolysis zone length increase with characteristic diameter. This trend agrees with the trends obtained experimentally as shown in Figure 7.10.

There is good agreement between the experimentally determined and calculated flaming pyrolysis times (Figure 7.11). For the smaller 4.52 mm diameter wood chips, the agreement is less good. The calculated flaming pyrolysis time is within 3% of the experimental value for the 9.46 mm diameter wood chips and 30% of the experimental value for the 15 mm diameter beads.

There is good agreement between the calculated and experimentally determined flaming pyrolysis zone lengths for each of the feedstocks considered. The calculated flaming pyrolysis zone lengths are within 4% of the measured values for the 4.52 mm diameter wood chips and the 15 mm diameter beads.

204

Equation 2.14 is sensitive to variations in the pyrolysis zone temperature. The sensitivity of the output from Equation 2.14 to the pyrolysis zone temperature is shown in Table 7.5. This data is presented graphically by Figure 7.11. Increasing the flaming pyrolysis zone temperature by 50% from 600°C to 900°C reduces the flaming pyrolysis time by 50%. The sensitivity analysis shows that the assumption of a 600°C flaming pyrolysis zone temperature is accurate.

Table 7.5
Model of Flaming Pyrolysis Zone - Sensitivity to Temperature

Feed: 15 mm diameter beads

Temperature °C	Flaming pyrolysis time, seconds	Temperature °C	Flaming pyrolysis time, seconds
500	152.76	800	68.96
600	110.28	900	57.91
700	85.13	1000	49.98
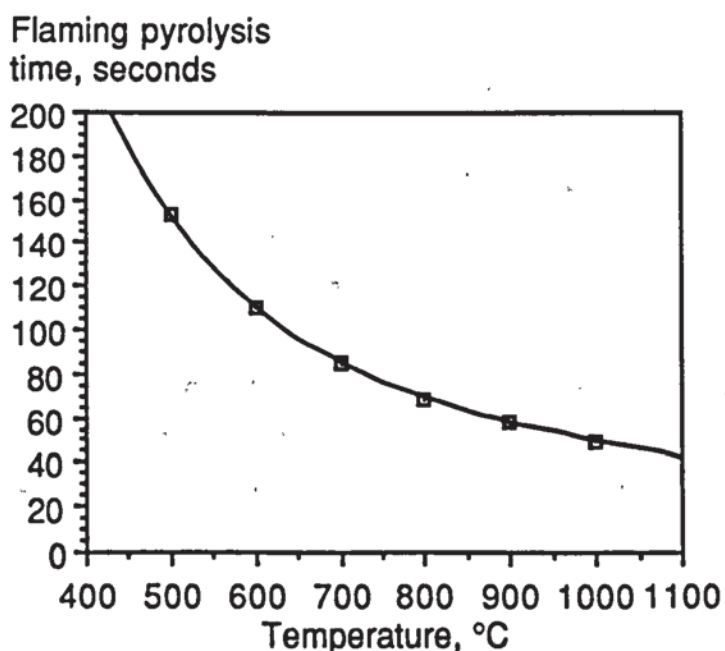
Figure 7.12
Effect of Temperature on Flaming Pyrolysis Zone Model (15 mm Diameter Beads)

Equations 2.14 and 2.15 have been used to predict the flaming pyrolysis time and flaming pyrolysis zone length in the open-core downdraft gasifier.

The model predicts that the average calculated flaming pyrolysis zone length in terms of characteristic diameters is 1.30 feed particle diameters. This compares well with the measured flaming pyrolysis zone length of 1.20 feed particle diameters. However, care must be taken when using this model to input an accurate pyrolysis zone temperature.

7.4.1.4   Flaming Pyrolysis Zone Length and Time For Flaming Pyrolysis in the Insulated Reactor

In this section, the measured times for flaming pyrolysis and the flaming pyrolysis zone lengths in the insulated and uninsulated gasifier are reported and compared. Insulation will reduce the heat losses from the reaction zones. The measured temperatures in the flaming pyrolysis zone during insulated and uninsulated gasifier operation were 710.6°C (experiment 25) and 561.7°C (experiment 26) respectively. The flaming pyrolysis time for a single particle and flaming pyrolysis zone length decrease to an asymptotic minimum with pyrolysis temperature as shown in Figure 7.12 produced from data calculated using Equation 2.15. An increase in temperature will, therefore, reduce the flaming pyrolysis time and the flaming pyrolysis zone length.

The flaming pyrolysis zone length and flaming pyrolysis time in the insulated gasifier were measured using wood chips sieved to between 6.35 mm and 12.7 mm during experiment 25. The flaming pyrolysis time was measured using a stopwatch. The flaming pyrolysis zone length was measured using a ruler mounted vertically next to the sight strip.

A comparison of the experimental observations of flaming pyrolysis time and flaming pyrolysis zone length in both an insulated and uninsulated gasifier for wood chips sieved to between 6.35 and 12.7 mm (experiments 25 and 26) are shown in Table 7.6.

It can be seen that insulating the gasifier reduces the flaming pyrolysis time by 20% and the flaming pyrolysis zone length by up to 10%. This confirms the trend shown in Figure 7.12.

Table 7.6
Comparison of Measured Insulated and Uninsulated Reactor Flaming Pyrolysis Times and Flaming Pyrolysis Zone Lengths

Feedstock: Wood chips, characteristic diameter: 9.46 mm

	Uninsulated reactor*	Insulated reactor
Flaming pyrolysis time, seconds	46.7	37.2
Flaming pyrolysis zone length, mm	10.0	9-10
Flaming pyrolysis zone length, characteristic diameters	1.06	0.95-1.06

* Table 7.3

The data in Table 7.6 can be compared with the flaming pyrolysis time and the flaming pyrolysis zone length for both the uninsulated and insulated gasifier calculated using Huff's model of flaming combustion modified by Reed to describe the flaming pyrolysis zone (Equation 2.14). The calculated flaming pyrolysis times and flaming pyrolysis zone lengths for the uninsulated and insulated gasifier are shown in Table 7.7. There is good agreement between the experimental and calculated results for both the flaming pyrolysis time and flaming pyrolysis zone length for the insulated gasifier. The calculated values for the flaming pyrolysis zone length clearly show a decrease in the flaming pyrolysis zone length between the insulated and uninsulated reactor.

7.4.2 Char Gasification Step During Stable Operation

In this section, the char gasification zone length and the measured time for a single particle to undergo char gasification in the uninsulated gasifier is reported and compared with a calculated particle char gasification time and char gasification zone length.

7.4.2.1 Char Gasification Zone Length

The start and end of the char gasification zone are not clearly defined in the literature. Two definitions are presented in this project.

Table 7.7

Comparison of Insulated and Uninsulated Reactor Flaming Pyrolysis Times and Flaming Pyrolysis Zone Lengths (Calculated Results)

Feedstock: Wood chips, characteristic diameter: 9.46 mm

	Uninsulated reactor	Insulated reactor
Flaming pyrolysis time, seconds	45.25	34.09
Flaming pyrolysis zone length, mm	13.22	9.39
Flaming pyrolysis zone length, characteristic diameters	1.40	0.99

Definition 1

The start of the char gasification zone is defined as the end point of flaming pyrolysis (the point at which the char particle about to undergo gasification is fully charred and no flames are emitted by the particle). The end of the char gasification zone is defined as the interface between the glowing zone of char and the black zone of char in the gasifier since glowing bodies indicate temperatures above 700°C (below which gasification is reported not to occur [19],[20]). The length of the char gasification zone may, therefore, be defined by the length of the glowing char zone in the gasifier (Figure 7.13).

The length of the char gasification zone as defined by definition 1 can be measured during an experiment or from photographs of the gasifier in operation. From Plate 7.12 and Figure 7.5, the length of the zone of glowing char is 28-55 mm (1.9-3.7 unreacted feed particle diameters). The length of the char gasification zone during the gasification of wood chips sieved between 6.35 mm and 12.7 mm was 4.5 cm equivalent to 4.8 mean representative feed particle diameters. These result are greater than the char gasification zone length reported by Earp (one feed particle diameter). However, Earp does not provide a definition for the start and end of the char gasification zone.
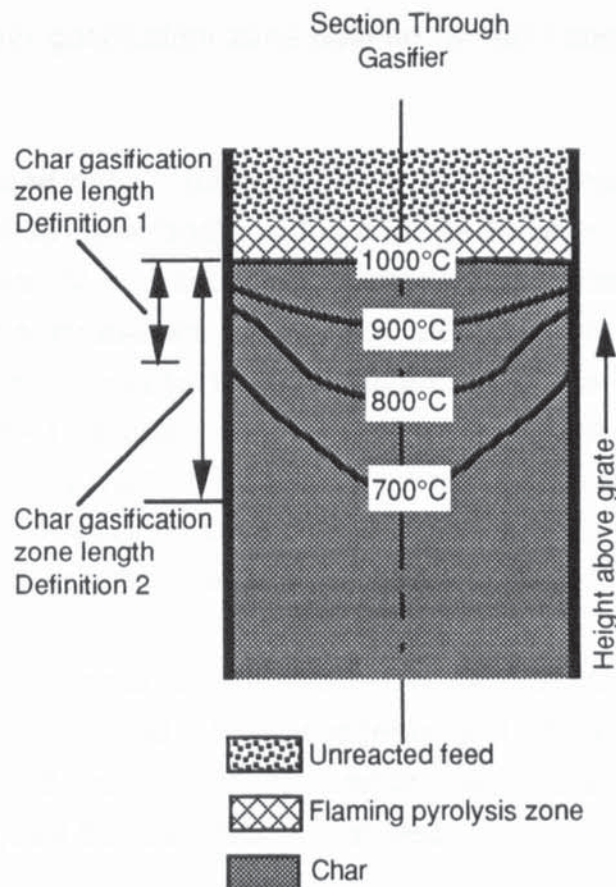
Figure 7.13
Char Gasification Zone Definitions

Definition 2

The determination of the char gasification zone length according to definition 1 does not account for the fact that the temperature of the char in the centre of the gasifier could be higher than the temperature of the char observed at the gasifier walls due to heat losses from the gasifier to the surroundings. Gasification may occur in the zone of black coloured char below the visibly glowing char (Figure 7.5).

The char gasification zone length is defined here from the vertical temperature profile through the gasifier (see Figures 8.14 and 8.15 later). The start of the char gasification zone is defined as the point at which the temperature in the gasifier is a maximum since when the gasification reactions start, the temperature in the gasifier will reduce. The bottom of the char gasification zone is defined as the point at which the temperature is 700°C (below·which gasification is reported not to occur [19],[20]). The

length of the char gasification zone defined by definition 2 is illustrated by Figure 7.13.

For the uninsulated reactor using wood chips sized between 6.35 and 12.7 mm (experiment 26), the length of the char gasification zone (definition 2) was 9 cm equivalent to 9.5 unreacted mean representative feed particle diameters. This measured value calculated from the gasifier vertical temperature profile is greater than the length of the observed glowing zone of char (definition 1) during experiment 26 of 4.5 cm (4.8 unreacted mean representative feed particle diameters), however. Both of these results are greater than those reported by both Reed [20] and Earp [12]. However, neither Reed or Earp clearly define the start and end of char gasification.

The variation in results arising from the two definitions of the char gasification start and end points suggests that the bottom of the char gasification zone forms an inverted bowl shape (Figure 7.13). In addition, definition 2 suggests that definition 1 is limited.

It is concluded that it is difficult to evaluate the length of the char gasification zone as it is difficult to observe the end of the char gasification zone. A suggested method to locate the end of the char gasification zone is to find the position at which the average char particle particle diameter in the gasifier is a minimum (Section 10). Defining the char gasification zone as the height of the glowing area of char results in a char gasification zone length of 4.5 unreacted mean representative feed particle diameters for wood chips sized between 6.35 mm and 12.7 mm. The length of the char gasification zone measured using the vertical temperature profile through the reactor during stable operation was found to be 9.5 unreacted mean representative feed particle diameters in length for wood chips sized between 6.35 mm and 12.7 mm.

7.4.2.2 Time of Char Gasification

Observations of the gasification of single char particles were carried out to determine the char gasification time for single particles. The char gasification time for seven particles is shown in Table 7.8 (including the particles illustrated by Figures 7.2-7.4). These data were obtained using a video of experiment 8. It was found to be difficult to observe particles nearing the end of char gasication since particles disappeared from view

before the end of gasification. However, it was possible to observe particles undergoing gasification to an average of 86.9% completion by volume (Table 7.8). The average gasification time for 86.9% conversion was 200.0 seconds (Table 7.8). The fastest gasification time was 71.8 seconds and the slowest gasification time was 359.4 seconds. Bead C moved very slowly downwards through the glowing zone of char and, therefore, remained near the top of the char gasification zone where the gasifier temperature is highest and where the gasification reaction rates are fastest. Beads B, H and I were observed to more quickly move towards the base of the glowing zone of char where the temperature is reduced and where gasification rates will be slower compared with the top of the gasification zone. Bead I was observed positioned near the base of the glowing zone of char for approximately 100 seconds (260-359.4 seconds) before becoming too small to observe. Linear extrapolation of the char particle gasification time (200 seconds for 86.9% mass conversion) to 100% mass conversion results in a total gasification time for char particles formed from 15 mm diameter beads of 230 seconds.

Table 7.8
Single Char Particle Gasification Times

Particle	Percent reduction in mass	Measured time, seconds
Beads B (Figure 7.2)	89.8	240.8
Bead C (Figure 7.3)	98.6	71.8
Bead D (Figure 7.4)	85.4	174.5
Bead E	81.4	180.7
Bead F	80.6	117.2
Bead G	90.9	181.4
Bead H	82.6	274.6
Bead I	85.9	359.4
Average	86.9	200.0

The average gasification time shown in Table 7.8 is greater than that reported by Earp [12] and Reed [20]. Earp reports that wood chips sized between 4.75 and 6.35 mm were completely gasified in 36 seconds and that

dowels (5 mm diameter, 6.35 mm length) were completely gasified in 65 seconds. The number of particles used for the determination and method of determination used are not reported. Reed suggests that gasification is 90% complete (at 1200 K) in about 100 - 140 seconds [20]. He does not, however, report the particle size.

Single char particles have been observed undergoing gasification and the time for a single char particle to undergo gasification measured. The average char gasification time for 15 mm diameter beads has been found to be 200.0 seconds for 86.9% char conversion. However, it was not possible to observe the particles to 100% conversion since, in each case, the particles disappeared from view.

7.4.2.3 Char Gasification Zone Modelling

Modelling of the char gasification zone length is important, since, in combination with a model to measure the flaming pyrolysis zone length, a prediction of gasifier dimensions can be made.

The char gasification model presented by Reed is simple and consists of the length of reactor that the fuel will travel through in 100 seconds (Section 2.1.2.3) [24]. This model has been applied to the feedstocks tested in this project using a char gasification time of 100 seconds to initially determine the accuracy of the model (Table 7.9 and Figure 7.14). The actual feed throughput for each feed type measured in this project was used to determine the char gasification zone length leading to the spread of data points. The observed char gasification zone length (definition 1) results are superimposed on Figure 7.14.

Table 7.9 Calculated Char Gasification Zone Lengths (Reed's Model)						
Feed characteristic diameter, mm	4.52	6.71	9.28	9.46	11.77	15.00
Zone length, cm	3.25	1.85	3.66	2.76	3.02	1.74

Char gasification
zone length, cm

Model results

Measured results (15 mm
diameter beads - definition 1)
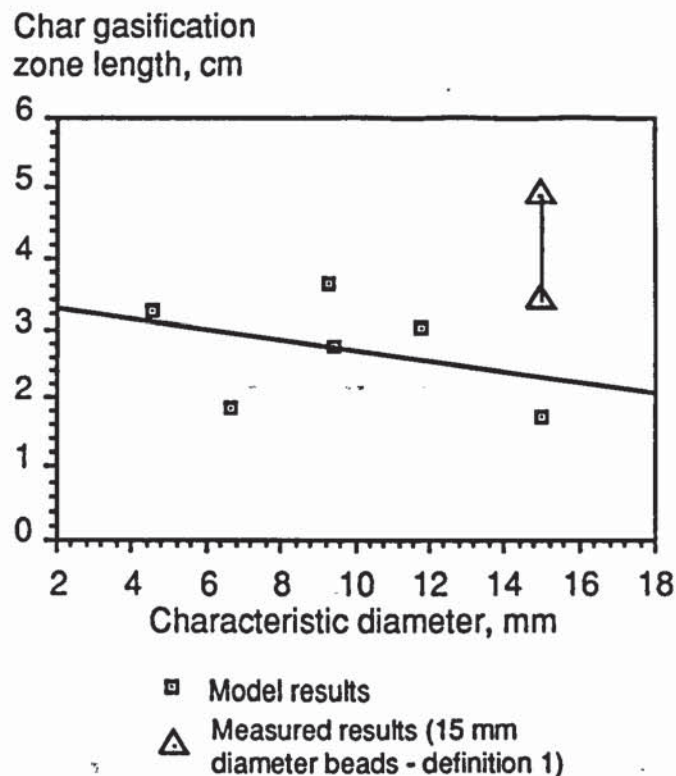
Figure 7.14

**Calculated Char Gasification Zone Length versus Feed Particle
Characteristic Diameter (Reed's Model)**

It can be seen that as the feed particle characteristic diameter is increased, there is a small decrease in the calculated char gasification zone length although the curve fit is less than satisfactory. This trend disagrees with the results of Reed which show that the char gasification zone length increases with particle size [26].

The calculated char gasification zone lengths (Table 7.9) are lower than the char gasification zone lengths measured according to both definitions 1 and 2. The model is also limited since it calculates the char gasification zone length from the feed velocity through the gasifier and not the char velocity.

It was decided, therefore, to develop a new model to calculate the length of the char gasification zone in an open-core downdraft gasifier. It was suggested in Section 7.3.2 that the base of the char gasification zone forms an inverted cone. By considering the char gasification to be wholly cone shaped (Figure 7.15), the modelling process can be simplified since the same number of particles can be considered entering and leaving a number of imaginary zones (into which the gasification zone can be split to permit modelling).

213
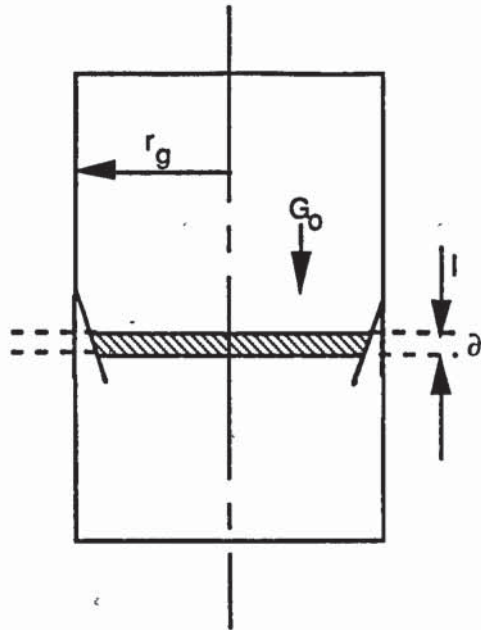
Figure 7.15

Pictorial Representation of Parameters in Char Gasification Zone Length Model

Nomenclature:

a   Surface area of particles per unit volume of packed bed

a_l Surface area of particles per unit volume of packed bed at distance l below star t of the char gasification zone

ε_c Char bed voidage at start of char gasification zone

ε_l Char bed voidage in section through char gasification zone, ∂l where ∂l is the length of a section through the char gasification zone

ε_w Wood bed voidage, (Table 4.4),

G_o Mass flow rate of char into imaginary char gasification zone, gs^{-1}

G_w Mass flow rate of wood into gasifier, gs^{-1},

L   Length of char gasification zone, cm

∂l Length of section of char gasification zone at a distance l below the start of the char gasification zone

N_p Number of particles entering the gasification zone in unit time:

$$N_p = \frac{3.G_o}{4.\pi.R_c^3 \rho}$$

R_w Radius of wood particle entering reaction zone, cm

ρ Char particle density (0.36 gcm^{-3} [56]),

R_c Radius of char particle entering char gasification zone, cm

r_c Internal radius of reaction zone at the start of the gasification zone, cm

R_t Char particle radius at time t, cm

r_g Internal radius of gasifier, 3.75cm

R_l Radius of char particle at the start of the section through the char gasification zone, cm

S_c Cross sectional area of reaction zone at the start of the gasification zone, cm^2

S_l Cross sectional area of imaginary zone in gasifier, cm^2

S_w Cross sectional area of gasifier $(\pi.r_g^2)$, cm^2

To calculate the length of the char gasification zone in an open-core downdraft gasifier the following assumptions were made:

*   The order of reaction is assumed to be zero such that $-r_A = k$
*   The reaction zone is conical (inverted) in shape. The number of particles under consideration is constant,
*   The movement of particles in the horizontal plane is not considered,
*   The bed voidage is constant.

At the start of the char gasification zone,

$$G_o = N_p. \left(\tfrac{4}{3}.\rho.\pi.R_c^3\right) \dots\dots\dots\dots\dots\dots\dots\dots\dots [7.16]$$

$$a = \frac{3.(1 - \varepsilon)}{R_c} \dots\dots\dots\dots\dots\dots\dots [7.17]$$

Taking the reaction zone to be conically shaped, the theoretical diameter of the reaction zone at the start of the char gasification zone is calculated assuming that the number of particles entering reaction zone equals the number of particles entering the char gasification zone. If the particles always remain closely packed, then S (the cross sectional area for flow) will also be a function of l (Figure 7.15).

$$S_c = \frac{S_w . (1 - \varepsilon_w)}{\pi R_w^2} \cdot \frac{\pi R_c^2}{(1 - \varepsilon_c)} \dots\dots\dots\dots [7.18]$$

Assuming $\varepsilon_w = \varepsilon_c$ since the voidages of the various feeds used in this project were similar (Table 4.4);

then
$$S_c = \pi \cdot \frac{r_g^2}{R_w^2} \cdot R_c^2 \quad \text{.............................} [7.19]$$

$$r_c = \left(\frac{r_g \cdot R_c}{R_w} \right) \quad \text{.............................} [7.20]$$

Calculation of the surface area of the imaginary section in the gasifier, I.

$$S_I = \left(\frac{S_c \cdot (1 - \varepsilon_c)}{\pi \cdot R_c^2} \right) \frac{\pi \cdot R_I^2}{(1 - \varepsilon_I)} \quad \text{.............................} [7.21]$$

Assuming $\varepsilon_c = \varepsilon_I$

$$= S_c \cdot \left(\frac{R_I}{R_c} \right)^2 \quad \text{.............................} [7.22]$$

$$= \pi \cdot \left(\frac{r_c}{R_c} \right)^2 \cdot R_I^2 \quad \text{.............................} [7.23]$$

Carry out a mass balance over the section through the char gasification zone defined by $S.\partial I$,

$$G_I = G_{I+\partial I} + (-r_{A,I}) \cdot a_I \cdot S_I \cdot \partial I \quad \text{.............................} [7.24]$$

$$0 = \frac{dG_I}{dI} + (-r_{A,I}) \cdot a_I \cdot S_I \quad \text{.............................} [7.25]$$

substituting:

$$G_I = N_p \cdot \rho \cdot \left(\frac{4}{3} \cdot \pi \cdot R_I^3 \right) \quad \text{.............................} [7.26]$$

$$\text{and } -r_A = k \quad \text{.............................} [7.27]$$

$$a_I = \frac{3 \cdot (1 - \varepsilon_I)}{R_I} \quad \text{.............................} [7.28]$$

$$\text{let: } \beta = \pi \cdot \left(\frac{r_c}{R_c} \right)^2 \quad \text{.............................} [7.29]$$

$$S_I = \beta \cdot R_I^2 \quad \text{.............................} [7.30]$$

$$0 = N_p.\rho.\frac{4}{3}.\pi.3.R_l^2.\frac{dR_l}{dl} + \frac{3.k.(1 - \varepsilon_l)}{R_l}.\beta.R_l^2 \,..\,[7.31]$$

$$-\int_{R_c}^{R_l} R_l\,.\,dR_l = \frac{3.k.(1 - \varepsilon_l).\beta}{N_p.\rho.4.\pi}\int_0^l dl \,.................[7.32]$$

$$\left(\frac{R_c^2 - R_l^2}{2}\right) = \frac{3.k.(1 - \varepsilon_l).\beta.l}{N_p.\rho.4.\pi} \,.........................[7.33]$$

For complete gasification, R_l will equal zero:

$$\frac{R_c^2}{2} = \frac{3.k.(1 - \varepsilon_l).\pi.L}{N_p.\rho.4.\pi}.\left(\frac{r_c}{R_c}\right)^2 \,.....................[7.34]$$

$\Rightarrow$
$$L = \left(\frac{R_c^4}{r_c^2}\right).\frac{2.N_p.\rho}{3.k.(1 - \varepsilon_l)} \,.........................[7.35]$$

substituting for N_p:

$\Rightarrow$
$$L = \frac{R_c.G_0}{2.k.\pi.r_c^2.(1 - \varepsilon_l)} \,.........................[7.36]$$

From Table 7.2, mass loss during flaming pyrolysis is 81% (for 15 mm diameter beads).

$$G_0 = 0.19\,G_w \,.........................[7.37]$$

substituting for r_c from Equation 7.20,

$$L = \frac{0.19.G_w.R_w^2}{2.\pi.k.(1 - \varepsilon_l).r_g^2.R_c} \,.........................[7.38]$$

k can be calculated from the following:
Using the shrinking particle model.
Rate $\propto$ surface area of particle

217

$$- \frac{\rho}{M_c} \cdot \frac{d}{dt}\left(\frac{4}{3} \cdot \pi \cdot R_t^3\right) = 4 \cdot \pi \cdot R_t^2 \cdot k' \cdot C_G \quad \text{..} [7.39]$$

$$- \frac{\rho}{M_c} \cdot 4 \cdot \pi \cdot R_t^2 \frac{dR_t}{dt} = 4 \cdot \pi \cdot R_t^2 \cdot (k' \cdot C_G) \quad \text{................................} [7.40]$$

$$- \int_{R_c}^{R_t} dR = (k' \cdot C_G \cdot \frac{\rho}{M_c}) \int_0^t dt \quad \text{................................} [7.41]$$

$$\frac{(R_c - R_t)}{R_c} = \frac{\alpha \cdot t}{R_c} \quad \text{..} [7.42]$$

where:

$$\alpha = \left(\frac{k' \cdot C_G \cdot M_c}{\rho}\right) \quad \text{..} [7.43]$$

$$\frac{R_t}{R_c} = 1 - \frac{\alpha}{R_c} \cdot t \quad \text{..} [7.44]$$

The relative particle volume change:

$$\frac{V_t}{V_c} = \frac{\frac{4}{3} \cdot \pi \cdot R_t^3}{\frac{4}{3} \cdot \pi \cdot R_c^3} = \frac{R_t^3}{R_c^3} \quad \text{................................} [7.45]$$

$$\left(\frac{R_t^3}{R_c^3}\right) = (1 - \frac{\alpha}{R_c} \cdot t)^3 \quad \text{................................} [7.46]$$

When $\frac{R_t}{R_c}$ is zero, the processing time t (obtained experimentally) is:

$$t = \frac{R_c}{\alpha} = \left(\frac{R_c \cdot \rho}{k' \cdot C_G \cdot M_c}\right) \quad \text{................................} [7.47]$$

Let $k = k' \cdot C_G \cdot M_c$

giving

$$\frac{k}{\rho} = \frac{R_c}{t} \quad \text{..} [7.48]$$

Equation 7.48 can, therefore, be used to calculate the length of the char gasification zone.

$$L_{CG} = \frac{G_o.R_w^2.t}{2.\pi.R_c^2.\rho.(1 - \varepsilon).r_g^2} \quad\text{............................}\text{[7.49]}$$

where:

ε	Char bed voidage (Table 4.4)
G_o	Char feed rate to char gasification zone*, gs^{-1}
k	Rate constant, cms^{-1}
L_{CG}	Length of char gasification zone, cm
ρ	Char density, 0.36 gcm^{-3} [56]
R_c	Diameter of char particles entering the char gasification zone, cm
r_g	Internal radius of gasifier, 3.75 cm

* The char feed rate to the gasifier is calculated from the fuel feed rate to the gasifier assuming a 81 % reduction in mass during flaming pyrolysis (Table 7.2).

Equation 7.49 has been used to calculate the length of the char gasification zone for beads used in experiment 8. Following flaming pyrolysis, the average char particle radius was 0.57 cm (Figures 7.1-7.4), the average char gasification time was 200 seconds (Table 7.8) and the wood feed rate was 1.41 kgh^{-1} (Section 5). The voidage in the char bed is assumed to be equivalent to the voidage of the wood chips sieved to between 9.5 mm and 12.7 mm as the equivalent char particle diameter (11.36 mm calculated from the data in Table 7.2) is similar to the mean representative diameter of the C5 wood chips (11.77 mm). This results in a char gasification zone length of 1.593 cm. This model predicts that the char gasification zone length is smaller than that observed. During experiment 8, the height of the char gasification zone according to definition 1 (Section 7.3.2.1) was between 28 mm and 55 mm (equivalent to 1.9 - 3.7 unreacted feed particle diameters). This may be due to simplifications and assumptions made during the development of the model and incorrect measurement of the char gasification time (Section 7.3.2.2). A sensitivity analysis (Table 7.10) testing the effect of char gasification time, t, on the char gasification zone length (calculated using Equation 7.31) shows that a char gasification time of 350 - 700 seconds is required for the calculated char gasification zone to match the observed char gasification zone length (definition 1).

It is concluded from the modelling carried out that the char gasification zone length is very small. This model is, however, limited as it:

- Does not account for the effect on the rate constant of the reduction in temperature as char gasification proceeds.
- Does not account for the "squashing" of particles in the char gasification zone and the change in bed voidage as the particles shrink.
- Does not include gasification on the internal surface of the char particle. Plates 7.3-7.6 show that during pyrolysis, the char formed often cracks permitting gases to enter the particle undergoing gasification. This would increase the rate of char gasification reducing the length of the char gasification zone.

Table 7.10
Char Gasification Zone Length Model - Sensitivity Analysis

Time seconds	Char gasification zone length, cm	Time seconds	Char gasification zone length, cm
0	0	500	3.98
50	0.40	550	4.38
100	0.80	600	4.78
150	1.19	650	5.18
200	1.59	700	5.58
250	1.99	750	5.98
300	2.39	800	6.38
350	2.79	850	6.77
400	3.19	900	7.17
450	3.59	950	7.57

It is recommended that future workers develop this model further to include the reduction in char gasification zone temperature as gasification proceeds and the convective heat transfer from the flames flowing downwards from the flaming pyrolysis zone through the char gasification zone (Section 10).

7.4.2.4   Char Gasification Zone in the Insulated Gasifier
Gasifier insulation will reduce the heat losses from the reaction zones in the gasifier reducing the rate at which the temperature falls to the point at which

char gasification is terminated. It could be seen that when using an insulated reactor, there was a deeper zone of orange and cherry red coloured char below the flaming pyrolysis zone (125 mm - experiment 25) compared with the length of the orange and cherry red zone of char in the uninsulated gasifier (60 mm - experiment 26). Bodies glowing red and orange indicate temperatures above 700°C [110] below which temperature gasification rates are reported to be insignificant [20].

The effect of insulation on the char gasification zone can be studied by measuring the depth of char at temperatures between the maximum gasifier temperature and 800°C (the char temperature at the grate of experiment 25). For experiment 25 (insulated reactor), the depth of char above 800°C was 125 mm while for experiments 22 and 26 (uninsulated reactor) the depths of char above 800°C were 80 and 65 mm respectively. During insulated gasifier operation, therefore, there was no cool char zone.

It is concluded that insulating the gasifier increases the maximum temperature at the top of the gasification zone and increases the length of the char gasification zone by between 56% and 92%. This will increase the rate of char consumption by gasification and will reduce the air/feed ratio required to maintain stable operation (see Section 8.6).

7.5   Summary
Two physical models reported in the literature (Section 2.1.2) showing the zonal operation of an open-core downdraft gasifier have been refined based on observations and measurements made in this project. Particles commencing gasification are firstly pyrolysed in a narrow flaming pyrolysis zone and subsequently gasified in a deeper, char gasification zone. Combustion of some of the pyrolysis products in the flaming pyrolysis zone provides energy for the char gasification process. During stable gasifier operation (ie, when there is no net production or consumption of char in the gasifier), sufficient pyrolysis products are combusted to ensure that the char produced by flaming pyrolysis is completely consumed in the char gasification zone.

Measurements of the lengths of the flaming pyrolysis and char gasification zones and the times for single particles to undergo flaming pyrolysis and char gasification have been presented.

The length of the flaming pyrolysis zone has been found to be 1.20 mean representative feed particle diameters and the time for a single 15 mm diameter bead to undergo flaming pyrolysis was 85.4 seconds. These measurements compare well with a model of flaming pyrolysis reported in the literature.

The length of the char gasification zone was difficult to measure. Two definitions of the start and end of the char gasification zone have been presented. The length of the observable char gasification zone (ie the height of the glowing char in the gasifier), has been found to be 4.5 mean representative feed particle diameters. The length of the char gasification zone according to the vertical temperature profile through the gasifier has been found to be 9.5 mean representative feed particle diameters suggesting that the length of the char gasfication zone is longer than the observable length of glowing char in the gasifier. A new model to calculate the char gasification zone length has been developed. This model predicts that the char gasification zone length is small. However, the model requires further development.

The time for char particles to undergo complete consumption could not be measured. Char particles produced from 15 mm diameter beads were observed to undergo 86.9% consumption in 200 seconds.

Combining the times for flaming pyrolysis and char gasification for the 15 mm beads results in an individual particle reaction time for 97.3% mass conversion in 285.4 seconds.

8. GASIFIER PERFORMANCE RESULTS AND DISCUSSION

One of the aims of this project was to assess the effect of process parameters on gasifier performance (Table 5.1). This section presents and discusses the results of variations in process parameters compared with a standard case performance (Section 8.1).

8.1 Standard Case Performance

A standard performance was defined to compare the performance of the gasifier under different conditions. Standard case performance is defined as operation under steady conditions (ie. there is no net production or consumption of char in the gasifier) with a feed consisting of wood chips sieved to between 6.35 and 12.7 mm.

8.1.1 <u>Data Collection and Treatment</u>

Gasifier standard case performance was achieved in experiments 22 and 26. The gasifier operating procedure and the parameters measured are detailed in Section 5.2.

8.1.2 <u>Results and Discussion</u>

Stable operation in experiments 22 and 26 is shown in Figures 8.1 and 8.2.
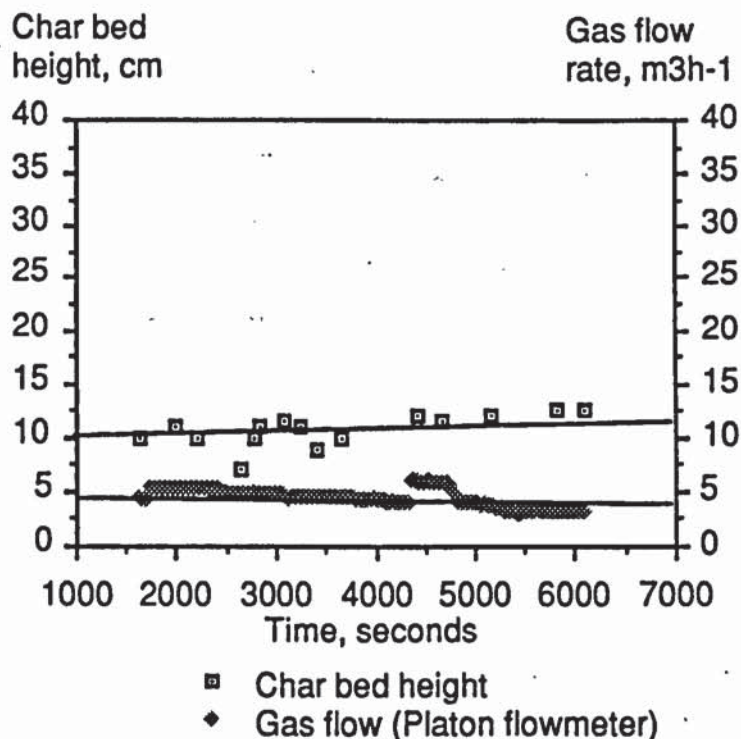
Figure 8.1
Char Bed Height v Time - Experiment 22
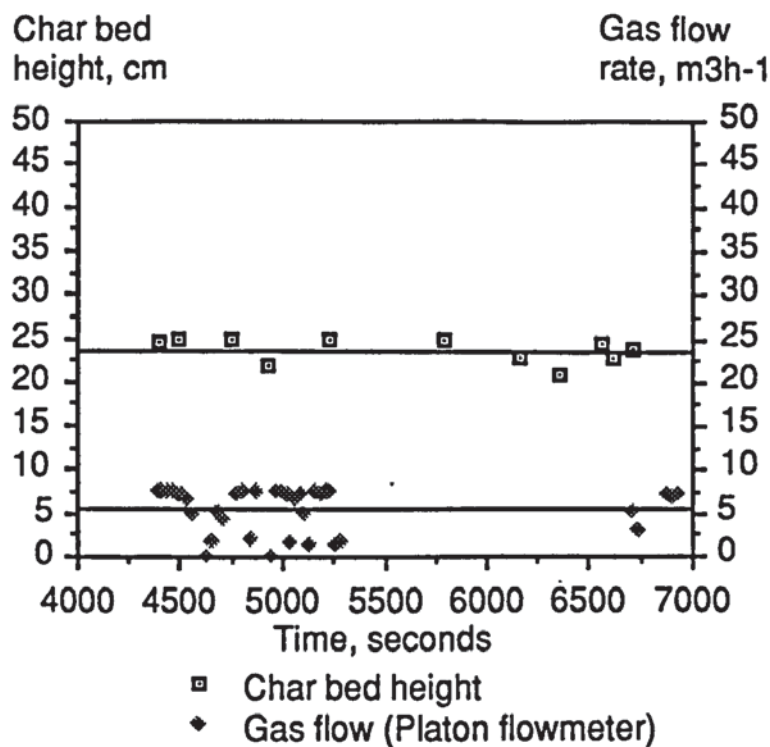
Figure 8.2
Char Bed Height v Time - Experiment 26

Plate 8.1 shows uninsulated gasifier operation during stable operation with wood chips (sized between 6.35 and 12.7 mm). Standard case performance data are presented in Table 8.1.

The results from the uninsulated mark II Aston gasifier (standard case operation) are similar to those of the mark I uninsulated Aston gasifier operating using a wood chip feed sieved to between 4.75 and 6.35 mm (Table 8.2). However, it is now possible to run the gasification system for much longer periods. The average experiment length during Earp's project (total of six experiments) was 7.38 minutes while the average experiment length during this project was 35.25 minutes [12]. The venturi system was reliable and easy to operate.

No variations in performance or damage to the venturi system were noted during this project. This is attributed to the simpler and more robust method of gasifier operation compared with the previous system of gasifier operation. The average pH of the scrubber water was 5.60. This is lower than the predicted pH of the water of 6.2 (Appendix II). No corrosion problems were experienced during this project.

224

Plate 8.1
Uninsulated Gasifier Operation with Wood Chips

Table 8.1
Gasifier Standard Case Performance Data

Feed: Wood chips (6.35-12.7 mm)

	Average value
Experiment length, hours (minutes)	0.97 (58.5)
Feed moisture content, % wb	9.49
Char bed height, cm	17.23
Specific capacity, $kgm^{-2}h^{-1}$	276.39
Mass yield, $kgkg^{-1}$	3.23
Volumetric yield, Nm^3kg^{-1}	2.94
Equivalence ratio, %	39.24
Air/feed ratio	2.81
Gas higher heating value, $MJNm^{-3}$	3.38
H_2/CO ratio	0.66
CO/CO_2 ratio	1.07
Gasifier gas outlet temperature, °C	440.39
Raw gas efficiency, %	61.44
Hot gas efficiency, %	55.40
Cold gas efficiency, %	46.69
H_2 in product gas, % volume	9.25
CO in product gas, % volume	14.22
CO_2 in product gas, % volume	13.69
CH_4 in product gas, % volume	1.01
N_2 in product gas, % volume	61.82

Earp's results also show two experiments with gas nitrogen contents of greater than 70% indicating an air leak into the gasification system [12]. During this project, air leaks into the gasification system were encountered on two occasions causing the experiments to be abandoned. Following these experiments, the gasification system was leak tested and the gasifier refitted into its support collar for re-use.

Comparison between the performance of the mark I Aston open-core downdraft gasifier and open-core downdraft gasifiers in the literature was made in Section 2.3. Due to the similarity between the performance of the mark I and uninsulated mark II Aston gasifiers, comparison of the uninsulated mark II Aston gasifier performance with other open-core

downdraft gasifiers in the literature will not be made. Comparison of the insulated Aston gasifier performance with other open-core downdraft gasifiers in the literature is made in Section 8.6.3.

<div style="border:1px solid black">

Table 8.2
Aston Open-Core Downdraft Gasifier (Mark I and II) Performance [12],[17]

Mark I Gasifier Feed: wood chips (4.75-6.35 mm)

Mark II Gasifier Feed: Wood chips (6.35-12.7 mm)

	Mark I gasifier performance	Mark II gasifier performance
Experiment length, hours (minutes)	0.15 (9.15)	0.97 (58.5)
Feed moisture content, % wb	10.77	9.49
Char bed height, cm	11.25	17.23
Specific capacity, $kgm^{-2}h^{-1}$	278.40	276.39
Mass yield, $kgkg^{-1}$	3.20	3.23
Volumetric yield, Nm^3kg^{-1}	2.80	2.94
Equivalence ratio, %	45.10	39.24
Air/feed ratio	2.73	2.81
Gas higher heating value, $MJNm^{-3}$	4.13	3.38
Cold gas efficiency, %	58.70	46.69
H_2 in product gas, % volume	12.60	9.25
CO in product gas, % volume	15.93	14.22
CO_2 in product gas, % volume	10.10	13.69
CH_4 in product gas, % volume	1.30	1.01
N_2 in product gas, % volume	60.10	61.82

</div>

8.1.3 Comparison of Mark II Aston Gasifier Standard Case Performance with the Aston Carbon Boundary Model

The adiabatic carbon boundary model, described fully by Double, requires the input of the feed carbon, hydrogen, oxygen, nitrogen, ash and moisture contents and reactor heat loss [45]. Based on this information and the assumption that there is 100% conversion of carbon to product gas with no tar or char production (ie the gasifier operates at the carbon boundary), the model employs thermodynamic equilibrium relationships to predict the product gas composition and gasifier air requirement.

The output from the Aston carbon boundary model for typical input conditions for a standard case experiment (the average of experiments 22 and 26) is compared with mark II Aston gasifier standard case performance in Table 8.3. The gasifier heat loss calculated from the gasifier temperature profile could not be entered into the carbon boundary model program as the program would not accept gasifier heat losses in excess of 20%. The model was run for heat losses in steps of 5% from 10% for comparison purposes, therefore.

Table 8.3
Comparison of Aston Carbon Boundary Model Predictions with Actual Mark II Standard Case Gasifier Performance

	Model predictions			Standard case performance
Reactor heat loss, %	10.00	15.00	20.00	38.56
Gas composition, % volume, dry				
Hydrogen	18.65	16.88	15.24	9.25
Carbon monoxide	19.02	16.02	13.31	14.22
Carbon dioxide	11.80	13.38	14.80	13.69
Methane	0.82	0.85	0.89	1.01
Nitrogen	49.71	52.87	55.76	61.82
Calculated gas HHV, MJNm^{-3}	4.84	4.28	3.77	3.38
Cold gas efficiency, %	68.67	63.31	57.99	46.69
Equivalence ratio, %	23.93	26.62	29.29	39.24
Equilibrium temperature, °C	647.09	628.05	609.70	440.40*

* Measured gas exit temperature

It can be seen from the model results that as the gasifier heat loss is increased, the model predictions in terms of product gas higher heating value, equivalence ratio and cold gas efficiency approach the results from the mark II Aston gasifier (Figure 8.3). The measured results lie closely to the extrapolated curves shown on Figure 8.3. It can also be seen that the gas exit temperature in the Aston gasifier is much lower than the equilibrium temperature for the gas in the model.
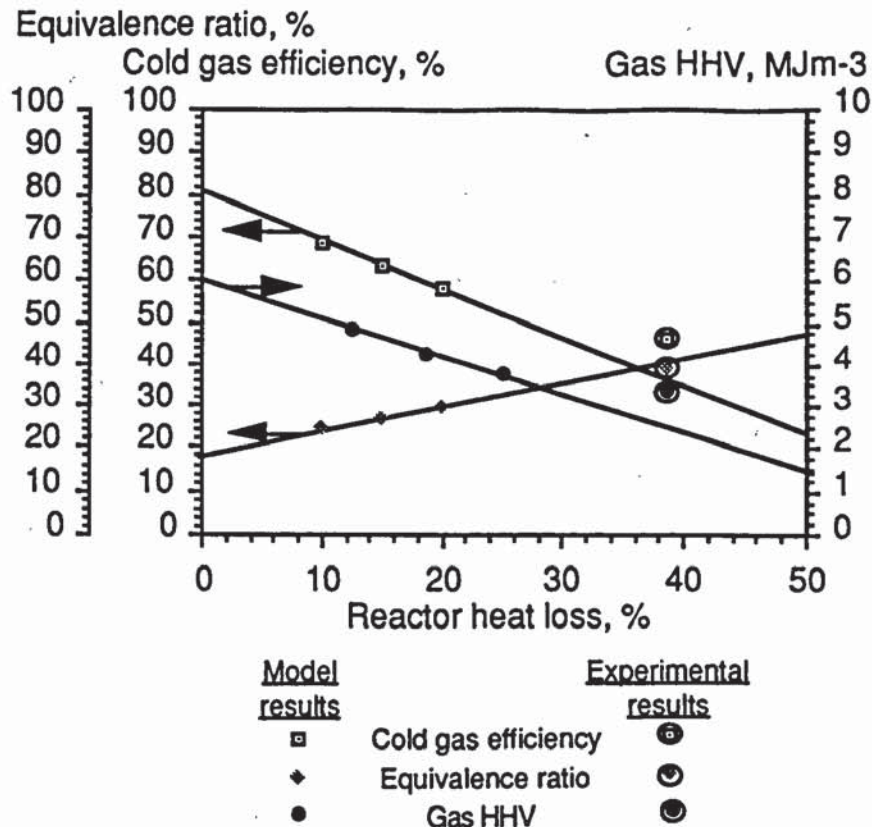
Figure 8.3

Predicted Gasifier Equivalence Ratio, Cold Gas Efficiency and Product Gas Higher Heating Value as a Function of Gasifier Heat Loss

Insulated mark II Aston gasifier performance is compared with the Aston carbon boundary model in Section 8.6.4.

8.2 Gasifier Performance During Char Consumption (Gasification) Dominant Operation

According to Reed [11] and Earp [12] an open-core downdraft gasifier can be operated in three regimes as described in Section 2.1.3:

a)   Char consumption (gasification) dominating;

b)   Pyrolysis dominating and;

c)   Stable operation.

The mode of operation is affected mainly by the gasifier equivalence ratio. At a particular equivalence ratio, the reaction zone will remain in a stable position relative to the grate since the rate of char production by pyrolysis will equal the rate of char consumption by gasification. Increasing the air flowrate into the gasifier will result in char consumption or gasification

dominant operation and the reaction zone will move downwards towards the grate. Decreasing the air flowrate into the gasifier will result in pyrolysis dominating operation and the reaction zone will move upwards away from the grate.

8.2.1 Data Collection and Treatment

The gasifier was operated in the char consumption (gasification) dominant regime during experiment 14 as shown by Figure 8.4 (uninsulated gasifier). The method of gasifier operation was the same as that used for the standard case experiments. Char bed height was measured manually at a frequency of approximately once every two to three minutes.
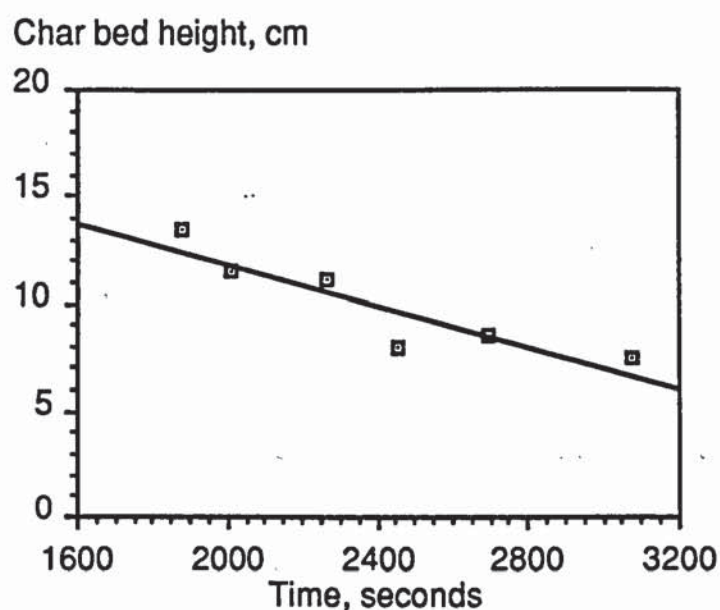
Char bed height, cm

Figure 8.4
Char Bed Height v. Time (Experiment 14)

8.2.2 Results and Discussion

As predicted by theory, the gasifier operates at a lower equivalence ratio during stable operation compared with the char consumption (gasification) dominant regime as shown in Table 8.4. Increasing the air input rate to the gasifier will reduce the product gas heating value as shown in Table 8.4 as the equivalence ratio approaches one indicating combustion.

Table 8.4
Comparison of Gasifier Performance in Char Consumption and Steady State Operational Modes (Uninsulated Reactor)

Experiments	14	22/26
Mode	Char consumption	Stable operation
Average rate of increase of char depth, cm.min^{-1}	-0.27	0.00
Equivalence ratio, %	43.50	39.13
Gasifier heat loss as % of dry wood input	22.78	28.30
H_2 in product gas, % volume	9.15	9.27
CO in product gas, % volume	12.97	14.24
CO_2 in product gas, % volume	16.27	13.687
CH_4 in product gas, % volume	0.80	1.01
N_2 in product gas, % volume	60.81	61.783
HHV, MJNm^{-3}	3.12	3.38
Specific capacity, kgm^{-2}h^{-1}	294.09	276.39
Volumetric gas yield, Nm^{3}kg^{-1}	3.25	2.94
Mass gas yield, kgkg^{-1}	4.05	3.56
Cold gas efficiency, %	47.77	46.69

Operation in the char consumption (gasification) dominant mode occurs because the rate of char consumption by gasification is increased relative to the rate of char production by pyrolysis. Char consumption (gasification) dominant operation is brought about by increasing the air flow rate entering the gasifier. Increasing the air flow rate into the gasifier increases the quantity of pyrolysis products oxidised. Increased oxidation of the pyrolysis products will increase the gasification agent concentration (carbon dioxide and water) and energy produced. The increased energy will be transferred by radiation to the flaming pyrolysis zone and by radiation and convection to the char gasification zone. Increased radiative heat transfer to the flaming pyrolysis zone will increase the rate of char production as indicated by the increased gasifier specific feed capacity during char consumption (gasification) dominating operation (Table 8.4). However, the increase in the rate of char production during pyrolysis is limited since only biomass particles "seeing" radiation will commence pyrolysis (see Figures 7.5 and 7.8). The increase in energy transferred to the char gasification zone will be greater than the increase in energy transferred to the flaming pyrolysis zone

and the rate of char consumption by gasification will be increased relative to the rate of char production by pyrolysis. The increase in energy in the gasification zone during char consumption (gasification) dominant operation compared with stable operation is indicated by the higher average temperature measured at the top of the gasification zone during char consumption (gasification) dominant operation (1045°C) compared with the average temperature measured at the same position during standard case operation (1018°C). When the rate of char consumption by gasification is greater than the rate of char production by pyrolysis, then the reaction zone will move downwards through the reactor. The mode of gasifier operation during char consumption (gasification) dominant operation is illustrated by a modification of Figure 7.7 shown in Figure 8.5.

Char consumption or gasification dominant operation does not occur as a result of char consumption by combustion in the char gasification zone as suggested in Section 2. It was shown in Section 7.1.1 that there is incomplete combustion of the gaseous pyrolysis products during stable gasifier operation since the pyrolysis products contain carbon monoxide and hydrogen. This supports the theory that char combustion in the char gasification zone with excess oxygen not consumed in the flaming pyrolysis zone does not occur during stable gasifier operation. During char consumption (gasification) dominant operation, the air input rate into the gasifier is increased leading to the possibility of char consumption by oxidation with oxygen. The additional air entering the gasifier during gasification dominant operation will be available, therefore, to react with the combustible gas leaving the flaming pyrolysis zone. If the volume of air entering the gasifier additional to that required for stable gasifier operation is greater than that required for stoichiometric combustion of the gases leaving the flaming pyrolysis zone (calculated in Section 7.1.1), then it can be inferred that char consumption by combustion will occur in the char gasification zone (Figure 7.6). The calculated air requirement for stoichiometric combustion of the gaseous products of pyrolysis is shown in Table 8.5. It can be seen from Table 8.5 that the additional air entering the gasifier during char consumption or gasification dominant operation (experiment 14) is insufficient to stoichiometrically combust the gases leaving the flaming pyrolysis zone. Char consumption in the char gasification zone by combustion during char consumption (gasification) dominant operation is, therefore, unlikely.
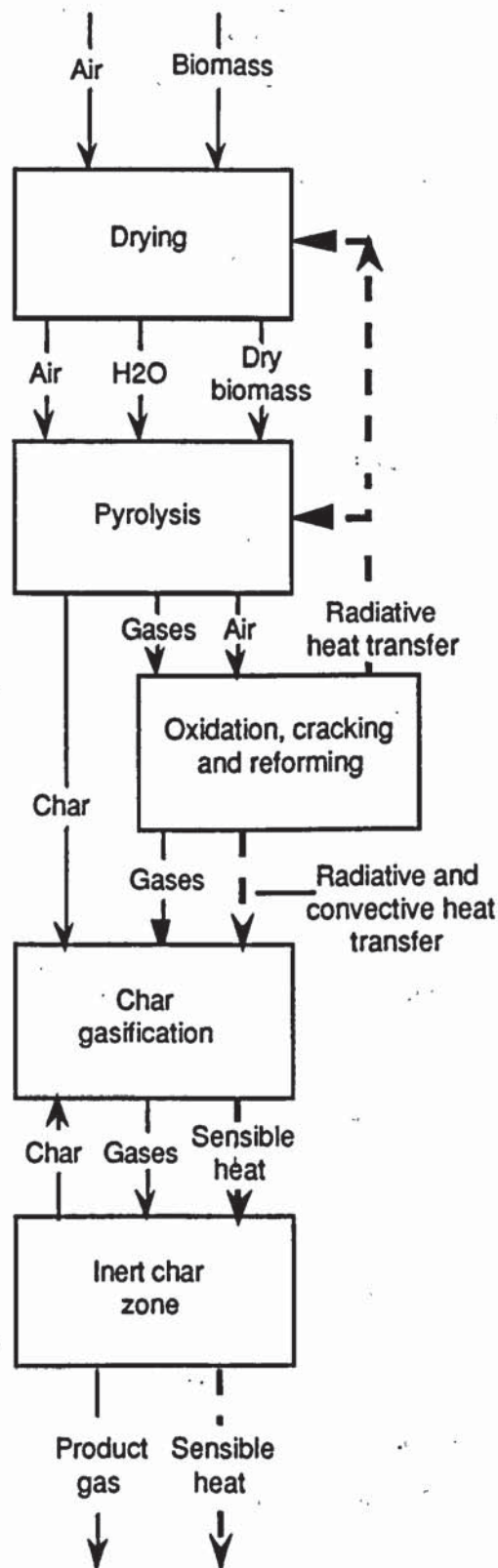
Figure 8.5

Flow Diagram of Gasification Process in an Open-Core
Downdraft Gasifier During Char Consumption (Gasification)
Dominant Operation

Table 8.5
Calculation of Air Requirement for Stoichiometric Combustion of Pyrolysis Gases During Char Consumption (Gasification) Dominant Operation

a) Calculation of Gas Production Rate by Mass Balance Over Flaming Pyrolysis (FP) Zone

Inputs, kgh^{-1}		Outputs, kgh^{-1}	
Wood (daf)	1.30	Char	0.24
Air	4.05	Gas (by difference)	5.11
Total	5.35	Total	5.35

b) Calculation of Stoichiometric Air Requirement for Combustion of Gaseous FP Products

Flaming pyrolysis gas carbon monoxide content (% by mass)*	16.48
Flaming pyrolysis gas hydrogen content (% by mass)*	1.37
Oxygen required for stoichiometric combustion of CO, kg	0.48
Oxygen required for stoichiometric combustion of H_2, kg	0.56
Total oxygen required for stoichiometric combustion of FP gases, kg	1.04
Total air required for stoichiometric combustion of FP gases, kg	4.91
Air to feed ratio during stable operation (experiments 22 + 26)	2.81
Air to feed ratio during char gasification dominant operation (experiment 14)	3.12
Additional air entering gasifier during gasification dominant operation compared with stable operation, kg	0.40

* see Section 7.1.1

Gasifier operation in the char consumption (gasification) dominant regime was difficult since, during gasifier operation, an accumulation of small ash particles at the interface between the char gasification and inert char zones leads to an increasing pressure drop during the experiment (Table 8.6). To operate in the char consumption (gasification) dominant regime, it was necessary to regularly adjust the water flowrate through the venturi to overcome the increasing pressure drop across the gasifier (Table 8.6).

It is concluded that during char consumption (gasification) dominant operation, there is a higher gasifier air requirement leading to a reduction in the product gas heating value compared with stable operation. Operation in the char consumption (gasification) dominant regime occurs as a result of an increase in the rate of char consumption by gasification compared with the rate of char production by pyrolysis. The increase in char consumption is

due to increased heat transfer from increased oxidation of pyrolysis products and hence increased gasification zone temperatures.

Table 8.6 Pressure Drop Across Gasifier During Char Consumption (Gasification) Dominant Operation (Experiment 14)		
Time Seconds after start of experiment 14	Pressure Drop cm.H_2O	Setting of Rotameter indicating water flowrate to venturi
0	53.0	6.0
120	62.5	6.0
420	79.5	8.2
1020	55.5	9.0
1200	87.0	7.2
1320	96.0	7.3

8.3 Effect of Pyrolysis Dominant Operation on Insulated Gasifier Performance

The effect on gasifier performance of operating the uninsulated Aston open-core downdraft gasifier during pyrolysis dominant operation and stable operation was studied by Earp [12]. He concluded that during pyrolysis dominant operation, the equivalence ratio is reduced relative to that at stable operation, but this change is masked by gasifier heat losses. The aim of this section is to compare insulated gasifier performance during stable and pyrolysis dominant operation and to test this conclusion.

8.3.1 Data Collection and Treatment

Data from experiments 24 and 25 was used for this analysis (insulated gasifier). The reaction zone rose throughout experiment 24 and the reaction zone was stable during experiment 25. Data collection was performed in the same way as for the standard case experiments. Char bed height was measured manually at a frequency of approximately once every two to three minutes.

8.3.2 Results and Discussion

A comparison of the insulated mark II Aston gasifier performance during pyrolysis dominating and stable operation is shown in Table 8.7.

Table 8.7

Comparison of Gasifier Performance in Pyrolysis Dominating and Steady State Operational Modes (Insulated Reactor)

Feed: Woodchips (6.35-12.7 mm)

Experiments	24	25
Mode	Pyrolysis dominating	Stable operation
Average rate of increase of char depth, $cm.min^{-1}$	0.72	0.00
Equivalence ratio, %	40.42	39.13
Gasifier heat loss as % of dry wood input	15.94	10.78
Carbon conversion efficiency, %	93.83	95.03
H_2 in product gas, % volume	11.58	13.08
CO in product gas, % volume	13.85	15.28
CO_2 in product gas, % volume	14.02	13.77
CH_4 in product gas, % volume	1.26	1.46
N_2 in product gas, % volume	59.28	56.41
HHV, $MJNm^{-3}$	3.73	4.18
Specific capacity, $kgm^{-2}h^{-1}$	282.74	328.15
Volumetric gas yield, Nm^3kg^{-1}	3.22	3.07
Mass gas yield, $kgkg^{-1}$	3.78	3.51
Cold gas efficiency, %	56.45	60.32

During pyrolysis dominant operation, the energy produced by oxidation of some of the products of pyrolysis is reduced. Heat transfer by radiation to both the pyrolysis and char gasification zones will be reduced by a similar extent. Heat transfer by convection to the zones below the flaming pyrolysis zone only will also be reduced suggesting that the rate of char consumption by gasification has been reduced to a greater extent than the rate of char production by pyrolysis. Char accumulation at the bottom of the char gasification zone (Figure 5.1) will occur and the reaction zone will move upwards through the reactor. This process is described by a modification of Figure 7.7 shown in Figure 8.6.
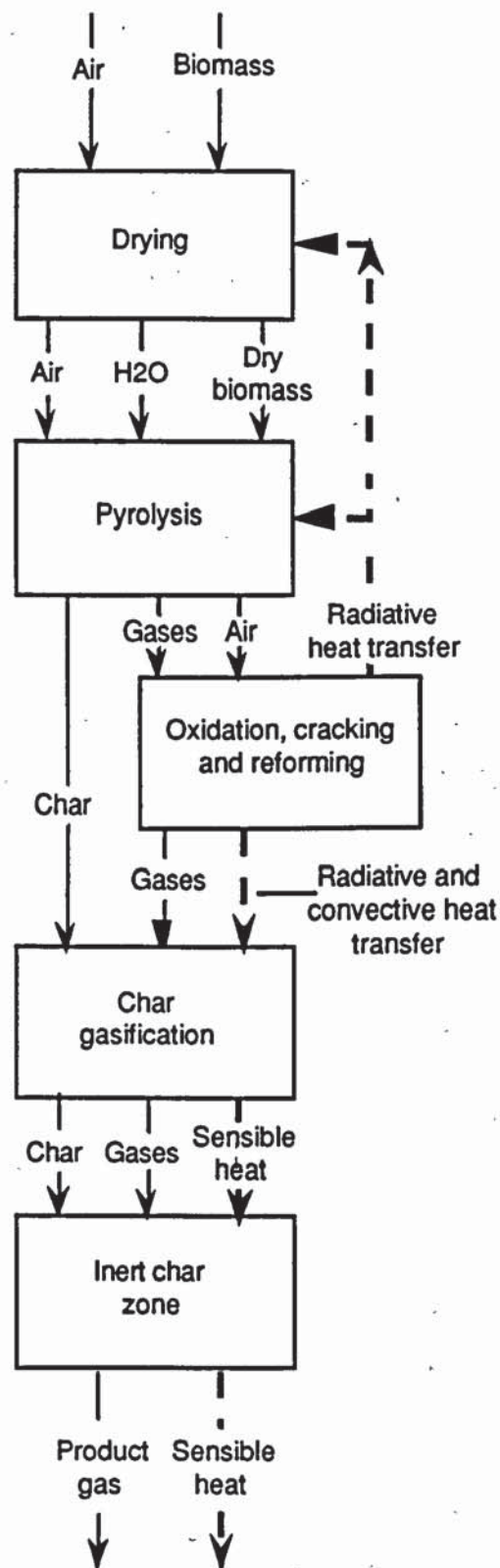
Figure 8.6

Flow Diagram of Gasification Process in an Open-Core Downdraft Gasifier During Pyrolysis Dominant Operation

It would be expected that during pyrolysis dominant operation, there would be a lower air requirement than during stable gasifier operation. It can be seen from Table 8.7, however, that during pyrolysis dominant operation, there is a higher air requirement compared with stable operation. This contradicts the theory and agrees with the results of Earp for an uninsulated reactor [12]. The increased equivalence ratio during pyrolysis dominant operation is explained by considering the gasifier heat loss presented as a percentage of the feed energy input in Table 8.7. Increasing the gasifier heat loss will increase the equivalence ratio necessary to maintain a stable reaction zone. During pyrolysis dominant operation in experiment 24 when the reaction zone was moving upwards away from the grate, the equivalence ratio was not increased sufficiently to offset the increased gasifier heat loss compared with experiment 25.

In this project, the heat loss from the insulated reactor has been measured using thermocouples attached to the external surface of the insulation. It can be seen from Table 8.7 that the heat loss when operating with a rising reaction zone is greater than when operating with a stable reaction zone. As Earp indicated, the higher heat loss when operating with an unstable reaction zone manifests itself in lower hydrogen and carbon monoxide in the product gas and a lower cold gas efficiency [12]. This also results in a lower product gas heating value when operating in the pyrolysis dominating mode. When operating in the pyrolysis dominating mode, theory suggests that the product gas heating value should be increased relative to the heating value of the product gas produced during stable gasifier operation (see Section 2.1.3).

The conclusion of Earp is confirmed (Section 2.1.3). The effect of operation in the pyrolysis dominant mode on gasifier performance is masked by heat losses from the reactor which increase the system air requirement.

8.4 Effect of Carbon Dioxide Injection into Gasifier

Three experiments were carried out to investigate the effect of carbon dioxide enrichment of the input air to the gasifier. The aim of enriching the air with carbon dioxide was to increase the volume of gasification agent in the char gasication zone and hence increase the rate of char consumption by gasification compared to the rate of char production by pyrolysis. It was expected that carbon dioxide enrichment of the air entering the gasifier

would reduce the input air flowrate during stable operation and increase the product gas heating value due to a reduction in the nitrogen content.

8.4.1   Data Collection and Treatment

Three experiments were carried out in which carbon dioxide was introduced to the gasifier (experiments 10, 11 and 12). Bottled carbon dioxide was injected into the unreacted feed zone using a copper pipe. The action of the venturi was used to draw the carbon dioxide down into the reaction zones. Carbon dioxide flowrates of 2, 5 and 10 $l.min^{-1}$ were used to initially investigate the effect of carbon dioxide injection. These correspond to percentage carbon dioxide concentrations in the input air of 7.8%, 12.2% and 22.6% (by mass) respectively. The method of gasifier operation and the data collected is described in Section 5.2.

8.4.2   Results and Discussion

Results from the operation of the gasifier with carbon dioxide enrichment of the input air are shown in Table 8.8.

Table 8.8
Aston Open-Core Gasifier Performance with Carbon Dioxide Enrichment of Input Air

Feed: Woodchips (6.35-12.7 mm)

CO_2 flowrate, $l.min^{-1}$	0	2	5	10
Percentage CO_2 in total gaseous input to gasifier	0	7.8	12.2	22.6
Experiment time, minutes	58.5	15.0	14.4	17.4
Feedrate, daf kgh^{-1}	1.22	1.13	0.77	1.32
Specific capacity, $kgm^{-2}h^{-1}$	328.89	283.85	174.00	299.35
Air flow rate, m^3h^{-1}	3.43	2.63	1.97	3.91
Air/feed ratio	2.81	2.37	2.63	2.97
Equivalence ratio, %	39.13	40.12	44.49	53.28
CO_2 flow, m^3kg^{-1} daf	0	0.17	0.39	0.43
H_2 in product gas, % volume	9.25	8.81	8.33	8.99
CO in product gas, % volume	14.22	13.35	14.09	13.49
CO_2 in product gas, % volume	13.69	18.40	19.92	18.73
CH_4 in product gas, % volume	1.01	1.33	1.20	1.43
N_2 in product gas, % volume	61.82	58.11	56.45	57.35
H_2/CO (output gas stream)	0.66	0.66	0.59	0.67
CO/CO_2 (output gas stream)	1.07	0.73	0.71	0.72
Gas flow m^3h^{-1}	4.70	3.01	3.52	4.43
HHV, $MJNm^{-3}$	3.38	3.34	3.32	3.42

Mass and energy balances were performed for the three experiments in which carbon dioxide was injected into the reactor (see Appendix VII). It was not possible to ensure that all of the carbon dioxide flowing through the injection system entered the gasifier and this may account for the poor mass and energy balances shown in Tables 6.5 and 6.6.

Carbon dioxide enrichment of the input air to the gasifier was not found to have a beneficial effect on gasifier performance. Increasing the carbon dioxide flowrate to the gasifier did not greatly affect the product gas higher heating value. The carbon dioxide concentration in the product gas is shown to increase with increasing carbon dioxide injection rate indicating that carbon dioxide injected into the gasifier is passing through the gasifier unreacted.

The air to feed ratio does not vary with increasing carbon dioxide flowrate and the equivalence ratio is increased to maintain a stable reaction zone. It was decided not to further investigate carbon dioxide enrichment of the input air to the gasifier.

8.5 Effect of Char Bed Height on Gasifier Performance

The aim of this section is to assess the effect of the char bed height on gasifier performance. This area was investigated by Earp [12]. However, Earp presented no results with char bed heights of 0 cm and Earp's data were collected under pyrolysis dominating conditions [12]. The aim of operating the gasifier with a char bed height of zero was to ascertain whether operation without a char bed would have a disproportionally detrimental effect on gasifier performance compared with the gasifier performance with a char bed.

The aim of this section, therefore, is to investigate the effect of char bed height over the range 0-20 cm on gasifier performance in terms of product gas composition, product gas heating value and reactor throughput during stable operation. The effects of char bed on gasifier performance is discussed in Section 2.1.4.2. .

8.5.1 Data Collection and Treatment

Earp investigated the effect of char bed over the range 7-16 cm on gasifier performance [12]. However, the effect of operating with no char bed as in experiment 9 of this project was not reported. The data used in this section were collected under stable operating conditions. Earp concluded that the char bed has little effect on gas quality although there is increased production of hydrogen and carbon monoxide suggesting increased char conversion by the Boudouard and water gas reactions [12]. This may have been due to the effect of gasifier operation in pyrolysis dominant mode.

Char bed height measurements were taken manually every two to three minutes in the same way as for the standard case experiments. The gasifier was uninsulated.

241

8.5.2 Results and Discussion

Table 8.9 presents the effect of char bed height on gasifier performance. This data is presented graphically in Figures 8.7-8.14. The lines drawn on each graph show the "best fit" line calculated using "Cricket Graph" graph plotting software.

Table 8.9
Effect of Char Bed on Gasifier Performance

Experiment	9	2	14	22	7	15	5	6	26
Char bed height, cm	1.1	6.8	9.8	10.9	12.0	16.6	19.7	20.9	23.6
Specific capacity, kgm^{-2}	254.9	360.4	294.1	274.0	253.8	369.7	285.7	281.7	278.8
Gas mass yield, $kgkg^{-1}$	3.43	3.55	4.04	3.74	3.95	3.59	3.4	3.29	3.44
Gas vol. yield Nm^3kg^{-1}	2.74	3.03	3.25	3.06	3.21	2.93	2.82	2.75	2.83
Equivalence ratio	42.7	43.11	48.77	45.95	46.88	49.11	38.72	39.01	43.79
Air/feed ratio	2.82	2.85	3.22	3.04	3.1	2.64	2.56	2.45	2.90
HHV MJm^{-3}	3.09	4.19	3.12	3.31	3.64	3.89	4.10	4.29	3.45
Raw gas efficiency %	65.82	87.78	77.22	74.75	84.73	80.15	78.76	82.96	68.65
Hot gas efficiency %	60.03	81.77	70.4	68.44	78.07	74.12	73.05	77.18	62.88
Cold gas efficiency %	49.79	70.04	59.46	58.16	67.59	65.61	65.55	69.43	68.65
Gas composition, % volume									
H_2	7.84	12.45	9.15	9.75	9.67	10.97	11.98	12.33	8.74
CO	12.82	16.85	12.97	12.88	14.54	15.67	15.24	15.81	15.55
CO_2	15.11	11.85	16.27	15.34	15.24	16.91	15.56	15.44	12.05
CH_4	1.18	1.19	0.8	1.09	1.43	1.29	1.63	1.82	0.93
N_2	63.04	57.62	60.81	60.92	59.11	55.16	55.58	54.60	62.73
Gas exit temp. °C	524.0	549.7	484.2	489.3	466.0	427.1	391.2	400.2	391.5

Increasing the char bed height in an open-core downdraft gasifier slightly reduces the air requirement of the gasification process as shown by Figures 8.10 and 8.12. Increasing the char bed height has little effect on the feed throughput (Figure 8.9). The decrease in air flow rate into the gasifier increases the product gas higher heating value due to the reduction in nitrogen content (see Figures 8.10 and 8.12). This leads to a slight increase in the gasifier cold gas efficiency (Figure 8.13). There is also a slight increase in the product gas hydrogen and carbon monoxide content suggesting that increased char conversion is occurring. Earp stated that the

increase in product gas heating value with increasing char bed height was due to increased char reduction and tar cracking. The reduced product gas nitrogen content with increasing char bed height was not reported by Earp.

Earp carried out no experiments with char bed heights less than 5 cm. He carried out extrapolations, therefore, to assess the effects on gasifier performance of operating with a char bed height of less than 5 cm [12]. He estimated that the gas heating value drops to approximately 85% of the gas heating value of the gas produced when operating with a 10 cm deep char bed [12]. From Table 8.9 it can be seen that the gas heating value drops to between 85 and 99% of the heating value of the gas produced with a char bed depth of between 10 and 12 cm.

Figure 8.13 shows the effect of char bed height on gasifier thermal efficiency. Increasing the char bed height leads to a decrease in the product gas temperature below the grate as shown in Figure 8.7. As noted above, the reduction in air to feed ratio as the char bed height increases leads to an increase in the gasifier cold gas efficiency. However, the hot and raw gas efficiencies reach a maximum at a char bed height of approximately 13.5 cm. This is due to heat losses from the char bed offsetting the increases in product gas heating value with increasing char bed height.

It is concluded that increasing the char bed height in an open-core downdraft gasifier leads to a slight improvement in the product gas quality. The hot gas efficiency has been found to be a maximum in the uninsulated gasifier when operating with a char bed height of 13.5 cm. Operation with little or no char bed does not have a disproportionally detrimental effect on the product gas quality. Further investigations should be carried out to investigate the effect of char bed height on the product gas tar content (see Section 10).

Gas temperature
below grate, °C
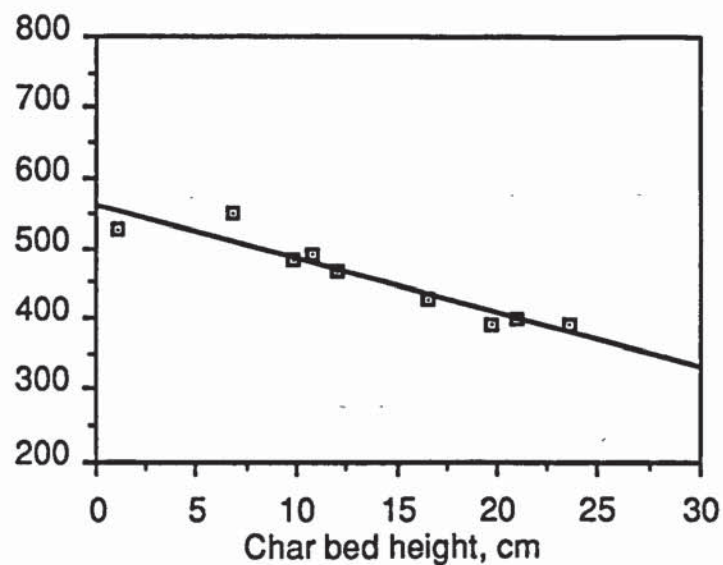
Figure 8.7

Effect of Char Bed Height on Product Gas Exit Temperature

Mass yield,
kgkg-1

Volumetric yield,
Nm3kg-1

□   Mass yield
♦   Volumetric yield
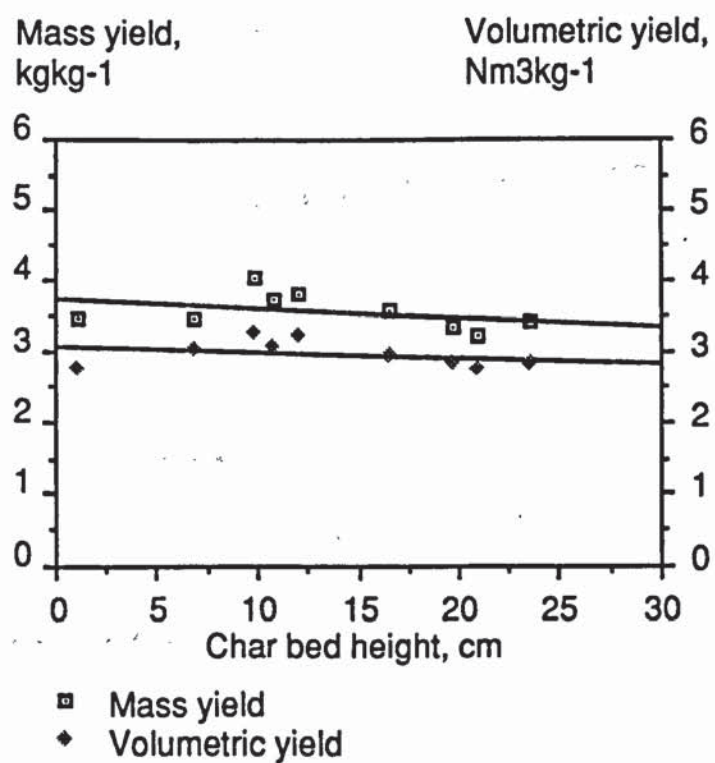
Figure 8.8

Effect of Char Bed Height on Product Gas Mass and Volumetric Yields

244

Specific capacity, kgm-2h-1
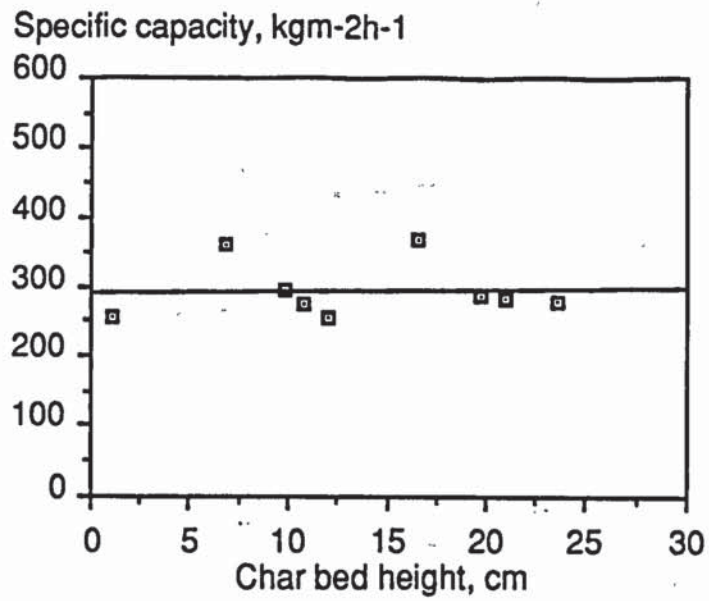
Char bed height, cm

Figure 8.9

Effect of Char Bed Height on Reactor Throughput

HHV, MJNm-3
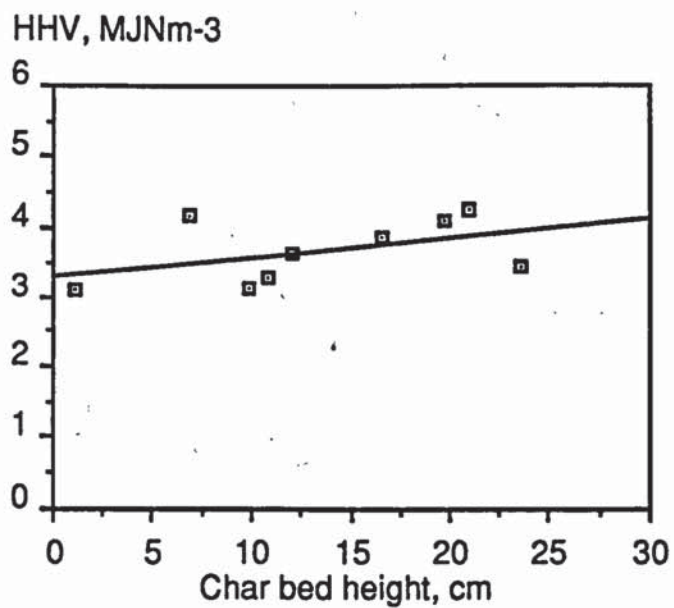
Char bed height, cm

Figure 8.10

Effect of Char Bed Height on Product Gas Higher Heating Value

245

% volume
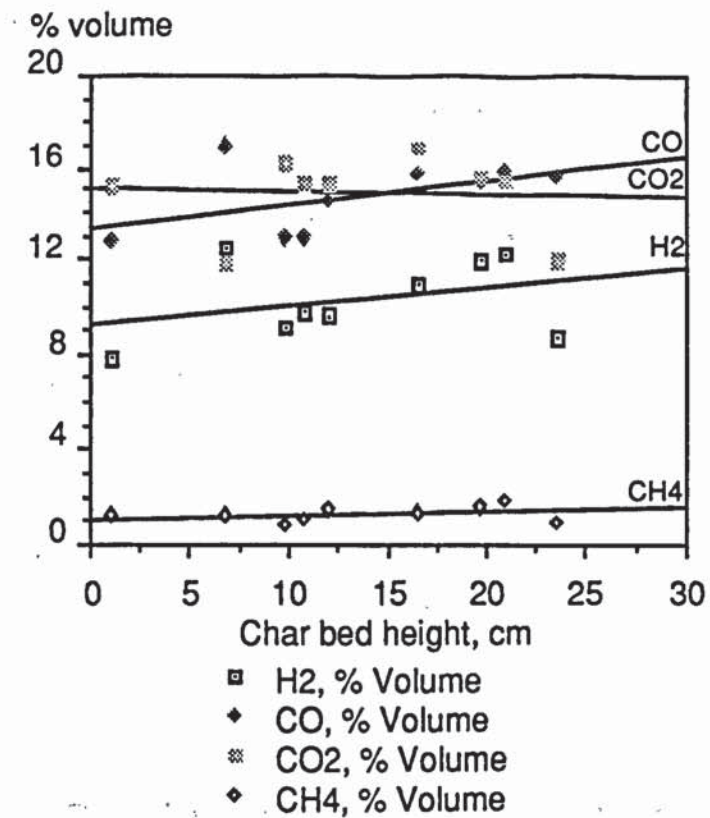
Figure 8.11

Effect of Char Bed Height on Product Gas Composition

N2, % Volume
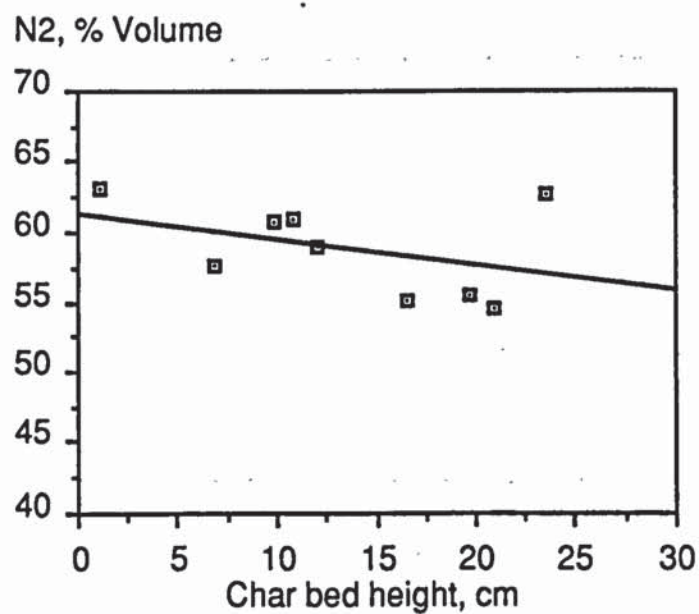
Figure 8.12

**Effect of Char Bed Height on Product Gas Nitrogen Content
(Calculated)**
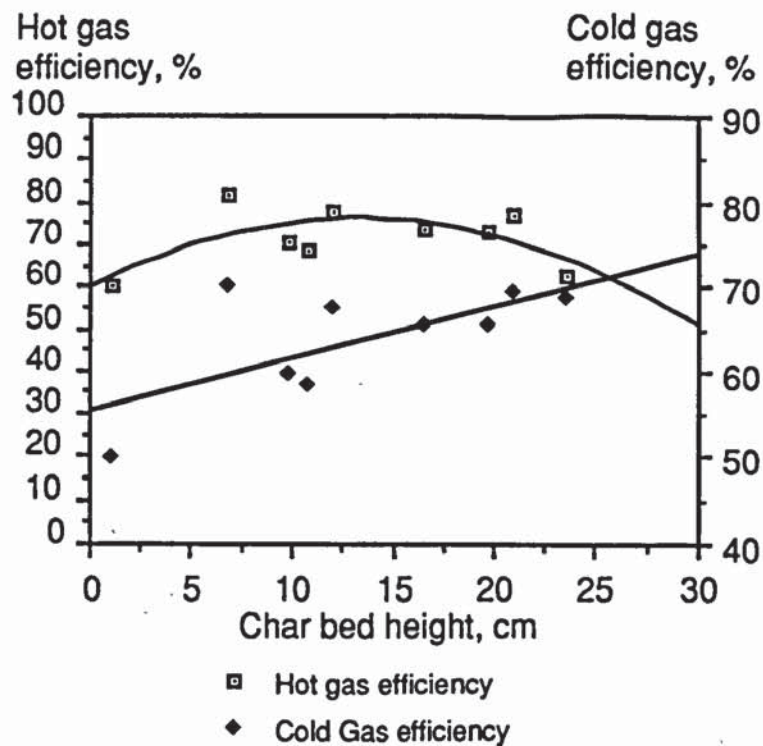
Figure 8.13

Effect of Char Bed Height on Gasifier Hot and Cold Gas Efficiencies
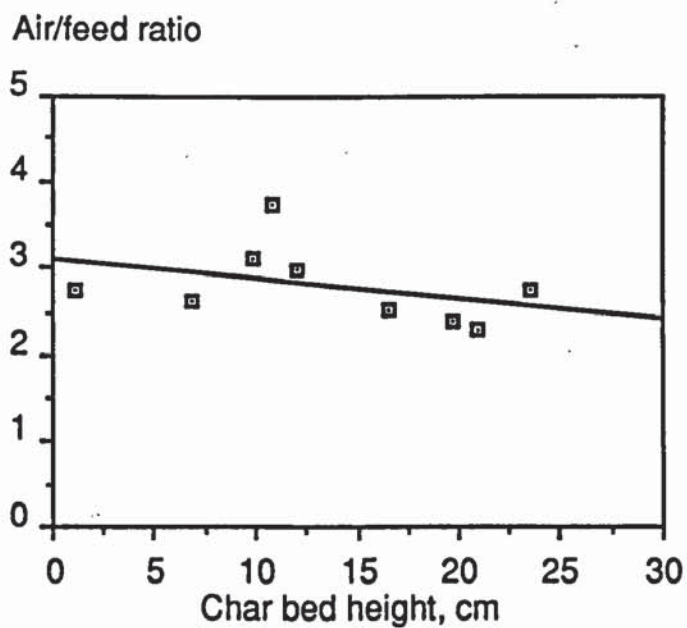
Figure 8.14

Effect of Char Bed Height on Air to Feed Ratio

247

8.6 Effect of Gasifier Insulation on Gasifier Performance

The aim of this section is to compare the performance of the gasifier when fitted with insulation to minimize heat losses with the performance of the uninsulated gasifier (standard case performance). The effects of heat loss on gasifier performance is discussed in Section 2.1.4.3 and the design of the insulation fitted to the gasifier is presented in Section 3.3.3. Assessments of the effect of insulation on the lengths of the flaming pyrolysis and char gasification zones was presented in Sections 7.2.4 and 7.3.4.

8.6.1 Data Collection and Treatment

The methods of data collection and gasifier operation were carried out in the same way as for the standard case experiments. The char bed heights and feed moisture contents for the insulated experiments are similar to those of the standard case experiments (10%). The gasification process within the insulated gasifier was observed through a 20 mm wide and 50 mm high sight strip (see Plate 3.2)

Four experiments were performed using an insulated reactor. Experiment 1 was performed using wood chips in the size range 4.75-6.35 mm and was used as a shakedown run. Wood chips in the size range 6.35-12.7 mm were used for the remaining three insulated reactor experiments (experiments 23, 24 and 25). The reaction zone in experiment 24 rose throughout the test and the experimental data were used to assess the effect of operating in the pyrolysis dominating mode on gasifier performance (see Section 8.3). The data from experiments 23 and 25 are, therefore, used to study the effect of gasifier insulation on gasifier performance. These data are presented in Table 8.10.

8.6.2 Results and Discussion

Gasifier insulation has the effect of reducing the heat losses from the gasifier and increasing available energy produced by flaming pyrolysis for gasification (Figures 8.15 and 8.16). The heat losses (convective and radiative) from the gasifier are reduced by the 38 mm thick mineral fibre (Kaowool) insulation from 39% to 16.6% of the wood input to the gasifier (experiments 25 and 26).

248

Gasifier insulation will increase the maximum gasifier temperature at the start of the char gasification zone favouring gasification both kinetically and thermodynamically (see Figures 8.15 and 8.16). The maximum temperature measured using a search thermocouple in the uninsulated gasifier was 930°C (measured at the top of the char bed) while the maximum temperature recorded in the insulated gasifier was 1040°C (Figures 8.15 and 8.16). The maximum temperature measured using a disappearing filament pyrometer was 1024.5°C in the uninsulated gasifier (standard case experiments) and 1040°C in the insulated gasifier (experiment 25).

Table 8.10
Insulated Gasifier Performance Data

Feed: Wood chips 6.35-12.7 mm

	Insulated Gasifier	Standard Case
Length of experiment, hours (minutes)	0.79 (46.6)	0.97 (58.5)
Feed moisture content, % wb	9.42	9.49
Char bed height, cm	18.97	17.23
Specific capacity, $kgm^{-2}h^{-1}$	320.57	276.39
Mass yield, $kgkg^{-1}$	3.39	3.23
Volumetric yield, Nm^3kg^{-1}	2.98	2.94
Equivalence ratio, %	36.06	39.19
Air/feed ratio	2.48	2.81
Gas higher heating value, $MJNm^{-3}$	4.49	3.38
H_2/CO ratio	0.77	0.66
CO/CO_2 ratio	1.46	1.07
Gasifier gas outlet temperature, °C	637.38	440.39
Raw gas efficiency, %	83.41	61.44
Hot gas efficiency, %	77.44	55.40
Cold gas efficiency, %	63.52	46.69
H_2 in product gas, % volume	13.25	9.25
CO in product gas, % volume	17.41	14.22
CO_2 in product gas, % volume	12.36	13.69
CH_4 in product gas, % volume	1.50	1.01
N_2 in product gas, % volume	55.48	61.82
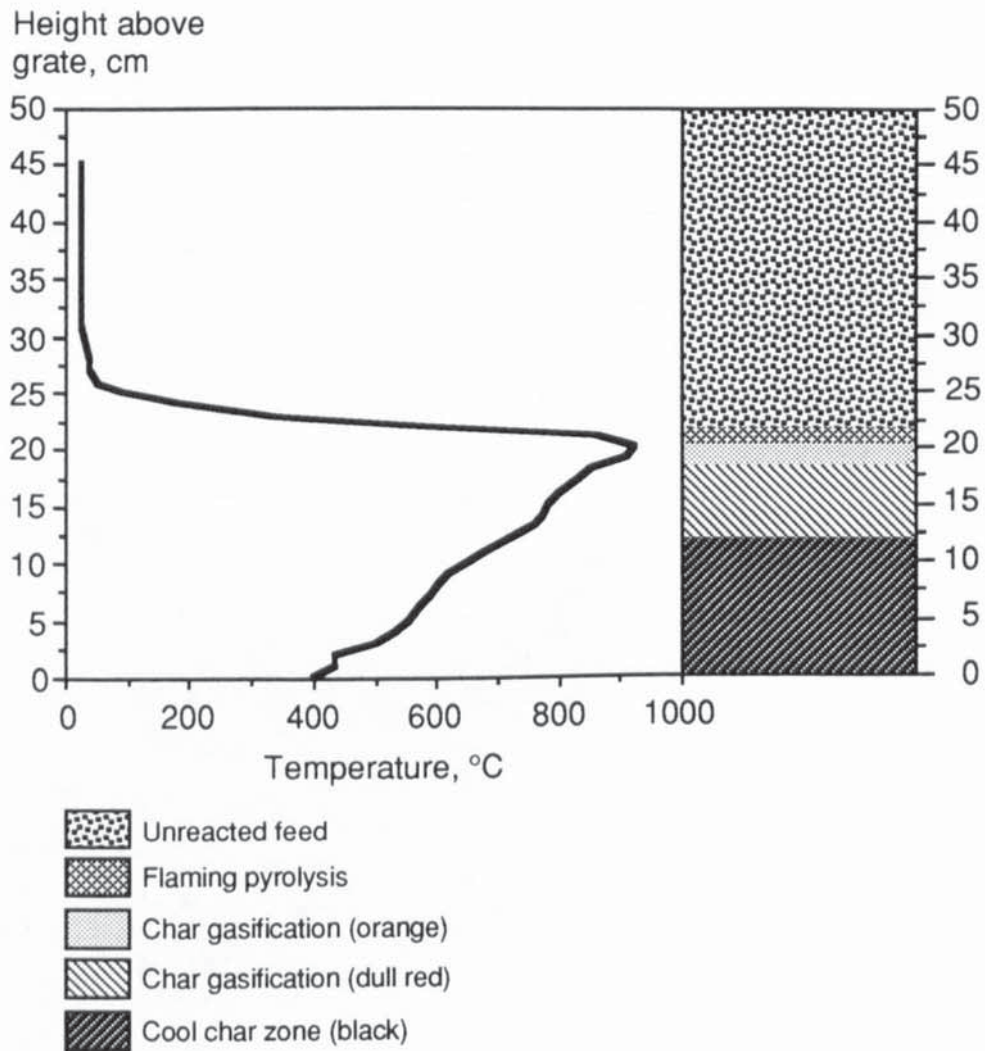
Figure 8.15

Vertical Temperature Profile Through the Uninsulated Gasifier

Height above
grate, cm

Unreacted feed
Flaming pyrolysis
Char gasification (orange)
Char gasification (dull red)
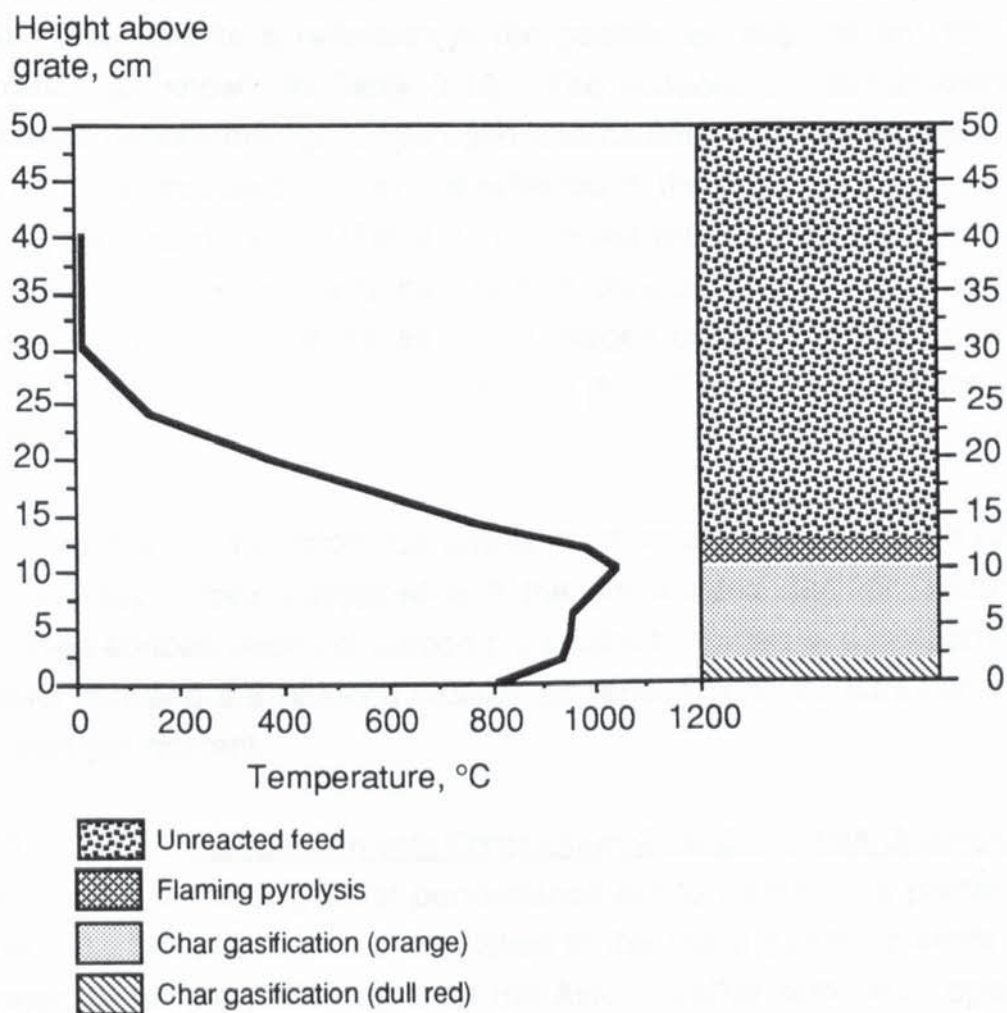
Figure 8.16

Vertical Temperature Profile Through the Insulated Gasifier

The higher temperatures obtained at the top of the char gasification zone during insulated gasifier performance compared with uninsulated gasifier operation lead to a higher gasifier specific capacity. This is caused by an increase in the rate of char production by pyrolysis and an increase in the rate of char consumption by gasification (Table 8.10). Reduced gasifier heat losses also lead to a reduction in the gasifier air requirement for stable operation as shown in Table 8.10. The reduced air requirement and increased concentrations of hydrogen and carbon monoxide in the product gas from the insulated gasifier are reflected in the 33% increase in product gas higher heating value (Table 8.10). Reed reports that the gasifier cold gas efficiency and product gas carbon dioxide concentration are very sensitive to gasifier heat losses for an oxygen blown open-core downdraft gasifier operating at atmospheric pressure [99]. This is shown by the results in Table 8.10.

Insulating the gasifier improves gasifier performance due to a reduction in gasifier heat losses compared with the uninsulated gasifier. There are increased concentrations of carbon monoxide, hydrogen and methane in the product gas and the reduced gasifier air requirement reduces the product gas nitrogen content.

8.6.3   Comparison with Other Open-Core Downdraft Gasifiers
Open-core donwdraft gasifier performance in the literature is presented in Table 2.6. The application of insulation to the Aston gasifier permits closer comparison of the performance of the Aston gasifier with other open-core downdraft gasifiers in the literature as most open-core downdraft gasifiers reported in the literature are insulated.

Insulating the Aston gasifier results in a product gas higher heating value and volumetric yield similar to the higher heating value and volumetric yield of the gas produced by the NREL 5 cm diameter gasifier (Tables 8.10 and 2.6) [11]. The higher product gas higher heating value produced by the Kansas State University gasifier is attributed to secondary air injection into the reaction zone converting tars to lower molecular weight components [32]. Secondary air injection maintains the reaction zone in the KSU gasifier at a constant position relative to the grate. The cold gas efficiency of the Twente University rice husk gasifier is more similar to the cold gas efficiency of the uninsulated Aston gasifier than the insulated Aston gasifier (Table

8.10) [31]. The lower specific capacity and cold gas efficiency of this gasifier compared with the insulated gasifier will be due to the poor flow characteristics and the small particle size of rice husk. A char/ash removal system is used in this case to maintain a stable reaction zone. The Univeristy of California, Davis reactor also operates with a rice husk feed resulting in a lower specific capacity and cold gas efficiency compared with the insulated Aston gasifier [29]. This gasifier was operated in a batch mode of operation with a rising reaction zone. The Syngas gasifier operates with a propane burner adding energy to the reaction zone [41]. Coupled with the blasting of air into the reaction zone, this results in a very high specific capacity (1450 $kgm^{-2}h^{-1}$) compared with the insulated Aston gasifier (320.57 $kgm^{-2}h^{-1}$).

The insulated Aston gasifier produces a product gas similar in composition to other air blown open-core downdraft gasifiers reported in the literature (Table 2.6). The volumetric gas yield is in the range of those published for other similar gasifiers. The product gas higher heating value from the Aston gasifier is lower than the higher heating values reported for the APWM and Syngas gasifiers as these gasifiers can operate at a lower equivalence ratio to maintain a stable reaction zone as a result of the use of char/ash removal systems. As discussed in Section 2.1.4.1, the effect of operation at lower equivalence ratios is to move the gasification reaction towards pyrolysis operation and to increase the product gas higher heating value. However, this results in the production of char as a waste stream.

8.6.4   Comparison with Aston Carbon Boundary Model
Insulated gasifier performance is compared with the output from the Aston carbon boundary model (for typical insulated gasifier inputs) in Table 8.11.

It can be seen that the output from the carbon boundary model compares well with the experimental results obtained. However, the equivalence ratio predicted by the carbon boundary model is lower than the measured equivalence ratio for the insulated Aston gasifier. Open-core downdraft gasifiers, however, operate at higher equivalence ratios compared with the theoretical equivalence ratio required for complete carbon conversion. Additional air is required to combust a high proportion of pyrolysis products to provide sufficient energy in the char gasification zone to ensure that stable

253

operation is maintained (ie. the rate of char production by pyrolysis equals the rate of char consumption by gasification).

<div style="border:1px solid">

Table 8.11
Comparison of Aston Carbon Boundary Model Predictions with Actual Mark II Standard Case Gasifier Performance

	Model predictions	Insulated gasifier performance
Reactor heat loss, %	16.59	16.59
Gas composition, % volume, dry		
Hydrogen	16.34	13.25
Carbon monoxide	15.13	17.41
Carbon dioxide	13.85	12.36
Methane	0.86	1.50
Nitrogen	53.82	55.48
Calculated gas HHV, MJNm^{-3}	4.11	4.49
Cold gas efficiency, %	61.61	63.52
Equivalence ratio, %	27.47	36.06
Equilibrium temperature, °C	622.16	637.38*

* Measured gas exit temperature

</div>

The higher methane, lower carbon dioxide and lower hydrogen concentrations of the gas from the Aston gasifier compared with the gas from the model may be due to increased methanation according to Equation 2.12. This reaction mechanism is not included in the procedures used in the carbon boundary model [45]. The high equivalence ratio at which the insulated gasifier operates compared with the carbon boundary model may also result in hydrogen consumption by oxidation according to Equation 2.8 forming water. The water concentration of the product gas was not measured in this research (see Section 10).

8.7 Effect of Feed Moisture Content on Gasifier Performance

The aim of this section is to assess the effect of feed moisture content on the gasifier performance. An investigation into the effect of feed moisture

content on gasifier performance will aid identification of the feed moisture content at which gasifier performance becomes unacceptable.

The effect of moisture on gasifier performance was discussed in Section 2.1.4.5. Increasing the feed moisture content is reported to have a detrimental effect on gasifier performance in terms of gas heating value, reactor throughput and gasifier efficiency to cold clean gas. Energy is required to remove any moisture in the biomass feed prior to the start of any gasification reactions. The latent heat provided to convert feed moisture to water vapour is lost and can not be recovered for use in the gasification process.

8.7.1 Data Collection and Treatment

The variable moisture content was obtained by chipping and gasifying the wood for use prior to drying. For standard case experiments, wood was dried to approximately 10% (wet basis) by storing the wood in the laboratory until the moisture content was constant. In addition to the standard case experiments, wood chip feeds (sieved to between 6.35 and 12.7 mm) with moisture contents of 18.6% wet basis (experiments 19-21) and 32.1% wet basis (experiments 15 and 17) were gasified. The moisture content was determined using the oven dry method described by TRADA (see Section 4.2.2) [92].

8.7.2 Results and Discussion

Table 8.12 presents the data for the experiments performed using variable moisture content feeds.

The results from the chip moisture content variation experiments are presented graphically in Figures 8.17 - 8.24. The lines drawn on each graph show the "best fit" line calculated using "Cricket Graph" graph plotting software. These graphs show the effect of the feedstock moisture content on the performance of the Aston open-core downdraft gasifier.

There is a reduction in gasifier performance with increase in feed moisture content (Table 8.12). The energy for evaporation of moisture reduces the energy available for char production by pyrolysis and char consumption by gasification (see Figure 8.20). Measured using a disappearing filament pyrometer, the maximum gasifier temperature (located at the top of the char

255

gasification zone) during standard case operation was 1024.5°C. During operation with wood chips with a moisture content of 18.63%, the average maximum gasifier temperature was 992.2°C and during operation with wood chips with a moisture content of 32.13%, the average maximum gasifier temperature was 996°C. The higher temperature recorded for operation with the feedstock containing 32% moisture compared with the feedstock containing 18% moisture is attributed to a measurement error. The reduced energy available in the gasifier with increase in feed moisture content leads to a reduction in the specific capacity as shown in Table 8.12 and Figure 8.18. In addition, Huff states that the burning time of wood particles increases with feed moisture content [23]. An increased feed moisture content should, therefore, increase the reaction time of a wood particle reducing the gasifier specific capacity (dry) as shown by Figure 8.18.

Table 8.12

Gasifier Performance Data - Effect of Feed Moisture Content

Feed: Woodchips (6.35-12.7 mm)

Feed moisture content, % wb	**9.49**	**18.63**	**32.13**
Length of experiment, hours	0.97	0.63	0.54
Char bed height, cm	17.23	10.26	8.29
Specific capacity, $kgm^{-2}h^{-1}$	276.39	252.49	126.40
Mass yield, $kgkg^{-1}$	3.59	3.55	3.82
Volumetric yield, Nm^3kg^{-1}	2.94	2.85	3.00
Equivalence ratio, %	44.87	42.99	41.70
Air/feed ratio	2.97	2.85	2.75
Gas higher heating value, $MJNm^{-3}$	3.38	3.05	3.30
H_2/CO ratio	0.66	0.82	0.77
CO/CO_2 ratio	1.07	0.67	0.60
Gasifier gas outlet temperature,°C	440.39	421.60	332.17
Raw gas efficiency, %	61.44	54.74	55.45
Hot gas efficiency, %	55.40	48.76	50.10
Cold gas efficiency, %	46.69	40.62	43.66
H_2 in product gas, % volume	9.82	9.52	8.99
CO in product gas, % volume	14.70	11.54	11.46
CO_2 in product gas, % volume	14.77	17.16	21.35
CH_4 in product gas, % volume	1.10	0.95	1.35
N_2 in product gas, % volume	59.60	60.83	56.85

Increasing the feed moisture content reduces the product gas carbon monoxide concentration, increases the product gas carbon dioxide concentration and slightly increases the product gas hydrogen concentration (Figure 8.21). This can be explained by the increased demand for combustion for drying biomass inside the gasifier and the simultaneously occurring water gas shift reaction in which there is more water available to convert carbon monoxide to hydrogen and carbon dioxide. The reduction in the proportion of combustible gases in the product gas leads to a decrease in the product gas heating value (Figure 8.19) and gasifier cold gas efficiency (Figure 8.23). The heating value of the gas produced from wood chips containing approximately 19% moisture (wet basis) is approximately 10% lower thàn wood chips containing approximately 10% moisture (Table 8.12). This compares well with the reduction in heating value of about 12%

from a gas produced from wood chips containing 13.5% and a gas produced from wood chips containing 21.6% of moisture for a throated downdraft gasifier in the literature [100]. There is a loss in cold gas efficiency of approximately 21% when the feed moisture content on a wet basis increases from 10 to 32%. There is good agreement between this figure and the loss in efficiency (26%) for a throated downdraft gasifier calculated by Graham when the poplar moisture content on a wet basis increased from 13 to 34% [94].

From the data presented in this project, it is confirmed that increasing feed moisture content has a detrimental effect on product gas quality. Providing a 5% reduction on cold gas efficiency is acceptable (compared with standard operation), then the maximum acceptable feed moisture content is 17.5%. A 10% reduction in gasifier cold gas efficiency compared with standard operation results in a maximum acceptable feed moisture content of 27.5%.

Gas mass yield, kg/kg   Gas volumetric yield, Nm3kg-1

Moisture, % wb

□ Mass yield, kg/kg
♦ Volumetric yield, Nm3/kg
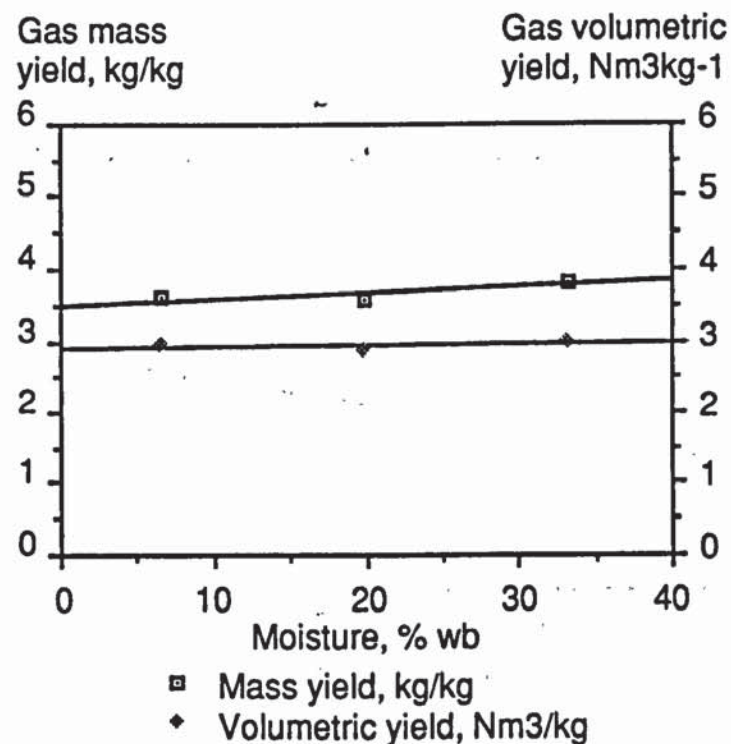
Figure 8.17
Dry Gas Mass and Volumetric Yields v Feed Moisture Content (wb)

Specific capacity,
kgm-2h-1

■ Specific capacity (wet feed)

✦ Specific capacity (dry feed)
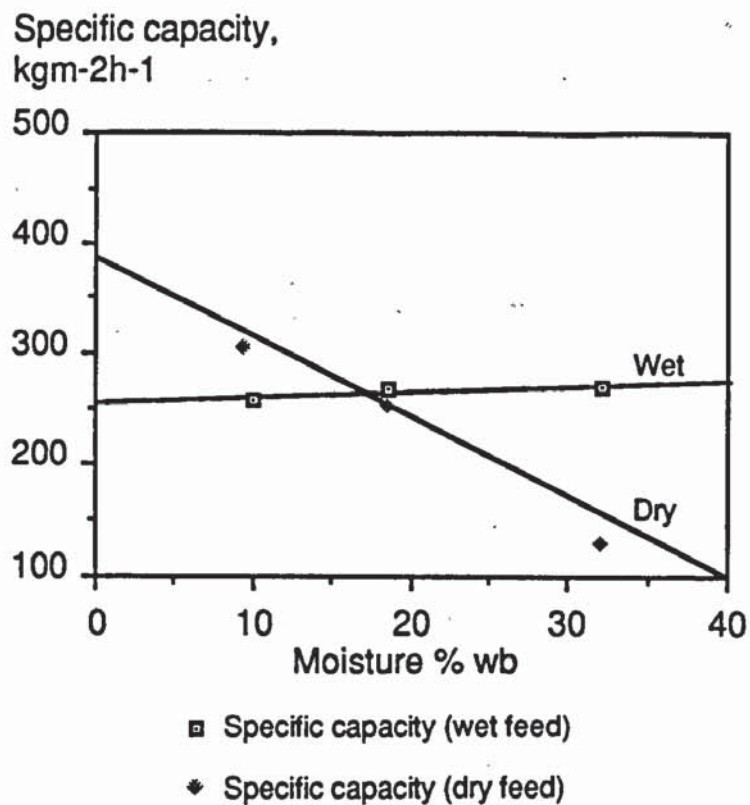
Figure 8.18

Gasifier Specific Capacity v Feed Moisture Content (wb)

HHV MJ/m3
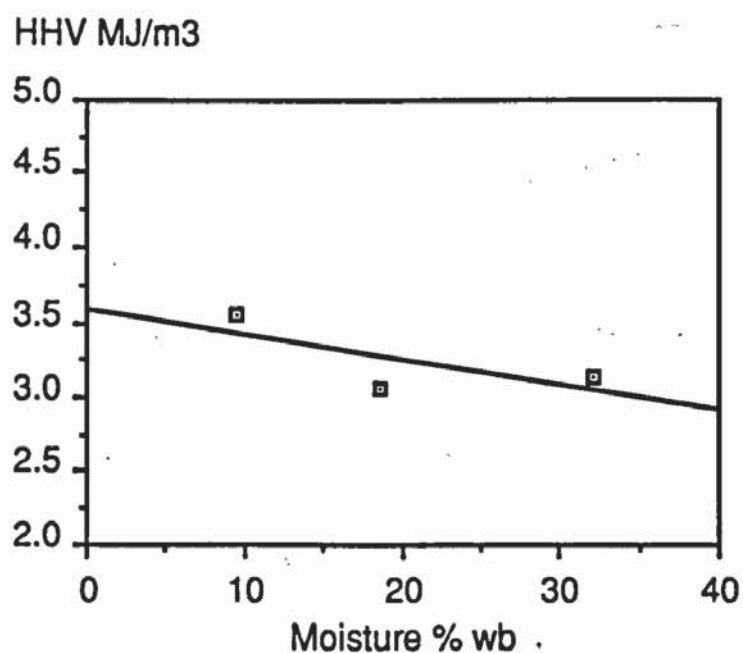
Figure 8.19

Product Gas Higher Heating Value v Feed Moisture Content (wb)

259

H2/CO ratio   CO/CO2 ratio

CO/CO2

H2/CO

Moisture % wb
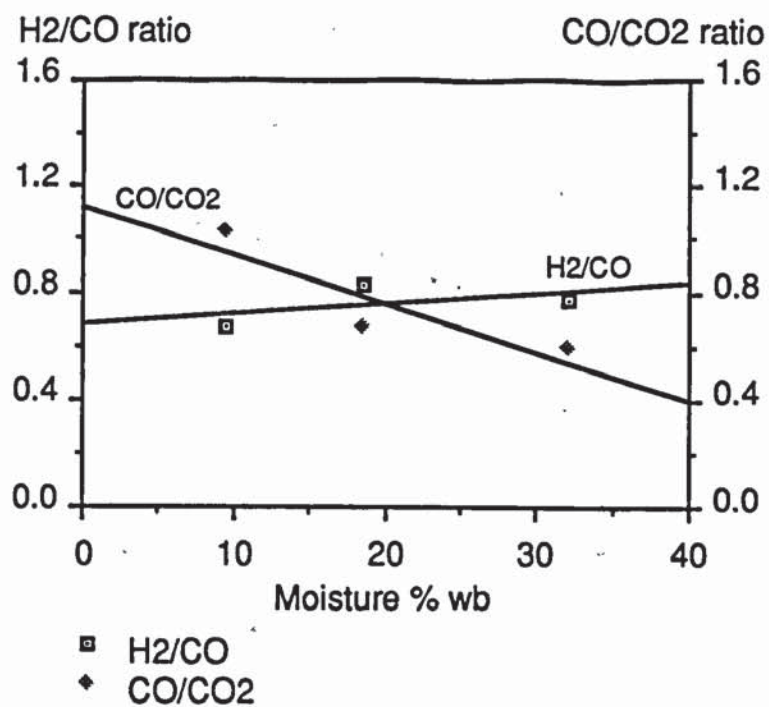
□   H2/CO
♦   CO/CO2

Figure 8.20

H$_2$/CO and CO/CO$_2$ Ratios v Feed Moisture Content (wb)

% volume

Moisture, % wb

□   H2   ※   CO2
♦   CO   ◇   CH4
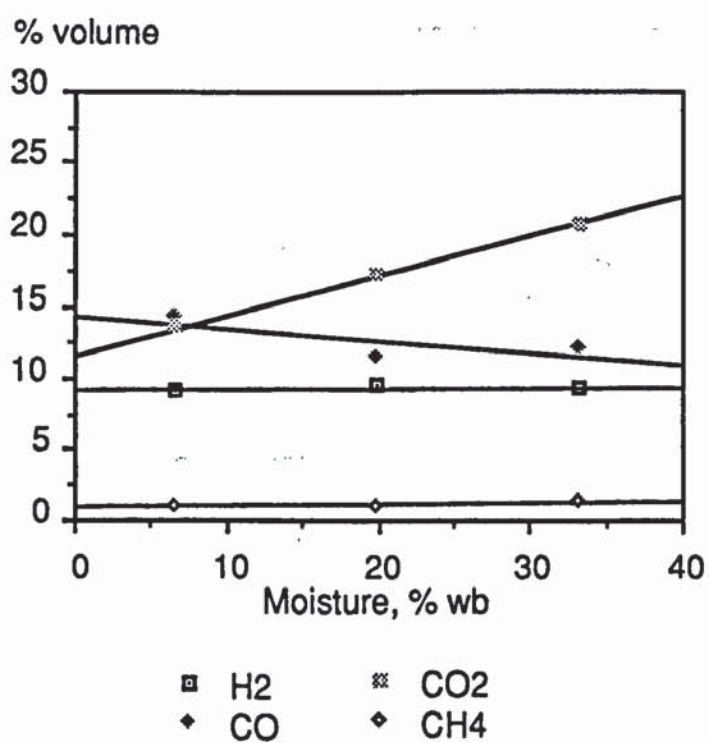
Figure 8.21

Product Gas Composition v Feed Moisture Content (wb)

Gas nitrogen content,
% volume
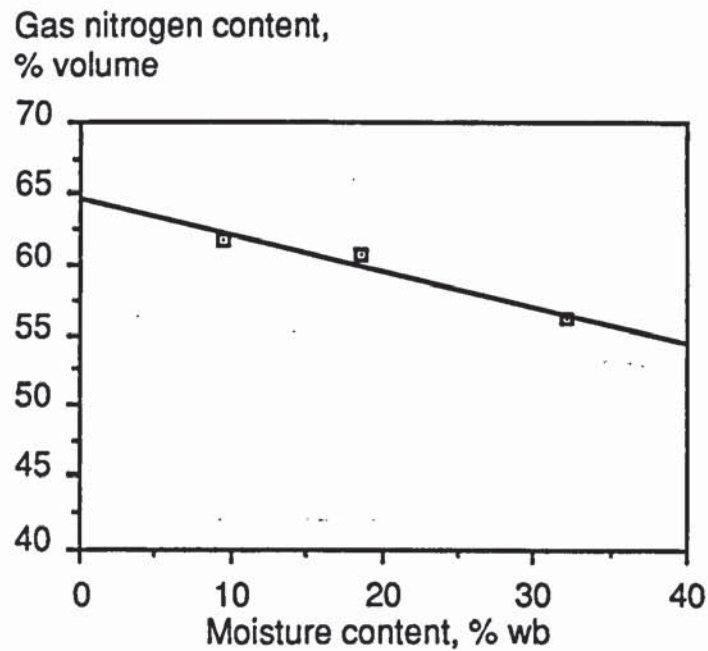
Figure 8.22

Product Gas Nitrogen Content v Feed Moisture Content (wb)

Efficiency, %

□ Raw gas efficiency
◆ Hot gas efficiency
▧ Cold gas efficiency
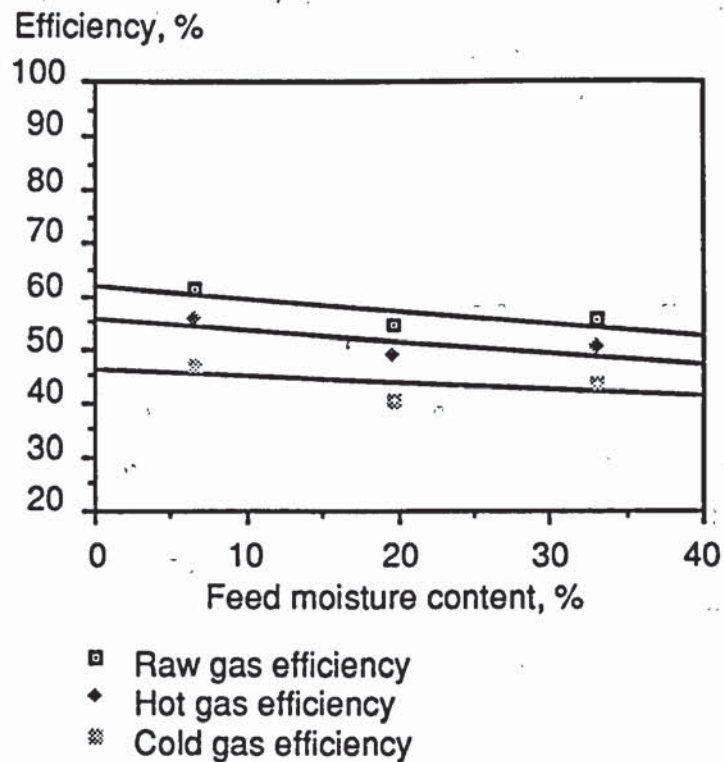
Figure 8.23

Gasifier Thermal Efficiency v Feed Moisture Content (wb)

261
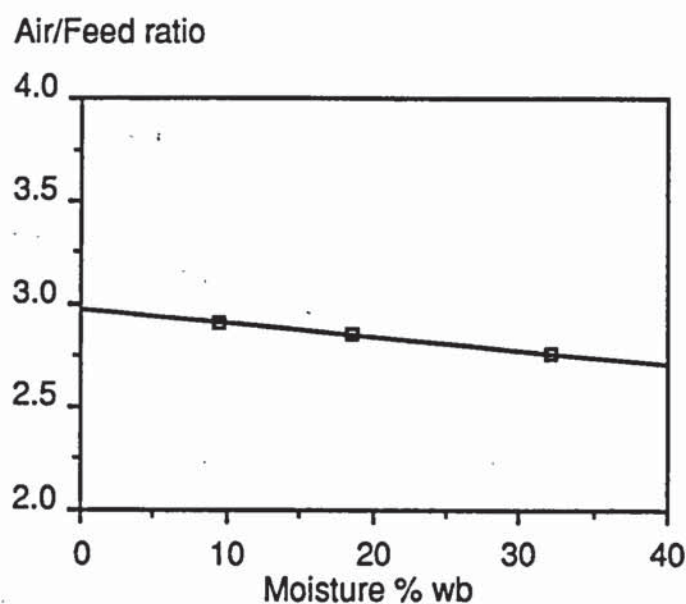
Air/Feed ratio

Figure 8.24
Air to Feed Ratio v Feed Moisture Content (wb)

8.8   Effect of Feed Size on Gasifier Performance

The aim of this section is to assess the effect of feed size on gasifier performance. The effect of feed size on gasifier performance in the literature is discussed in Section 2.1.4.4.

8.8.1   Data Collection and Treatment

Feed size can be quantified in terms of the particle characteristic diameter or the particle characteristic size. The characteristic diameter is defined as the diameter of a sphere having the same volume as the particle under consideration while the characteristic size is defined as the length of side of cube having the same volume as the particle under consideration. The characteristic size and diameter for ten particles from each feed type was obtained and the average used for this analysis. This procedure is fully described in Section 4.2.4.

Six different feed sizes were gasified in eight experiments. Feed production and preparation is described in Section 4.1. Table 8.13 shows the experiments corresponding to the feeds tested. Due to the loss of computer recorded data during experiment 8, the results for the spherical feed (15 mm diameter beads) are not used in this section. The feed moisture content for each of the experiments shown in Table 8.13 was approximately 10% (wet basis).

262

<div align="center">

Table 8.13

Effect of Feed Size - Experiments Performed

</div>

Feed Description	Wood chips	Dowels	Wood chips	Wood chips	Wood chips
Characteristic diameter, mm	4.52	6.71	9.28	9.46	11.77
Sphericity	0.71	0.87	0.77	0.76	0.68
Experiment(s)	5,7	6	15	22,26	14

The method of gasifier operation, data collected and data treatment methods were the same as those used for the standard experiments.

8.8.2   Results and Discussion

The results of the effect of feed size expressed as the particle characteristic diameter and feed shape expressed as the particle sphericity (see Section 8.9) on gasifier performance are shown in Table 8.14.

The effect of feed size on gasifier performance is presented graphically in Figures 8.25 to 8.32. It can be seen that there is apparently an ideal feed particle size (6.4 mm characteristic diameter equivalent to a cube of side 5.2 mm) for the Aston gasifier at which the air to feed ratio for stable operation is a minimum (Figure 8.32) leading to a reduction in the product gas nitrogen content and hence, the dry gas mass and volumetric yields (Figure 8.25). Feeds containing particles with characteristic diameters less than 6.4 mm will increase the pressure drop through the gasifier and were observed to flow poorly within the gasifier. During the gasification of feeds containing wood chips sieved to between 4.75 and 6.35 mm, the reaction zone was often badly defined and sloping and voids were observed in the unreacted feed zone (see Plate 8.2) resulting in poor gasifier performance. The char yield from feeds consisting of particles with characteristic diameters larger than 6.4 mm will be greater than the char yield from feeds consisting of particles with characteristic diameters less than 6.4 mm [32]. Large particles are reported to yield a greater amount of char during pyrolysis than smaller particles [37]. As the feed particle size increases, the residence time of the volatiles in the particle during pyrolysis will increase and allow sufficient time for some of the reactive components of pyrolysis to deposit carbon in the

particle. This will lead to an increase in the gasifier air requirement to maintain stable operation when operating with feeds consisting of particles with characteristic diameters greater than 6.4 mm (Figure 8.32). It was shown in Table 7.1 that the char yield from 15 mm diameter beads was greater than the char yield from wood chips sieved to between 4.75 mm and 6.35 mm. In addition, it is reported that the char yield from the pyrolysis of a 5 mm particle was 19% and from a 15 mm particle was 24% [36].

Table 8.14
Gasifier Performance Data - Effect of Feed Size and Shape

Characteristic diameter, mm*	4.52	6.71	9.28	9.46	11.75
Length of experiment, hours	0.40	0.74	0.74	0.97	0.37
Sphericity	0.71	0.87	0.77	0.76	0.68
Feed moisture content, % wb	9.64	9.76	9.71	9.49	9.71
Char bed height, cm	15.86	20.93	16.58	17.23	9.80
Specific capacity, $kgm^{-2}h^{-1}$	269.77	281.67	369.66	276.39	294.09
Mass yield, $kgkg^{-1}$	3.63	3.23	3.57	3.23	4.05
Volumetric yield, Nm^3kg^{-1}	3.01	2.75	2.93	2.94	3.25
Equivalence ratio, %	37.38	33.62	35.02	39.24	43.50
Air/feed ratio	2.68	2.28	2.51	2.81	3.12
Gas higher heating value, $MJNm^{-3}$	3.87	4.29	3.90	3.38	3.12
H_2/CO ratio	0.72	0.78	0.70	0.66	0.71
CO/CO_2 ratio	0.98	1.03	0.93	1.07	0.80
Gasifier gas outlet temperature,°C	428.60	400.17	427.06	440.39	484.22
Raw gas efficiency, %	69.78	71.44	68.06	61.44	65.53
Hot gas efficiency, %	63.60	65.66	62.02	55.40	58.71
Cold gas efficiency, %	54.61	57.91	53.51	46.69	47.77
H_2 in product gas, % volume	10.83	12.33	10.97	9.25	9.15
CO in product gas, % volume	14.89	15.81	15.67	14.22	12.97
CO_2 in product gas, % volume	15.40	15.44	16.91	13.69	16.27
CH_4 in product gas, % volume	1.53	1.82	1.29	1.01	0.80
N_2 in product gas, % volume	57.35	54.60	55.16	61.82	60.81

* See Table 4.4

Walawender reports that the gasifier cold gas efficiency is higher for feeds consisting of small particles compared with feeds consisting of larger

264

particles [32]. However, the effect of particle size on gasifier performance was only investigated using two feedstocks and a comparison with this work can not be made.

Hoi investigated the effect of feed particle size on throated downdraft gasifier performance (Section 2.1.4.4) [39]. Hoi's results show an ideal particle size at which the product gas higher heating value is a maximum [39]. However, the cold gas efficiency is shown by Hoi to decrease linearly with increase in feed particle size although a quadratic curve similar to those shown in Figure 8.31 could be drawn through the data points presented (Figure 2.11) [39].

The optimum feed particle diameter for the Aston gasifier has been found to be 6.4 mm at which the gasifier air requirement to maintain a stable reaction zone is a minimum. The use of feeds consisting of small particles (less than 6 mm diameter) can lead to bridging in the unreacted feed zone and the formation of mis-shaped reaction zones resulting in poor gasifier performance and difficult gasifier control.
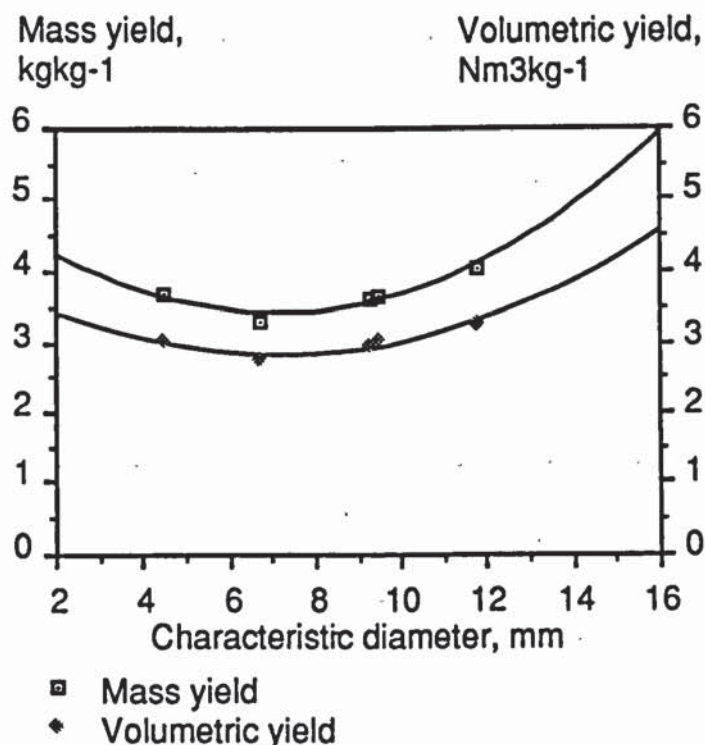
Figure 8.25
Dry Gas Mass Yield and Gas Volumetric Yield v Feed Size
(Characteristic Diameter)

265
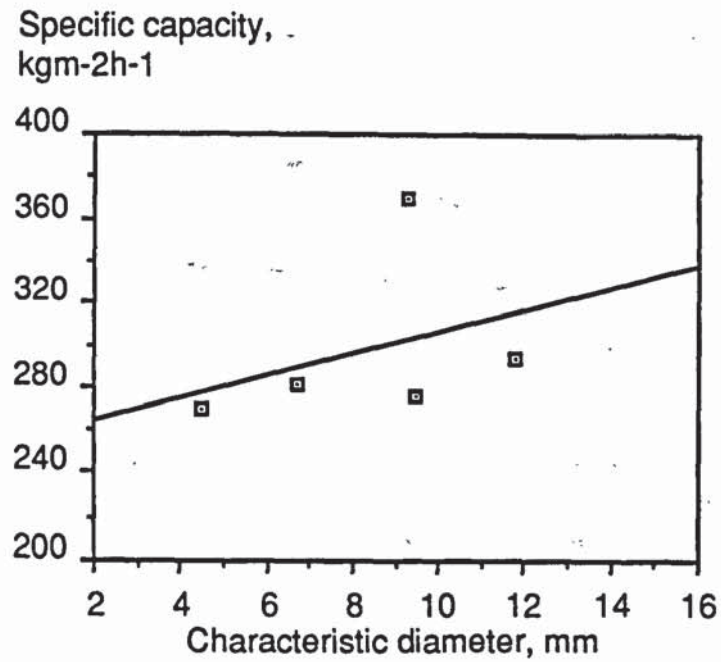
Figure 8.26

Specific Capacity v Feed Size (Characteristic Diameter)
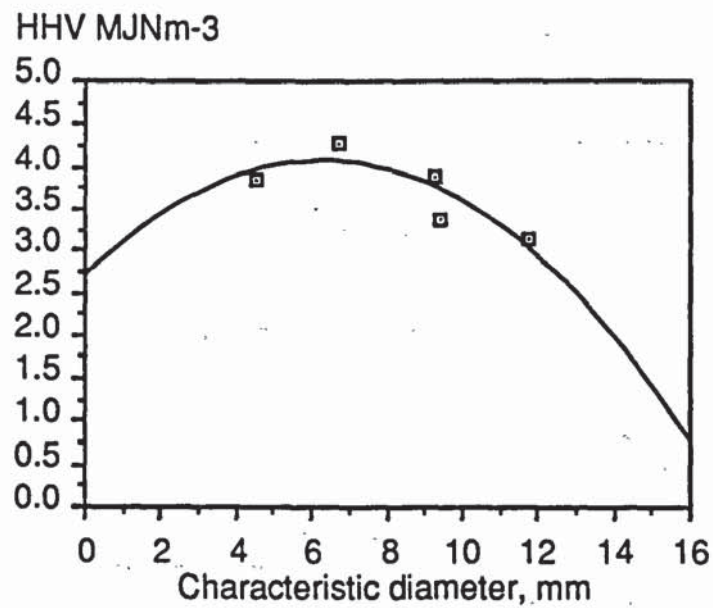
Figure 8.27

Gas Higher Heating Value v Feed Size (Characteristic Diameter)
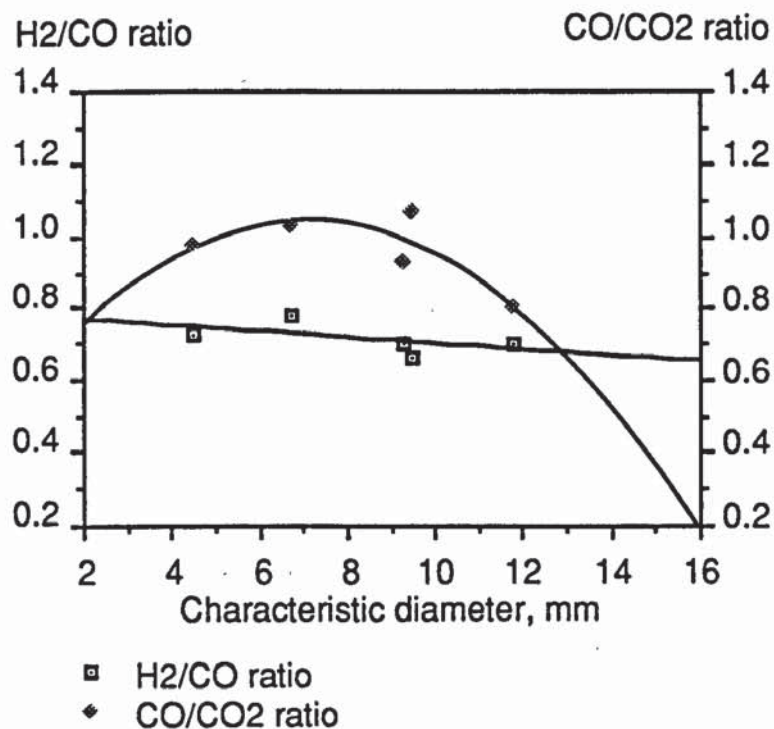
Figure 8.28

Gas H$_2$/CO and CO/CO$_2$ Ratios v Feed Size (Characteristic Diameter)
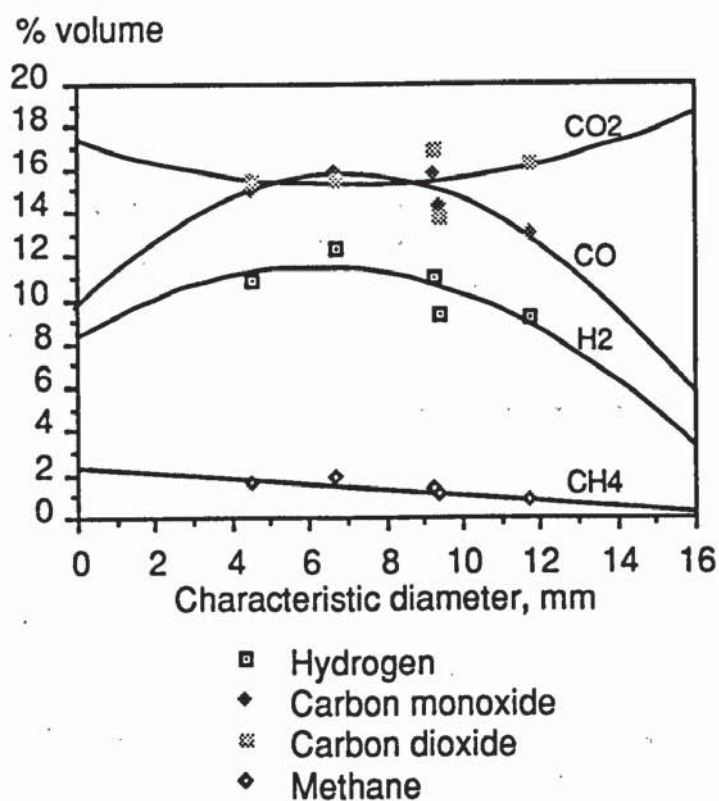
Figure 8.29

Gas Compositions v Feed Size (Characteristic Diameter)
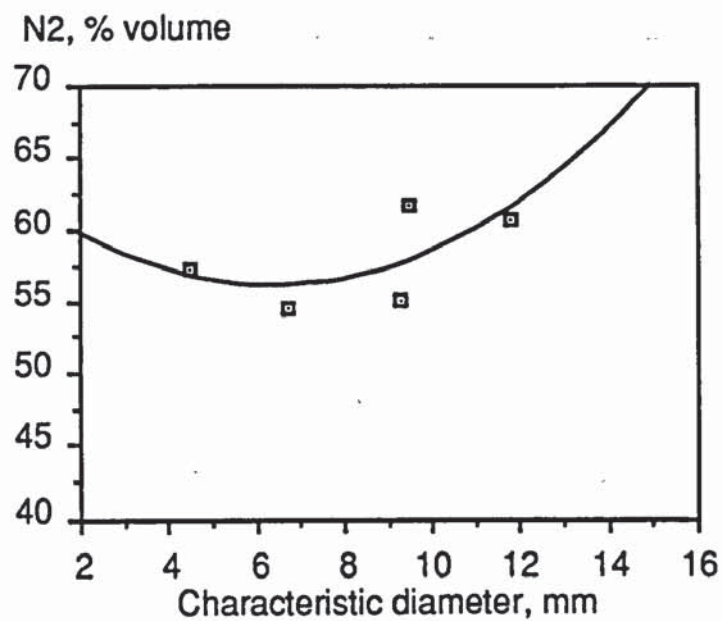
Figure 8.30

Gas Nitrogen Content v Feed Size (Characteristic Diameter)

- □ Raw gas efficiency, %
- ♦ Hot gas efficiency, %
- ▓ Cold gas efficiency, %
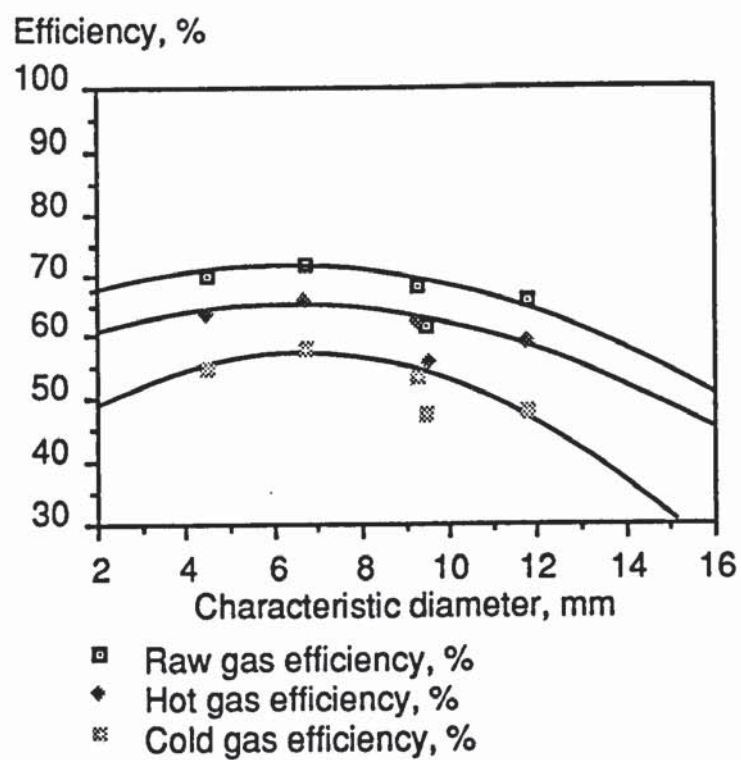
Figure 8.31

Gasifier Efficiency v Feed Size (Characteristic Diameter)
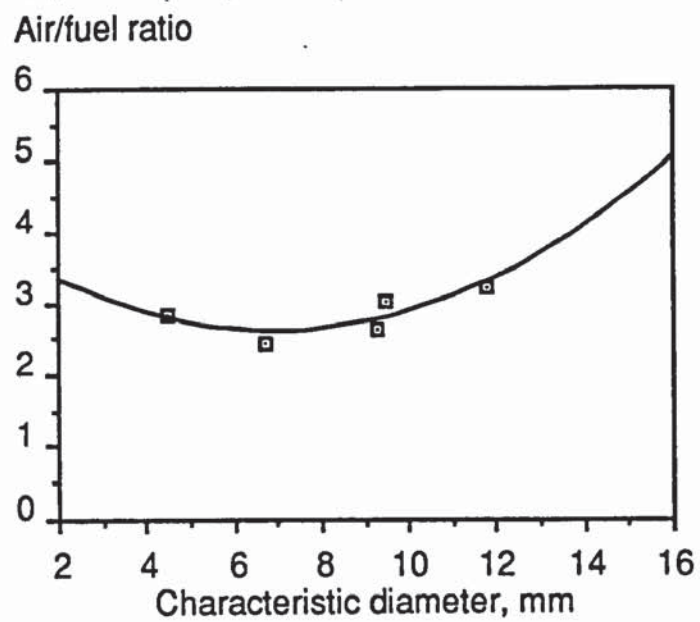
Figure 8.32

Air to Feed Ratio v Feed Size (Characteristic Diameter)

Plate 8.2
Feed Bridging in Gasifier (Experiment 7)

8.9 Effect of Feed Shape on Gasifier Performance

The aim of this section is to assess the effect of feed shape on gasifier performance. The effect of feed shape on the performance of open-core downdraft gasifiers in the literature is discussed in Section 2.1.4.4.

8.9.1 Data Collection and Treatment

Feed shape can be quantified in terms of the particle sphericity. Sphericity is defined as the ratio of the particle surface area of a sphere having the same volume as the particle to the surface area of the particle [23]. The procedure used to measure the sphericity of the feeds used in this project is described in Section 4.2.4.

The six feeds presented in Table 8.13 are used to study the effect of feed shape. The gasifier performance data for beads (experiment 8) are not presented in this section due to the loss of computer recorded data during the experiment.

The data collected, method of gasifier operation and method of data treatment were the same as for the standard experiments.

8.9.2 Results and Discussion

Table 8.14 shows the effect of feed shape on gasifier performance. The results from the chip shape variation experiments are presented graphically in Figures 8.33 - 8.40. The lines on each graph show the best fit line calculated using "Cricket Graph" graph plotting software.

Feed shape affects the flow of solids through the gasifier. It was found that during the gasification of commercially produced wood chips consisting of a mixture of pin and slab shaped particles, material flow through the gasifier was poor leading to a sloping reaction zone and the formation of voids (experiment 13). Gasifier control was difficult and it was concluded that feeds consisting of mixed shape particles are not suitable for the Aston gasifier. Hoi reports that uniformly shaped particles improve fuel flow resulting in better gas-solid reactions [39]. No fuel flow problems were encountered during the gasification of 15 mm beads (experiment 8) and the interfaces between the various zones in the gasifier were observed to be broadly horizontal (see Plate 7.12).

Increasing the feed particle sphericity towards 1.0 (spherical particles) is shown to improve gasifier performance. Figure 8.50 shows that the air to feed ratio is reduced as the feed particle sphericity is increased leading to a reduction in the product gas nitrogen content (Figure 8.38) and gas mass and volumetric yields (Figure 8.33). Improved material flow through the reactor will result in improved gas-solid reaction leading to higher concentrations of carbon monoxide and hydrogen in the product gas (Figures 8.36 and 8.37). The reduced product gas concentrations of nitrogen and carbon dioxide at high feedstock particle sphericity lead to an increase in the product gas higher heating value (Figure 8.35).

It is concluded that gasifier performance is improved with increasing feed particle sphericity. Gasifier control (to maintain a stable reaction zone) was easiest when operating with the feed consisting of 15 mm beads. In addition, the interfaces between each zone in the gasifier were broadly horizontal and the reaction zones were regular in shape when operating using the feed consisting of 15 mm beads.

□ Mass yield
◆ Volumetric yield
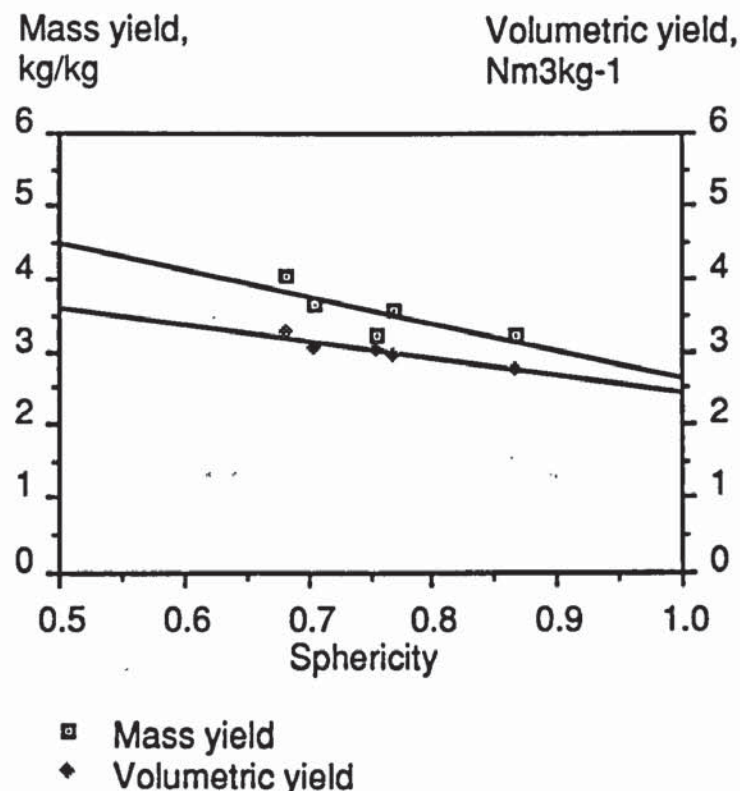
Figure 8.33
Gas Mass Yield and Gas Volumetric Yield v Feed Shape
(Sphericity)

272
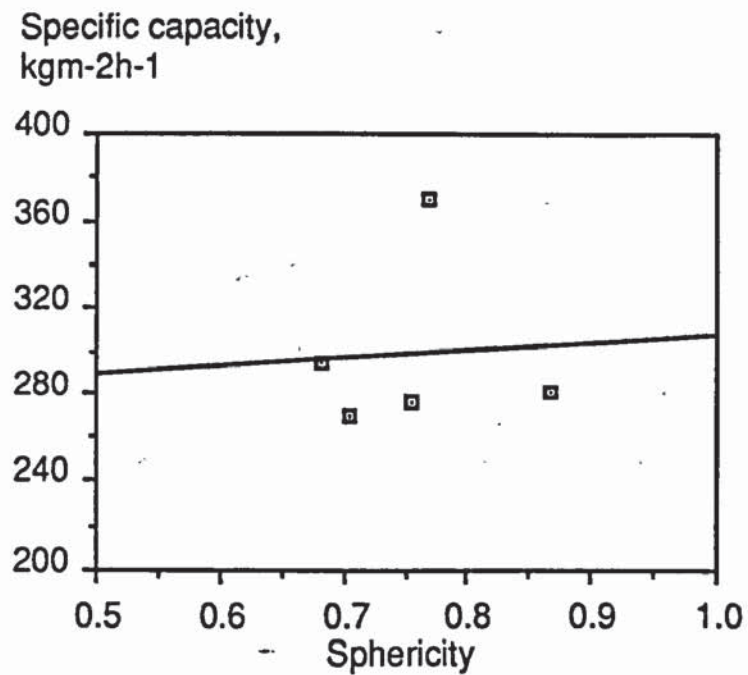
Figure 8.34

Specific Capacity v Feed Shape (Sphericity)
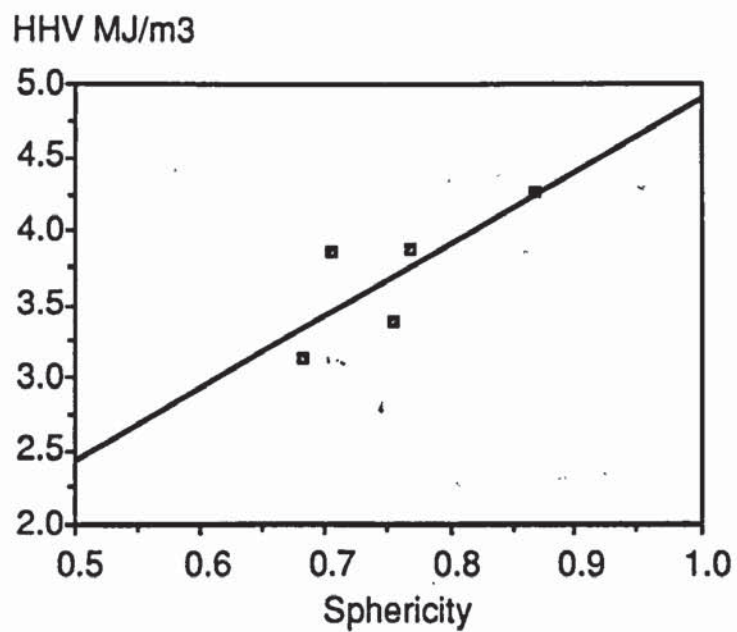
Figure 8.35

Product Gas Higher Heating Value v Feed Shape (Sphericity)

273
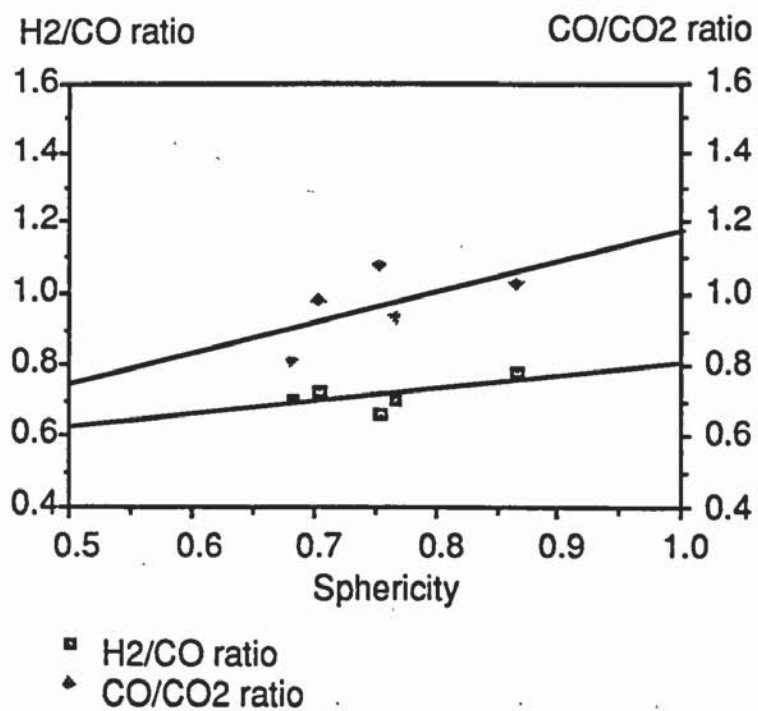
Figure 8.36

Gas H$_2$/CO and CO/CO$_2$ Ratios v Feed Shape (Sphericity)
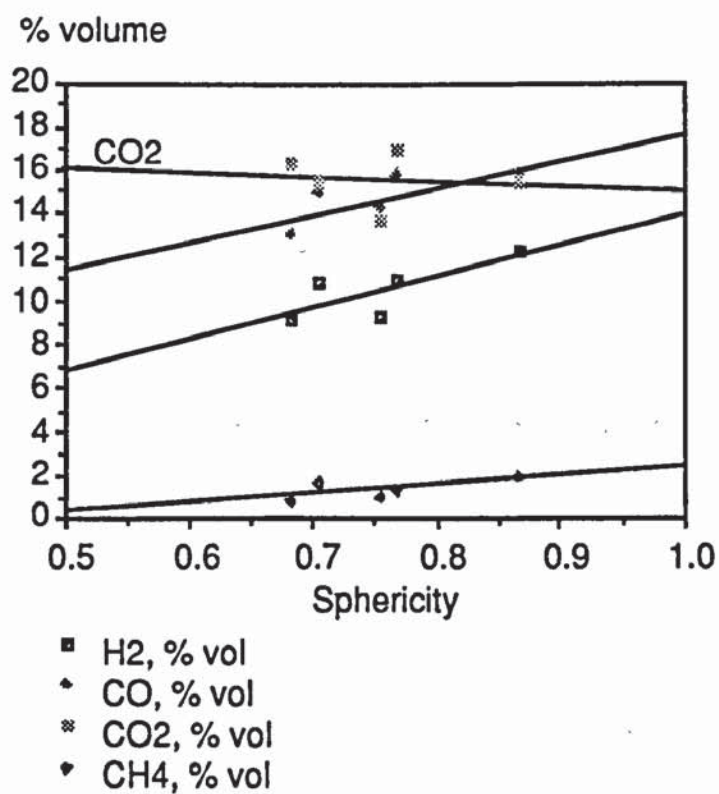
Figure 8.37

Gas Composition v Feed Shape (Sphericity)

274
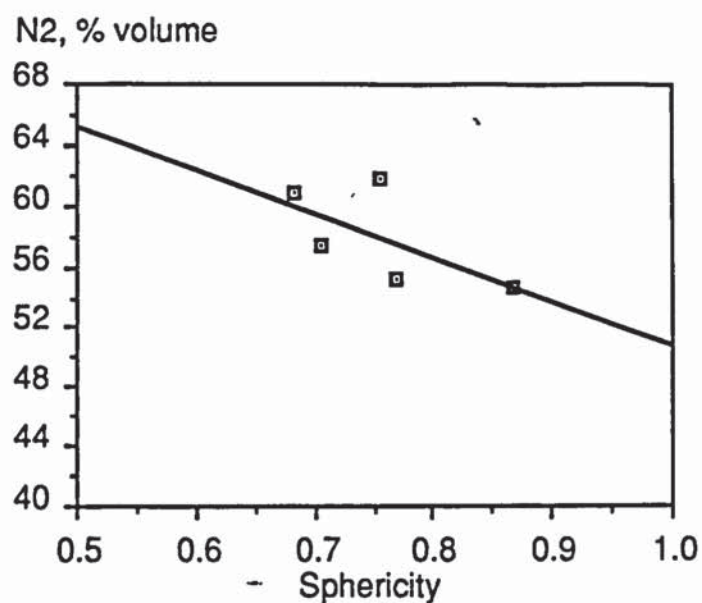
Figure 8.38

Gas Nitrogen Content v Feed Shape (Sphericity)

□   Raw gas efficiency
♦   Hot gas efficiency
❊   Cold gas efficiency
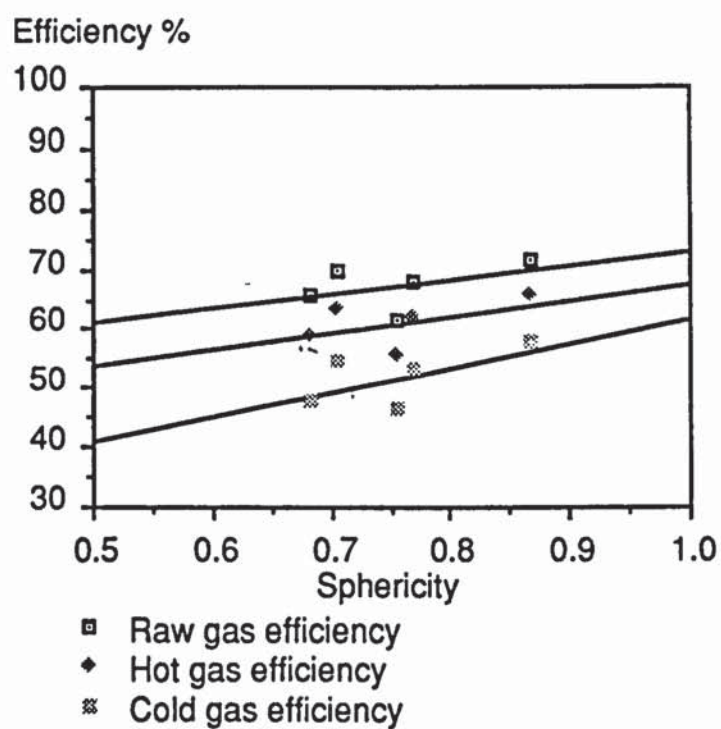
Figure 8.39

Gasifier Efficiency v Feed Shape (Sphericity)
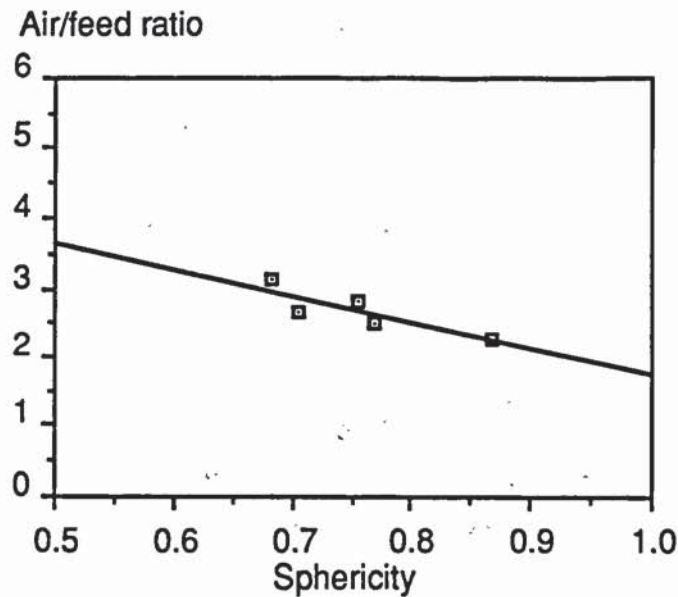
Figure 8.40

Air to Feed Ratio v Feed Shape (Sphericity)

8.10 Effect of Gasifier Operation Using Sewage Sludge Feed

The aim of this experiment was to test the suitability of dried sewage sludge in the Aston downdraft gasifier.

8.10.1 Data Collection and Treatment

The sewage sludge was received in the form of 40 mm long pellets. These were ground using an Atlas hand mill and sieved and the fraction between 4.75 and 6.35mm was selected for the gasification test. The method of gasifier operation was the same as that used for standard case experiments and is described in Section 5.2.

8.10.2 Results and Discussion

Table 8.15 shows the performance of the gasifier with sewage sludge feed.

The gasifier was operated for approximately 40 minutes with sewage sludge. During this period, the reaction zone rose due to the accumulation of ash and unreacted carbon in the gasifier at a rate of 0.5 cm.min^{-1}. To maintain a stable reaction zone and to overcome the increasing reactor pressure drop, the air flow rate was progressively increased throughout the experiment. This failed to increase the rate of char consumption by gasification and resulted in the gasification process during experiment 4 approaching combustion as evidenced by the poor gas composition and

heating value (Table 8.15). The high airflow rate into the gasifier during sewage sludge gasification is shown by the high air to feed ratio and mass and volumetric gas yields compared with standard case operation. The maximum height of the glowing hot zone (including the flaming pyrolysis zone) in the gasifier (appearing as an orange zone of char in the reactor) was 9.5 cm while the temperature 2 cm above the bottom of this zone was 640.9°C.

<div style="border: 1px solid black;">

Table 8.15
Aston Open-Core Downdraft Gasifier Performance - Sewage Sludge Feed (Experiment 4)

	Standard case	Sewage sludge
Experiment length, hours (minutes)	0.97 (58.5)	0.665 (39.9)
Feed moisture content, % wb	9.49	10.26
Feed ash content, % wt	0.07	31.80
Feed carbon content, % wt daf	53.04	45.19
Feed hydrogen content, % wt daf	6.12	5.29
Feed oxygen content, % wt daf	39.90	45.09
Feed nitrogen content, % wt daf	0.93	4.51
Average char bed height, cm	17.23	12.39
Specific capacity, $kgm^{-2}h^{-1}$	276.39	101.59
Mass yield, $kgkg^{-1}$	3.23	5.62
Volumetric yield, Nm^3kg^{-1}	2.94	4.33
Equivalence ratio, %	39.24	90.10
Air/feed ratio	2.81	5.24
Gas higher heating value, $MJNm^{-3}$	3.38	1.58
H_2/CO ratio	0.66	0.76
CO/CO_2 ratio	1.07	0.50
Gas outlet temperature, °C	440.39	410.44
Hot gas efficiency, %	55.40	58.91
Cold gas efficiency, %	46.69	42.82
H_2 in product gas, % volume	9.25	4.97
CO in product gas, % volume	14.22	6.61
CO_2 in product gas, % volume	13.69	13.20
CH_4 in product gas, % volume	1.01	0.28
N_2 in product gas, % volume	61.82	74.95

</div>

Dried sewage sludge is not a suitable feedstock for the Aston open-core downdraft gasifier in its current configuration due to the absence of a char/ash removal system required to maintain the reaction zone at a constant height above the grate. It should be noted that the use of a char/ash removal system would result in a reduced gasifier thermal efficiency due to the removal of unreacted carbon from the gasifier. Mixing the sewage sludge feedstock with wood would reduce the overall feed ash content making the use of dried sewage sludge more feasible. Alternatively, an external burner such as that used in the Syngas gasifier (see Section 2.3.7) could be used to increase the rate of char gasification [41]. The further use of sewage sludge and alternative feedstocks in the Aston open-core reactor is discussed in Section 10.

9.   CONCLUSIONS

9.1   Gasification System Operation

A gasification system utilizing a novel transparent quartz glass open-core downdraft gasifier has been modified to permit easier, safer and more reliable operation. The mark II Aston gasifier system can be operated for longer periods of time and the average start-up time has been significantly reduced compared with the mark I Aston gasifier. The average run time during this project was 35.25 minutes while the average run time in the previous project (mark I Aston gasifier) was 7.38 minutes. A low heating value gas was produced and when operating with an uninsulated gasifier, similar performance to the mark I gasifier was realised. The gasification system can now be used for further gasification studies with few further modifications (see Section 10).

9.1.1   Wood Feeding

Two methods of wood feeding were used during this project. It was found that when using the automatic screw feeder, it was difficult to obtain the correct screw feeder feed setting during a run to ensure that the gasifier was neither over nor under fed. In addition, the feed particles in the feed used for standard case runs were too large for use in the screw feeder. Manual batch feeding ensuring that the upper feed level in the gasifier never fell below 3 cm under the top rim of the gasifier was found to be easier to control and record.

9.1.2   Gasifier

During this project, no major problems concerning the gasifier were encountered. During insulated gasifier operation, some heat damage to the gasifier vessel occurred. This was not severe and the gasifier could be re-used several times before transparency was lost. It is concluded that the quartz glass gasifier was adequate for the experiments carried out during this project.

9.1.3   Venturi Ejector and Gas Separation

The venturi system worked reliably and was simple to operate. It is concluded that the venturi system is more efficient and reliable than the gas pump and scrubber system used previously on the mark I Aston gasifier. However the product gas was wet on exit from the demister as evidenced by water condensation in the 18A Rotameter used in runs 2, 3 and 4. The

demisting device did not work as well as predicted by the design calculations and it is recommended that future workers modify the demister (see Section 10).

9.1.4 Instrumentation

The instrumentation fitted to the gasifier except for the Platon gas flow meter worked well (see Section 6). The gas flow rate was measured using a cumulative gasmeter, therefore.

Some computerised data were lost during run 8 as a result of a disk error. However, no other problems were encountered with the data-logging equipment. The computer data-logging system, therefore, is suitable for the purpose of recording data from the mark II Aston gasification system.

9.2 Experimental Programme

A total of 26 experimental runs have been performed. Detailed observations of the gasification process have been made and an investigation of several parameters which affect the gasifier performance has been carried out.

9.2.1 Mass and Energy Balances

Mass and energy balances were performed for each successful run using a spreadsheet program. Overall mass balance closures were in the range 88.5% to 108.0%. The average mass balance closure was 97.3%. Energy balance closures were in the range 81.4 to 137.9%. The average energy balance closure was 104.6%. Poor energy balance closures are due to over estimations of the gasifier heat losses. Heat losses from the uninsulated Aston gasifier during standard case operation were estimated to be 45.0% of the chemical energy of the feed. The average heat losses from the insulated gasifier were estimated to be 13.1% of the chemical energy of the feed. This heat loss compares well with reported heat losses for similar, insulated gasifiers in the literature.

9.2.2 Gasification Process in an Open-Core Downdraft Gasifier

Observations of the gasification process within the gasifier show the process to occur in two steps. These are the pyrolysis and oxidation step (flaming pyrolysis) and the char gasification step. The average time for a single 15 mm diameter bead to undergo these two steps undergoing 97.3% mass conversion has been found to be 285 seconds.

9.2.2.1   Pyrolysis and Oxidation Step (Flaming Pyrolysis)

Measurements of the flaming pyrolysis zone in the uninsulated Aston gasifier show the average flaming pyrolysis zone length to be 1.20 feed particle diameters. The time for flaming pyrolysis has been shown to increase with feed particle size. The average time for the flaming pyrolysis of 15 mm diameter beads was 85.4 seconds.

The experimentally determined time for flaming pyrolysis and flaming pyrolysis zone length were compared with a published model of flaming pyrolysis.   There is good agreement between the experimental and calculated results for the 15 mm diameter beads and the wood chips sieved to between 6.35 mm and 12.7 mm. For the smaller chips, the agreement is less good.

The average particle weight loss during during flaming pyrolysis was found to be 87.8% which is in agreement with the published weight loss data on pyrolysis for wood of between 80 and 95%. Approximately 10% by mass of the original particle remains as char following flaming pyrolysis.

It is confirmed that the main method of heat transfer to the particles approaching the reaction zone is radiation. Radiative heat transfer from the oxidation of volatiles to the incoming feed controls the rate of reaction in the gasifier. This confirms that there will be only one air to feed ratio at which the gasifier will operate for stable operation.

Gasifier insulation slightly reduced the flaming pyrolysis zone length to 1 feed particle diameter and reduced the flaming pyrolysis time from 46.7 to 37.2 seconds for wood chips sieved between 6.35 and 12.7 mm.

9.2.2.2   Char Gasification Step

Measurement of the time for the gasification of single char particles was difficult since in most cases, particles undergoing gasification disappeared from view prior to complete consumption. The average gasification time for char particles produced from 15 mm diameter beads was 200 seconds (for 97.3% mass conversion). This value is greater than that reported by Earp (15 - 18 seconds) and less than that predicted by NREL models (100 - 140 seconds). However, the start and end points of the char gasification step are

281

not clearly defined by Earp and NREL. In addition, the particle size is not reported by NREL.

The char gasification zone length has been measured in two ways. The height of the glowing char zone in the gasifier during the gasification of 15 mm diameter beads was 28-55 mm equivalent to 1.9-3.7 feed particle diameters. The height of the glowing char zone in the gasifier during the gasification of wood chips sieved to between 6.35 mm and 12.7 mm was 45 mm, equivalent to 4.8 mean representative feed particle diameters. From the gasifier vertical temperature profile of the uninsulated gasifier, the char gasification zone length (during the gasification of wood chips sieved to between 6.35 mm and 12.7 mm) was 9 cm, equivalent to 9.5 mean representative feed particle diameters. The differential between the measured temperature at the centre of the gasifier and the temperature of the char at the periphery of the gasifier (indicated by the char colour) suggests that the the bottom of the char gasification zone is an inverted cone in shape.

A model has been developed to calculate the char gasification zone length. The calculated char gasification zone length for 15 mm diameter beads (15.93 mm) has been found to be smaller than the observed char gasification zone length (28-55 mm). It is concluded from the results from the model that the length of the char gasification zone is very small.

Gasifier insulation increased the depth of the char gasification zone. The effect of insulation on the char gasification zone was studied by measuring the depth of char at temperatures between the maximum gasifier temperature and 800°C (the char temperature at the grate of run 25). For run 25 (insulated reactor), the depth of char above 800°C was 125 mm while for runs 22 and 26 (uninsulated reactor) the depth of char above 800°C was 80 and 65 mm respectively. During insulated gasifier operation, therefore, there was no cool char zone.

9.2.3   Parameters Affecting Gasifier Performance

A standard (base) case performance was defined to permit comparison of gasifier performance under various conditions. Standard case performance was similar to the performance of the mark I Aston gasifier. The average gas heating value (during standard case operation) was found to be 3.38 MJm^{-3}

while the cold gas efficiency was found to be 46.69%. The low efficiency is due to the high heat losses from the uninsulated gasifier. Standard case performance was compared with the output from the Aston carbon boundary model [45]. It was not possible to enter the actual heat losses into the computer model. Output from the model with the highest possible heat loss entered (20%) does not compare well with the performance of the uninsulated gasifier performance.

The operating parameters varied were:

a) Gasifier stability
b) Carbon dioxide enrichment of input air
c) Char bed depth
d) Gasifier insulation
e) Feed moisture content
f) Feed size and shape
g) Feed type (sewage sludge)

9.2.3.1 Gasifier Stability

Open-core downdraft gasifiers can be operated in three regimes. These are:

- Stable operation (the rate of char production by pyrolysis equals the rate of char consumption by gasification);
- Char consumption (gasification) dominant operation (the rate of char consumption by gasification exceeds the rate of char production by pyrolysis) and;
- pyrolysis dominant (char production) operation (the rate of char production by pyrolysis exceeds the rate of char consumption by gasification).

The mark II Aston gasifier has been operated in each of the three different modes of operation and the results presented.

During operation in the char consumption (gasification) dominant mode, it was found that the gasifier operated at a higher equivalence ratio than during stable operation. This observation is in agreement with theory.

Uninsulated gasifier operation in the pyrolysis dominant (char production) mode was carried out by Earp. Earp concluded that the effects of operating

283

were masked by gasifier heat losses. A comparison was made between stable operation and pyrolysis dominant (char production) operation using an insulated gasifier in this project. It was confirmed that the equivalence ratio during char production operation (40.42%) was slightly greater than the equivalence ratio during stable operation (39.19%) although the difference was less marked than those reported by Earp for the uninsulated reactor (41.9% for char production operation and 38.4% for stable operation) [12].

9.2.3.2 Carbon Dioxide Enrichment of Input Air

Carbon dioxide enrichment of the air was investigated to attempt to reduce the gasifier air requirement and hence reduce the extent of oxidation of the pyrolysis products. It was found that enrichment of the input air with small quantities of carbon dioxide had little effect on gas quality and increased the gasifier air requirement. Excessive quantities of carbon dioxide extinguished the gasification process as would be expected and were found to be a suitable method of ending runs and "freezing" the gasification process to enable extraction of particles undergoing gasification.

9.2.3.3 Char Bed Depth

Increasing the height of the char bed below the reaction zone was found to improve the product gas quality although the improvement was small. The hot gas efficiency was found to be a maximum when operating the gasifier with a char bed height of approximately 13.5 cm. The reduction in gasifier hot gas efficiency when operating with char bed heights greater than 13.5 cm is due to heat losses from the char bed reducing the product gas temperature at the grate.

9.2.3.4 Gasifier Insulation

Gasifier insulation was found to improve product gas quality. Insulation reduced the overall gasifier heat losses by radiation and convection by 22% of the feed input and increased the maximum temperature in the gasifier from 931.8°C in an uninsulated gasifier to 1029°C in the insulated reactor. To compensate for heat losses, the uninsulated gasifier operates at a higher equivalence ratio (39.19%) compared with the insulated reactor (36.06%). The product gas from the insulated reactor has a higher heating value (4.49 $MJNm^{-3}$) compared with the gas from the uninsulated gasifier (3.38 $MJNm^{-3}$). This is because of higher concentrations of hydrogen, carbon monoxide and methane in the product gas from the insulated gasifier.

Insulated gasifier performance compares well with the output from the Aston carbon boundary model although the product gas methane content predicted by the model was lower than that measured in the actual product gas from the insulated gasifier.

9.2.3.5 Feed Moisture Content

There is a reduction in gasifier performance with increase in feed moisture content. There is an increase in product gas carbon dioxide content with increase in feed moisture content indicating that there is increased conversion of biomass by oxidation to provide energy for drying. Product gas carbon monoxide content decreases with increased feed moisture content due to the action of the water gas shift reaction and the product gas methane content increases with increased feed moisture content indicating that there is increased tar production.

9.2.3.6 Feed Size and Shape

Feed size was defined as the characteristic size of a particle (the length of the side of a cube having the same volume as the particle) and the characteristic diameter (the diameter of a sphere having the same volume as the particle). There was found to be an ideal particle characteristic diameter (6.4 mm, equivalent to a cube of side 5.2 mm) at which the gasifier air requirement for stable operation was a minimum. This led to a maximum product gas higher heating value. It was also observed that feeds consisting of small particles did not flow through the gasifier as freely as the feed used for standard case runs.

Feed shape was defined as the particle sphericity - the ratio of the particle surface area of a sphere having the same volume as the particle to the surface area of the particle. It is concluded that gasifier performance is improved by increasing the sphericity of the particles in the feed. The superior flow of spherical particles as shown during run 8 resulted in a well defined reaction zone with no voids.

9.2.3.7 Feed Type (Sewage Sludge)

Sewage sludge was not found to be a suitable feedstock for the Aston gasifier due to the combination of an absence of a gasifier ash removal system and a high feed ash content. Excess ash in the char bed led to

channelling leading to poor oxidant distribution to the reaction zone indicated by a irregularly shaped reaction zone.

10. RECOMMENDATIONS

This section describes the areas in which further work is recommended and modifications which should be carried out to the gasification system to improve system performance.

10.1 Future Work

This project has highlighted the following areas in which further study should be considered:

A raw gas liquids and solids sampling system should be constructed to enable a more complete determination of process streams to be made. Time constraints prevented the construction of a raw gas liquids and solids sampling system although an iso-kinetic sampling probe was installed in the pipework connecting the gasifier to the venturi ejector. The liquids and solids sampling system should be used to evaluate the following:

- Mass and energy balances over the gasifier including the measured raw gas char and tar contents;
- The effect of reactor insulation on the gasifier tar production rate;
- The effect of char bed height within the gasifier on the tar production rate;
- A comparison of the raw gas tar and char content of the Aston gasifier with other downdraft throated and open-core gasifiers in the literature.
- The effectiveness of the venturi ejector as a gas scrubber by comparison of the raw and cleaned gas solid and liquid contents. This will enable more accurate identification and evaluation of opportunities for the utilization of the product gas from open-core downdraft gasifiers cleaned using a venturi ejector (eg. internal combustion engines).

The primary feedstock used in this project was rough sawn timber purchased from a local timber yard and chipped. This proved to be a satisfactory feedstock. Commercially produced woodchips representative of real woodchips were gasified in this and the previous project [12]. It was found, however, that the commercially bought 'real' woodchips exhibited poor flow characteristics causing frequent feed bridging within the gasifier leading to poor gasifier performance. It is recommended that the gasification

287

of alternative feedstocks such as straw pellets and sawdust pellets should be investigated. A small quantity of dried sewage sludge was gasified in this project. However, it was concluded that sewage sludge is not a suitable feedstock for the existing mark II gasification system due to the high ash content. To enable use of existing quartz glass reactors and to reduce overall system design and construction time, the collar and grate used in the mark I Aston gasifier was re-used in the mark II Aston gasifier. It is recommended that a new reactor support collar is constructed incorporating a char/ash removal system to enable operation with high ash fuels. This would also enable an investigation of continuous operation in the pyrolysis dominant mode to maximise the product gas heating value to be made. A suggested design for a collar incorporating an ash removal system is shown in Figure 10.1. It can be seen that the seal preventing product gas contamination with air is located at the top of the gasifier where the gasifier temperature is low. The reactor would be supported by legs mounted on the grate.
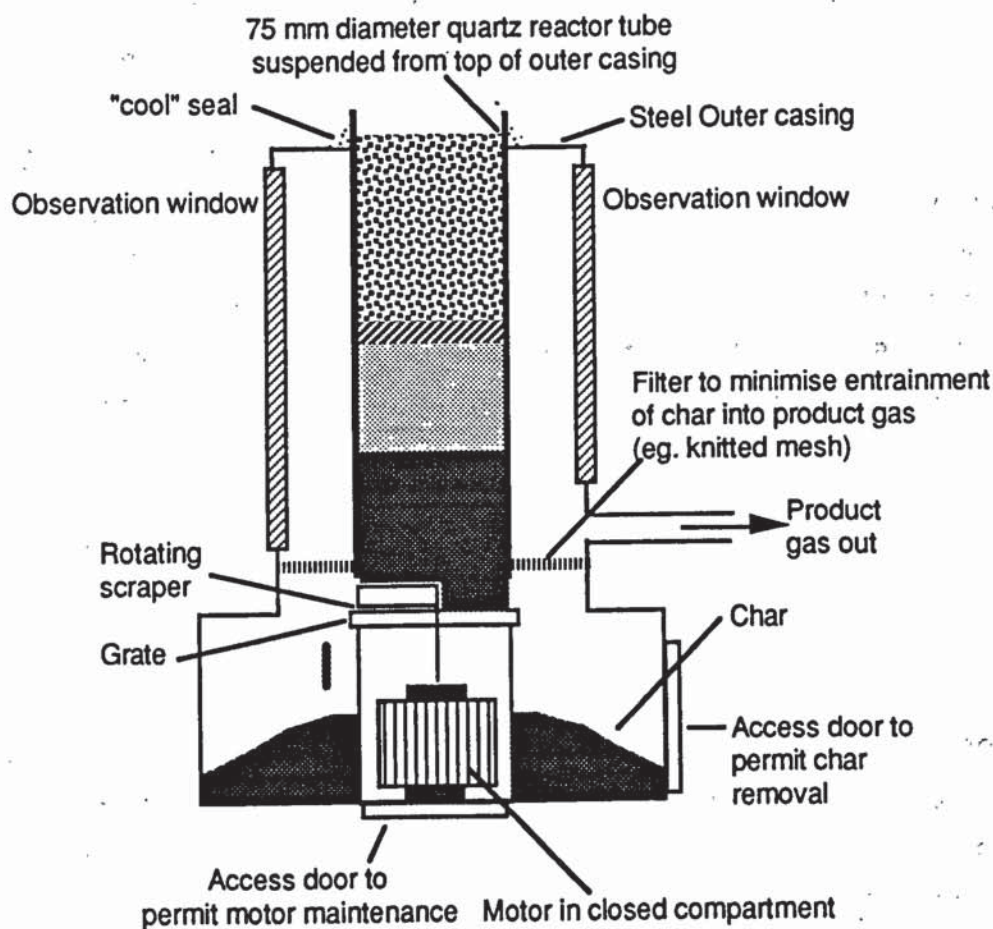
Figure 10.1

Suggested Design for Collar for 75 mm diameter Quartz Glass Reactor Incorporating Char/Ash Removal System

Following completion of this experimental programme, gasification research using the mark II gasification system has continued [69]. To prevent possible damage caused by dismantling the water pump, an inspection of the internal components of the pump was not carried out at the end of this experimental programme. In addition, the water pump was operating satisfactorily and repair was not required. If open-core gasification research is terminated following the project currently underway [69] or if major system modifications were to be undertaken, then it is recommended that the water pump is inspected for possible damage from small grits which may have passed through the in-line filter upstream of the water pump.

A model to predict the char gasification zone length in an open-core downdraft gasifier was developed in this project. It is recommended that future workers develop this model further to include the reduction in char gasification zone temperature as gasification proceeds and the convective heat transfer from the flames flowing downwards from the flaming pyrolysis zone through the char gasification zone.

10.2   System Modifications

It was noted in Section 6 that the Platon flowmeter was unreliable and that product gas flow measurements were taken using the cumulative flowmeter installed in the gasifier system downstream of the Platon flowmeter. It is recommended that a new on-line flowmeter is installed in addition to the existing gasmeter. Experience has shown Rotameter flowmeters to be unsuitable. Flowmeter types for consideration include:

- Orifice plates
- Venturi flowmeters
- Ultrasonic gas flow meters.

The method of measuring the insulated gasifier outside wall temperature was found to be satisfactory. The method of measuring the uninsulated gasifier outside temperature was found to be less satisfactory. Assuming the gasifier radial temperature distribution to be constant led to over estimations of the gasifier heat loss from the uninsulated gasifier. Measuring the vertical temperature profile of the gasifier was also time consuming. It is recommended that a quicker, more accurate method, of measuring the

uninsulated gasifier outside temperature is employed to calculate the gasifier heat loss. For temperatures below 600-700°C, it is suggested that a contact thermocouple is used while for temperatures above 600-700°C, two colour pyrometry could be used. Two colour pyrometry offers the opportunity of measuring the outside temperature of the gasifier from colour photographs of the gasifier in operation provided a heat source of known temperature is included in the photograph.

Feed production was found to be time consuming although a mechanical grinding machine was utilised towards the end of this project. Sieving was carried out manually. To increase the wood production rate and reduce the hazards associated with wood sieving, the purchase of a sieving machine for the existing 36 inch diameter sieves might be considered. This would enable feed of smaller particle size to be made more quickly and hence enable use of the existing screw feeder.

The product gas analysis system purchased in 1985 was overhauled in January 1989. It was found that towards the end of the experimental programme, the carbon dioxide analyser gave unstable readings. This instrument, therefore, now requires a major overhaul. Since the air flow rate into the gasifier is determined by nitrogen balance, the purchase of a nitrogen analyser might also be considered.

To increase the accuracy of mass and energy balances and to determine the efficiency of the demisting device, the gas moisture content on exit from the disentrainment tank should be measured. This could be carried out by passing a measured volume of gas through a pre-weighed dryer assembly containing dessicant. The gas moisture content can then be calculated from equation 8.1.

$$\text{Moisture, weight \%} = \frac{100 \times \text{weight gain}}{\text{Sample volume} \times \text{gas density}} \quad \text{...........[8.1]}$$

The demisting device did not work as will as predicted by the design calculations as indicated by water condensation in the glass Rotameters used for product gas flow measurements (fitted downstream of the demister). Currently, water separated from the product gas by the demister is returned to the disentrainment tank through the gas inlet aperture (Section 3). It is recommended that the demister is modified to permit water separated from

the product gas by the demister to go to drain thereby preventing possible re-entrainment of water removed from the product gas by the demister.

It is suggested that a cyclone for the removal of solids be fitted into the process prior to the venturi ejector thus increasing the system gas cleaning efficiency.

Appendix I
Published Work

(i)   Earp D M, Reyes-Nunez L R, Evans G D, Bridgwater A V, "Mass and Energy Balances over an Open-Core Downdraft Gasifier". Published in: "Biomass for Energy and Industry, Volume 2, Conversion and Utilization of Biomass", Grassi G, Gosse G, dos Santos G (eds.), pp729-733, Elsevier, 1990.

(ii)   Evans G D, Milligan J M, Bridgwater A V, "The Development of an Open-Core Downdraft Gasifier", in: "Biomass for Energy, Industry and Environment - 6th EC Conference", Grassi G, Collina A, Zibetta H (eds.), Elsevier, pp787-791, 1992

(iii)   Milligan J B, Evans G D, Bridgwater A V, "Results from an Open-Core Downdraft Gasifier", presented at "Advances in Thermochemical Biomass Conversion", May 11-15 1992.

Pages removed for copyright restrictions.

Appendix II
Design Calculations

II.1   Calculation of Venturi Size [65]

For a 10 m^3h^{-1} air handling capacity and a required suction capacity of 635 mmHg abs (25"Hg abs) and assuming a water temperature of 70°F (21.1°C):

Capacity of a 1 inch ejector at a water pressure of 40 psig (giving 25"Hg abs suction pressure) = 1.9375 scfm (taken from graph supplied by AVE).

$$\text{Capacity ratio} = \frac{5.9}{1.9375} = 3.045$$

From the table supplied by AVE [65], a 2 inch ejector is required for this duty.

Oversizing by 40% (ie: 14 m^3h^{-1} air moving capacity).

Using a water pressure of 60 psig, a water temperature of 60°F and a required suction pressure of 25"Hg abs,

$$\text{Capacity ratio} = \frac{14 \times 0.59}{2.75} = \frac{8.26}{2.75} \text{ sfcm} = 3.00$$

From the tables supplied by AVE, a 2 inch ejector using water at 60 psig would be suitable for this duty.

The maximum gas moving capacity of a 2 inch ejector using water at 60 psog (suction pressure, 25"Hg abs, water temperature, 21.1°C)

$$= 2.75 \times 4 = 11 \text{ scfm} \times \frac{10}{5.9} = 18.6 \text{ } m^3h^{-1}$$

II.2 Calculation of Air Flow Requirement for Stoichiometric Combustion of Wood and Hence That Required for Gasification of Wood

<u>Assumptions</u> [12]

Biomass feedrate: 1.5 kgh-1

Biomass CV   19.5 MJkg-1

Biomass elemental analysis (% weights)

C	50.74
H	5.62
O	43.05
S	<0.01
N	<0.2
Moisture	0
Ash	0.38

$$\text{Equivalence ratio} = 100 * \frac{\text{Actual oxidant to feed ratio}}{\text{Stoichiometric oxidant to feed ratio}} \quad \text{.......[II.1]}$$

From Earp, the average equivalence ratio used for stable operation in the mark I Aston gasifier was 49.4% [12].

Using a basis, 100kg of biomass;

Oxygen required to burn 50.74 kg of carbon $= \frac{74}{12}$ x 50.74 = 312.90 kg

Oxygen required to burn 5.62 kg of hydrogen $= \frac{5}{2}$ x 5.62 = 4.05 kg

Oxygen required to burn 0.01 kg of carbon $= \frac{32}{32}$ x 0.01 = 0.01 kg

Total oxygen   =   326.96 kg/100 kg Biomass

Oxygen in Biomass   =   43.05 kg

∴ Oxygen to be supplied for stoichiometric combustion

=   (326.96 - 43.05)   =   283.91 kg/100kg biomass

∴ Air to be supplied   =   283.91 x $\frac{100}{23}$ =   1234.4 kg/100 kg biomass

Density of air   =   1.2928 kgm-3 at STP

∴ The theoretical air requirement for complete combustion $= \frac{12.34}{1.2928}$

$= 9.55 \text{ m}^3\text{kg}^{-1}$ biomass

For gasification using equivalence ratio of 49.4% [12].
Air required for gasification $= 0.494 \times 9.55 = 4.7 \text{ m}^3\text{kg}^{-1}$ of biomass
At a feedrate of 1.5 kgh^{-1} [12], air required $= 7.1 \text{ m}^3\text{h}^{-1}$

II.3 Calculation of Pressure Drop from Top of Disentrainment Vessel to Burner (Previous Gasifier Design)

From the readings taken by Reyes [17],
ΔP from the top of the disentrainment vessel to the top of the gasmeter.
At a gas flowrate (q) $\approx$ 8.5 m^3h^{-1}

ΔP_3 = 543 mmHg guage
ΔP_2 = 581 mmHg guage
ΔP_{2-3} = 38 mmHg

At an air flow rate of approximately 5 m^3h^{-1} the measured pressure drop from the previous pump outlet to the burner = 134 mmHg.

∴ The total pressure drop from the top of the disentrainment vessel to the burner should be of the order of 172 mmHg (0.234 barg, 3.33 psig)

II.4   Mark II Aston Gasifier Pressure Drop Measurements

The system pressure drop measurements were taken with 26cm of wood chips (sized between 6.35 and 12.7mm) in the gasifier and without lighting the gasifier. The static pressure was measured at the points indicated at various air flow rates using mercury and oil manometers (see Figure IV.1).

Nomenclature

Q   Air flowrate through gasifier system (measured using test dial on gasmeter)

R   Water rotameter setting (adjusted by opening or closing valve V3)

II.4.1   Static Pressure Upstream of Venturi (at Valve V4), ΔP_0

ΔP_0 = Static pressure upstream of venturi, mm water

R	Q	ΔP_0
	m^3h^{-1}	mmH_2O
2	0.82	2.3
3	1.77	3.9
4	2.55	5.5
5	3.34	8.6
6	4.00	11.0
7	4.63	13.3
8	5.23	18.1
9	6.00	25.1
10	6.68	33.0
11	7.15	41.6
12	7.84	52.6

II.4.2   Static Pressure at Disentrainment Tank, ΔP_1

ΔP_1 = Static pressure at disentrainment tank

R	Q	ΔP_1
	m^3h^{-1}	mmHg
2	0.87	9.0
3	1.87	14.0
4	2.71	22.0
5	3.43	35.5
6	4.08	46.0

7	4.63	60.0
8	5.29	72.0
9	5.91	94.0
10	6.80	112.0
11	7.15	134.0
12	7.84	161.0

II.4.3 Static Pressure at Demister (PT1), ΔP_2

ΔP_2 = Static pressure at demister

R	Q	ΔP_2
	m^3h^{-1}	mmHg
2	0.67	9.0
3	1.48	12.0
4	2.46	20.0
5	3.29	36.0
6	3.92	48.0
7	4.53	60.0
8	5.29	77.0
9	5.91	97.0
10	6.58	118.0
11	7.15	139.0
12	7.99	166.0

II.4.4 Static Pressure at Gasmeter (PT2), ΔP_3

ΔP_3 = Static pressure at gasmeter

R	Q	ΔP_3
	m^3h^{-1}	mmHg
2	0.65	7.5
3	1.56	15.0
4	2.22	23.0
5	2.79	31.0
6	3.43	33.0
7	3.96	45.0
8	4.53	55.0
9	5.51	70.0
10	6.58	84.0
11	7.28	103.0
12	7.99	126.0

II.4.5   <u>Pressure Drop Across Lean Gas Burner, ΔP_4</u>

ΔP_4 = Pressure drop across lean gas burner, mmHg

R	Q $m^3 h^{-1}$	ΔP_4 mmHg
2	0.65	8.0
3	1.54	10.0
4	2.22	11.5
5	2.85	18.0
6	4.38	22.0
7	5.23	52.0
8	6.00	66.0
9	6.00	66.0
10	6.58	78.0
11	7.15	95.2
12	7.84	115.0
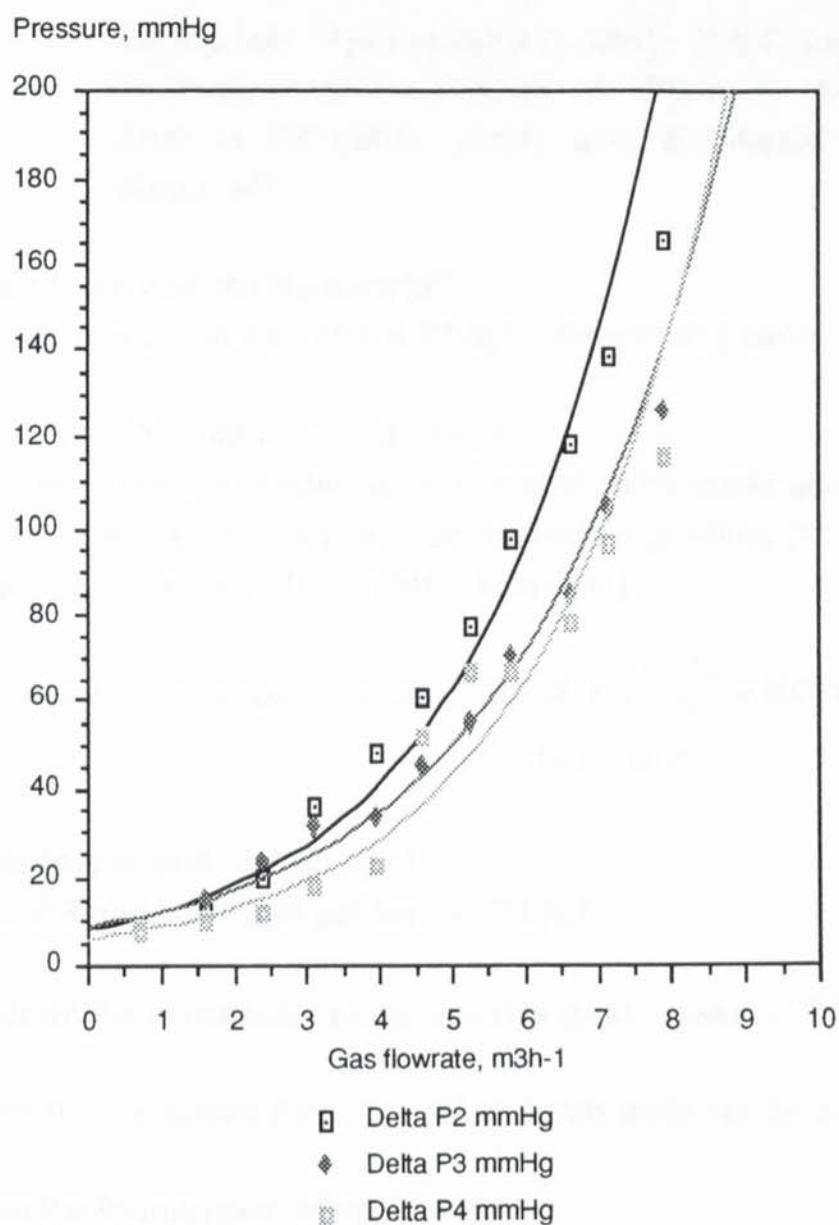
Pressure, mmHg

Figure II.1

Pressure Drops Across Mark II Aston Gasifier System

Figure II.1 presents the pressure measurements graphically. Polynomial regresions have been fitted to $\Delta P2$, $\Delta P3$ and $\Delta P4$ and their expressions are shown below (Equations II.2-II.4):

$$\Delta P2 = 7.744 \times 10^{(0.180Q)} \dotfill [II.2]$$
$$\Delta P3 = 8.134 \times 10^{(0.156Q)} \dotfill [II.3]$$
$$\Delta P4 = 5.465 \times 10^{(0.177Q)} \dotfill [II.4]$$

II.5   **Estimated Pyroligneous Acid Production Rate, Estimated Concentration of Phenols and Acetic Acid in Scrubber Water and Estimated Scrubber Water pH**

Using data taken from the literature [67];
Condensate production rate from a 73 kgh^{-1} downdraft gasifier = 9.2 % of outputs.
Outputs = 127.19 + 42.17 = 169.36 kgh^{-1}
If it is assumed that the condensates consist of 100% acetic acid (the major componant of actual condensates from downdraft gasifiers [101]) then the density will be 1.0498 gcm^{-3} = 1049.8 kgm^{-3} [71]

$$\therefore \text{Volume of condensables produced} = 0.092 \times \frac{169.36}{1049.8} = 0.01484 \text{ } m^3h^{-1}$$

$$= 14.84 \text{ } l.h^{-1}$$

Aston gasifier feedrate = 1.5 kgh^{-1}
Feedrate of Esplin downdraft gasifier = 73 kgh^{-1}

Scaling down the condensate production rate gives a value of 305 cm^3h^{-1}

If it is therefore assumed that 500 cm^3 of condensate will be produced per hour;
then, from the figures taken from Table 3.4

$$\text{Mass phenol} = \frac{4990}{2} = 2495 \text{ mg}$$

Molecular weight phenol (MW) = 94
$\therefore$ Number of moles of phenol = 0.02654 moles

$$\text{Mass acetic acid} = \frac{37430}{2} = 18715 \text{ mg}$$

Molecular weight of acetic acid = 60
$\therefore$ Number of moles of acetic acid = 0.3119 moles

Working water capacity of the venturi circuit and disentrainment vessel
= 140 litres = 140 kg

Number of moles of water = 7777 moles

Percentage concentration of phenol
after one hour of operation $= \dfrac{0.0265 \times 100}{7777 + 0.0265} = 3.4 \times 10^{-4}\%$

Percentage concentration of acetic acid
after one hour of operation $= \dfrac{0.3119 \times 100}{7777 + 0.3119} = 4.01 \times 10^{-3}\%$

To calculate the pH of the scrubber water, it is assumed that the scrubber water is saturated with CO_2. To calculate the molality, Henry's law is used [102].

$$x_i = \frac{p}{K} \quad\text{..[II.5]}$$

where:
x_i is the mole fraction of solute,
p is the partial pressure of the solute,
K is the Henry constant (1.25×10^6 mmHg for CO_2)

The amount of CO_2 dissolved in 1 kg of water is given by:

$$x_{(CO_2)} = \frac{n_{(CO_2)}}{n_{(H_2O)}} \quad\text{..[II.6]}$$

since the amount of CO_2 dissolved is small.

$$\text{so that: } n_{(CO_2)} = x_{(CO_2)} {}^* n_{(H_2O)} = \frac{p \cdot n_{(H_2O)}}{K} \quad\text{....................[II.7]}$$

The partial pressure of the CO_2 in the water will be (see Appendix II.3) [17]:
0.15 x 0.21 barg = 0.0315 barg = 23.63 mmHg.

from the data shown, the molality is:
$$n_{(CO_2)} = \frac{23.63}{18.02 {}^* 1.25 \times 10^6} = 1.05 \times 10^6 \text{ mol.kg}^{-1}$$

The pH of a solution of a weak acid is given by [102]:
$$pH = 0.5K_a - 0.5\log A \quad\text{......................................[II.8]}$$

where:

K_a is ionization constant in water (6.37 for H_2CO_3)

A is the molality mol.kg^{-1}

Expected pH of water in scrubber is, therefore,

$$pH = (0.5 * 6.37) - (0.5 * log (1.05 \times 10^6)) = 6.2$$

II.6   Gas Velocities in Pipework from Disentrainment Vessel to Gasmeter

Pipework diameter (existing) to input of gasmeter = 15 mm

Pipework diameter (existing) from output of gasmeter to burner = 12 mm

Expected gas yield = 860 $Nm^3m^{-2}h^{-1}$ at STP [12]

Grate diameter = 75 mm

Actual gas flowrate at 60°C = 1.29 m^3s^{-1}

If $15ms^{-1} <$ fluid velocity $< 18ms^{-1}$ [103]

Then if pipe diameter = 15 mm, gas velocity = $\dfrac{(1.29 \times 10^{-3}) \times 4}{\pi \times 0.015^2}$

$\qquad\qquad\qquad\qquad\qquad\qquad\qquad\qquad\quad = 7.3\ ms^{-1}$

If pipe diameter = 12 mm, gas velocity = 11.41 ms^{-1}

If pipe diameter = 9.5 mm, gas velocity = 18.2 ms^{-1}

II.7 Force Acting on Lid of Disentrainment Vessel and Hence the Number of Toggle Clamps required to Clamp the Lid Shut

If the pressure in the air space above the water in the disentrainment tank
$$= 5 \text{ psig } (3\,515 \text{ kgm}^{-2})$$

$$\text{from Force} = \text{Pressure} \times \text{Area} \dots\dots\dots\dots\dots\dots [\text{II.9}]$$

$$\text{Area} = 0.6^2 = 0.36 \text{ m}^2$$

$$\text{Force} = 1265.4 \text{ kgf}$$

The use of 12 brauer V150/2B toggle clamps each capable of remaining shut against 150 kgf will therefore be sufficient to keep the tank lid shut (allowing up to a 42 % margin for error in the above calculation).

II.8   Disentrainment Vessel Material Thickness [103]

Assumptions:

i)   Space above the water is filled with air at a pressure of 5psig,

ii)   The tank is fully closed,

iii)   The water is clean,

Specific weight of water ($\mu = \rho.g$) = 1.0 x 9.81 = 9.81 KNm^{-3} so that the incremental pressure ΔP due to the water is:

$$\Delta P = \mu \Delta h = 9.81 \times 0.4 = 3.924 \, KPa \quad \text{.....................[II.10]}$$

The resultant force is :

$$3.924 + 34.464 = 38.3883 \, KNm^{-2} = 38388.3 \, Nm^{-2}$$

Material thickness is given by Equation II.11 [72]:

$$t = C \times D \times \sqrt{\frac{P}{f}} \quad \text{..............................[II.11]}$$

where:

f = the maximum allowable stress

(for 316 stainless steel, tensile strength = 520 Nmm^{-2})

D = the equivalent plate diameter

C = a constant depending upon the edge support of the plate; C = 0.43 for steels

Equivalent diameter of 60cm x 60cm plate

$$D = \sqrt{\frac{(4 \times 0.6^2)}{\pi}} = 0.677m$$

Plate thickness required for 5psig = 2.50mm
Plate thickness required for 10psig = 3.45mm

II.9 Disentrainment Tank Gas Exit Aperture Size

For a gas velocity of 6m^{3}h^{-1} and a gas density of 0.7 kgm^{-3},

$$\rho v^2 = 11 \ [104]$$

$$\text{Aperture diameter} = \sqrt{\left(\sqrt{\frac{0.7}{11}} \times \frac{4 \times 6}{3600 \times \pi}\right)} \quad \text{............ [II.12]}$$

Aperture diameter = 23.16mm

the velocity should be 75% of this value [104]

Aperture diameter should, therefore, be 30mm

11.10   Demisting Device Sizing

The size of the demister was calculated using Equation II.13 and a nomogram for sizing demisters which also takes into account other variables such as liquid and vapour densities and operating pressure [77].

$$V = K\sqrt{\frac{D-d}{d}} \quad ....[II.13]$$

where:

V = Allowable velocity, ms^{-1}

K = Constant. For clean conditions, K = 0.107 ms^{-1}

D = Liquid density at operating temperature and pressure, kgm^{-3}

d = Vapour density at operating temperature and pressure, kgm^{-3}

Taking the liquid density (water) as 1000 kgm^{-3} and the gas density as 0.7 kgm^{-3} (approximating the product gas to air), this yields a superficial gas velocity of 3.14 ms^{-1}. Applying this figure and the liquid and vapour densities to the demister sizing nomogram yields a demister pad diameter of 22 cm for a gas flow of $3m^3h^{-1}$ at 15°C (average mark I Aston gasifier gas flow - see Table 3.4) [77].

II.1   Iso-Kinetic Sampling Probe Design

It was decided during the design stage that an accurate determination of the tar and condensate concentration of the product gas was required to give a complete evaluation of the gasification system. It was, therefore, decided to incorporate into the design of the venturi to gasifier support collar connection an iso-kinetic sample probe which would remove representative gas samples from the raw gas stream. The installation of the sample probe through the solids catchpot permits its removal for inspection and maintenance.

In the sampling of fluids containing particulate matter, there is a risk of obtaining a sample containing a non-representative concentration of particulate matter. Iso-kinetic condtions (equal gas velocity) ensure that particle distribution in the chamber and sample pipe are the same thus minimizing this risk (see Figure II.2). The error from a correctly designed iso-kinetic sampling is zero for particles less than 3 microns and less than 5% for 5 micron particles [105].

In this case, the raw product gas emerges from the gasifier, passes through a 1 inch diameter aperture, a 1 inch diameter pipe and into the venturi ejector (see Figure II.3). The collar supporting the gasifier will cause a disturbance to the gas flow. Treating this disturbance as a bend [106], the sampling position was placed two pipe diameters (2 inches) downstream of the gasifier support collar [107] (see Figure II.3). In addition, one pipe diameter (1 inch) of straight pipe was allowed downstream of the probe to minimize disturbance to the flow of fluid. This led to a minimum length of straight pipe between the gasifier support collar and the first bend in the collar to venturi pipework of 3 inches.

Design procedures for the sampling probe are set out in BS 893: 1978 [68] and Reed [2]. Reed's calculations provide a limiting value for the nozzle internal diameter dependant on the internal diameter of the pipework. In this case, the internal diameter of the pipework is 25.4 mm (1 inch) suggests that the nozzle diameter should be 2.12mm. However, BS 893 suggests that the diameter of the entry nozzle should be no less than 10mm [68]. Since this diameter of probe would be less prone to blockages, it was decided, therefore, to use this figure and derive all the other dimensions from it (see Figure II.4).

As the raw gas emerging from the gasifier could be up to 1000°C and contain corrosive constituents, 316 stainless steel was used for the construction of this probe.

BS 893 states that the gas velocity at the sampling point should be such that the pitot static pressure difference is not less than 10 Nm^{-2} [68]. This is equivalent to an air velocity of approximately 5 ms^{-1} at 200°C. The maximum gas velocity expected in the connector is approximately 1.5 ms^{-1} at 200°C (equivalent to 10 m^3h^{-1} at 50°C measured by the on-line flowmeter downstream of the disentrainment tank). True iso-kinetic sampling according to BS 893 may, therefore, not be possible although sampling according to the spirit of BS 893 is possible

(a)
Iso-kinetic Sampling

(b)
Sampling velocity too low (Particle lost)

(c)
Sampling velocity too high (Extra particle collected)
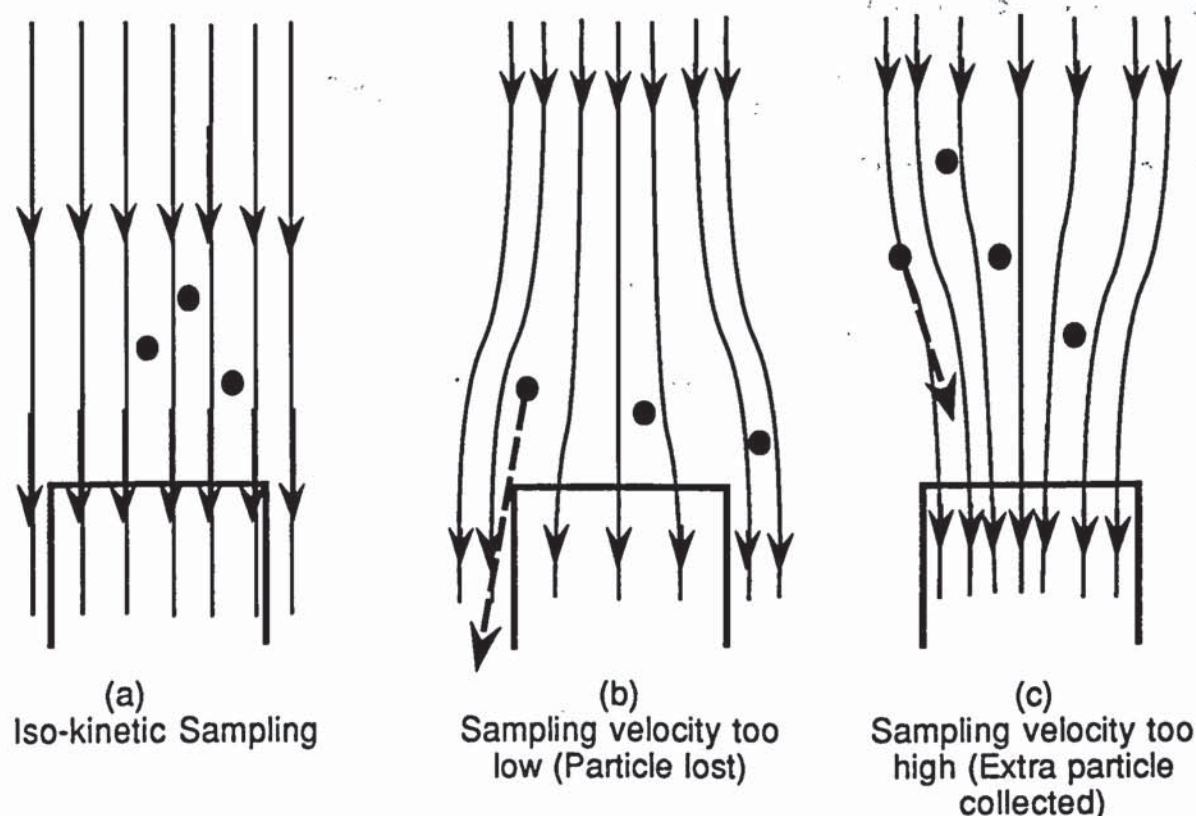
Figure II.2
Iso-Kinetic Sample Conditions Showing Gas Stream Lines [2]

333
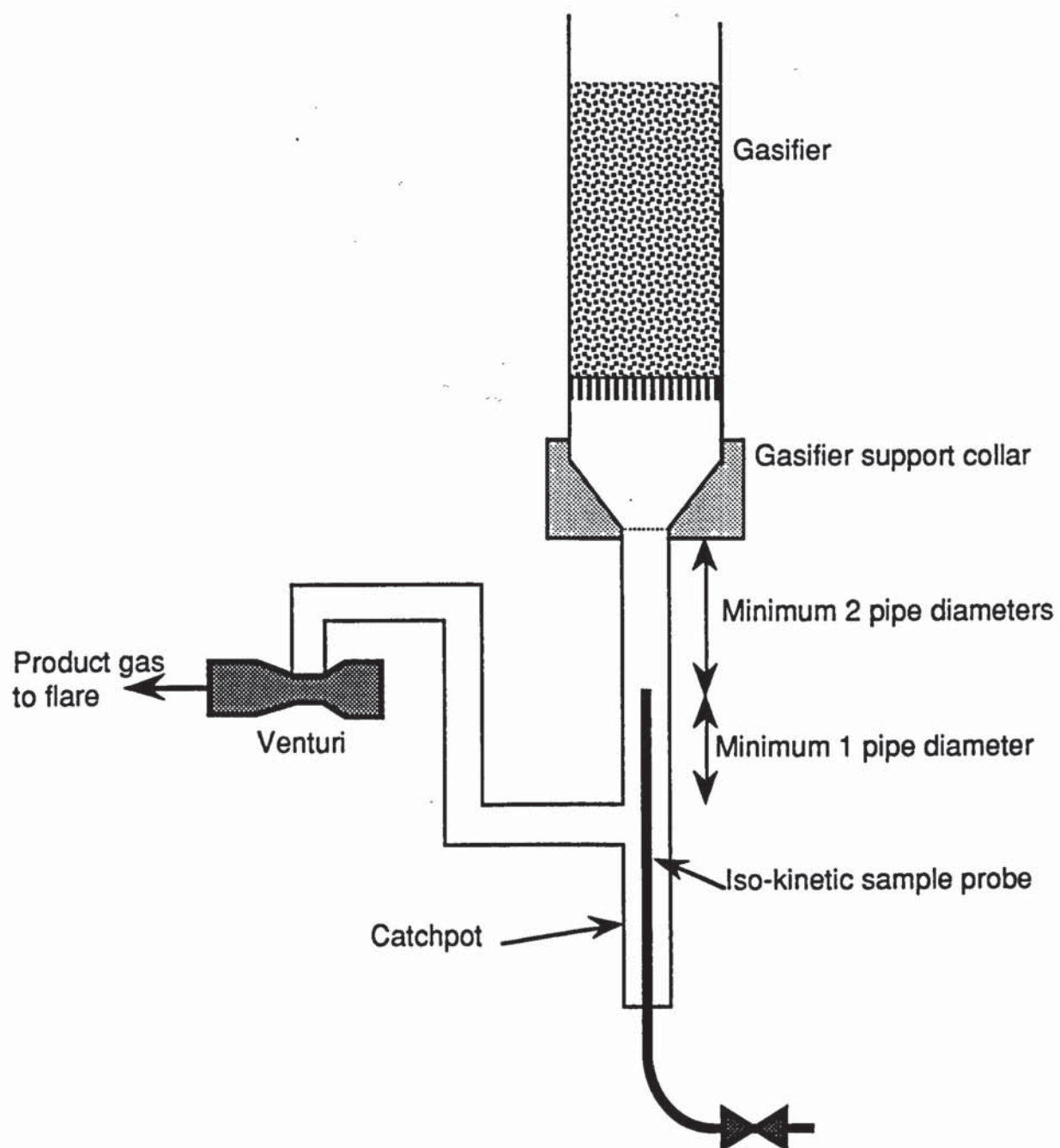
Figure II.3
Venturi to Collar Pipework Configuration

Gasifier

Gasifier support collar

Minimum 2 pipe diameters

Minimum 1 pipe diameter

Product gas
to flare

Venturi

Iso-kinetic sample probe

Catchpot
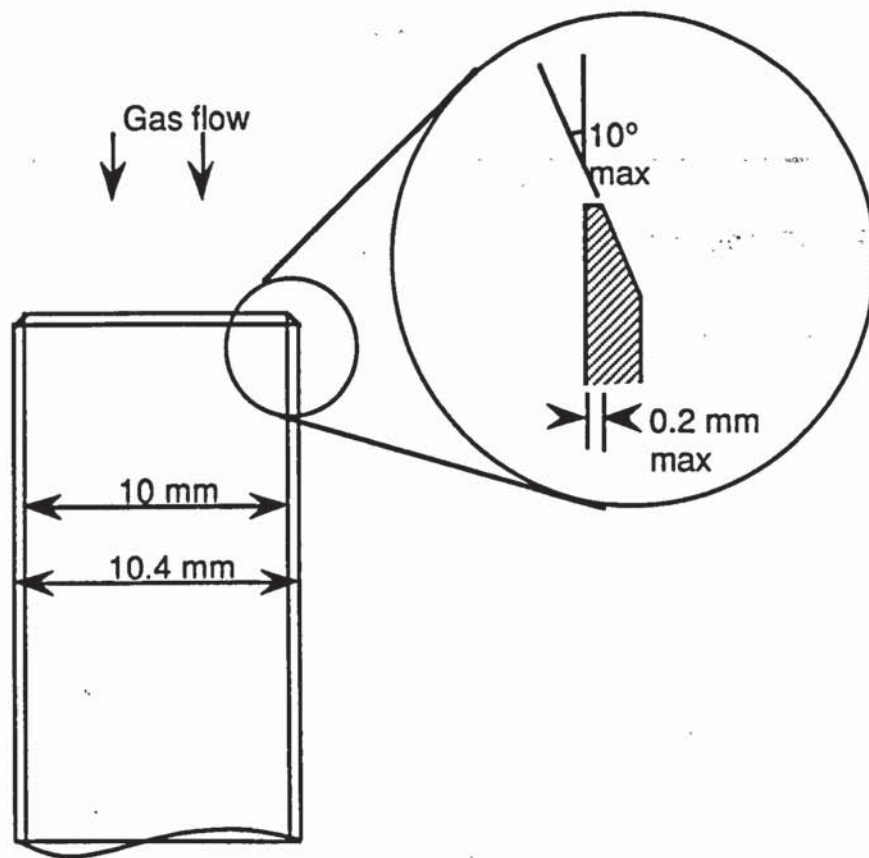
Figure II.4
Nozle Design of Iso-Kinetic Sampling Probe [68]

Appendix III
Gas Solubilities

Table III.1

Solubility of Some Gases Found in Product Gas[97]

Gas	Coefficient of Solubility in Water
Oxygen	0.0489
Nitrogen (pure)	0.0239
Nitrogen (atmospheric)	-
Air	0.0294
Carbon dioxide	1.7130
Carbon monoxide	0.0354
Hydrogen	0.0215
Methane	0.0556

Appendix IV
Piping and Instrumentation Diagram
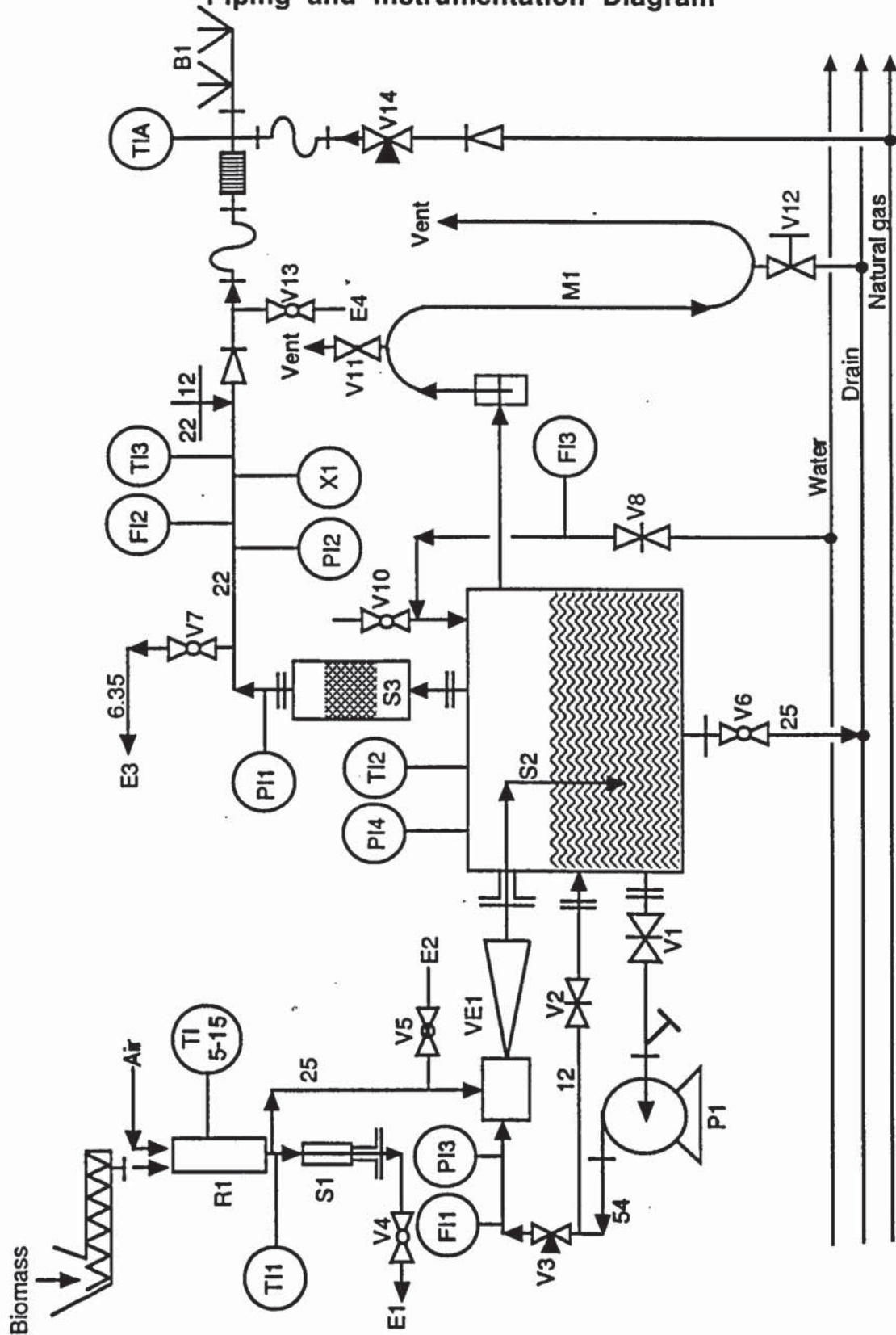
Figure IV.1
Piping and Instrumentation Diagram of Gasification System
The symbols used in the drawing are those listed by Austin [78]

IV.1 Key to Plant Items and Instruments

Plant Items

Miscellaneous

Code	Function
R1	Gasifier
B1	Burner
P1	Pump
VE1	Venturi ejector

Sample Points

E1	Iso-kinetic sample point
E2	Sample point at venturi
E3	On-line gas analysis
E4	Batch gas analysis

Valves

Code	Duty	Type
V1	Pump isolation (on/off)	Gate
V2	Pump bypass shut off (on/off)	Gate
V3	Venturi circuit control	Needle
V4	Iso-kinetic sample probe isolation (on/off)	Ball
V5	Sample point 1 (on/off)	Ball
V6	Tank drain (on/off)	Ball
V7	Sample Point 2 (on/off)	Ball
V8	Mains water control	Gate
V9	Compressed air control to hot box (not illustrated)	Gate
V10	Tank access	Ball
V11	Water manometer make-up point	Gate
V12	Manometer drain	Gate
V13	Sample point 3	Ball
V14	Natural gas control	Needle

338

Instruments

Thermocouples

Code	Function
TI1	Gas temperature below reactor grate
TI2	Water temperature in disentrainment tank
TI3	Gas temperature just downstream of demister
TI4	Gas temperature at gas meter
TI5	Reactor search thermocouple
TI6-TI14	Reactor temperature measurement

Pressure Instruments

Code	Function
PI1	Gas pressure downstream of demister (PT1, mmHg abs)
PI2	Gas pressure at gas meter (PT2, mmHg abs)
PI3	Venturi circuit water pressure (Bourdon gauge, psig)
PI4	Disentrainment tank pressure (Bourdon gauge, psig)
PI5	Pressure below reactor grate (Manometer, cmH_2O)

Flowmeters

Code	Function
FI1	Venturi circuit water flowrate (Series 1000 Rotameter 65S metric)
FI2	Product gas flowrate (Platon flowmeter - recorded by datalogger)
FI3	Water flowrate into disentrainment tank (Rotameter)

Miscellaneous

Code	Function
XI	Cumulative gas volume meter
TIA	Pilot light alarm

Appendix V
Gasifier Start-up and Shut-Down Procedures

V.1   Gasification Start-up Procedure

1)   Close all valves except V1, V2 and V3.
2)   Switch on pilot light alarm.
3)   Test carbon monoxide alarm.
4)   Open V11 and V8 and fill disentrainment tank with water until tank is approximately two thirds full of water. Close V11 and V8.
5)   Fill reactor to a depth of 2-3 cm with charcoal.
6)   Add a small amount of low ash paper to the charcoal.
7)   Add a small amount of wood shavings to the reactor.
8)   Check water pump is primed.
9)   Place burner on balcony outside laboratory.
10)   Calibrate instruments (gas analysers, pressure transducers, flowmeters).
11)   Switch on analyser pump.
12)   Switch on compressed air and electricity supplies to hot box.
13)   Connect pipe from CO_2 cylinder to V4.
14)   Open V4. Turn flow of CO_2 from cylinder to approximately $25 lmin^{-1}$.
15)   Switch on water pump and adjust V3 to give a water flowrate of 4 as indicated by the Series 1000 rotameter above V3.
16)   Using soapy water, check the gasification system for gas leaks.
17)   Open V13 (natural gas supply to burner)
18)   Light burner pilot light.
19)   Check pilot light alarm.
20)   Allow the CO_2 to flow through the system for 15 minutes.
21)   Switch off CO_2 supply to venturi.
22)   Switch on CO alarm.
23)   Throw one match into gasifier.
24)   Once gasifier lit, start feeding wood.
25)   Continue.

Valve Position Checklist at Start Up
The following are the positions of the valves prior to start-up:
Closed: V4,V5,V6,V7,V8,V9,V10
Open: V1,V2

Partially open: V3

V.2   Shut Down Procedure

1)   Stop feeding wood

2)   Close V7 (gas supply to analysers).

3)   Switch of hot box and analysers' pump.

4)   Slowly close V3 until Series 1000 water rotameter reads approximately 4.

5)   When pressure in the disentrainment tank is approximately 0.5 psig or less, fully close V3 slowly and switch of the water pump.

6)   Close V3 (natural gas supply to burner).

7)   Check that the pilot light alarm operates.

8)   Switch off computer system.

9)   Using CO_2, extinguish any fire in the gasifier.

10)   Allow gasifier to cool for 15 to 20 minutes.

11)   Connect CO_2 line to V4.

12)   Open V4

13)   Set CO_2 flow to approximately 25 $lmin^{-1}$.

14)   Open V3. Switch on pump and adjust V3 so that the Series 1000 water rotameter reads approximately 3.

15)   Allow the CO_2 to flow for 15 minutes to permit full evacuation of combustible gas from the gas space above the water in the disentrainment tank.

16)   Close V4 and switch of CO_2 supply at bottle.

17)   Slowly close V3 and switch off water pump.

18)   Switch off pilot light alarm.

19)   Allow system to cool for at least 1 hour.

20)   Open V11 to release any pressure in the disentrainment tank.

21)   Make back-up copies of computer data and transfer data file from the BBC to the Vax Cluster.

22)   Switch off fumehood.

23)   Switch off CO alarm.

V.3   Emergency Shut Down Procedure

1) All people not involved with the gasifier operation to evacuate the laboratory.

2) Switch off all electrical switches on the fumehood roof (above yellow pump).

3) Switch off biomass feeder if in use (switch at back of gas analyser cubicle).

4) Extinguish reactor using sand, or foam fire extinguisher or carbon dioxide if possible/necessary.

5) Switch off natural gas supply to burner (if possible)

6) Evacuate laboratory.

7) Re-enter laboratory (using breathing apparatus) to follow normal shut down procedure if conditions allow. Monitor CO alarm.

In the event of a major fire and/or explosion, immediately evacuate the laboratory, sound the fire alarms, inform security (dial 222) and follow the building evacuation procedures.

Vessel - GASIFIER			
Intention - Conversion of wood to a gaseous fuel			
Guide Word	Deviation	Cause	Consequences & Action
Line No. A1			
Intention - Transfers the product gas from the gasifier to the Venturi			
NO/NONE	Flow	Pump off or broken Blockage	Insufficient air will reach reaction zone - pyrolysis will dominate. Wood could burn causing damage to reactor. Possible release of toxic/explosive gases. Action: Stop run, extinguish fire as necessary by pouring sand into reactor. High pressure indisentrainment tank may force gas followed by water into low pressure pipework (between venturi and gasifier) and gasifier. Slight risk of explosion. More possibly, blow back will force hot contents of gasifier upwards and out of the gasifier. Possible release of toxic gases into lab. Switch off pump, Evacuate lab if necessary. Carry out emergency shut down procedure. Investigate cause of problem.
		Needle valve closed . Blocked venturi Valve on closed	Open valve to give required flow Stop run and investigate No water will reach pump - damageinput side to pump may occur to pump. Switch off pump. Open valve
REVERSE	Flow	No water flow to pump - possible blockage in line filter, blocked venturi, broken	As above for NO/NONE flow

Guide Word	Deviation	Cause	Consequences & Action
		pump	
LESS	Flow	Loss of pressure in venturi pipework	Pyrolysis will dominate in reaction zone and zone will rise until fuel reserve is burnt out. Extinguish using sand if necessary. Turn off automatic fuel feeder if in operation. If a rapid decrease in flow occurs, high pressure in disentrainment tank may force gas followed by water into low pressure pipework (between venturi and gasifier) and gasifier. Slight risk of explosion. More possibly, blow back will force hot contents of gasifier upwards and out of the gasifier.
		Blocked line filter	Stop run and clean or replace filter.
		Leak in pipework	Stop run according to set shut down procedure, fix leak

Vessel - VENTURI

Intention - To draw air through the gasifier and to mix the product gas thoroughly with water

Guide Word	Deviation	Cause	Consequences & Action

Line No. A2

Intention - transfers product gas and water into the disentrainment tank

Guide Word	Deviation	Cause	Consequences & Action
NO/NONE	Flow	Pump failure Needle valve closed. Blocked line filter. Valve on input side to pump closed	As above for NO/NONE - Stop run and nvestigate. Open valve V3 to obtain correct flow. No water will reach pump - damage may occur to pump. Switch off pump, open valve V1. High pressure in disentrainment tank may force gas followed by water into low pressure pipework (between venturi and gasifier) and gasifier. Slight risk of explosion. More possibly, blow back will force hot contents of gasifier upwards and out of

344

			the gasifier. Possible release of toxic gases into lab.
REVERSE	Flow	Pump fitted incorrectly	No suction produced by venturi - Stop run and re-fit pump
LESS	Flow	Line filter blocked	As above for NO/NONE Flow. Stop run and investigate. Possible release of toxic/explosive gases to atmosphere.
MORE	Flow		Excess water flow. Reaction zone will descend towards grate. Possible damage to grate if not checked (gasification will dominate reactions in gasifier). Adjust valve V3 to give correct flowrate and pressure. Pump bypass line valve possibly shut

Vessel - WATER PUMP

Intention - To provide water at high pressure (up to 60 psig) to the venturi ejector

Guide Word	Deviation	Cause	Consequences & Action

Line No. A3

Intention - transfers water at high pressure to the water ejector

| NO/NONE | Flow | One or more valves shut | Pump may be damaged by lack of water - reset/open appropriate valve. Gasification process will stop. Possible fire in reactor. Follow shut down procedure and extinguish fire using sand as required. High pressure in disentrainment tank may force gas followed by water into low pressure pipework (between venturi and gasifier) and gasifier. Slight risk of explosion. More possibly, blow back will force hot |

Guide Word	Deviation	Cause	Consequences & Action
			contents of gasifier upwards and out of the gasifier. Possible release of toxic gases into lab. Switch off pump, evacuate lab if necessary. Carry out emergency shut down procedure. Investigate cause of problem.
LESS	Flow	One or more valves incorrectly set	Insufficient suction provided for gasifier. Reaction zone will rise. Reset valves V2, V3 (ensuring that V1 is open) to give required water flowrate. If not possible, follow shut down procedure - reaction will stop automatically when all fuel used. If automatic fuel feeding is in use, switch off feeder.
		Blocked line filter	Shut down rig and investigate. As above for NO/NONE.
		Blocked venturi	As above for blocked line filter
MORE	Flow	One or more valves incorrectly set	Excess suction provided in gasifier - reaction zone will descend and cause possible damage to grate (gasification will dominate reactions in gasifier). Adjust valve(s) to give correct flowrate and pressure. Pump bypass line valve (V2) possibly shut.

Vessel - ROTAMETER		
Intention - Measures water flowrate in venturi circuit		
Guide Word	Deviation Cause	Consequences & Action
Line No. A4		
Intention - transfers water at high pressure to the water ejector		
Possible deviations, causes and consequences same as for line A4		

Vessel - DISENTRAINMENT/SEPARATION TANK			
Intention - Separates gas phase from water phase			
Guide Word	Deviation	Cause	Consequences & Action

Line No. A5

Intention - transfers gas from tank to demister

Guide Word	Deviation	Cause	Consequences & Action
NO/NONE	Flow	Pump off or broken	No suction provided by venturi - possible release of toxic/flammable gases from reactor - switch on pump, stop run. Possible fire in reactor, xtinguish. High pressure in disentrainment tank may force gas followed by water into low pressure pipework (between venturi and gasifier) and gasifier. Slight risk of explosion. More possibly, blow back will force hot contents of gasifier upwards and out of the gasifier. Possible release of toxic gases into lab. Switch off pump, Evacuate lab if necessary. Carry out emergency shut down procedure. Investigate cause of problem.
		No flow in venturi Valves V1, V2 and/or V3 incorrectly set	Possible fire in gasifier. Reset valves to give correct water flowrate
		Blockage in water circuit	Shut down test and investigate. Extinguish fire in reactor. Possible explosion in tank due to build up of pressure in disentrainment tank. Venturi will stop providing suction at high backback pressures (approx 10-12 psig) - gasification reaction will stop and unreacted fuel may burn. Stop test immediately - investigate cause of
		Blockage in downstream pipework/ flowmeter/burner	

347

			possible blockage. Extinguish fire as necessary.
		Blocked water input to tank	Water may gush up into reactor. Reactor may smash (catastrophically), reaction should stop. Stop run immediately and when safe investigate cause.
LESS	Flow	Incorrectly set valves	Pyrolysis may be dominating gasification process and reaction zone may be rising. Reaction will stop when all fuel used. Possible burn back into automatic feeder if in use. Reset valves to give correct water flowrate
		Blocked line filter	Unable to raise sufficient water pressure. Pyrolysis will dominate - reaction zone will rise. Stop run and investigate. As above for NO/NONE if decrease in flow is rapid.
		Blocked demister	Pressure will rise in tank. If pressure reaches 3.3psig, safety u-tube will release pressure in tank. Following any tank pressure release through safety u-tube, stop run, switch off pump, open lab windows and evacuate lab.
MORE	Flow	Incorrectly set valves	Reaction zone may descend. May damage grate. Reset valves
REVERSE	Flow	Tank drain valve may be open allowing water to empty from the tank; or tank may be leaking	Water level in tank will be seen to fall. Close valve, make up lost water. If the tank is allowed to empty, the pump will run dry thus causing damage. No or tank may besuction will be provided by venturi leakingand fumes will escape through top of gasifier. Switch off pump if tank level is too low.

Vessel - Demister

Intention - Removes water droplets from product gas stream

Guide Word	Deviation	Cause	Consequences & Action

Line No. A6

Intention - transfers gas from demister via flowmeters to gas burners

Guide Word	Deviation	Cause	Consequences & Action
NO/NONE	Flow	No flow in venturi. Valves V1, V2 and/or V3 incorrectly set.	Possible fire in gasifier. Reset valves to correct water flowrate
		Blockage in water circuit	Shut down test and investigate. Extinguish fire in reactor as necessary. High pressure in disentrainment tank may force gas followed by water into low pressure pipework (between venturi and gasifier). Slight risk of explosion. More possibly, blow back will force hot contents of gasifier upwards and out of the gasifier. Possible release of toxic gases into lab. Switch off pump, Evacuate lab if necessary. Carry out emergency shut down procedure. Investigate cause of problem.
		Blockage in downstream pipework/ flowmeters/burners	Possible explosion in tank due to build up of pressure in disentrainment tank. If the tank pressure reaches 3.3psig, safety u-tube will release pressure in tank. Following any tank pressure release through the safety u-tube, stop run (follow emergency shut-down procedure), open lab windows and evacuate lab. Venturi only will stop providing suction at high back pressures (approx. 10-12 psig). Investigate cause of possible blockage when safe.

	Comp-osition	Air in leak to system	Product gas composition readings odd. Stop run and check for leaks. Nitrogen composition of product gas will be excessive.
LESS	Flow	Incorrectly set valves	Pyrolysis may be dominating gasification process and reaction zone may be rising. Reaction will stop when all fuel used. Possible burn back into automatic feeder if in use. Reset valves to give correct water flowrate.
MORE	Flow	Incorrectly set valves	Reaction zone may descend. May damage grate. Reset valves

Figure VI.1
Gasifier Configuration Showing Line Numbers for Hazop Analysis

351
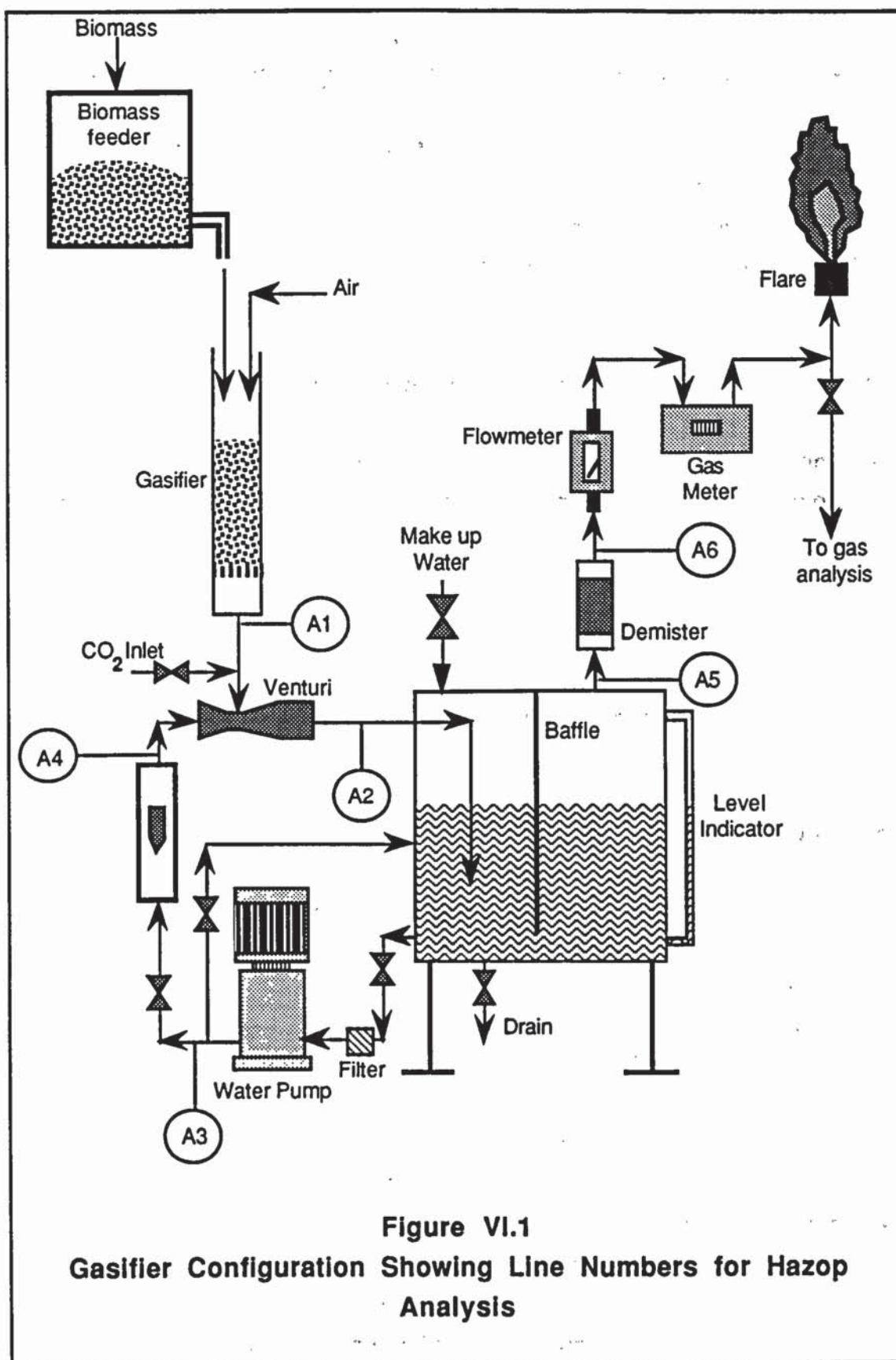
Mass Balance and Energy Balance Calculation Procedures

VII.1   Mass Balance Method

In any process, mass is neither created or destroyed (Equation VII.1). This applies to the total mass of the system and to the components within that system. Table VII.1 shows the total inputs and outputs of the gasifier during normal operation.

{Mass in} = {Mass out}+{accumulation (or depletion) within system} ...... [VII.1]

At steady state the accumulation of material within a system is zero and the amount of material within a system does not enter into the calculation. A mass balance closure is, therefore defined as:

$$\text{Mass balance closure} = \frac{\text{Total mass out}}{\text{Total mass in}} \times 100\% \dots\dots\dots [VII.2]$$

The mass balance closure should equal 100%. The size of any deviation from 100% will indicate the quality of the balance.

Figure VII.1 shows the boundary over which the mass balances have been performed and the streams entering and leaving the system. Table VII.1 lists the input and output streams to the system.

Elemental balances (C, H and O) were also performed. The nitrogen input rate to the gasifier was calculated from the nitrogen output rate. The nitrogen balance by definition equals 100%.

When performing mass balances on the gasification system, it was assumed that:

1)   The gasifier is operating at steady state when the char bed height is constant and the product gas flowrate is constant.

2)   Product gas flowrate is constant.

3)   Ash takes no part in the gasification process.

4)   No char or ash passes through the grate.

5)   No carbon dioxide is absorbed by the scrubber water as the scrubber water has been pre-saturated with carbon dioxide before the start of the run (see Section 3).

6)   The gas is saturated with water on exit from the disentrainment tank.
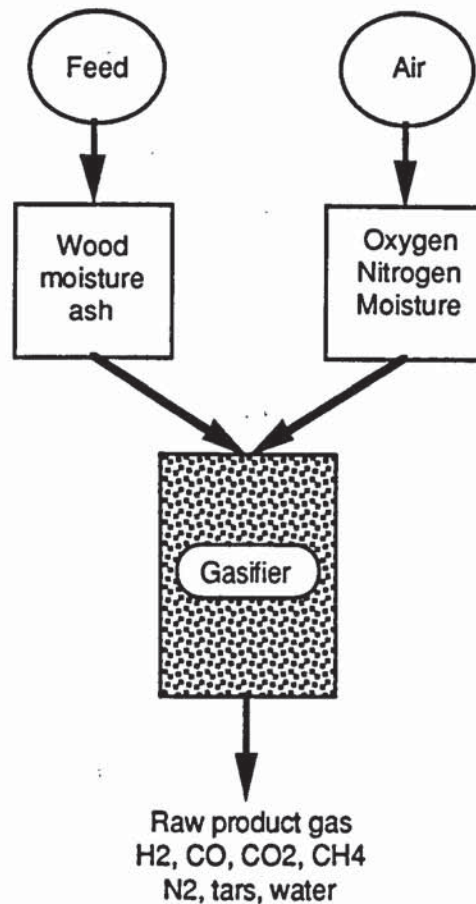
Figure VII.1
Mass Balance Flow Diagram

The results from the mass and energy balances performed over the gasifier are presented in tabular format in this Appendix.

VII.1.1   Gasifier Inputs
As shown in Figure VII.1, the gasifier inputs are air and fuel.

VII.1.1.1   Feed Input
The ultimate analyses including the ash content carried out by British Gas of the feed inputs (except sewage sludge) used in this project are presented in Tables 4.3. The feed moisture content was determined prior to each run as described in Section 4.4.2.

From the wood flowrate measured during the run, the dry and dry ash free wood flowrates into the gasifier can be calculated using the following equations:

353

Wet feed mass flowrate, kgh^{-1} (measured) = G^f_{wet}

Feed moisture content, % = m^f

Mass input flow of moisture in feed, kgh^{-1},

$$G^{input}_m = G^f * \left(\frac{m^f}{100}\right) \quad \text{........................ [VII.3]}$$

Dry feed mass flow rate, kgh^{-1},

$$G^f_{dry} = G^f_{wet} * (1 - \frac{m^f}{100}) \quad \text{........................ [VII.4]}$$

Feed ash content, % = ash
Dry ash flow, kgh^{-1},

$$G^{input}_{ash} = G^f_{dry} * \frac{ash}{100} \quad \text{........................ [VII.5]}$$

Dry ash free feed flow, kgh^{-1},

$$G^f_{daf} = G^f_{dry} * (1 - \frac{ash}{100}) \quad \text{........................ [VII.6]}$$

VII.4.1.2   Air Input

Air contains 78.8% nitrogen and 21.2% oxygen and has a molecular weight (dry) of 28.85 kg.kgmole^{-1} [108]. Moisture in the air stream was measured using a wet and dry hygrometer situated in the laboratory. From the air moisture content, the wet air molecular weight is calculated.

The mass flow of air into the gasifier is calculated by assuming that all the nitrogen in the product gas is supplied by the air flow into the gasifier (Equations VII.7 and VII.8).

Mass flow rate of wet air, G^a_{wet}, kgh^{-1},

$$G^a_{wet} = \frac{1}{0.788} * G^{output}_{N_2} \quad \text{........................ [VII.7]}$$

$$G^a_{wet} = G^g_{dry} * X_{N_2} * \frac{1}{0.788} \quad \text{........................ [VII.8]}$$

Volumetric flowrate of wet air, V_{wet}^a, Nm^3h^{-1}

$$V_{wet}^a = \frac{G_{wet}^a * R * 273}{MW_{wet}^a * P} \qquad\text{......................} \text{[VII.9]}$$

Mass input flow of moisture in air, G_m^a kgh^{-1},

$$G_m^a = W^a * G_{wet}^a \qquad\text{..}\text{[VII.10]}$$

Dry air input rate to gasifier, G_{dry}^a, kgh^{-1},

$$G_{dry}^a = G_{wet}^a - G_m^a \qquad\text{...............................}\text{[VII.11]}$$

Volumetric dry air input rate to gasifier, V_{dry}^a, Nm^3h^{-1}

$$V_{dry}^a = \frac{G_{dry}^a * R * 273}{MW_{dry}^a * P} \qquad\text{...............................}\text{[VII.12]}$$

VII.4.2   Gasification System Outputs

The outputs from the gasifier are the product gas (consisting of H_2, CO, CO_2, CH_4 and N_2), tars, condensates, char and ash. It was not possible to measure the char, ash, condensate and tar mass flowrates as no time was available to construct a particulate and tar sampling system for use with the iso-kinetic sampling probe. From the literature and a simple evaluation of the tars produced in runs 1 and 2, the gas tar and condensate content was assumed to be 1% of the product gas mass flowrate (see Section 6.3).

VII.4.2.1   Product Gas Flowrate

Due to the unreliable readings obtained from the Platon on-line flowmeter (see Section 6.3), the average gas flowrate measured using the gasmeter have been used to record the product gas flowrate. The Platon on-line

355

flowmeter was used to give an indication of the variations in gas flowrate during a run.

Wet product gas volumetric flowrate $= U_{wet}^g$, m^3h^{-1}

From the dry gas analysis, (measured using the gas analysers), the molecular weight of the dry gas stream can be calculated using Equation VII.13.

$$MW_{dry}^g = \sum_i x_i * MW_i \quad \text{............................[VII.13]}$$

where MW_i is the molecular weight of component i in the gas and x_i is the molar fraction of component i.

On exit from the disentrainment tank, the gas will be saturated with water. The molar fraction of water in the gas, W^g can be calculated using Equation VII.14 .

$$W^g = \frac{P_{H_2O}}{PT2 - P_{H_2O}} \quad \text{............................[VII.14]}$$

P_{H_2O} is the vapour pressure of the water at the gas temperature, mmHg

PT2 is the pressure of the gas at outlet conditions, mmHg

Using this value for the product gas water content, the composition of the wet gas is calculated and its molecular weight, MW_{wet}^g calculated using Equation VII.13 .

The wet gas mass flowrate is then calculated, G_{wet}^g,

$$G_{wet}^g = \frac{V_{wet}^g * PT2 * MW_{wet}^g}{760 * R * TC3} \quad \text{............................[VII.15]}$$

The dry gas mass flowrate is, G_{dry}^g, kgh^{-1}

$$G^g_{dry} = G^g_{wet} * (1 - W^g) \dots\dots\dots\dots\dots\dots\dots [VII.16]$$

VII.4.2.2   Tar Output

For the purposes of the mass balance calculation, it is assumed that the amount of tars in the product gas equals 1% of the product gas mass flowrate (see Section 6.1.3). The tar analysis used is that presented by Reyes (see Table VII.1). Tars were collected in this project but British Gas were unable to analyse them.

Table VII.1
Tar Ultimate Analysis [17]

Component	Analysis, weight %
C	72.2
H	9.6
O	18.2

Tar molecular formula (based on above CHO analysis), $C_6H_{9.6}O_{1.1}$.
tar molecular weight, $MW_{tar} = 99.2$ kg.kg mole tar^{-1}

Tar mass flowrate, expressed as a weight fraction of the dry product gas can be estimated using Equation VII.17.

$$G^g_{tar} = 0.01 * G^g_{dry} \dots\dots\dots\dots\dots\dots\dots [VII.17]$$

VII.5   Elemental Mass Balance
VII.5.1   Carbon Balance
VII.5.1.1   Inputs

Only the feed contains carbon. Therefore, the carbon input will equal the carbon in the feedstock.

$$G^{input}_C = G^f_C \dots\dots\dots\dots\dots\dots\dots\dots\dots\dots [VII.18]$$

$$G^{input}_C = G^f_{daf} * Y_C \dots\dots\dots\dots\dots\dots\dots\dots [VII.19]$$

where, Y_C = weight fraction of carbon in the wood

VII.5.1.1   Outputs

Carbon is found in the product gas (CO, CO_2 and CH_4) and in the tars. No char is assumed to pass through the grate (see assumptions).

The carbon outputs of the system are calculated using the Equation VII.20.

$$G_C^{output} = G_{CO_2}^g * \frac{12}{44} + G_{CO}^g * \frac{12}{28} + G_{CH_4}^g * \frac{12}{16} + 0.722 * G_{tar}^g \quad [VII.20]$$

The carbon balance closure can be calculated using Equation VII.21.

$$\text{Carbon closure} = \frac{G_C^{output}}{G_C^{input}} * 100\% \quad\quad\quad [VII.21]$$

VII.5.2   Hydrogen Balance

VII.5.2.1   Inputs

Hydrogen is contained within the feed and in the moisture entering the gasifier with the air.

$$G_H^{input} = G_H^f + G_H \text{ (feed moisture)} + G_H \text{ (air moisture)} \quad\quad [VII.22]$$

$$G_H^{input} = \left(G_{daf}^f * Y_H\right) + \left(G_m^a * \frac{2}{18}\right) + \left(G_{wet}^f * \frac{m^f}{100} * \frac{2}{18}\right) \quad [VII.23]$$

where, Y_H = weight fraction of hydrogen in the wood
and m^f = feed moisture content, %.

VII.5.2.2   Outputs

Hydrogen is found in the product gas (H_2, H_2O and CH_4) and in the tars.

The hydrogen outputs of the system are calculated using Equation VII.24.

$$G_H^{output} = \left(G_{CH_4}^g * \frac{4}{16}\right) + X_H + \left(0.096 * G_{tar}^g\right) + \left((G_{wet}^g - G_{dry}^g) * \frac{2}{18}\right)$$

$$\quad\quad\quad\quad\quad\quad\quad\quad\quad\quad\quad\quad\quad\quad\quad\quad [VII.24]$$

358

The hydrogen balance closure can be calculated using Equation VII.25.

$$\text{Hydrogen closure} = \frac{G_H^{output}}{G_H^{input}} * 100\% \quad\text{......................[VII.25]}$$

VII.5.3 Oxygen Balance

VII.5.3.1 Inputs

Oxygen is contained within the feedstock, the feed moisture and the moisture in the air entering the gasifier.

$$G_O^{input} = G_O^f + G_O \text{ (feed moisture)} + G_O \text{ (air moisture)} \quad\text{...........[VII.26]}$$

$$G_O^{input} = \left(G_{daf}^f * Y_O\right) + \left(G_m^a * \frac{16}{18}\right) + \left(G_{wet}^f * \frac{m^f}{100} * \frac{16}{18}\right) \text{..[VII.27]}$$

where, Y_O = weight fraction of oxygen in the wood

VII.5.3.2 Outputs

Oxygen is found in the product gas (CO, CO_2 and H_2O) and the tars.

The oxygen outputs of the system are calculated using the Equation VII.28.

$$G_O^{output} = (G_{CO_2}^g * \frac{16}{44}) + (G_{CO}^g * \frac{16}{28}) + (G_{H_2O}^g * \frac{16}{18}) + (0.182 * G_{tar}^g) \text{.........}$$

$$\text{..[VII.28]}$$

The oxygen balance closure can be calculated using Equation VII.29.

$$\text{Oxygen closure} = \frac{G_O^{output}}{G_O^{input}}) * 100\% \quad\text{......................[VII.29]}$$

VII.5.3 Nitrogen Balance

The nitrogen balance is used to calculate the air input rate to the gasifier and by definition, therefore, equals 100%.

$$V_N^g = V_N^a \dots\dots\dots\dots\dots [VII.30]$$

VII.6   Mass Balance Efficiency Indicators

The following indicators have also been calculated to aid evaluation of the Aston open-core gasifier.

VII.6.1   Mass Yield

This is defined as the ratio of the mass of dry product gas and the mass of dry feed input to the gasifier (Equation VII.31).

$$\text{Mass yield MY} \atop \text{kgkg}^{-1} = \frac{\text{Dry gas mass flowrate + Tar mass flowrate}}{\text{Dry feed input rate to gasifier}} \dots [VII.31]$$

VII.6.2   Volumetric Yield

The volumetric yield is defined as the ratio of the dry gas normal volumetric flowrate and the dry feed input rate to the gasifier.

$$\text{Volumetric yield VY} \atop \text{Nm}^3\text{kg}^{-1} = \frac{\text{Normal dry gas volumetric flowrate}}{\text{Dry feed input rate to gasifier}} \dots [VII.32]$$

VII.6.3   Air / Fuel Ratio

This is defined as the ratio of dry air mass flow into the gasifier and the dry feed input rate to the gasifier.

$$\text{Air/fuel ratio} \atop \text{A/F kgkg}^{-1} = \frac{\text{Dry air mass flowrate into gasifier}}{\text{Dry feed input rate to gasifier}} \dots [VII.33]$$

VII.6.4   Equivalence Ratio

This is defined as the ratio of the actual oxidant to fuel ratio to the oxidant to fuel ratio required for stoichiometric combustion.

$$\text{Equivalence ratio, \%} = \frac{\text{Actual oxidant/fuel ratio}}{\text{stoichiometric oxidant/fuel ratio}} \times 100\% \dots [VII.34]$$

The stoichiometric air requirement is calculated from the molecular formula of the feed.

$$C_6H_\xi O_\psi + \alpha O_2 = \beta CO_2 + \chi H_2O \quad\text{............................[VII.35]}$$
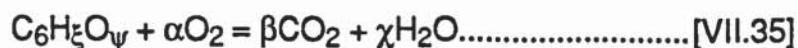
The coefficients ξ, ψ, α, β and χ are calculated using Equations VII.36, VII.37 and VII.38.

$$\chi = \frac{\xi}{2} \quad\text{...[VII.36]}$$

$$\beta = 6 \quad\text{...[VII.37]}$$

$$\alpha = \frac{12 + \chi - \psi}{2} \quad\text{.............................[VII.38]}$$

The mass of oxygen required for stoichiometric combustion will, therefore, be:

> Mass oxygen required
> for stoichiometric combustion, $\text{kg.kgmol}^{-1} = 32 * \alpha$ ....[VII.39]

The ratio of the mass of oxygen required per kg molecule of wood and the mass of 1 mole of dry wood will give the stoichiometric oxidant to fuel ratio. The actual oxidant to fuel ratio is the defined by Equation VII.40.

$$\text{Actual oxidant to feed ratio} = \frac{\text{Oxygen flowrate into gasifier}}{\text{Dry feed mass flowrate into gasifier}} \text{..[VII.40]}$$

VII.6.5 Mass Conversion to Dry Product Gas

This is the ratio, expressed as a percentage, of the dry gas mass flowrate to the sum of the dry feed flow and the dry air input rate to the gasifier.

$$MC, \% = \frac{G^g_{dry}}{G^f_{dry} + G^a_{dry}} * 100\% \quad\text{...........................[VII.41]}$$

VII.6.6 Carbon Conversion Efficiency

This the ratio, expressed as a percentage, of the mass of carbon in the dry, clean product gas to the mass of carbon in the dry feed.

$$\eta_{cc} = \frac{G^g_{daf} * Y_C}{12 * \left(\dfrac{G^g_{CO_2}}{44} + \dfrac{G^g_{CO}}{28} + \dfrac{G^g_{CH_4}}{16} \right)} * 100\% \quad\text{...............[VII.42]}$$

VII.6.7 Specific Capacity

This is the dry fuel flow rate divided by the grate cross sectional area $(kg.h^{-1}.m^{-2})$.

$$SC = \frac{G^g_{daf}}{4.418 \times 10^{-3}} \quad \text{.....................................[VII.43]}$$

VII.7 Energy Balance

In any plant or unit, energy is conserved. Equation VII.44 illustrates the principle of energy balances.

$$\begin{pmatrix} \text{Heat added or removed} \\ \text{from a process} \end{pmatrix} = \begin{pmatrix} \text{enthalpy of} \\ \text{products} \end{pmatrix} - \begin{pmatrix} \text{enthalpy of feed} \\ \text{streams} \end{pmatrix} \text{..[VII.44]}$$

The energy inputs and outputs to the gasifier are shown in Figure VII.2.

Energy inputs to the gasifier are:

i)   Feed (chemical energy and sensible energy)
ii)   Air (sensible energy and latent energy of any moisture)

Energy outputs from the gasifier are:

i)   Hot, wet, raw gas (chemical energy, latent energy, chemical energy of tars, sensible energy of tars, latent heat of tars, sensible heat of moisture and latent heat of moisture,
ii)   Heat losses from the gasifier.

VII.7.1 Energy Inputs to Gasifier

The energy inputs to the gasifier consist of the heat of combustion of the wood, the sensible heat of the wood, the sensible heat of the moisture within the wood, the sensible heat of the air and the sensible and latent heats of the moisture in the air.

VII.7.1.1 Energy Inputs from Feed

The chemical energy of the feedstock was calculated using Equation VII.45.
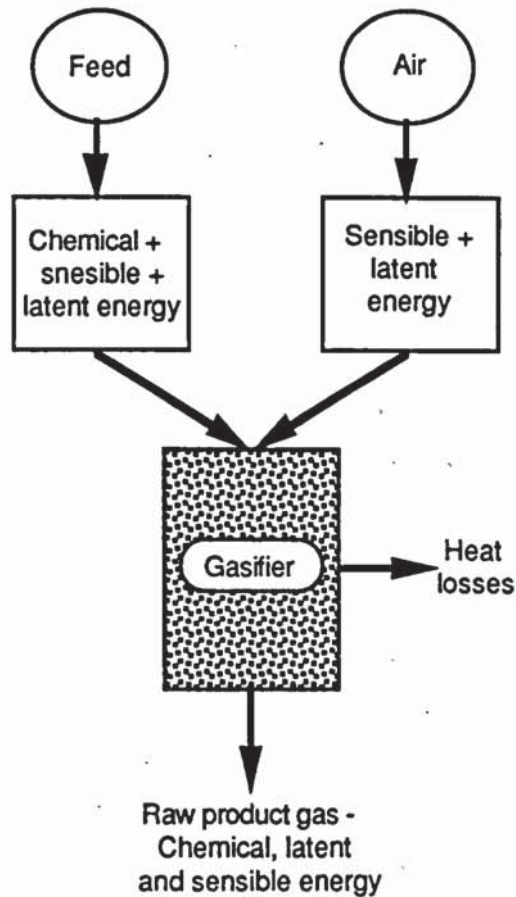
Figure VII.2
Energy Balance Flow Diagram

$$E_{chem}^f = G_{daf}^f * HHV^f \dots\dots\dots\dots\dots\dots\dots\dots[VII.45]$$

The sensible energy of the feed can be calculated using Equation VII.46. However, in this project, the reference temperature was taken as room temperature and in all cases, the feed sensible energy was zero.

$$E_{sens}^f = C_p^f * G_{daf}^g * (T^f - T_{ref}) \dots\dots\dots\dots\dots\dots[VII.46]$$

VII.7.1.2   Energy Inputs from Air

Energy is provided by the air as the sensible heat of the dry air and as the latent heat of the moisture contained within the air. The sensible energy of the dry air can be calculated using Equation VII.47. However, since the reference temperature was taken as room temperature, the sensible energy of the air was zero.

363

$$E_{sens}^a = G_{dry}^a * C_p^a * (T_i^a - T_{ref}) \dots\dots\dots\dots\dots\dots [VII.47]$$

$$E_{lat}^a = G_{dry}^a * L^a * \frac{m^a}{100} \dots\dots\dots\dots\dots\dots\dots [VII.48]$$

VII.7.2   Energy Outputs from the Gasifier

The energy outputs from the gasifier consist of the heat losses from the gasifier and the heat of combustion of the raw product gas consisting of the energy of the dry product gas (sensible and chemical), the energy of the water (sensible and latent) and the energy of the tars (sensible and chemical).

VII.7.2.1   Gasifier Heat Losses

The major mechanisms by which heat will be lost from the gasifier are convection and radiation. Both of these mechanisms will be affected by the surface temperature of the gasifier. The measurement of the gasifier outside wall temperature was found to be difficult. The most successful method used was that of a search thermocouple. A single thermocouple fitted into a close fitting stainless steel sheath positioned inside the gasifier near the gasifier's vertical centreline permitted a vertical temperature profile (using 1cm intervals) of the gasifier during steady state operation to be measured. The gasifier was split into zones or segments 1cm deep and 75mm in diameter. Using the search thermocouple, the temperature in each segment was measured (this was repeated 3 times). This provided the temperature data necessary to perform the heat loss calculations on the gasifier (assuming the gasifier temperature to be constant over the whole volume of each segment). At heights 30cm above the grate, the gasifier outside temperature was assumed to be equal to room temperature as it was difficult to accurately note the position of the thermocouple (measurements within the gasifier are made using a 30cm steel ruler mounted vertically alongside the gasifier - 0cm is the position of the grate). Back heat transfer from the reaction zones is extremely limited and in all cases during temperature search experiments, the reaction zone was no further than 25cm above the grate

In addition to this method, during insulated gasifier operation, thermocouples were fitted tightly in between the inside surface of the insulation and the outside surface of the gasifier. Due to the breakage of

some of the straps fitting the insulating sleeve to the gasifier, however, this method was not wholly successful. Thermocouples were also fitted to the outside face of the insulation during runs 29 and 30. Silicone sealant was used to hold the thermocouples in place. The results from these measurements are used to perform the heat loss calculations for these runs.

Natural Convection Heat Losses

Heat transferred from a body by natural convection is governed by Equation VII.49.

$$q_{conv} = h_{conv} * Area * (T_1 - T_2) \dots\dots\dots\dots\dots [VII.49]$$

For the special case of convection from a hot body to air with streamline flow, the convective heat transfer coefficient is given by Equation VII.50 [109].

$$h_{conv} = 1.18 * \sqrt[4]{\frac{(T_1 - T_2)}{d_o}} \dots\dots\dots\dots\dots [VII.50]$$

Combining Equations VII.49 and VII.50, Equation VII.51 is used to calculate the convective heat transfer rate from each segment of the gasifier selected.

$$q_{c_k} = 1.18 * \pi * d_o^{0.75} * (T_i - T_2)^{1.25} * K_k \dots\dots\dots\dots [VII.51]$$

The total convective heat transfer rate from the gasifier will be the sum of the convective heat transfer rates from each of the segments.

Radiative Heat Losses

The radiative heat losses from the gasifier are calculated in a similar way to the convective heat losses. Heat transferred from a grey body of area by radiation is governed by the Stefan-Boltzmann law (Equation VII.52) [110].

$$q_{rad} = Area * \varepsilon * \sigma * (T_1^4 - T_2^4) \dots\dots\dots\dots\dots [VII.52]$$

The emissivity of the quartz glass tube has been taken as 0.935 [17]. No value for the emissivity of Kaowool ceramic fibre insulation could be obtained. A value for the emissivity of asbestos paper was, therefore used (0.93) [111].

For a segment of gasifier K_k in depth, the radiative heat loss from the segment will be:

$$q_{rad_k} = \pi * d_o * \varepsilon * \sigma * (T_k^4 - T_2^4) * K_k \dots\dots\dots [VII.53]$$

The total radiative heat transfer rate from the gasifier will be the sum of the radiative heat transfer rates from each gasifier segment.

Total Heat Loss from Gasifier

The total heat loss from the gasifier will be the sum of the radiative and convective heat losses (Equation VII.54).

$$Q_{tot} = q_{rad} + q_{conv} \dots\dots\dots\dots\dots\dots [VII.54]$$

The heat loss is converted from watts to MJh^{-1} by multiplying the total heat loss by 0.0036.

VII.7.2.2 Raw Product Gas Energy

The raw gas energy consists of the sensible and chemical heats of the dry gas, the sensible and latent heats of the water in the gas and the sensible and chemical heats of the tars (assumed to be equal to 1% of the dry gas mass flowrate).

Chemical Energy of the Dry Gas

This is calculated from Equation VII.55.

$$E_{chem}^g = HHV^g * V_{dry}^g \dots\dots\dots\dots [VII.55]$$

The gas higher heating value is calculated from the dry gas analysis by multiplying the volume fractions of hydrogen, carbon monoxide and methane with their respective heating values (Equation VII.56).

$$HHV^g = 12.761 * X_{H_2} + 12.634 * X_{CO} + 39.748 * X_{CH_4} \dots [VII.56]$$

Sensible Heat of the Dry Gas

The sensible heat of the dry gas can be calculated using Equation VII.57.

$$E_{sens}^g = G_{dry}^g * \Delta H_G \dots\dots\dots\dots [VII.57]$$

For pure materials with no phase change, the specific sensible heat of the dry gas is given by Equation VII.58.

$$\Delta H_G = \int_{T_{ref}}^{T_o} C_p^g \, dT \dots\dots\dots\dots\dots\text{[VII.58]}$$

The specific heat of the gas at constant pressure will vary with temperature. C_p must, therefore, be calculated as a function of temperature. For solids and gases, this is usually expressed as an empirical power series equation (Equation VII.59).

$$C_p = A + BT + CT^2 + DT^3 \dots\dots\dots\dots\text{[VII.59]}$$

For a gas mixture as in this situation, the heats of mixing are usually negligible and the mean specific heat capacity of the mixture can be taken as the sum of the individual heat capacities multiplied by the respective mol fractions of the components (Equation VII.60) [72].

$$C_p^g = \left(X_{H_2} {}^* C_{P_{H_2}}\right) + \left(X_{CO} {}^* C_{P_{CO}}\right) + \left(X_{CO_2} {}^* C_{P_{CO_2}}\right) + \left(X_{CH_4} {}^* C_{P_{CH_4}}\right) + \left(X_{N_2} {}^* C_{P_{N_2}}\right) \dots\text{[VII.60]}$$

To calculate the coefficients A, B, C and D in Equation VII.59 for a gas mixture, the following summations are performed:

$$A = \sum_i a_i {}^* X_i \dots\dots\dots\dots\text{[VII.61]}$$
$$B = \sum_i b_i {}^* X_i \dots\dots\dots\dots\text{[VII.62]}$$
$$C = \sum_i c_i {}^* X_i \dots\dots\dots\dots\text{[VII.63]}$$
$$D = \sum_i d_i {}^* X_i \dots\dots\dots\dots\text{[VII.64]}$$

Table VII.2 lists the coefficients used in Equations VII.61 to VII.64.

Table VII.2
Coefficients for the Ideal Gas Specific Heat Capacity Equation [72]

Gas	a	b x10^3	c x10^5	d x10^9
Hydrogen	27.143	9.273	-1.380	7.645
Carbon monoxide	30.869	-12.850	2.789	-12.710
Carbon dioxide	19.795	73.430	-5.601	17.150
Methane	19.251	52.120	1.197	-11.310
Nitrogen	31.150	-13.560	2.679	11.680

Integrating Equation VII.59 between T_o and T_{ref}:

$$C_p^g = \frac{A.(T_o - T_{ref}) + \frac{B}{2}.(T_o^2 - T_{ref}^2) + \frac{C}{3}.(T_o^3 - T_{ref}^3) + \frac{D}{4}.(T_o^4 - T_{ref}^4)}{(T_o - T_{ref})} \quad \text{.......[VII.65]}$$

The resultant specific heat can be used to calculate the sensible heat of the raw product gas (MJh^{-1}) at the outlet temperature of the gasifier using Equation VII.66.

$$E_{sens}^g = \frac{C_p^g * (T_o - T_{ref}) * G_{dry}^g}{1000 * MW_{dry}^g} \quad \text{...................[VII.66]}$$

Chemical Energy of the Tars

The chemical energy of the tars is calculated by multiplying the gas tar content (estimated at 1% of the dry gas mass flowrate) with the higher heating value of the tar. The higher heating value used is that calculated by Reyes using the IGT Equation (Equation 4.1) using the elemental tar analysis data performed by British Gas (35.137 MJkg^{-1}).

$$E_{chem}^t = G^t * HHV^t \quad \text{...................[VII.67]}$$

Sensible Energy of the Tars

The sensible heat of the tars is calculated using Equation VII.68.

$$E^t_{sens} = C^t_p * (T_o - T_{ref}) * G^t \dots\dots\dots\dots\dots [VII.68]$$

The specific heat of the tars used was calculated from the elemental analysis of the tar and its corresponding molecular formula using a modified form of Kopp's law (see Table VII.3) [72].

Table VII.3
Calculation of Tar Specific Heat Capacity [72]

Tar molecular formula: $C_6H_{9.6}O_{1.1}$

Element	Molecular weight	Heat Capacity $J.mol^{-1}.°C^{-1}$
Carbon	12 * 6.0	7.5 * 6.0
Hydrogen	1 * 9.6	9.6 * 9.6
Oxygen	16 * 1.1	16.7 * 1.1
	99.2	155.53 $Jmol^{-1}°C^{-1}$

Specific heat capacity $= \dfrac{155.53}{99.2} = \underline{1.5678}$ $kJkg^{-1}°C^{-1}$

VII.8   Energy Balance Efficiency Indicators

Three indicators have been calculated to examine the energy efficiency of the gasifier; the cold clean gas efficiency (Equation VII.69), the hot clean gas efficiency (Equation VII.70) and raw gas efficiency (Equation VII.71).

$$\eta_{cold} = \left(\frac{E^g_{cold}}{E^f_{chem}} \right) * 100\% \dots\dots\dots\dots [VII.69]$$

where:

$$E^f_{chem} = HHV^f * G^f_{daf} \dots\dots\dots\dots\dots [VII.45]$$

$$\eta_{hot} = \left(\frac{E^g_{chem} + E^g_{sens}}{E^f_{chem}} \right) * 100\% \dots\dots [VII.70]$$

369

$$\eta_{raw} = \left(\frac{E^g_{chem} + E^g_{sens} + E^t_{chem} + E^t_{sens}}{E^f_{chem}} \right) * 100\% \ldots\ldots[VII.71]$$

Nomenclature

A, B, C, D		Constants for the ideal gas specific heat capacity equation
a_i, b_i, c_i, d_i		Coefficients of the ideal gas specific heat capacity equation
Area	m^2	Area
ash	%	Feed ash content
C_p	$KJ.kmol^{-1}.K^{-1}$	Mean specific heat capacity
d	m	Gasifier outside diameter
ΔH_g	$MJ.kg^{-1}.K^{-1}$	Specific sensible heat of the dry gas
E	$MJ.h^{-1}$	Energy
ε		Quartz glass emmissivity, 0.935 for quartz glass [56]
F	%	Feed ash content
G	$kg.h^{-1}$	Mass flowrate
η	%	Efficiency
h	$W.m^{-2}.K^{-1}$	Convective heat transfer coefficient
HHV	$MJ.kg^{-1}/MJ.Nm^{-3}$	Higher heating value
K	m	Depth of gasifier segment
L	$MJ.kg^{-1}.K^{-1}$	Latent heat of water vapour at room temperature
m	%	Moisture content
MW	$kg.kgmole^{-1}$	Molecular weight
N	$kg.h^{-1}$	Elemental mass flowrate
P	atm	Gas pressure at NTP (273K, 760mmHg)
PT2	mm.Hg	Gas pressure at gasmeter
Q	W	Total gasifier heat loss due to radiative and convective heat losses
q	W	Heat transfer or loss
R	$m^3.atm.kgmol^{-1}.K^{-1}$	Universal gas constant
S	$kg.h^{-1}$	Air moisture content
σ	$W.m^{-2}.K^{-4}$	Stefan Boltzmann constant. 5.67×10^{-8}
SC	$kg.h^{-1}.m^{-2}$	Specific capacity
T	K	Temperature
TC3	K	Gas temperature at gasmeter
U	$m^3.h^{-1}$	Volumetric flowrate

V	$Nm^3.h^{-1}$	Volumetric flowrate at standard conditions, 273K, 760mmHg)
VY	$Nm^3.kg^{-1}$	Gasifier volumetric yield
W^a	kg (water).kg (air)$^{-1}$	Air moisture content
W^g	kg (water).kg (gas)$^{-1}$	Molar fraction of water in gas
X	fraction	Molar fraction
Y	fraction	Weight fraction
Z	m^2	Area available for heat transfer

Subscripts

amb	Ambient
ash	ash
C	Carbon
cc	Carbon conversion
CH_4	Methane
chem	chemical
CO	Carbon monoxide
CO_2	Carbon dioxide
conv	Convective
daf	Dry ash free
dry	Dry
H_2	Hydrogen
H_2O	Moisture
i	Fraction i (i = H_2, CO, CO_2 or CH_4)
j	Fraction j (j = C, H, O or N)
k	segment number
lat	latent
m	Moisture
N_2	Nitrogen
o	Outer
O_2	Oxygen
r	Radiative
ref	Reference temperature
sens	sensible
wet	Wet

Superscripts

a	Air

f	Feed
g	Gas
input	Input
output	Output
t	Tar

Mass and Energy Balances for Runs Performed

Run 1				Elemental Balance		
Mass Balance						
			Carbon	Hydrogen	Oxygen	Nitrogen
Feed Moisture content % (wb)	7.90					
Carbon % weight (daf)	53.04					
Hydrogen % weight (daf)	6.12					
Oxygen % weight (daf)	39.90					
Inputs Kg/h						
Wood	1.09					
Wood moisture	0.09					
Ash	0.00					
Oxygen in air	0.52					
Nitrogen in air	1.92					
Air moisture	0.01					
Total	3.53		0.58	0.07	0.95	1.92
Outputs Kg/h						
H2	0.04					
CO	0.61					
CO2	0.70					
CH4	0.03					
N2 (by difference)	1.92					
Tar	0.03					
Ash	0.00					
Total	3.32		0.50	0.05	0.86	1.92
Closure %	94.19		85.59	69.86	90.45	
Closure* %			90.87	74.17	96.03	
Efficiency indicators						
Mass yield kg/kg	3.01					
Volumetric yield Nm3/kg	2.70					
air/fuel ratio	2.22					
Mass conv. to dry prod. gas %	93.22					
Carbon conversion to gas %	81.34					
Equivalence ratio, %	31.00					
Specific capacity kg/m2h	247.60					
Energy Balance - Summary						
		MJ/h	% dry wood			
Energy input						
Dry wood	Chemical	23.28	100.00			
	Sensible	0.00	0.00			
Dry air	Sensible	0.00	0.00			
Air	Latent	0.04	0.15			
TOTAL		23.32				
Energy output						
Dry gas	Chemical	13.01	55.87			
	Sensible	2.64	11.36			
	Total	15.65	67.23			
Tars	Chemical	1.20	5.16			
	Sensible	0.03	0.13			
	Total	1.23	5.30			
Losses	Radiative	4.12	17.68			
	Convective	1.29	5.53			
	Total	5.40	23.21			
TOTAL		22.29	95.74			
Closure %		95.59				
EFFICIENCIES						
Cold gas %		55.87				
Hot gas %		67.23				
Raw gas %		72.53				

Run 2						
Mass Balance				Elemental Balance		
			Carbon	Hydrogen	Oxygen	Nitrogen
Feed Moisture content % (wb)		12.00				
Carbon % weight (daf)		53.04				
Hydrogen % weight (daf)		6.12				
Oxygen % weight (daf)		39.90				
Inputs Kg/h						
Wood		1.59				
Wood moisture		0.22				
Ash		0.00				
Oxygen in air		0.88				
Nitrogen in air		3.26				
Air moisture		0.02				
Total		5.73	0.84	0.10	1.51	3.26
Outputs Kg/h						
H2		0.05				
CO		1.01				
CO2		1.11				
CH4		0.04				
N2 (by difference)		3.26				
Tar		0.06				
Ash		0.00		.		
Total		5.53	0.81	0.07	1.40	3.26
Closure %		96.54	95.52	70.70	92.27	
Closure* %			98.94	73.23	95.58	
Efficiency indicators						
Mass yield kg/kg		3.44				
Volumetric yield Nm3/kg		3.03				
air/fuel ratio		2.60				
Mass conv. to dry prod. gas %		95.55				
Carbon conversion %		90.68				
Equivalence ratio, %		36.23				
Specific capacity kg/m2h		360.36				
Energy Balance - Summary						
		MJ/h	% dry wood			
Energy input						
Dry wood	Chemical	33.88	100.00			
	Sensible	0.00	0.00			
Dry air	Sensible	0.00	0.00			
Air	Latent	0.06	0.18			
TOTAL		33.94				
Energy output						
Dry gas	Chemical	20.22	59.66			
	Sensible	3.97	11.73			
	Total	24.19	71.39			
Tars	Chemical	1.99	5.87		.	
	Sensible	0.05	0.14			
	Total	2.04	6.01			
Losses	Radiative	10.17	30.01			
	Convective	1.59	4.70			
	Total	11.76	34.71			
TOTAL		37.99	112.11			
			.			
Closure %		111.91				
EFFICIENCIES						
Cold gas %		59.66				
Hot gas %		71.39				
Raw gas %		77.40				
	.					
				.		

Run 3				Elemental Balance		
Mass Balance						
			Carbon	Hydrogen	Oxygen	Nitrogen
Feed Moisture content % (wb)	11.07					
Carbon % weight (daf)	53.04					
Hydrogen % weight (daf)	6.12					
Oxygen % weight (daf)	39.90					
Inputs Kg/h						
Wood	1.50					
Wood moisture	0.19					
Ash	0.00					
Oxygen in air	0.70					
Nitrogen in air	2.60					
Air moisture	0.02					
Total	4.80		0.80	0.09	1.30	2.60
Outputs Kg/h						
H2	0.04					
CO	0.68					
CO2	0.85					
CH4	0.03					
N2 (by difference)	2.60					
Tar	0.04					
Ash	0.00					
Total	4.25		0.58	0.05	1.02	2.60
Closure %	88.50		73.06	54.70	78.29	
Closure* %			82.55	61.81	88.46	
Efficiency indicators						
Mass yield kg/kg	2.80					
Volumetric yield Nm3/kg	2.43					
air/fuel ratio	2.20					
Mass conv. to dry prod. gas %	87.60					
Carbon conversion %	69.14					
Equivalence ratio, %	30.65					
Specific capacity kg/m2h	339.91					
Energy Balance - Summary						
		MJ/h	% dry wood			
Energy input						
Dry wood	Chemical	31.96	100.00			
	Sensible	0.00	0.00			
Dry air	Sensible	0.00	0.00			
Air	Latent	0.05	0.17			
TOTAL		32.02				
Energy output						
Dry gas	Chemical	14.26	44.61			
	Sensible	2.37	7.43			
	Total	16.63	52.04			
Tars	Chemical	1.52	4.76			
	Sensible	0.03	0.09			
	Total	1.55	4.85			
Losses	Radiative	10.17	31.84			
	Convective	1.61	5.03			
	Total	11.78	36.87			
TOTAL		29.97	93.76			
Closure %		93.60				
EFFICIENCIES						
Cold gas %		44.61				
Hot gas %		52.04				
Raw gas %		56.90				

Run 4 - Sewage sludge				Elemental Balance		
Mass Balance						
			Carbon	Hydrogen	Oxygen	Nitrogen
Feed Moisture content % (wb)		10.26				
Carbon % weight (daf)		45.19				
Hydrogen % weight (daf)		5.29				
Oxygen % weight (daf)		45.09				
Inputs Kg/h						
Feed		0.45		3.13		
Feed moisture		0.08				
Ash		0.23				
Oxygen in air		0.50				
Nitrogen in air		1.85				
Air moisture		0.02				
Total		3.03	0.20	0.02	0.70	1.85
Outputs Kg/h						
H2		0.01				
CO		0.16				
CO2		0.50				
CH4		0.00				
N2 (by difference)		1.85				
Tar		0.00				
Ash		0.23				
Total		2.76	0.21	0.01	0.45	1.85
Closure %		90.86	102.13	40.04	64.71	
Closure* %			112.39	44.07	71.22	
Efficiency indicators						
Mass yield kg/kg		5.62				
Volumetric yield Nm3/kg		4.33				
air/fuel ratio		5.24				
Mass conv. to dry prod. gas %		90.10				
Carbon conversion %		69.65				
Equivalence ratio, %		90.10				
Specific capacity kg/m2h		101.59				
Energy Balance - Summary						
		MJ/h	% dry wood			
Energy input						
Dry wood	Chemical	7.17	100.00			
	Sensible	0.00	0.00			
Dry air	Sensible	0.00	0.00			
Air	Latent	0.04	0.55			
TOTAL		7.21				
Energy output						
Dry gas	Chemical	3.07	42.82			
	Sensible	1.15	16.09			
	Total	4.22	58.91			
Tars	Chemical	0.00	0.00			
	Sensible	0.00	0.00			
	Total	0.00	0.00			
Losses	Radiative	1.36	18.95			
	Convective	0.54	7.48			
	Total	1.89	26.43			
TOTAL		6.12	85.34			
Closure %		84.88				
EFFICIENCIES						
Cold gas %		42.82				
Hot gas %		58.91				
Raw gas %		58.91				

Run 5							
Mass Balance				Elemental Balance			
				Carbon	Hydrogen	Oxygen	Nitrogen
Feed Moisture content % (wb)		9.78					
Carbon % weight (daf)		53.04					
Hydrogen % weight (daf)		6.12					
Oxygen % weight (daf)		39.90					
Inputs Kg/h							
Wood		1.26					
Wood moisture		0.14					
Ash		0.00					
Oxygen in air		0.64					
Nitrogen in air		2.39					
Air moisture		0.02					
Total		4.29		0.67	0.08	1.15	2.39
Outputs Kg/h							
H2		0.04					
CO		0.67					
CO2		1.08					
CH4		0.04					
N2 (by difference)		2.39					
Tar		0.04					
Ash		0.00					
Total		4.26		0.65	0.05	1.18	2.39
Closure %		99.38		96.44	67.67	102.96	
Closure* %				97.05	68.10	103.61	
Efficiency indicators							
Mass yield kg/kg		3.34					
Volumetric yield Nm3/kg		2.82					
air/fuel ratio		2.40					
Mass conv. to dry prod. gas %		98.38					
Carbon conversion %		91.82					
Equivalence ratio, %		33.44					
Specific capacity kg/m2h		285.70					
Energy Balance - Summary							
		MJ/h	% dry wood				
Energy input							
Dry wood	Chemical	26.86	100.00				
	Sensible	0.00	0.00				
Dry air	Sensible	0.00	0.00				
Air	Latent	0.04	0.17				
TOTAL		26.91					
Energy output							
Dry gas	Chemical	14.60	54.34				
	Sensible	2.01	7.49				
	Total	16.61	61.83				
Tars	Chemical	1.51	5.61				
	Sensible	0.03	0.09				
	Total	1.53	5.71				
Losses	Radiative	7.60	28.29				
	Convective	1.55	5.77				
	Total	9.15	34.06				
TOTAL		27.29	101.60				
Closure %		101.43					
EFFICIENCIES							
Cold gas %		54.34					
Hot gas %		61.83					
Raw gas %		67.54					

Run 6						
Mass Balance				Elemental Balance		
			Carbon	Hydrogen	Oxygen	Nitrogen
Feed Moisture content % (wb)	9.76					
Carbon % weight (daf)	50.13					
Hydrogen % weight (daf)	6.34					
Oxygen % weight (daf)	42.32					
Inputs Kg/h						
Wood	1.24					
Wood moisture	0.14					
Ash	0.01					
Oxygen in air	0.60					
Nitrogen in air	2.24					
Air moisture	0.03					
Total	4.09		0.62	0.08	1.13	2.24
Outputs Kg/h						
H2	0.04					
CO	0.67					
CO2	1.03					
CH4	0.04					
N2 (by difference)	2.24					
Tar	0.04					
Ash	0.01					
Total	4.07		0.63	0.05	1.14	2.24
Closure %	99.41		101.10	66.31	100.94	
Closure* %			101.70	66.70	101.54	
Efficiency indicators						
Mass yield kg/kg	3.23					
Volumetric yield Nm3/kg	2.75					
air/fuel ratio	2.28					
Mass conv. to dry prod. gas %	98.41					
Carbon conversion %	96.36					
Equivalence ratio, %	33.62					
Specific capacity kg/m2h	281.67					
Energy Balance - Summary						
		MJ/h	% dry wood			
Energy input						
Dry wood	Chemical	25.34	100.00			
	Sensible	0.00	0.00			
Dry air	Sensible	0.00	0.00			
Air	Latent	0.07	0.29			
TOTAL		25.41				
Energy output						
Dry gas	Chemical	14.67	57.91			
	Sensible	1.96	7.75			
	Total	16.64	65.66			
Tars	Chemical	1.44	5.68			
	Sensible	0.02	0.10			
	Total	1.46	5.78			
Losses	Radiative	7.59	29.97			
	Convective	1.54	6.06			
	Total	9.13	36.03			
TOTAL		27.23	107.47			
Closure %		107.17				
EFFICIENCIES						
Cold gas %		57.91				
Hot gas %		65.66				
Raw gas %		71.44				

Run 7							
Mass Balance				Elemental Balance			
				Carbon	Hydrogen	Oxygen	Nitrogen
Feed Moisture content % (wb)		9.50					
Carbon % weight (daf)		53.04					
Hydrogen % weight (daf)		6.12					
Oxygen % weight (daf)		0.93					
Inputs Kg/h							
Wood		1.12					
Wood moisture		0.12					
Ash		0.00					
Oxygen in air		0.70					
Nitrogen in air		2.62					
Air moisture		0.02					
Total		4.45		0.59	0.07	1.15	2.62
Outputs Kg/h							
H2		0.03					
CO		0.65					
CO2		1.07					
CH4		0.04					
N2 (by difference)		2.62					
Tar		0.04					
Ash		0.00					
Total		4.45		0.63	0.04	1.16	2.62
Closure %		100.15		105.95	64.54	100.54	
Closure* %				105.79	64.44	100.39	
Efficiency indicators							
Mass yield kg/kg		3.93					
Volumetric yield Nm3/kg		3.21					
air/fuel ratio		2.97					
Mass conv. to dry prod. gas %		99.15					
Carbon conversion %		100.50					
Equivalence ratio, %		41.33					
Specific capacity kg/m2h		253.84					
Energy Balance - Summary							
		MJ/h	% dry wood				
Energy input							
Dry wood	Chemical	23.87	100.00				
	Sensible	0.00	0.00				
Dry air	Sensible	0.00	0.00				
Air	Latent	0.05	0.21				
TOTAL		23.92					
Energy output							
Dry gas	Chemical	13.10	54.89				
	Sensible	2.50	10.48				
	Total	15.60	65.37				
Tars	Chemical	1.56	6.53				
	Sensible	0.03	0.13				
	Total	1.59	6.66				
Losses	Radiative	10.18	42.63				
	Convective	1.61	6.75				
	Total	11.79	49.38				
TOTAL		28.98	121.41				
Closure %		121.16					
EFFICIENCIES							
Cold gas %		54.89					
Hot gas %		65.37					
Raw gas %		72.03					

Run 8 (based on assumed data)						
Mass Balance				Elemental Balance		
			Carbon	Hydrogen	Oxygen	Nitrogen
Feed Moisture content % (wb)		10.00				
Carbon % weight (daf)		49.47				
Hydrogen % weight (daf)		6.47				
Oxygen % weight (daf)		0.48				
Inputs Kg/h						
Wood		1.41				
Wood moisture		0.16				
Ash		0.00				
Oxygen in air		0.88				
Nitrogen in air		3.28				
Air moisture		0.02				
Total		5.57	0.70	0.09	1.49	3.28
Outputs Kg/h						
H2		0.04				
CO		0.78				
CO2		1.38				
CH4		0.03				
N2 (by difference)		3.28				
Tar		0.05				
Ash		0.00				
Total		5.55	0.77	0.05	1.46	3.28
Closure %		99.79	110.88	53.15	97.53	
Closure* %			111.12	53.26	97.73	
Efficiency indicators						
Mass yield kg/kg		3.91				
Volumetric yield Nm3/kg		3.13				
air/fuel ratio		2.96				
Mass conv. to dry prod. gas %		98.80				
Carbon conversion %		105.19				
Equivalence ratio, %		44.47				
Specific capacity kg/m2h		318.28				
Energy Balance - Summary						
		MJ/h	% dry wood			
Energy input						
Dry wood	Chemical	28.37	100.00			
	Sensible	0.00	0.00			
Dry air	Sensible	0.00	0.00			
Air	Latent	0.06	0.22			
TOTAL		28.43				
Energy output						
Dry gas	Chemical	14.72	51.87			
	Sensible	3.07	10.81			
	Total	17.78	62.68			
Tars	Chemical	1.93	6.80			
	Sensible	0.04	0.14			
	Total	1.97	6.94			
Losses	Radiative	10.18	35.87			
	Convective	1.61	5.68			
	Total	11.79	41.55			
TOTAL		31.54	111.16			
Closure %		110.92				
EFFICIENCIES						
Cold gas %		51.87				
Hot gas %		62.68				
Raw gas %		69.61				

Run 9						
Mass Balance				Elemental Balance		
			Carbon	Hydrogen	Oxygen	Nitrogen
Feed Moisture content % (wb)		9.50				
Carbon % weight (daf)		53.04				
Hydrogen % weight (daf)		6.12				
Oxygen % weight (daf)		39.90				
Inputs Kg/h						
Wood		1.13				
Wood moisture		0.12				
Ash		0.00	.			
Oxygen in air		0.66				
Nitrogen in air		2.43				
Air moisture		0.02				
Total		4.22	0.60	0.07	1.10	2.43
Outputs Kg/h						
H2		0.02		.		
CO		0.49				
CO2		0.91				
CH4		0.03				
N2 (by difference)		2.43				
Tar		0.04				
Ash		0.00				
Total		3.92	0.51	0.03	0.95	2.43
Closure %		93.01	84.66	45.88	85.92	
Closure %			91.03	49.33	92.39	
Efficiency indicators						
Mass yield kg/kg		3.45				
Volumetric yield Nm3/kg		2.74				
air/fuel ratio		2.74				
Mass conv. to dry prod. gas %		92.09				
Carbon conversion %		80.00				
Equivalence ratio, %		38.24				
Specific capacity kg/m2h		254.92				
Energy Balance - Summary						
		MJ/h	% dry wood			
Energy input						
Dry wood	Chemical	23.97	100.00			
	Sensible	0.00	0.00			
Dry air	Sensible	0.00	0.00			
Air	Latent	0.05	0.19			
TOTAL		24.01				
Energy output						
Dry gas	Chemical	9.54	39.80			
	Sensible	2.46	10.24			
	Total	12.00	50.05			
Tars	Chemical	1.36	5.66			
	Sensible	0.03	0.13			
	Total	1.39	5.79			
Losses	Radiative	6.85	28.59			
	Convective	0.85	3.55			
	Total	7.70	32.14			
TOTAL		21.09	87.98			
Closure %		87.81				
EFFICIENCIES						
Cold gas %		39.80				
Hot gas %		50.05				
Raw gas %		55.84				

Run 10				Elemental Balance		
Mass Balance						
			Carbon	Hydrogen	Oxygen	Nitrogen
Feed Moisture content % (wb)		9.54				
Carbon % weight (daf)		53.04				
Hydrogen % weight (daf)		6.12				
Oxygen % weight (daf)		39.90				
Inputs Kg/h						
Wood		1.32				
Wood moisture		0.14				
Ash		0.00				
Oxygen in air		0.96				
Nitrogen in air		2.99				
CO2 input		1.14				
Air moisture		0.03				
Total		6.41	1.01	0.10	1.94	2.99
Outputs Kg/h						
H2		0.03				
CO		0.70				
CO2		1.53				
CH4		0.04				
N2 (by difference)		2.99				
Tar		0.05				
Ash		0.00				
Total		5.36	0.79	0.05	1.53	2.99
Closure %		83.62	78.10	49.61	78.72	
Closure %			92.81	58.95	93.55	
Efficiency indicators						
Mass yield kg/kg		4.01				
Volumetric yield Nm3/kg		3.17				
air/fuel ratio		2.97				
Mass conv. to dry prod. gas %		124.28				
Carbon conversion %		93.33				
Equivalence ratio, %		53.28				
Specific capacity kg/m2h		299.35				
Energy Balance - Summary						
		MJ/h	% dry wood			
Energy input						
Dry wood	Chemical	28.15	100.00			
	Sensible	0.00	0.00			
Dry air	Sensible	0.00	0.00			
Air	Latent	0.07	0.23			
TOTAL		28.21				
Energy output						
Dry gas	Chemical	14.36	51.03			
	Sensible	2.42	8.58			
	Total	16.78	59.61			
Tars	Chemical	1.86	6.62			
	Sensible	0.03	0.11			
	Total	1.90	6.73			
Losses	Radiative	9.42	33.46			
	Convective	1.60	5.67			
	Total	11.01	39.13			
TOTAL		29.69	105.47			
Closure %		105.22				
EFFICIENCIES						
Cold gas %		51.03				
Hot gas %		59.61				
Raw gas %		66.34				

384

Run 11						
Mass Balance				Elemental Balance		
			Carbon	Hydrogen	Oxygen	Nitrogen
Feed Moisture content % (wb)		9.54				
Carbon % weight (daf)		53.04				
Hydrogen % weight (daf)		6.12				
Oxygen % weight (daf)		0.93	.			
Inputs Kg/h						
Wood		0.72				
Wood moisture		0.08				
Ash		0.00				
Oxygen in air		0.62				
Nitrogen in air		2.04				
CO2 input		0.22				
Air moisture		0.02				
Total		0.00	0.44	0.05	1.05	2.04
Outputs Kg/h						
H2		0.02				
CO		0.47				
CO2		1.02				
CH4		0.03				
N2 (by difference)		2.04				
Tar		0.04				
Ash		0.00				
Total		3.61	0.52	0.03	1.01	2.04
Closure %		#DIV/0!	117.74	58.83	96.43	
Closure* %			116.70	58.31	95.58	
Efficiency indicators						
Mass yield kg/kg		4.94				
Volumetric yield Nm3/kg		3.91				
air/fuel ratio		3.71				
Mass conv. to dry prod. gas %		99.15				
Carbon conversion %		77.02				
Equivalence ratio, %		62.90				
Specific capacity kg/m2h		163.65				
Energy Balance - Summary						
		MJ/h	% dry wood		.	
Energy input						
Dry wood	Chemical	15.39	100.00			
	Sensible	0.00	0.00			
Dry air	Sensible	0.00	0.00			
Air	Latent	0.05	0.30			
TOTAL		15.43				
			.			
Energy output						
Dry gas	Chemical	9.44	61.35			
	Sensible	1.37	8.93			
	Total	10.81	70.28			
Tars	Chemical	1.26	8.16			
	Sensible	0.03	0.21			
	Total	1.29	8.37			
Losses	Radiative	6.58	42.74			
	Convective	1.47	9.52			
	Total	8.04	52.26			
TOTAL		20.14	130.90			
Closure %		130.52				
EFFICIENCIES						
Cold gas %		61.35				
Hot gas %		70.28				
Raw gas %		88.22				

Run 12				Elemental Balance			
Mass Balance				Carbon	Hydrogen	Oxygen	Nitrogen
Feed Moisture content % (wb)		9.50					
Carbon % weight (daf)		53.04					
Hydrogen % weight (daf)		6.12					
Oxygen % weight (daf)		0.93					
Inputs Kg/h							
Wood		0.77					
Wood moisture		0.08					
Ash		0.00					
Oxygen in air and added		0.46					
Nitrogen in air		1.51					
CO2 input		0.56					
Air moisture		0.01					
Total		3.31		0.56	0.06	1.01	1.53
Outputs Kg/h							
H2		0.02					
CO		0.38					
CO2		0.85					
CH4		0.02					
N2 (by difference)		1.53					
Tar		0.03					
Ash		0.00					
Total		2.82		0.43	0.02	0.84	1.53
Closure %		85.33		76.51	40.77	83.40	
Closure* %				89.67	47.78	97.74	
Efficiency indicators							
Mass yield kg/kg		3.64					
Volumetric yield Nm3/kg		2.85					
air/fuel ratio		2.63					
Mass conversion to wet produc		81.71					
Carbon conversion %		99.70					
Equivalence ratio, %		44.49					
Specific capacity kg/m2h		174.00					
Energy Balance - Summary							
		MJ/h	% dry wood				
Energy input							
Dry wood	Chemical	16.36	100.00				
	Sensible	0.00	0.00				
Dry air	Sensible	0.00	0.00				
Air	Latent	0.03	0.21				
TOTAL		16.40					
Energy output							
Dry gas	Chemical	7.27	44.41				
	Sensible	1.32	8.04				
	Total	8.58	52.45				
Tars	Chemical	0.98	6.00				
	Sensible	0.03	0.18				
	Total	1.01	6.19				
Losses	Radiative	9.42	57.59				
	Convective	1.60	9.77				
	Total	11.02	67.36				
TOTAL		20.61	126.00				
Closure %		136.40					
EFFICIENCIES							
Cold gas %		44.41					
Hot gas %		52.45					
Raw gas %		69.32					

Run 13						
Mass Balance				Elemental Balance		
			Carbon	Hydrogen	Oxygen	Nitrogen
Feed Moisture content % (wb)	9.54					
Carbon % weight (daf)	50.74					
Hydrogen % weight (daf)	5.62					
Oxygen % weight (daf)	43.05					
Inputs Kg/h						
Wood	1.02					
Wood moisture	0.11					
Ash	0.00					
Oxygen in air	0.39					
Nitrogen in air	1.46					
Air moisture	0.02					
Total	2.87		0.52	0.06	0.83	1.46
Outputs Kg/h						
H2	0.02					
CO	0.37					
CO2	0.66					
CH4	0.02					
N2 (by difference)	1.46					
Tar	0.03					
Ash	0.00					
Total	2.56		0.37	0.02	0.70	1.46
Closure %	88.99		71.82	40.55	84.22	
Closure* %			80.71	45.57	94.65	
Efficiency indicators						
Mass yield kg/kg	2.48					
Volumetric yield Nm3/kg	1.99					
air/fuel ratio	1.82					
Mass conv. to dry prod. gas %	88.09					
Carbon conversion %	68.29					
Equivalence ratio, %	25.37					
Specific capacity kg/m2h	230.18					
Energy Balance - Summary						
		MJ/h	% dry wood			
Energy input						
Dry wood	Chemical	19.83	100.00			
	Sensible	0.00	0.00			
Dry air	Sensible	0.00	0.00			
Air	Latent	0.04	0.19			
TOTAL		19.87				
Energy output						
Dry gas	Chemical	8.85	44.64			
	Sensible	1.08	5.44			
	Total	9.93	50.08			
Tars	Chemical	0.89	4.46			
	Sensible	0.01	0.07			
	Total	0.90	4.54			
Losses	Radiative	10.17	51.29			
	Convective	1.60	8.06			
	Total	11.77	59.35			
TOTAL		22.60	113.96			
Closure %		113.74				
EFFICIENCIES						
Cold gas %		44.64				
Hot gas %		50.08				
Raw gas %		54.61				

Run 14				Elemental Balance		
Mass Balance						
			Carbon	Hydrogen	Oxygen	Nitrogen
Feed Moisture content % (wb)		9.71				
Carbon % weight (daf)		53.04				
Hydrogen % weight (daf)		6.12				
Oxygen % weight (daf)		39.90				
Inputs Kg/h						
Wood		1.30				
Wood moisture		0.14				
Ash		0.00				
Oxygen in air		0.86				
Nitrogen in air		3.19				
Air moisture		0.03				
Total		5.35	0.69	0.08	1.38	3.19
Outputs Kg/h						
H2		0.03				
CO		0.68				
CO2		1.34				
CH4		0.02				
N2 (by difference)		3.19				
Tar		0.05				
Ash		0.00				
Total		5.32	0.71	0.05	1.37	3.19
Closure %		99.36	103.10	56.82	99.36	
Closure* %			103.76	57.18	99.99	
Efficiency indicators						
Mass yield kg/kg		4.05				
Volumetric yield Nm3/kg		3.25				
air/fuel ratio		3.12				
Mass conv. to dry prod. gas %		98.38				
Carbon conversion %		97.60				
Equivalence ratio, %		43.50				
Specific capacity kg/m2h		294.09				
Energy Balance - Summary						
		MJ/h	% dry wood			
Energy input						
Dry wood	Chemical	27.58	100.00			
	Sensible	0.00	0.00			
Dry air	Sensible	0.00	0.00			
Air	Latent	0.07	0.25			
TOTAL		27.65				
Energy output						
Dry gas	Chemical	13.18	47.77			
	Sensible	3.02	10.94			
	Total	16.19	58.71			
Tars	Chemical	1.84	6.69			
	Sensible	0.04	0.14			
	Total	1.88	6.82			
Losses	Radiative	10.16	36.85			
	Convective	1.58	5.73			
	Total	11.74	42.57			
TOTAL		29.82	108.11			
Closure %		107.84				
EFFICIENCIES						
Cold gas %		47.77				
Hot gas %		58.71				
Raw gas %		65.53				

Run 15				Elemental Balance			
Mass Balance				Carbon	Hydrogen	Oxygen	Nitrogen
Feed Moisture content % (wb)		9.71					
Carbon % weight (daf)		53.04					
Hydrogen % weight (daf)		6.12					
Oxygen % weight (daf)		39.90					
Inputs Kg/h							
Wood		1.63					
Wood moisture		0.18					
Ash		0.00					
Oxygen in air		0.87					
Nitrogen in air		3.23					
Air moisture		0.03					
Total		5.74		0.87	0.10	1.52	3.23
Outputs Kg/h							
H2		0.05					
CO		0.93					
CO2		1.57					
CH4		0.04					
N2 (by difference)		3.23					
Tar		0.06					
Ash		0.00					
Total		5.89		0.90	0.06	1.69	3.23
Closure %		102.59		104.16	62.96	110.83	
Closure* %				101.53	61.37	108.03	
Efficiency indicators							
Mass yield kg/kg		3.57					
Volumetric yield Nm3/kg		2.93					
Air/fuel ratio		2.51					
Mass conv. to dry prod. gas %		101.56					
Carbon conversion %		99.27					
Equivalence ratio, %		35.02					
Specific capacity kg/m2h		369.66					
Energy Balance - Summary		MJ/h		% dry wood			
Energy input							
Dry wood	Chemical	34.76		100.00			
	Sensible	0.00		0.00			
Dry air	Sensible	0.00		0.00			
Air	Latent	0.07		0.21			
TOTAL		34.83					
Energy output							
Dry gas	Chemical	18.60		53.51			
	Sensible	2.96		8.51			
	Total	21.56		62.02			
Tars	Chemical	2.06		5.92			
	Sensible	0.04		0.11			
	Total	2.10		6.03			
Losses	Radiative	10.17		29.25			
	Convective	1.59		4.58			
	Total	11.76		33.83			
TOTAL		35.41		101.88			
Closure %		101.67					
EFFICIENCIES							
Cold gas %		53.51					
Hot gas %		62.02					
Raw gas %		68.06					

Run 16				Elemental Balance		
Mass Balance						
			Carbon	Hydrogen	Oxygen	Nitrogen
Feed Moisture content % (wb)		32.13				
Carbon % weight (daf)		53.04				
Hydrogen % weight (daf)		6.12				
Oxygen % weight (daf)		39.90				
Inputs Kg/h						
Wood		0.46				
Wood moisture		0.22				
Ash		0.00				
Oxygen in air		0.25				
Nitrogen in air		0.92				
Air moisture		0.01				
Total		1.63	0.24	0.03	0.43	0.92
Outputs Kg/h						
H2		0.01				
CO		0.20				
CO2		0.50				
CH4		0.01				
N2 (by difference)		0.92				
Tar		0.02				
Ash		0.00				
Total		1.66	0.24	0.02	0.48	0.92
Closure %		101.77	99.17	55.00	111.07	
Closure* %			97.45	54.04	109.15	
Efficiency indicators						
Mass yield kg/kg		3.57				
Volumetric yield Nm3/kg		2.79				
air/fuel ratio		2.55				
Mass conv. to dry prod. gas %		100.77				
Carbon conversion %		94.30				
Equivalence ratio, %		35.53				
Specific capacity kg/m2h		104.07				
Energy Balance - Summary						
		MJ/h	% dry wood			
Energy input						
Dry wood	Chemical	9.76	100.00			
	Sensible	0.00	0.00			
Dry air	Sensible	0.00	0.00			
Air	Latent	0.02	0.20			
TOTAL		9.78				
Energy output						
Dry gas	Chemical	4.25	43.58			
	Sensible	0.68	6.98			
	Total	4.93	50.56			
Tars	Chemical	0.57	5.85			
	Sensible	0.01	0.09			
	Total	0.58	5.94			
Losses	Radiative	6.56	67.22			
	Convective	1.40	14.33			
	Total	7.96	81.56			
TOTAL		13.47	138.06			
Closure %		137.78				
EFFICIENCIES						
Cold gas %		43.58				
Hot gas %		50.56				
Raw gas %		56.50				

Run 17						
Mass Balance				Elemental Balance		
			Carbon	Hydrogen	Oxygen	Nitrogen
Feed Moisture content % (wb)		32.13				
Carbon % weight (daf)		53.04				
Hydrogen % weight (daf)		6.12				
Oxygen % weight (daf)		39.90				
Inputs Kg/h						
Wood		0.66				
Wood moisture		0.31				
Ash		0.00				
Oxygen in air		0.40				
Nitrogen in air		1.50				
Air moisture		0.01				
Total		2.57	0.35	0.04	0.67	1.50
Outputs Kg/h						
H2		0.02				
CO		0.31				
CO2		0.89				
CH4		0.02				
N2 (by difference)		1.50				
Tar		0.03				
Ash		0.00				
Total		2.77	0.41	0.03	0.83	1.50
Closure %		108.06	118.51	63.53	124.46	
Closure* %			109.67	58.79	115.18	
Efficiency indicators						
Mass yield kg/kg		4.18				
Volumetric yield Nm3/kg		3.21				
air/fuel ratio		2.90				
Mass conv. to dry prod. gas %		107.01				
Carbon conversion %		112.84				
Equivalence ratio, %		40.53				
Specific capacity kg/m2h		148.74				
Energy Balance - Summary						
		MJ/h	% dry wood			
Energy input						
Dry wood	Chemical	20.57	100.00			
	Sensible	0.00	0.00			
Dry air	Sensible	0.00	0.00			
Air	Latent	0.03	0.16			
TOTAL		20.60				
Energy output						
Dry gas	Chemical	6.96	33.82			
	Sensible	0.90	4.35			
	Total	7.85	38.17			
Tars	Chemical	0.95	4.61			
	Sensible	0.01	0.06			
	Total	0.96	4.67			
Losses	Radiative	6.56	31.91			
	Convective	1.40	6.82			
	Total	7.96	38.73			
TOTAL		16.78	81.57			
Closure %		81.44				
EFFICIENCIES						
Cold gas %		33.82				
Hot gas %		38.17				
Raw gas %		42.84				

Run 18	Platon gas flow only, gasmeter flow unavailable					
Mass Balance				Elemental Balance		
			Carbon	Hydrogen	Oxygen	Nitrogen
Feed Moisture content % (wb)		32.13				
Carbon % weight (daf)		53.04				
Hydrogen % weight (daf)		6.12				
Oxygen % weight (daf)		39.90				
Inputs Kg/h						
Wood		0.48				
Wood moisture		0.23				
Ash		0.00				
Oxygen in air		0.42				
Nitrogen in air		1.55				
Air moisture		0.02				
Total		2.45	0.26	0.03	0.61	1.55
Outputs Kg/h						
H2		0.01				
CO		0.26				
CO2		0.90				
CH4		0.02				
N2 (by difference)		1.55				
Tar		0.03				
Ash		0.00				
Total		2.77	0.39	0.02	0.81	1.55
Closure %		112.85	151.53	73.75	132.09	
Closure* %			134.28	65.35	117.05	
Efficiency indicators						
Mass yield kg/kg		5.69				
Volumetric yield Nm3/kg		4.28				
air/fuel ratio		4.09				
Mass conv. to dry prod. gas %		111.76				
Carbon conversion %		143.99				
Equivalence ratio, %		57.05				
Specific capacity kg/m2h		109.19				
Energy Balance - Summary						
		MJ/h	% dry wood			
Energy input						
Dry wood	Chemical	10.24	100.00			
	Sensible	0.00	0.00			
Dry air	Sensible	0.00	0.00			
Air	Latent	0.04	0.40			
TOTAL		10.28				
Energy output						
Dry gas	Chemical	5.75	56.11			
	Sensible	0.78	7.60			
	Total	6.52	63.71			
Tars	Chemical	0.94	9.17			
	Sensible	0.01	0.10			
	Total	0.95	9.28			
Losses	Radiative	7.10	69.34			
	Convective	1.48	14.41			
	Total	8.58	83.76			
TOTAL		16.05	156.74			
Closure %		156.11				
EFFICIENCIES						
Cold gas %		56.11				
Hot gas %		63.71				
Raw gas %		72.98				

Run 19						
Mass Balance				Elemental Balance		
			Carbon	Hydrogen	Oxygen	Nitrogen
Feed Moisture content % (wb)		18.59				
Carbon % weight (daf)		53.04				
Hydrogen % weight (daf)		6.12				
Oxygen % weight (daf)		39.90				
Inputs Kg/h						
Wood		0.89				
Wood moisture		0.20				
Ash		0.00				
Oxygen in air		0.59				
Nitrogen in air		2.18				
Air moisture		0.02				
Total		3.65	0.47	0.05	0.94	2.18
Outputs Kg/h						
H2		0.02				
CO		0.41				
CO2		1.04				
CH4		0.02				
N2 (by difference)		2.18				
Tar		0.04				
Ash		0.00				
Total		3.71	0.50	0.03	1.00	2.18
Closure %		101.50	106.18	62.06	105.81	
Closure* %			104.61	61.14	104.25	
Efficiency indicators						
Mass yield kg/kg		4.11				
Volumetric yield Nm3/kg		3.27				
air/fuel ratio		3.09				
Mass conv. to dry prod. gas %		100.50				
Carbon conversion %		100.61				
Equivalence ratio, %		43.16				
Specific capacity kg/m2h		202.01				
Energy Balance - Summary						
		MJ/h	% dry wood			
Energy input						
Dry wood	Chemical	18.95	100.00			
	Sensible	0.00	0.00			
Dry air	Sensible	0.00	0.00			
Air	Latent	0.05	0.27			
TOTAL		19.00				
Energy output						
Dry gas	Chemical	9.06	47.80			
	Sensible	1.78	9.42			
	Total	10.84	57.22			
Tars	Chemical	1.28	6.77			
	Sensible	0.02	0.12			
	Total	1.31	6.89			
Losses	Radiative	12.40	65.44			
	Convective	1.65	8.70			
	Total	14.05	74.14			
TOTAL		26.19	138.25			
Closure %		137.88				
EFFICIENCIES						
Cold gas %		47.80				
Hot gas %		57.22				
Raw gas %		64.10				

Run 20				Elemental Balance			
Mass Balance							
				Carbon	Hydrogen	Oxygen	Nitrogen
Feed Moisture content % (wb)		18.59					
Carbon % weight (daf)		53.04					
Hydrogen % weight (daf)		6.12					
Oxygen % weight (daf)		39.90			·		
Inputs Kg/h							
Wood		1.73					
Wood moisture		0.40					
Ash		0.00					
Oxygen in air		0.77					
Nitrogen in air		2.86					
Air moisture		0.03					
Total		5.37		0.92	0.11	1.46	2.86
Outputs Kg/h							
H2		0.04					
CO		0.72					
CO2		1.37					
CH4		0.03					
N2 (by difference)		2.86					
Tar		0.05					
Ash		0.00					
Total		5.07		0.74	0.06	1.41	2.86
Closure %		94.50		80.48	51.90	96.68	
Closure* %				85.16	54.92	102.30	
Efficiency indicators							
Mass yield kg/kg		2.90					
Volumetric yield Nm3/kg		2.40					
air/fuel ratio		2.10					
Mass conv.n to dry prod. gas %		93.56					
Carbon conversion %		76.50					
Equivalence ratio, %		29.29					
Specific capacity kg/m2h		392.06			·		
Energy Balance - Summary							
		MJ/h	% dry wood				
Energy input							
Dry wood	Chemical	36.77	100.00				
	Sensible	0.00	0.00				
Dry air	Sensible	0.00	0.00				
Air	Latent	0.07	0.18				
TOTAL		36.84					
Energy output							
Dry gas	Chemical	15.18	41.27				
	Sensible	2.72	7.40				
	Total	17.90	48.67				
Tars	Chemical	1.78	4.84				
	Sensible	0.03	0.09				
	Total	1.81	4.93				
Losses	Radiative	12.40	33.72				
	Convective	1.65	4.48				
	Total	14.04	38.19				
TOTAL		33.75	91.79				
Closure %		91.63					
EFFICIENCIES							
Cold gas %		41.27					
Hot gas %		48.67			·		
Raw gas %		53.60					

Run 21				Elemental Balance		
Mass Balance						
			Carbon	Hydrogen	Oxygen	Nitrogen
Feed Moisture content % (wb)		18.72				
Carbon % weight (daf)		53.04				
Hydrogen % weight (daf)		6.12				
Oxygen % weight (daf)		39.90				
Inputs Kg/h						
Wood		0.72				
Wood moisture		0.17				
Ash		0.00				
Oxygen in air		0.47		.		
Nitrogen in air		1.74		.		
Air moisture		0.02			.	
Total		2.94	0.38	0.04	0.76	1.74
Outputs Kg/h						
H2		0.01				
CO		0.24				
CO2		0.66				
CH4		0.01				
N2 (by difference)		1.74				
Tar		0.03				
Ash		0.00				
Total		2.69	0.31	0.02	0.62	1.74
Closure %		91.75	80.80	42.69	81.95	
Closure* %			88.07	46.53	89.32	
Efficiency indicators						
Mass yield kg/kg		3.69				
Volumetric yield Nm3/kg		2.89				
air/fuel ratio		3.07				
Mass conv. to dry prod. gas %		90.85				
Carbon conversion %		75.84				
Equivalence ratio, %		42.79				
Specific capacity kg/m2h		163.40				
Energy Balance - Summary						
		MJ/h	% dry wood			
Energy input						
Dry wood	Chemical	15.32	100.00	.		
	Sensible	0.00	0.00	.		
Dry air	Sensible	0.00	0.00			
Air	Latent	0.05	0.30			
TOTAL		15.37				
Energy output						
Dry gas	Chemical	5.02	32.78			
	Sensible	1.17	7.61			
	Total	6.19	40.39			
Tars	Chemical	0.92	6.03			
	Sensible	0.02	0.10			
	Total	0.94	6.13			
Losses	Radiative	12.39	80.86			
	Convective	1.63	10.66			
	Total	14.03	91.52			
TOTAL		21.16	138.05			
Closure %		137.63				
EFFICIENCIES					*	
Cold gas %		32.78				
Hot gas %		40.39				
Raw gas %		46.52				

Run 22						
Mass Balance				Elemental Balance		
			Carbon	Hydrogen	Oxygen	Nitrogen
Feed Moisture content % (wb)	8.91					
Carbon % weight (daf)	53.04					
Hydrogen % weight (daf)	6.12					
Oxygen % weight (daf)	0.93					
Inputs Kg/h						
Wood	1.21					
Wood moisture	0.12					
Ash	0.00					
Oxygen in air	0.74					
Nitrogen in air	2.76					
Air moisture	0.03					
Total	4.72	0.64	0.07	1.23	2.76	
Outputs Kg/h						
H2	0.03		•			
CO	0.59					
CO2	1.10					
CH4	0.03					
N2 (by difference)	2.76					
Tar	0.05					
Ash	0.00					
Total	4.56	0.61	0.04	1.15	2.76	
Closure %	96.64	94.46	58.45	93.42		
Closure* %		97.74	60.48	96.67		
Efficiency indicators						
Mass yield kg/kg	3.73					
Volumetric yield Nm3/kg	3.06					
air/fuel ratio	2.89					
Mass conv. to dry prod. gas %	95.68					
Carbon conversion %	89.36					
Equivalence ratio, %	40.34					
Specific capacity kg/m2h	274.03					
Energy Balance - Summary						
		MJ/h	% dry wood			
Energy input						
Dry wood	Chemical	25.77	100.00			
	Sensible	0.00	0.00			
Dry air	Sensible	0.00	0.00			
Air	Latent	0.06	0.25			
TOTAL		25.83				
Energy output						
Dry gas	Chemical	12.24	47.49			
	Sensible	2.65	10.28			
	Total	14.89	57.77			
Tars	Chemical	1.59	6.18			
	Sensible	0.03	0.13			
	Total	1.63	6.31			
Losses	Radiative	10.16	39.42			
	Convective	1.57	6.09			
	Total	11.73	45.51			
TOTAL		28.24	109.59			
Closure %		109.32				
EFFICIENCIES						
Cold gas %		47.49				
Hot gas %		57.77				
Raw gas %		64.08				

Run 23						
Mass Balance				Elemental Balance		
			Carbon	Hydrogen	Oxygen	Nitrogen
Feed Moisture content % (wb)	8.76					
Carbon % weight (daf)	53.04					
Hydrogen % weight (daf)	6.12					
Oxygen % weight (daf)	39.90					
Inputs Kg/h						
Wood	1.45					
Wood moisture	0.14					
Ash	0.00					
Oxygen in air	0.86					
Nitrogen in air	2.96					
Air moisture	0.03					
Total	5.27		0.77	0.09	1.44	2.96
Outputs Kg/h						
H2	0.05					
CO	0.84					
CO2	1.19					
CH4	0.05					
N2 (by difference)	2.96					
Tar	0.05					
Ash	0.00					
Total	5.15		0.76	0.07	1.36	2.96
Closure %	97.61		98.74	76.74	94.32	
Closure* %			101.15	78.62	96.63	
Efficiency indicators						
Mass yield kg/kg	3.51					
Volumetric yield Nm3/kg	3.07					
air/fuel ratio	2.59					
Mass conv. to dry prod. gas %	96.62					
Carbon conversion %	93.81					
Equivalence ratio, %	39.13					
Specific capacity kg/m2h	328.15					
Energy Balance - Summary						
		MJ/h	% dry wood			
Energy input						
Dry wood	Chemical	30.85	100.00			
	Sensible	0.00	0.00			
Dry air	Sensible	0.00	0.00			
Air	Latent	0.07	0.22			
TOTAL		30.92				
Energy output						
Dry gas	Chemical	18.61	60.32			
	Sensible	4.34	14.08			
	Total	22.96	74.40			
Tars	Chemical	1.84	5.97			
	Sensible	0.05	0.16			
	Total	1.89	6.14			
Losses	Radiative	2.60	8.43			
	Convective	0.73	2.35			
	Total	3.33	10.78			
TOTAL		28.18	91.32			
Closure %		91.12				
EFFICIENCIES						
Cold gas %		60.32				
Hot gas %		74.40				
Raw gas %		80.54				

Run 24						
Mass Balance				Elemental Balance		
			Carbon	Hydrogen	Oxygen	Nitrogen
Feed Moisture content % (wb)		8.76				
Carbon % weight (daf)		53.04				
Hydrogen % weight (daf)		6.12				
Oxygen % weight (daf)		0.93				
Inputs Kg/h						
Wood		1.25				
Wood moisture		0.12				
Ash		0.00				
Oxygen in air		0.77				
Nitrogen in air		2.85				
Air moisture		0.02				
Total		4.87	0.66	0.08	1.27	2.85
Outputs Kg/h						
H2		0.04				
CO		0.69				
CO2		1.10				
CH4		0.04				
N2 (by difference)		2.85				
Tar		0.05				
Ash		0.00				
Total		4.77	0.66	0.05	1.20	2.85
Closure %		97.84	99.07	71.66	94.81	
Closure* %			101.26	73.24	96.90	
Efficiency indicators						
Mass yield kg/kg		3.78				
Volumetric yield Nm3/kg		3.22				
air/fuel ratio		2.90				
Mass conv. to dry prod. gas %		96.85				
Carbon conversion to gas %		93.83				
Equivalence ratio, %		40.42				
Specific capacity kg/m2h		282.74				
Energy Balance - Summary						
		MJ/h	% dry wood			
Energy input						
Dry wood	Chemical	26.59	100.00			
	Sensible	0.00	0.00			
Dry air	Sensible	0.00	0.00			
Air	Latent	0.06	0.23			
TOTAL		26.65				
Energy output						
Dry gas	Chemical	15.01	56.45			
	Sensible	3.98	14.98			
	Total	18.99	71.42			
Tars	Chemical	1.69	6.36			
	Sensible	0.05	0.17			
	Total	1.74	6.54			
Losses	Radiative	3.42	12.85			
	Convective	0.82	3.09			
	Total	4.24	15.94			
TOTAL		24.96	93.90			
Closure %		93.69				
EFFICIENCIES						
Cold gas %		56.45				
Hot gas %		71.42				
Raw gas %		77.96				

Run 25						
Mass Balance				Elemental Balance		
			Carbon	Hydrogen	Oxygen	Nitrogen
Feed Moisture content % (wb)		10.08				
Carbon % weight (daf)		53.04				
Hydrogen % weight (daf)		6.12				
Oxygen % weight (daf)		39.90				
Inputs Kg/h						
Wood		1.82				
Wood moisture		0.20				
Ash		0.00				
Oxygen in air		0.91				
Nitrogen in air		3.39				
Air moisture		0.03				
Total		6.12	0.96	0.11	1.64	3.39
Outputs Kg/h						
H2		0.06				
CO		1.30				
CO2		1.15				
CH4		0.06				
N2 (by difference)		3.39				
Tar		0.06				
Ash		0.00				
Total		6.03	0.96	0.08	1.59	3.39
Closure %		98.49	99.68	76.09	97.22	
Closure* %			101.21	77.26	98.71	
Efficiency indicators						
Mass yield kg/kg		3.28				
Volumetric yield Nm3/kg		2.96				
air/fuel ratio		2.37				
Mass conv. to dry prod. gas %		97.48				
Carbon conversion %		95.03				
Equivalence ratio, %		32.99				
Specific capacity kg/m2h		411.47				
Energy Balance - Summary						
		MJ/h	% dry wood			
Energy input						
Dry wood	Chemical	38.69	100.00			
	Sensible	0.00	0.00			
Dry air	Sensible	0.00	0.00			
Air	Latent	0.08	0.22			
TOTAL		38.77				
Energy output						
Dry gas	Chemical	25.81	66.71			
	Sensible	5.33	13.76			
	Total	31.14	80.47			
Tars	Chemical	2.18	5.65			
	Sensible	0.06	0.16			
	Total	2.24	5.80			
Losses	Radiative	0.65	1.68			
	Convective	0.36	0.94			
	Total	1.02	2.63			
TOTAL		34.40	88.90			
Closure %		88.71				
EFFICIENCIES						
Cold gas %		66.71				
Hot gas %		80.47				
Raw gas %		86.28				

Run 26						
Mass Balance				Elemental Balance		
			Carbon	Hydrogen	Oxygen	Nitrogen
Feed Moisture content % (wb)		10.08				
Carbon % weight (daf)		53.04				
Hydrogen % weight (daf)		6.12				
Oxygen % weight (daf)		39.90				
Inputs Kg/h						
Wood		1.23				
Wood moisture		0.14				
Ash		0.00				
Oxygen in air		0.71				
Nitrogen in air		2.66				
Air moisture		0.03				
Total		4.60	0.65	0.08	1.21	2.66
Outputs Kg/h						
H_2		0.03				
CO		0.67				
CO_2		0.82				
CH_4		0.02				
N_2 (by difference)		2.66				
Tar		0.04				
Ash		0.00				
Total		4.23	0.56	0.04	0.98	2.66
Closure %		91.97	85.26	48.64	81.52	
Closure* %			92.70	52.88	88.63	
Efficiency indicators						
Mass yield kg/kg		3.40				
Volumetric yield Nm3/kg		2.83				
air/fuel ratio		2.74				
Mass conv. to dry prod. gas %		91.05				
Carbon conversion %		80.52				
Equivalence ratio, %		38.15				
Specific capacity kg/m2h		278.76				
Energy Balance - Summary						
		MJ/h	% dry wood			
Energy input						
Dry wood	Chemical	26.21	100.00			
	Sensible	0.00	0.00			
Dry air	Sensible	0.00	0.00			
Air	Latent	0.07	0.25			
TOTAL		26.28				
Energy output						
Dry gas	Chemical	12.03	45.89			
	Sensible	1.88	7.16			
	Total	13.90	53.04			
Tars	Chemical	1.49	5.68			
	Sensible	0.02	0.09			
	Total	1.51	5.77			
Losses	Radiative	10.16	38.75			
	Convective	1.56	5.96			
	Total	11.72	44.71			
TOTAL		27.13	103.52			
Closure %		103.26				
EFFICIENCIES						
Cold gas %		45.89				
Hot gas %		53.04				
Raw gas %		58.81				

REFERENCES

1   Grassi G, Bridgwater A V, "Biomass for Energy, Industry and the Environment - A Strategy for the Future", Commission for the European Communities, Directorate General for Science Research and Development, Publication number EUR 12897EN. Publisher: Edizioni Esagonon - Sesto San Giovanni, Milan, Italy, 1990

2   Reed T B, Das A, "Handbook of Biomass Downdraft Gasifier Engine Systems", SERI Report SERI/SP-271-3022, Golden, Colorado, USA, March 1988

3   Anon, "BP Statistical Review of World Energy", BP Plc., Britannic House, Moor Lane, London, 1989

4   Anon, "BP Statistical Review of World Energy", BP Plc., Britannic House, Moor Lane, London, 1991

5   Reed T B et al. (eds), "A Survey of Biomass Gasification - Volume I", SERI Report number SERI/TR-33-239, Colorado, USA, 1979

6   Hos J J, Groeneveld M J, "Biomass Gasification", in "Biomass - Regenerable Energy", Hall D O, Overend R P (eds.), John Wiley and Sons, 1987, pp237-255

7   Groenveld M J, Van Swaaij W P M, "Potentials and Applications of the Co-Current Moving Bed Gasifier", Applied Energy 5 (1979) 165

8   Chern S M. Walawender W P, Fan L T, "Mass and Energy Balance Analyses of a Downdraft Gasifier", Biomass 18 pp127-151, 1989

9   Beenackers A A C M, van Swaaij W P M, "Gasification of Biomass, A State of the Art Review (Keynote Paper)", in, "Thermochemical Processing of Biomass", Bridgwater A V (ed.), Butterworths, 1984

10 Groeneveld M J, van Swaaij W P M, "The Design of Co-Current Moving-Bed gasifiers Fueled by Biomass", Chemical Age of India 31 (3), pp171-178, 1980

11 Reed T B, Markson M, "Biomass Gasification Reaction Velocities", in "Fundamentals of Thermochemical Biomass Conversion", Overend R P, Milne T A, Mudge L K (eds.), Elsevier, 1985

12 Earp D M, "Gasification of Biomass in a Downdraft Reactor", PhD Thesis, Aston University, 1988

13 Overend R, "Gasification - An Overview", Proceedings of Forest Product Research Society Conference, Seattle, USA, 1979

14 Van Swaaij W P M, "Gasification - The Process and the Technology", in, "Energy from Biomass - 1st EC Conference", Palz W, Chartier P, Hall D O (eds.), Applied Science, 1981

15 Beenackers A A C M, van Swaaij W P M, "Methanol from Wood, A State of the Art Review", in, "Energy from Biomass, 2nd EC Conference", Strub A, Chartier P, Schleser G (eds.), Applied Science, pp782-798, 1983

16 Buekens A G, Schoeters J G, "Modelling of Biomass Gasification", in, "Fundamentals of Thermochemical Biomass Conversion", Overend R P, Milne T A, Mudge L K (eds.), Elsevier, 1985

17 Reyes L R N, "Downdraft Gasification of Biomass and Opportunities in Chile", MPhil Thesis, Aston University, 1988

18 Buekens A G, Schoeters J G, "Mathermatical Modelling in Gasification (Keynote Paper)" in, "Thermochemical Processing of Biomass", Bridgwater A V (ed.), P177-199, Butterworths, 1984

19   Reed T B, Markson M, "A Predictive Model for Stratified Downdraft Gasification of Biomass", in "Proceedings 15th Biomass Thermochemical Contractors Meeting", March 16-17 1983, (Report No. PNL-SA-11306, Conf-830233

20   Reed T B, Markson M, "Stratified Bed Downdraft Gasification of Biomass", in "Progress in Biomass Conversion, Volume IV", Tilman D A, Jahn E C (eds.), Academic Press, New York, 1983

21   Chern S-M, "Equilibrium and Kinetic Modeling of Co-Current (Downdraft) Moving-Bed Biomass Gasifiers", PhD Thesis, Kansas State University, Manhattan, Kansas, U S A, 1989

22   Reed T B, Graboski M S, Levie B, "Fundamentals, Development and Scaleup of the Air-Oxygen Stratified Downdraft Gasifier", The Biomass Energy Foundation Press, Golden, CO 80402, USA, SERI/PR-234-2571, 1988

23   Huff E R, "Effect of Size, Density, Moisture and Furnace Wall Temperature on Burning Times of Wood Pieces", in "Fundamentals of Thermochemical Biomass Conversion", Overend R P, Milne T A, Mudge L K (eds.), Elsevier, 1985

24   Reed T B, Levie B, "A Simplified Model of a Stratified Downdraft Gasifier", in, "Bio-Energy 84", Bente P (ed.), Bio-Energy Council, Washington DC, 1983

25   Reed T B, Levie B, Das A, "Understanding, Operating, and Testing Fixed Bed Gasifiers", in, "Bioenergy 84, Volume I, Bio-Energy State of the Art", Egnéus H, Ellegård A (eds.) Elsevier, 1984

26   Reed T B, Levie B, Das A, "Low and Medium BTU Wood Gasification", NREL, 1617 Cole Blvd, Golden, CO, 80401, USA, 1984

27   Reed T B, "The Scientific Basis of Gasifier Design", in, "Symposium on Forest Products Research International - Achievements and the Future", Pretoria, South Africa, 22-26 April 1985, ISBN 0 7988 3373 4. Organised by the National Timber Research Institute of the South African Council for Scientific and Industrial Research

28   Reed T B, Levie B, Das A, "Biomass Gasification for Power, Fuels, and Chemicals", 5th Canadian Bioenergy R&D Seminar, Hasnain S (ed.), Elsevier, 1984

29   Kaupp A. "Air Blown Gasification of Rice Hulls: Dependance of Gas and Solid Properties on Operating Variables", PhD Thesis, University of California, Davis, USA, 1983

30   Wallace J B, "Technical Summary of the American Power and Waste Management Gasifier System", report. Prepared by: Novatech Consultants Inc., Suite 300-40 Powell Street, Vancouver, BC. V6A 1E7 for American Power and Waste Management Ltd., Suite 250-780 Beatty Street, Vancouver, BC, V6B 2M1, USA. 22 March 1991

31   Manurung R, Beenackers A A C M, "Gasification of Rice Husk in a Small Moving Bed Gasifier", 3rd EC Conference, Energy From Biomass, Venice, Italy, 1985

32   Walawender W P, Chern S M, Fan L T, "Influence of Operating Parameters on the Performance of a Wood-Fed Downdraft Gasifier", in, "Energy from Biomass and Wastes X", Klass D L (ed.), Elsevier, pp607-627, 1987

33   Cogliali G, "Gasification of Biomass for the Production of Synthesis Gas with the Intention to Produce Synthetic Fuel in a Further Process", in, "Advanced Gasification - Methanol Production from Wood - Results of

the EEC Pilot Programme", Beenackers A A C M, van Swaiij W P M (eds.), Reidel, 1986

34   Kaupp A, Goss J R, "State of the Art for Small Scale (to 50kW) Gas Producer Engine Systems", USDA report No 53-319R-0-141, Tippi Workshop Books, Colorado, USA, 1984

35   Walawender W P, Chee C S, Geyer W A, "Influence of Tree Species and Wood Deterioration on Downdraft Gasifier Performance", Department of Chemical Engineering, Kansas State University, Durland Hall, Manhattan, KS, 66506, USA, May 12, 1988

36   Chan W R, Kelbon M, Krieger B B, "Product Formation in the Pyrolysis of Large Wood Particles", in "Fundamentals of Thermochemical Biomass Conversion", Overend R P, Milne T A, Mudge L K (eds.), Elsevier, 1985

37   Shamsuddin A H, Williams P T, "Devolatisation Studies of Oil-Palm Solid Wastes by Thermo-Gravimetric Analysis", Journal of the Institute of Energy, March 12992, 65, pp31-34

38   Winship R D, "Evaluation of Fuels for Operation of a Fixed Bed Downdraft Commercial Gasifier", in "Proceedings of the Second Bioenergy Research and Development Seminar", Ottawa, Canada, pp 221-225, 1980

39   Hoi W K, "Gasification of Rubberwood in a Downdraft Reactor", PhD Thesis, Aston University, 1991

40   Hos J J, Beenackers A A C M, van den Aarsen F G, van Swaaij W P M "Production of a Low-Btu Gas by Cocurrent Gasification of Solid Wastes", Twente University of Technology, PO Box 217, Enschede, Netherlands, Received 1991

41   Graboski M S, Brogan T R, "Development of a Downdraft Modular Skid Mounted Biomass/Waste Gasification System", presented at "Energy from Biomass and Wastes XI", Orlando, Florida, USA, 1987

42   Hoi W K, Bridgwater A V, "Development of a Rubberwood Gasifier", in, "Biomass for Energy and Industry, 5th EC Conference, Volume 2", Grassi G, Gosse G, dos Santos G (eds.), pp 2.734-2.738, Elsevier, 1990

43   Groeneveld M J, van Amerongen J, Hos J J, "Production of a Tar-Free Gas in an Annular Co-Current Moving Bed Gasifier", presented at Symposion on Forest Products Research INternational - Achievements and the Future, Pretoria, South Africa, 22-26 April 1985

44   Bridgwater A V, Double J M, Earp D M, "Technical and Market Assessment of Biomass Gasification in the UK", Report to the Energy Technology Support Unit, UKAEA, Harwell, 1986

45   Double J M, "The Design, Evaluation and Costing of Biomass Gasfiers", PhD Thesis, The University of Aston in Birmingham, September 1988

46   Reines R G, "The Gasification of Carrot Fibre in a Cast Refractory Micro-Gasifier", in, "Thermochemical Processing of Biomass", Bridgwater A V (ed.), Butterworths, 1984

47   Anon., "Towards Improved Utilization of Forest Industry Mill Residues in British Columbia", Extractions from a report prepared for The Ministry of Forests Province of British Columbia Wood Residue Task Force, prepared by Simons Strategic Services Division. February 1991

48   Manurung R, Beenackers A A C M, "Field Test Performance of Open Core Down Draft Rice Husk Gasifiers", in, "Biomass for Energy and Industry, 5th EC Conference, Volume 2", Grassi G, Gosse G, dos Santos G (eds.), Elsevier, pp2.512-2.523, 1990

49 Henrikson U, Kofoed E, Gabriel S, Koch T, Christensen O. "Gasification of Straw", Laboratory of Energetics, The Technical University of Denmark, DTH byngning 403, DK-2800 Lyngby, undated, received April 1992

50 Henrikson U, Kofoed E, Christensen O, "Sensitivity Analysis of a Two Stage Biomass Gasifier by a Computer Based Model", Laborartory for Energetics, The Technical University of Denmark, DK-2800, Lyngby, Denmark, March 1992

51 Walawender W P, Chern S M, Fan L T, "Woodchip Gasification in a Commercial Downdraft Gasifier", in, "Fundamentals of Thermochemical Biomass Conversion", Overend R P, Milne T A, Mudge L K (eds.), Elsevier, 1985

52 Henrikson U, private communication at IEA Biomass Meeting, 30:3:92

53 Anon., "Triton Kaowool Ceramic Fibre Product Information Catalogue", Morganite Ceramic Fibres Ltd., Tebay Road, Bromborough, Wirral, Merseyside, L62 3PH. Undated

54 Coulson J F, Richardson J F, "Chemical Engineering, Volume 1, Fluid Flow, Heat Transfer and Mass Transfer", Pergamon, 1957

55 Chapman A J, "Heat Transfer", 2nd Edition, MacMillan, 1967

56 Perry, R H, Green, D, "Perry's Chemical Engineer's Handbook, 6th Edition", McGraw Hill, 1985

57 Incropera F P, Dewitt D P, "Introduction to Heat Transfer", 2nd edition, Wiley, 1990

58 Anon., Model AB Pressure Transducer Instruction Sheet. Data Instruments, 4 Hartwell Place, Lexington, MA 02173 USA, undated

59 Overend R P (Scientific Authority), "A Comparative Assessment of Forest Biomass Conversion to Energy Forms", Enfor Project C-258. Contractors Final Report. DSS Contract 43ss.KN107-1-4416. Energy, Mines and Resources Canada Requisition 23216-3-6238. December 1983

60 Harker J H, Backhurst J R, "Process Plant Design", Heinemann Educational Books, London, 1983

61 Coulson J M, Richardson J F, "Chemical Engineering, Volume 2, Unit Operations", Pergamon, 3rd edition, 1978

62 Calvert S, Goldschmid J, Leith D, Mehta D, "Wet Scrubber System Study, Volume 1, Scrubber Handbook", The US Environmental Protection Agency, EPA-R272118a, 1972

63 Reed T B, (ed), "Gasification - Principles and Technology - Energy Technology Review No 67", Noyes Data Corporation, New Jersey, 1981

64 Coulson J M, Richardson J F, "Chemical Engineering, Volume II", 3rd Edition, Pergamon, 1989

65 Anon., "Performance Data Supplement to Bulletin 4P", All Venturi Equipment Ltd., Venturi House, Edensor Road, Longton, Stoke on Trent, ST3 2QB

66 Emmett, P, "Private Communication", All Venturi Equipment, Venturi House, Edensor Road, Longton, Stoke-on-Trent, ST3 2QB, 1989

67 Esplin G J, Fung D P C, Hsu C C, "A Comparison of the Energy and Product Distribution from Biomass Gasifiers", The Canadian Journal of Chemical Engineering, Volume 64, pp652-663. August, 1986

68 BS 893: 1978, "Measurement of the Concentration of Particulate Material in Ducts Carrying Gases"

69 Milligan J B, "First Year Report", Department of Chemical Engineering, Aston University, UK. October, 1991

70 Anon., "CR Vertical Multistage In-Line Pumps", Catalogue, Grundfos Pumps Ltd., Grovebury Road, Leighton Buzzard, Beds., LU7 8TL, 1989

71 Anon.,"Durapipe catalogue", Glynwed Tubes and Fittings Ltd., Norton Canes, Cannock, Staffs., WS1 3NS

72 Coulson J F, Richardson J F, Sinnott R K, "Chemical Engineering, Volume 6, SI Units, Design", Pergamon, 1989

73 Anon., "Walflon Joint Sealant Catalogue". James Walker and Co. Ltd., Lion Works, Woking, Surrey, GU22 8AP. Undated

74 Anon., "Toggle Clamps, Pliers and Presses Catalogue". HMC Braur Ltd., Dawson Road, Mount Farm Estate, Bletchley, Milton Keynes, Bucks., MK1 1JP. Undated

75 Anon., "QVF Process Plant and Pipeline Catalogue". Corning Process Systems, Corning Ltd., Newstead Industrial Estate, Trentham, Stoke-on-Trent, ST4 8JG. Undated

76 Anon., "Graphite Bursting Discs". Le Carbone (Great Britain) Ltd., South Street, Portslade, Sussex, BN4 2LX. Undated

77 Anon., "Knitmesh Demister Catalogue", Knitmesh Ltd., Sanderson Station Approach, South Croydon, CR2 0YY. Undated

78 Austin D G, "Chemical Engineering Symbols", George Godwin Ltd., London, 1979

79 Perma Pure Sampling Systems, Bulletin 120. Perma Pure Products Inc., Farmingdale, New Jersey, USA. Undated

80 Anon., "Operation and Flow Control Manual OMM1006", Platon Flow Control Ltd., Platon Park, Viables, Basingstoke, Hampshire, RG22 4PS. Undated

81 Anon., "Thorn EMI Flow Measurement Catalogue", Thorn EMI Flow Measurement Ltd., PO Box 3, Talbot Road, Stretford, Manchester M32 0XX. Undated

82 Phillips A, "BBC Kermit User Guide", Lancaster University, 1986

83 Anon., "Explosivity Tests for Industrial Dusts - Fire Research Technical Paper No. .21 - 2nd Edition", Department of the Environment and Fire Officers' Committee - Joint Fire Research Organization. HMSO, 1974

84 Anon, "Occupational Exposure Limits, 1987", Health and Safety Guidance Note EH 40/87

85 Bretherick I (ed), "Hazards in the Chemical Laboratory - 3rd edition" Royal Society of Chemistry, London, 1981

86 Anon., "QVF General and Technical Information Catalogue", Corning Process Systems, Trentham, Stoke on Trent. Undated

87 Bjorseth O M et al, "Monitoring for Polycyclic Aromatic Hydrocarbon (PAH)Content and Mutagenic Activity in Products and Emissions from a Gasifier Demonstration Project", in, "Safe Handling of Chemical Carcinogens, Mutagens, Teratogens and Highly Toxic Substances - Volume 2", Walters D B (ed), Ann Arbor Science, Michigan, 1980

88 Wilson H T, Hill AN, "Fluidised Bed Gasification Facility, Operating and Safety Document", Foster Wheeler Power Products, January 1985, Report No. RD514/TN5

89 Knoef H A M, Stassen H E M, Hovestad A, Visser R, "Environmental Aspects of Condensates from Down-Draft Biomass Gasifiers", 4th EC Conference - Energy from Biomass, Orleans, France, 1987

90 Graboski M, Bain R, "Properties of Biomass Relevant to Gasification", in, "A Survey of Biomass Gasification, Volume II - Principles of Biomass

Gasification", Reed T B et al. (eds.), SERI report No. SERI/TR-33-239, Colorao, USA, 1980

91 Bridgwater A V, "Review of Thermochemical Biomass Conversion", Contractors Report, ETSU B 1202. Energy Research Group, Department Birmingham, UK. January 1991

92 Anon., "Moisture Content of Timber - its Importance, Measurement and Specification", TRADA Wood Information, Section 4, Sheet 14, Timber Research and Development Association, England, October 1985

93 Brown M D, Baber E G, Mudge L K, "Evaluation of Processes for Removal of Particulates, Tars and Oils from Biomass Gasifier Product Gases" in, "Energy from Biomass and Wastes X", Klass D L (ed.), Institute of Gas Technology, Chicago, USA. Elsevier, p 655-676, 1987

94 Graham R G, Huffman D R, "Gasification of Wood in a Commercial Scale Downdraft Gasifier", in, "Energy from Biomass and Wastes V", Klass D L (ed.), Elsevier, p632-651, 1981

95 Esplin G J, Fung D P C, Hsu C C, "Development of Sampling and Analytical Procedures for Biomass Gasifiers", Canadian Journal of Chemical Engineering, 63, p946-953, December 1985

96 Chee C S, Walawender W P, Fan L T, "Material Balance Analysis of Prototype Commercial Downdraft Gasifiers", in, "Proceedings of the International Conference on Research in Thermochemical Biomass Conversion", April 1988, Pheonix, Arizona, USA. Bridgwater A V, Kuester J L (eds.), Elsevier, p1034-1048, 1989

97 Spiers H M, "Technical Data on Fuel", British National Committee World Power Conference, 5th Edition, 1950

98 Milligan J B, private communication, 20th June 1992

99 Reed T B, Markson M, "The SERI High Pressure Oxygen Gasifier", in Proceedings of the Biomass to Methanol Specialist's Workshop, 3-5 March 1982, SERI report number SERI/CP-234-1590, Reed T B, Graboski M (eds.)

100 Carre J, Lacrosse L, Schenkel Y, "Comparison Between Gasification and Densified Products Gasification", in, Fundamentals of Thermochemical Biomass Conversion", Overend R P, Milne T A, Mudge L K (eds), Elsevier, 1985

101 Anon., "32 month Gasifier Mechanistic Study and Downstream Process Development Program for the Pressurized Ash-Agglomerating Fluidized Bed Gasification System. Quarterly Report, October 1 - December 31, 1985", KRW Energy Systems Inc., Madison, USA,. NTIS No. PC A09/MF A01; 1st March, 1988

102 Atkins P W, "Physical Chemistry", 3rd edition, OUP, 1986

103 Meriam J L, Kraige L G, "Engineering Mechanics, Volume 1, Statics", 2nd Edition, 1987, John Whiley and Sons

104 Nonhebel G, "Gas Purification Processes for Air Pollution Control", 2nd Edition, Newnes-Butterworths, 1972

105 Perry, R H, "Engineering Manual", 3rd edition, McGraw Hill, 1959

106 Temple R G, "Private Communication, Aston University, UK, June 1990

107 BS 3405: 1983, "Measurement of Particulate Emmission Including Grit and Dust (Simplified Method)

108 Spiers H M, "Technical Data on Fuel", 6th Edition, The British National Committee on World Power Conference, London, 1961

109 Coulson J M, Richardson J F, "Chemical Engineering", Volume 1, 3rd Edition, Pergamon, 1977

110 Gray W A, Müller R, "Engineering Calculations in Radiative Heat Transfer", 1st Edition, Pergamon, 1974

111 Schmidt F W, Henderson R E, Wolgemuth C H, "Introduction to Thermal Sciences. Thermodynamics, Fluid Dynamics, Heat Transfer", John Wiley and Sons, 1984